ANALYTICAL AND EXPERIMENTAL STUDIES ON IN-PLANE VIBRATIONS AND NOISE OF ROLLING DISKS SUBJECT TO NON-HOMOGENEOUS CONSTRAINTS

Salem Mohamed Bashmal

A Thesis

in

The Department

of

Mechanical and Industrial Engineering

Presented in Partial Fulfillment of the Requirements
for the Degree of Doctor of Philosophy at
Concordia University
Montreal, Quebec, Canada

November 2010

CONCORDIA UNIVERSITY
SCHOOL OF GRADUATE STUDIES

This is to certify that the thesis prepared

By: SALEM BASHMAL

Entitled: ANALYTICAL AND EXPERIMENTAL STUDIES ON IN-PLANE

              VIBRATIONS AND NOISE OF ROLLING DISKS SUBJECT TO

              NON-HOMOGENEOUS CONSTRAINTS

and submitted in partial fulfillment of the requirements for the degree of

              DOCTOR OF PHILOSOPHY (Mechanical Engineering)

complies with the regulations of the University and meets the accepted standards with respect to originality and quality.

Signed by the final examining committee:

Dr. A. R. Sebak	Chair
Dr. A. V. Singh	External Examiner
Dr. A. Bagchi	External to Program
Dr. C. Y. Su	Examiner
Dr. I. Stiharu	Examiner
Dr. R. Bhat and Dr. S. Rakheja	Thesis Supervisor

Approved by

              Chair of Department or Graduate Program Director

              Dean of Faculty

ABSTRACT

Analytical and Experimental Studies on In-plane Vibrations and Noise of Rolling Disks Subject to Non-homogeneous Constraints

Salem M. Bashmal
Concordia University, 2010

In many engineering applications involving circular disks such as railway wheels, grinding wheels and disk brakes, the in-plane dynamics play a prominent role causing disk noise and vibration. While the out-of-plane characteristics have been extensively investigated over the past many decades, only limited efforts have been made on the in-plane vibration behavior of circular and annular disks. This dissertation research aims at developing a generalized formulation for analysis of in-plane vibration behavior of circular annular rotating disks under different support conditions at the inner and outer boundaries.

The in-plane free vibration of the elastic and isotropic disk is first studied on the basis of the two-dimensional linear plane stress theory of elasticity. The exact solutions for the frequency equations are obtained for annular disks with uniform boundary conditions, including elastic boundaries. The results obtained are used to validate the accuracy of the approximate methods for cases involving uniform boundary conditions. The boundary characteristic orthogonal polynomials are employed in the Rayleigh-Ritz method to evaluate free in-plane vibration behavior of disks with free boundary conditions while artificial springs are used to realize clamped conditions at discrete points. The obtained results are compared with those attained from a finite element model to demonstrate the validity of the proposed method. For rotating disks, the frequencies

corresponding to the forward and backward traveling waves are obtained and compared with those available in the published studies. The expressions for the acoustic properties from thick annular disks subject to non-uniform boundary conditions are presented.

Analytical results suggest that the non-uniformity of the support affects the modal characteristics of disk along the in-plane and out-of-plane directions, while introducing additional coupling between the modes. Specifically, some of the peaks in the frequency response, obtained under uniform boundary conditions, split into two distinct peaks in the presence of a point support. Laboratory measurements are performed to investigate the effects of different support conditions on the in-plane and out-of-plane responses of stationary and rotating disks with different radius ratios. The proposed formulation is extended to study the three-dimensional problem of a rotating railway wheel under the effect of contact with rail.

ACKNOWLEDGEMENTS

إلى والديّ الكريمين ...... ثمرة من ثمار غرسهما وتربيتهما

إلى زوجتي العزيزة ...... زهرة اقطفها لها ناضرة زهية

إلى أبنائي الأعزاء ...... حافزاً لهم على العلم والعمل

إليكم جميعاً أهدي هذا العمل

Table of CONTENTS

LIST OF FIGURES

LIST OF TABLES

NOMENCLATURE

SYMBOL   DESCRIPTION

A_n, B_n, C_n, D_n Deflection coefficients of the exact solution

b Backward traveling wave

b_k, c_k Constants in the recurrence formula for orthogonal polynomials

BCOP   Boundary Characteristic Orthogonal Polynomials

BEM   Boundary element method

c_0 Speed of sound in air

D_{mn} Sound pressure directivity functions

$\bar{e}_r, \bar{e}_\theta, \bar{e}_z$ Unit vectors on the radial, circumferential and normal directions

E Young's modulus of disk

Ev, O Even and odd modes

f Forward traveling wave

F Magnitude of the harmonic force

FE   Finite element model

$\{F_s\}$ Force vector due to rotation

$\bar{G}$ Free space Green's function

$[G]$ Gyroscopic matrix

h Thickness of the annular disk

h' Web thickness in the railway wheel

H_n Hankel function of order n

$J_n(\xi)$	Bessel function of the first kind of order n
k	Acoustic wave number
k_z	Structural wave number
k_n	Modal acoustic wave number
K_r, K_θ	Radial and circumferential stiffness coefficients
$\bar{K}_r, \bar{K}_\theta$	Non-dimensional radial and circumferential stiffness parameters
$[K]$	Stiffness matrix
$[\bar{K}_q], [\bar{\bar{K}}_{qq}]$	Nonlinear stiffness matrices from the cubic and fourth order terms
m	Nodal circle number
M	Maximum number of polynomials along radial direction
$[M]$	Mass matrix
n	Nodal diameter number
N	Maximum number of modes along circumferential direction
$N_r, N_{r\theta}$	Radial and circumferential in-plane forces
P	Far-field sound pressure
$\tilde{P}$	Fourier transform of sound pressure
P_{mn}	Modal sound pressure
$\{q\}$	Generalized coordinate
$\{q_s\}$	Static displacement vector
$\{q_d\}$	dynamic displacement vector
r	Radial coordinate
$\bar{r}$	Instantaneous position vector

r_0	Undeformed position of a particle
rw	Reflected traveling wave
R	Distance between the sound receiver and the center of the disk
R_i	Inner radius of the annular disk
R_o	Outer radius of the annular disk
T	Kinetic energy of the disk
$\bar{u}$	Displacement vector
u_r, u_θ, u_z	Radial, circumferential and normal displacements of the disk
$U_n(\xi), V_n(\xi)$	Radial and circumferential deflection functions
$\bar{U}, \bar{V}$	Radial and circumferential deflection coefficients
w	Non-dimensional rotational speed of the disk
$\mathbb{U}$	Strain energy of the annular disk
$\mathbb{U}_d$	Potential energy of the uniform artificial springs
$\mathbb{U}_p$	Potential energy of the point-support
$Y_n(\xi)$	Bessel function of the second kind of order n
z	Normal coordinate
$Z(z)$	Acceleration distribution along z direction
β	Radius ratio
$\epsilon_r, \epsilon_\theta, \epsilon_z$	Normal strain components
$\epsilon_{r\theta}, \epsilon_{\theta z}, \epsilon_{rz}$	shear strain components
ζ	Non-dimensional normal coordinate of the disk
η	Circumferential coordinate in the fixed coordinate system

θ	Circumferential coordinate
θ_0	Circumferential coordinate of the point support
λ	Non-dimensional frequency parameters
v	Poisson's ratio
ξ	Non-dimensional radial coordinate of the disk
Π_{mn}	Sound power
ρ	Mass density of the disk
ρ_0	Mass density of air
σ_n	Radiation efficiency
$\sigma_r, \sigma_\theta, \sigma_z$	Normal stress components
$\sigma_{r\theta}, \sigma_{\theta z}, \sigma_{rz}$	shear stress components
ς_n	Modal damping ratio
$\bar{\phi}, \bar{\psi}$	Lamé Potentials
Φ, Ψ	Radial variations of Lamé Potentials
$\phi_n(\xi),$	Deflection polynomials along ξ directions
$\psi_l(\zeta)$	Assumed deflection polynomials along the normal direction
ω	Radian natural frequency
Ω	Angular velocity of the annular disk
$\vec{\Omega}$	Angular velocity vector
$\bar{\Omega}$	Non-dimensional rotational speed of the disk

SUBSCRIPTS	DESCRIPTION
c	Cosine component
i	Inner radius
mn	Mode indices
o	Outer radius
p	Point support
r	Radial component
s	Sine component
θ	Circumferential component

1. INTRODUCTION AND LITERATURE REVIEW

1.1.   General

Circular disks are commonly used in a wide variety of engineering applications including space structures, electronic components and rotating machinery. The vibration of such disks is known to cause vibration in itself and also of adjoining components which could lead to fatigue failure of the system. Moreover, rotating disks such as railway wheels, grinding wheels, disk brakes and gears have been found to be responsible for the major part of the radiated noise [1]. The out-of-plane vibration characteristics of rotating disks have been extensively investigated over the past many decades. Many engineering applications, however, involve in-plane vibration of rotating disks, which have received relatively little attention. The in-plane vibration of rotating disks also play a prominent role in the characteristics of the entire system suggesting that a study of in-plane vibration is also important in addressing the issue related to noise and vibration of the rotating machines.

For automotive rotors and thick annular disks, the frequencies of in-plane modes of vibration have frequencies that are both comparable to low-order bending modes and within the acknowledged brake noise range [2]. Although the sound radiation from the rotor occurs through its out-of-plane motion, the excitation force arises from the friction energy in the in-plane direction. Friction from the pads excites the in-plane vibration in the rotor which in turn couples with bending modes of vibration to produce noise [2]. Laboratory studies have also demonstrated that in-plane modes exist at frequencies

comparable to those associated with the out-of-plane bending even for disks with thickness to diameter ratios as small as 10^{-1} [2].

Furthermore, the in-plane dynamics of disks is more closely related to the sound radiation. The studies have generally assumed that the sound radiation from the in-plane modes of a disk is negligible compared to that attributed to the out-of-plane modes. The in-plane vibration, however, could contribute significantly to the sound especially for disks that are relatively thick. For example, the radial components of railway wheel are of most importance in rolling noise [3]. Moreover, squealing noise that occurs as the train traverses narrow curves is due to the frictional contact between the rail and wheels. A component of this friction load is oriented in the in-plane directions leading to potential in-plane vibration of the wheel. Furthermore, the in-plane vibration of the wheels could affect the magnitude of the friction and, consequently, the amplitude of the squeal [2, 4].

This dissertation research is concerned with the analysis of in-plane vibration behavior of stationary and rotating disks subject to various boundary conditions that may be found in engineering applications. An analytical method is proposed to study the in-plane vibration behavior of the disks subject to combinations of various classical boundary conditions, and single or multiple elastic or non-uniform supports. Laboratory experiments are also performed and the data are used to demonstrate the validity of the proposed approach.

1.2.   Review of Previous Literature

The analysis of any vibrating system necessitates appropriate modeling of the structural components and boundary conditions. Plates, cylinders and shells are,

obviously, used to represent two-dimensional (or three-dimensional) structural components. Therefore, a substantial body of literature could be found on the analysis of such structures with different geometries, material properties and boundary conditions. Rotating structures, such as railway wheel or disk brake, can also be modeled as circular disks with both in-plane and out-of-plane degrees-of-freedom (DOF). The relevant reported studies on circular disks are thus reviewed and discussed in the following sections to build the essential background and formulate the scope of this dissertation. Although numerous selected studies are cited in the following section, it needs to be noted that there are far more related works in the literature. For more related studies, references are made to the works by Leissa [5] and Rao [6]. The general scope of the problems and the related work presented in the literature are grouped under different relevant topics and briefly described in the following sub-sections.

1.2.1. In-plane Dynamics of a Disk

The vibration characteristics of circular disks subject to classical boundary conditions have been reported in a vast number of studies. In particular, the out-of plane flexural vibrations of the circular disks have been analytically investigated under different boundary conditions using several exact and approximate approaches [5, 6]. These studies have provided vast amount of information on out-of-plane vibration behavior of disks. The in-plane vibration characteristics of disks, however, have been reported in fewer studies. Although some of the studies have included in-plane dynamics in the analysis, the focus was primarily on the out-of-plane dynamics due to in-plane excitations [7- 10]. Ferguson and White [7] studied out-of plane dynamic response of a

plate under the effect of static, in-plane loading at the outer edge. Srinivasan and Ramamurti [8] studied the buckling and free vibration of an annular plate with clamped inner boundary and a concentrated, in-plane edge load at the outer boundary using semi-analytical finite element method. Yano and Kotera [9] studied the stability of a rotating disk with a fixed elastic restraint and, in a subsequent study, included the effect of static in-plane load [10]. While these models captured the effect of in-plane forces on out-of-plane vibration, the in-plane deformations of the disk were entirely ignored.

In-plane vibration of circular disks, however, have been gaining increasing attention only in recent years, in view of its applications in various practical problems including the vibration of railway wheels, disk brakes and hard disk drives [1, 3, 11]. Furthermore, the in-plane dynamics of rotating disks is considered to be of practical importance in view of its application in rolling noise emission arising from the wheel-rail interactions [12].

In-plane Vibration of Stationary Disk

The first attempt to tackle the problem of vibration within the plane of disks was by Love [13], who derived the essential equations of motion and presented the general solution for a thin circular disk with free edge conditions. No further investigations were performed on the modal characteristics of the disk since the physical significance of the problem was not apparent to the author to attempt the solution. The practical importance of Love's theory was highlighted by Onoe [14], who related it to problems involving piezoelectric vibrators and relatively thick disks. He evaluated the in-plane vibration of disks using numerical analysis and presented the frequency equations corresponding to

4

the different modes. The variations in the frequency parameters versus the Poisson's ratio were discussed briefly. A more generalized analysis of the in-plane vibration of disks was subsequently presented by Holland [15] in the late sixties, who reported the frequency parameters and normalized eigenmodes for a wide range of nodal diameter numbers and Poisson's ratios. The study also investigated the response due to an in-plane force excitation.

Another study evaluated the frequency parameters and associated mode shapes of in-plane vibration of solid disks clamped at the outer edge using assumed deflection modes in terms of trigonometric and Bessel functions [16]. The study examined the effect of Poisson's ratio and disk thickness on the natural frequencies. It was shown mathematically that the modes with circumferential wave number equal to unity are the only group of modes that involve displacement of the disk center. More recently, Park [17] followed an approach similar to that proposed by Love and obtained an exact frequency equation for a solid disk clamped at the outer edge. The two dimensional deformed shapes were derived from the finite element model and natural frequencies were compared with those reported in a previous study [16].

The above studies were limited to in-plane free vibration of solid disks. Such analyses of annular disks have been addressed only in a few studies. Ambati et al. [18] presented a generalized formulation for in-plane vibration analysis of annular disks and extended the application to solid disks as well as thin rings by varying the size of the opening. A relation was established between the in-plane modes of annular disks with their counterparts of the thin ring. The authors also illustrated verifications of the analytical results through experiments. The study, however, was limited to disks with free

5

boundary conditions at both the inner and the outer edges. The natural frequencies of an annular disk with clamped inner edge and free outer edge were obtained by Srinivasan and Ramamurti [19], who also obtained the stress distribution due to a rotating force. Irie et al. [20] evaluated the natural frequencies of in-plane vibration of annular disks using transfer matrix formulation with combinations of free and clamped conditions at the inner and outer edges, while the corresponding mode shapes were not presented. In a recent paper, Wu [21] focused on the torsional vibration of circular and annular disks subject to different boundary conditions. Mode shapes were presented and discussed along with torque distribution for different modes. The in-plane dynamic response due to external in-plane force was investigated by Leung and Pinnington [22]. The study obtained the transfer function between the rim and the center.

In recent studies, Lee and Singh [23, 24] calculated the modal radiation properties of a thick annular disk due to out-of-plane and radial excitations. The in-plane vibration characteristics were obtained using the transfer matrix method proposed by Irie et al. [20] and the finite element method. Two analytical methods were proposed for the calculation of the far field pressure from the radial structural modes of the thick annular disk with free boundaries. The first method employed the Rayleigh integral approach, while the second treated the inner and outer edges as two cylindrical radiators. The analytical results were also compared with the numerical results obtained using boundary element method and with the experimental measurements. Although both methods revealed acceptable accuracy when compared with the experimental results, the cylindrical radiator method provided more accurate results than the Rayleigh integral. The effect of

couplings between the in-plane and out-of-plane modes on the total acoustic radiation in thick annular disks was also studied [11].

Rotating Disks

The vast majority of the above-stated studies have considered non-rotating disks for the in-plane vibration analysis. In practice, the problem of rotating disks is far more relevant to applications such as railway wheels, circular saw blades and spur gears. A rotating disk imparts additional forces due to the centrifugal and gyroscopic effects. Furthermore, it has been shown that each resonance observed for a stationary disk splits into two resonances when rotation is introduced due to the gyroscopic effects [25]. Centrifugal forces can be considered as additional stiffeners as a function of the rotational speed. The vibration analysis of rotating disks, thus, involves far more complexities than that of a stationary disk subject to a rotating load as a result of the Coriolis and centrifugal terms associated with the relative motion between the spinning disk and the stationery edge loads [25]. The problems of in-plane vibration of rotating disks have been addressed in only a few studies. Bhuta and Jones [26] provided a solution to the axisymmetric in-plane vibrations of a thin rotating circular full disk and concluded that the effect of rotation is generally lowering the natural frequencies for the modes considered. Two types of instabilities were discussed. The first type was called the "static resonance" or "bursting" [27] which occurred when the radial displacements due to centrifugal force became unbounded at critical speed values. The second type of instability was attributed to couplings between the radial and torsional displacements causing the disk to become dynamically unstable when spinning at high speed. This was

referred to as dynamic instability and is the common type of instability discussed in the literature.

Burdess et al. [27] presented generalized formulations by implementing Lame's potentials to consider asymmetric in-plane vibrations. Unlike the axisymmetric modes, the rotational effects caused the natural frequencies to yield two distinct values. The effect of rotational speed on forward and backward traveling waves of a two nodal diameter mode was discussed for a solid disk with free outer edge. Chen and Jhu [25, 28] extended the analysis to study the divergence instability of spinning annular disks clamped at the inner edge and free at the outer. The effects of radius ratio on the natural frequencies and critical speeds of the disk were also investigated. The studies concluded that the critical speeds of in-plane modes with different nodal diameter numbers approached a single asymptotic value as the nodal diameter increases. This value was independent of the radius ratio but dependent on the Poisson's ratio. The same problem was analyzed by Hamidzadeh [30, 31] where the equations of motion were represented in terms of the dilatation and the elastic rotation of the disk.

In the previous studies, the critical speeds were determined using the classical theory of linear elasticity. It was further assumed that the equations of motion could be established around the equilibrium position, which permitted the decoupling of the static or steady state and dynamic responses. The additional stiffening due to the static displacement could thus be neglected in the dynamic analysis. In order to capture the stiffening effect of the rotation, it is essential to employ the nonlinear strain measures which couple the static solution with the dynamic problem. Several studies have considered stiffening effects on structures other than disks such as rings [32, 33] and

8

beams [34]. The effects of additional stiffening have been discussed extensively in the context of out-of-plane vibrations of disks [35]. For the in-plane modes of rotating disks, Deshpande and Mote [36] studied the stability of a spinning thin disk using a nonlinear strain measure in order to account for the stiffening of the disk due to rotation. The study suggested that the critical speeds were incorrectly predicted by the linear strain measure since the effect of stiffening due to initial deformation was ignored. The static equilibrium problem was subsequently solved to obtain the axisymmetric radial expansion and the associated additional stiffening effects. The study did not observe a critical speed in the range of rotational speeds considered for modes with two or less nodal diameters, when the initial stiffening effect was included in the in-plane vibration analysis. An upper limit for the rotational speed was identified where the assumption of linear strain measure would be applicable.

The analysis of dynamic response of a rotating disk also involves similar challenges associated with consideration of the external rotating force, namely the centrifugal and coriolis forces. Srinivasan and Ramamurti [19] investigated the problem of a stationary disk subject to a rotating edge load, while Chen and Jhu [25, 29] obtained the in-plane dynamic response of the rotating annular disk subject to a fixed load. The difference between the two studies lies in the treatment of additional terms arising from the centrifugal and coriolis forces in the rotating disks. The two studies may, thus, be expected to yield comparable responses at relatively low rotational speeds. The most significant deviations between the results of the two studies, the one involving a fixed disk with a rotating load and that of a rotating disk with fixed load, would be in the modes with zero nodal diameter number, i.e. axisymmetric modes. More recently, Koh et

9

al. [37] revisited both problems (stationary disk-rotating load and rotating disk-fixed load) using moving element method. The moving element method is similar to the conventional finite element method except that the elements can rotate relative to the disk and are not attached to material points. The study also presented analytical solution using the approach developed by Chen and Jhu [28] while using Fourier-Hankel functions instead of the Fourier-Bessel functions and confirmed the differences observed in [29]. Leung and Pinnington [38] conducted experiments to measure the in-plane response of stationary disk under rotating edge loads. The cited references mostly dealt with the vibration of disks with uniform boundary conditions. The effect of point support or contact has not been addressed in the literature. The stiffening due to rotation was also formulated with the assumption of uniform boundary conditions. It, therefore, became essential to investigate the effects of stiffening and constraint non-uniformity on the in-plane modes of vibration for annular disks.

Applications of In-plane modes

In order to reflect the importance of in-plane modes of vibrating structures, a few investigations have illustrated the contributions of in-plane modes to various practical problems. As discussed above, relatively thick disks exhibit in-plane modes. Common applications include the disk brakes and railway wheels. In both applications, the disks are relatively thick, rotating and are subject to external forces and/or contact forces. The contributions on in-plane modes in the coupled vibration characteristics and noise radiation have been discussed in a few studies. Tzou et al. [2] investigated the vibration characteristics of a disk brake through formulation and analysis of a three-dimensional

model for the disk (discussed in a subsequent section). Laboratory tests on disk brakes showed that in-plane modes exist at frequencies comparable to those of the out-of-plane modes even for disks with thickness ratio of 0.1. Figure 1.1 shows that the first radial mode (3.2 kHz) is located between the second and third bending modes, while the torsional mode is even lower than the first bending mode [2]. Lee [39] investigated the instability in brake system due to in-plane modes compared to instability due to the out-of-plane modes. More recently, Kirillov et al. [40] studied the coupled vibration of a rotating disk brake in the presence of a distributed frictional loading on its surface based on Kirchhoff's assumptions. The out-of-plane and in-plane modes of vibrations were decoupled due to the linearity of the problem. This study showed that the frictional pads must have both in-plane and out-of-plane components in order to introduce a linear coupling between the in-plane and the out-of-plane modes. The perturbation method was used to predict the stability boundaries of the coupled system.

Lee and Singh [41] extended their own work on the acoustic properties of thick disks to study the mutual radiations of the radial and out-of-plane modes contributing to the sound radiation of a disk brake rotor. The far-field sound radiation from the disk brake rotor was computed using a finite element model to obtain the vibration characteristics, while analytical methods were employed for deriving the sound radiation properties.

In railway vehicles, the interactions of the rotating wheel with the rail are considered as the primary source of noise radiation [42-44]. The rotation of the wheel, coupling between modes, contact forces and different types of excitation are significant

11

factors contributing to the noise radiation due to wheel-rail interactions (see Figure 1.2).

The dynamic railway wheel and track interactions in the presence of wheel flat defects
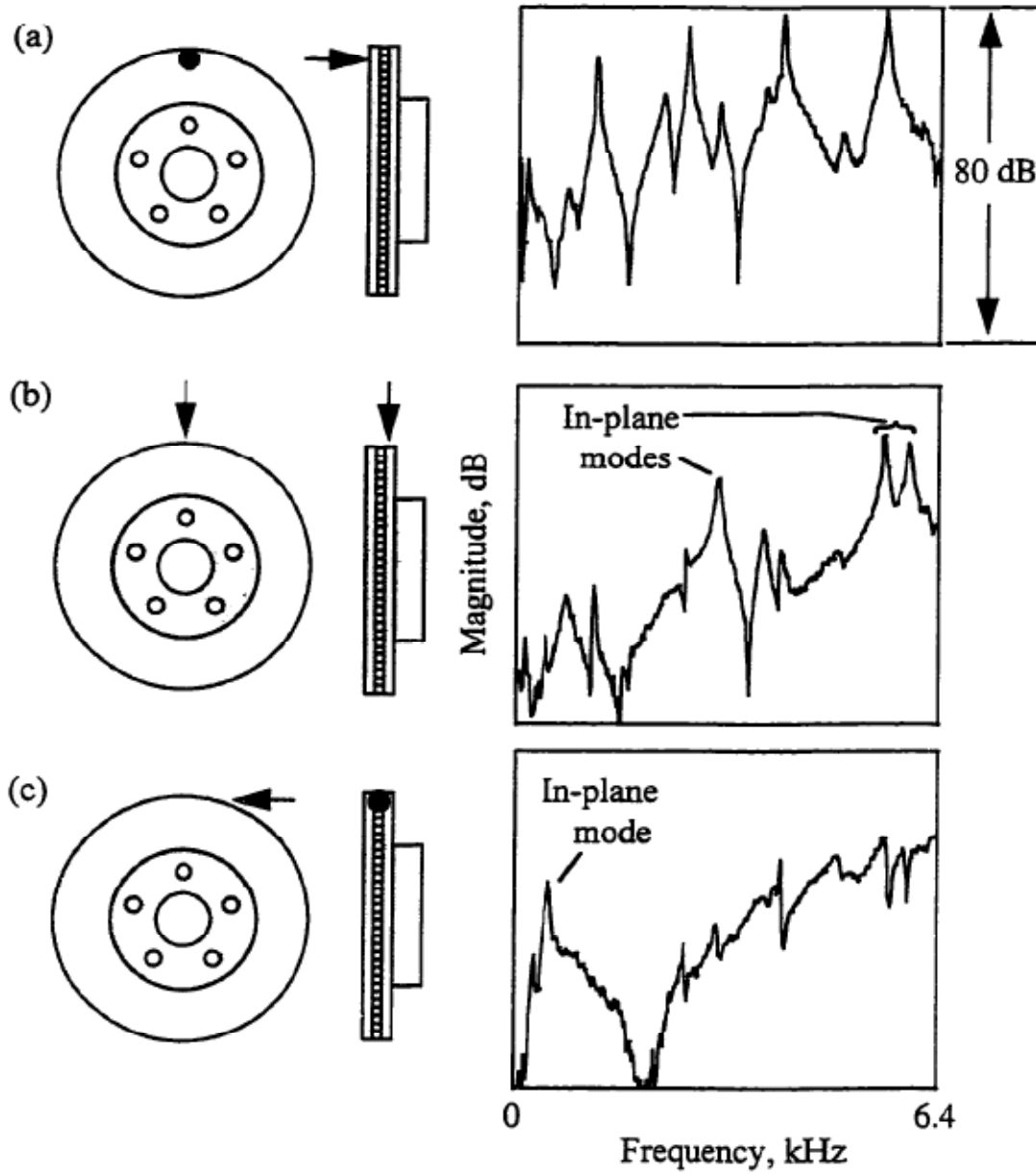
Figure 1.1: Frequency response of an automobile brake rotor system: (a) out-of-plane vibration, (b) in-plane radial modes, (c) in-plane torsional modes [2].

would be of particular interest in the context of in-plane wheel vibration, which may contribute to dynamic wheel impact loads and noise emission, although only minimal efforts have been made in identifying relation between the in-plane modes and noise radiated [12]. Detailed models of railway wheels are required to account for the in-plane deformations of the wheels. Furthermore, the gyroscopic and preload effects may be of particular importance [45]. A discussion on the available models in the literature will be given in a later section.
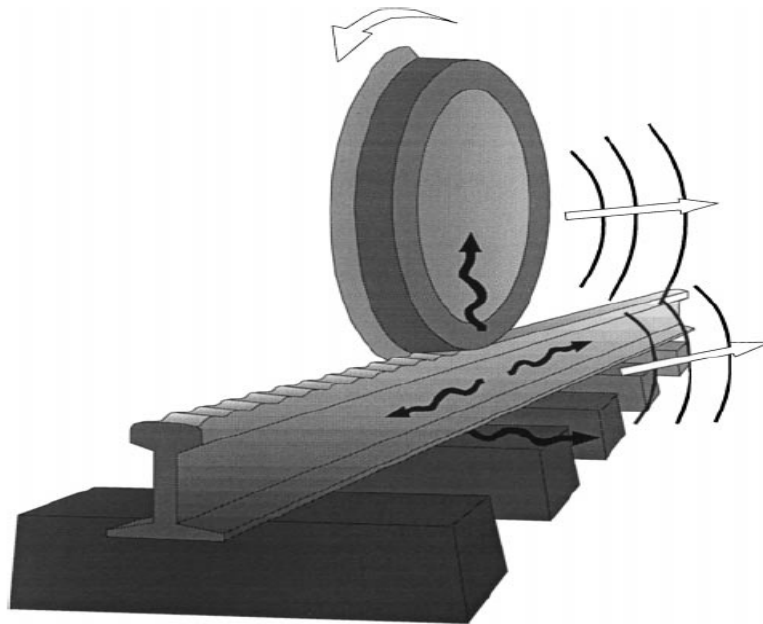
Figure 1.2: Schematic showing the sources associated with rolling wheel-rail interactions contributing to noise emission [12].

Baddour and Zu [46] presented a mathematical model of a spinning thin disk based on the linear Kirchhoff and nonlinear von Karman strain expressions incorporating both in-plane inertia and rotary inertia. For the stationary disks, the in-plane and out-of-plane modes were observed to be uncoupled and could be treated independently. For the spinning disks, it was shown that inclusion of the in-plane inertia results in additional

terms in the equation for the out-of-plane vibrations, which had been ignored in the previous studies. These additional terms were present in both the linear and nonlinear analysis of rotating disks and added additional stiffening to the out-of-plane displacement. The nonlinear equations of motion for the out-of-plane vibrations were linearized and solved for the natural frequencies to study the rotational effects [47]. It was concluded that the in-plane inertia could not be ignored for spinning disks, although its contribution to the out-of-plane vibrations could be neglected for stationary disks.

More recently, Baddour and Zu [48] revisited the nonlinear coupled problem of the spinning disk that included three nonlinear differential equations, which were simplified to two degrees-of-freedom (DOF) model using the Galerkin method. The study reported somewhat new phenomena such as internal resonance and instability of the disk which were attributed to the inclusion of the in-plane inertia. These observed phenomena were not present when the in-plane inertia was ignored. It was, thus, concluded that the consideration of in-plane mode is important in applications where high rotational speed is encountered.

1.2.2. Point and Line Contact

It is well known that the vibration characteristics of the disk are significantly affected by the type of boundary conditions. Circular disks with different boundary conditions are commonly encountered in many engineering applications including space structures, electronic components and rotating machinery. In most cases, the disk may be fastened or welded at different points suggesting that the boundary conditions may neither be rigid nor be uniform around the edge. Moreover, rotating disks are subject to

14

friction or contact forces from the adjacent structures such as friction pad in disk brakes and railway wheel contact with the rails. Several models have been proposed to study disks with contact or point clamped boundary conditions, which may be classified into two groups based on the treatment of the contact. In the first approach, the contact is considered as an external force applied to the disk. The time response due to the contact force is subsequently obtained. The most of the cited studies described in the previous section on the in-plane vibration of disks would fall within this first analysis approach. The second approach considers the contact as an additional constraint. This method allows for analyses of free vibrations of the disk under the effect of the contact. The additional constraint may be considered as a point support [7], a line support [49] or an elastic support [50]. The effects of such contacts on the out-of-plane vibration characteristics of circular disks have been extensively investigated, while such studies on the in-plane vibration have not been reported in the literature. The relevant reported studies on the out-of-plane vibrations are, thus, reviewed and discussed in this section since their proposed methods could also be applied to study the in-plane modes or the coupled vibrations of thick disks.

The study by Hirano and Okazaki [51] was among the first ones, which investigated the fundamental out-of-plane mode of a solid circular disk with mixed boundary conditions using the integral equations formulation proposed by Keer and Stahl [52] for rectangular plates. Combinations of free, clamped and simply-supported boundary conditions were considered at the outer edge of the solid disk. Numerical results were verified by experiments performed on a solid disk that was clamped over a portion of the edge and free over the remaining circumference. The free vibration of a

disk elastically supported at discrete points located arbitrarily inside the disk was investigated by Irie and Yamada [53]. The natural frequencies and mode shapes were calculated numerically for both symmetrical and anti-symmetrical modes of the disk supported at several points. This study showed that the natural frequencies and mode shapes vary considerably with variations in location of the supports. Leissa et al. [54] investigated the out-of-plane free vibration of a circular plate with elastic constraints varying along the outer periphery. The elastic constraints were represented in terms of a Fourier series along the periphery of the disk. The numerical results were evaluated for a single sinusoidal variation of the rotational spring along the outer edge. The proposed method was subsequently extended to include the vibration of disks with linearly varying thickness along the radial direction by Laura and Ficcadenti [55].

Narita and Leissa [56, 57] further investigated the free vibration of a disk with clamped or simply supported conditions only along a portion of the edge. This study showed variations in the frequency with respect to the angle formed by the constrained portion of the edge. Figure 1.3 shows that symmetric and anti-symmetric modes follow different paths as the span of the clamped edge increases, until they approach the same value of the natural frequencies at the totally clamped edge condition. In Figure 1.3, the numbers on the right and left vertical axes are the frequency parameters for the point-supported and totally-clamped conditions, respectively, while α represents the angle formed by the edge support. Amabili et al. [58] investigated the modal characteristics of a solid plate fixed by different number of bolts using the Fourier series expansion of the elastic constraints in conjunction with the Rayleigh-Ritz method. Based on the Mindlin's plate theory, Irretier [50] used a point elastic spring to represent a contact between the rail

16

and the railway wheel for predicting the natural frequencies and the mode shapes, and dynamic response to a harmonic excitation at the wheel-rail contact.
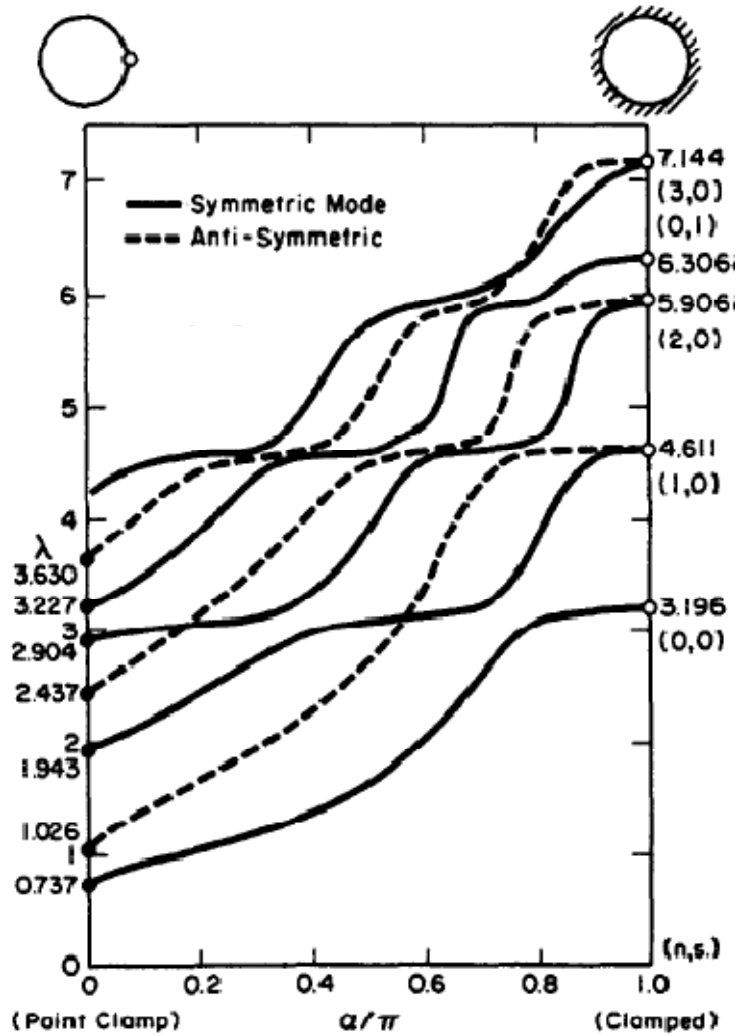
Figure 1.3: Variations in the frequency parameters of a solid circular disk with respect to the angle formed by the constrained portion of the edge ($v = 0.33$) [56].

Alternate methods, other than the elastic constraints, have also been used for analysis of free vibration of circular disks with mixed boundary conditions such as the variational approach [59], perturbation method [60] and Lagrange multipliers [7]. In a study by Ferguson and White [7], the free vibration characteristics of a stationary disk were obtained by an extension of the Rayleigh-Ritz method and the unknown Lagrange

17

multiplier. The disk was clamped at the inner boundary with a point constraint on the periphery. The effect of in-plane static loading applied between the centrally clamped region and the contact region were also examined, which resembled a railway wheel. The resulting study illustrated the changes in the natural frequencies and the mode shapes. The relation between the load and a natural frequency for a given rotational speed was further calculated using a combination of Fourier series along the circumferential direction and finite element analysis for the radial behavior.

It is more realistic to assume that the peripheral load is a distributed load. Chonan and Hayase [49] studied the in-plane stress distribution in a spinning annular disk through a Galilean transformation. The disk was clamped at the inner boundary and subjected to a stationary distributed load along a finite length of the outer boundary. Eastep and Hemmig [61] employed finite-element approach to investigate the vibration responses of a disk with partially free and partially clamped edges. The numerical results were verified using the experimental data and the effects of variations in the arc length of the free portion on the natural frequencies were discussed.

The reported studies have shown that the presence of non-uniform boundary conditions caused some of the modes to have two distinct natural frequencies [57]. This was clearly illustrated in Figure 1.3 when the disk is clamped along portion of the edge. This has been attributed to different effects of non-uniform conditions on the symmetric and anti-symmetric modes of vibrations. This frequency split was also observed in the experimental measurements conducted by Eastep and Hemmig [61]. This behavior has also been discussed extensively in a recent study on a solid disk with mixed boundary conditions [62].

The cited references, however, mostly investigated the out-of-plane dynamics only. The effect of an additional constraint or a point support on the in-plane modes has not been addressed. Furthermore, consideration of circular disks with either a point or a patch constraint with certain flexibility would be more representative of many situations such as automobile wheel/tire assembly and railway wheels. The in-plane vibration characteristics of disks with such partial supports and flexible boundary conditions have not yet been reported.

1.2.3. Three Dimensional Models

The reported studies on vibration characteristics of circular disks have generally considered classical thin plate theory which assumes that in-plane and out-of-plane displacements are uncoupled. This reduces the problem to single DOF (out-of-plane) two-dimensional problem. For a moderately thick disk, such theory would yield incorrect estimates of the natural frequencies of the disk because due to the presence of shear deformation and rotary inertia. Mindlin [63] proposed an alternate theory for thick plates where the shear deformation and rotary inertia were included in the analysis of the two-dimensional system. The Mindlin's theory has been extensively used to predict the natural frequencies of circular thick plates subject to different boundary conditions [64-66].

A three-dimensional model, however, could provide more comprehensive vibration characteristics of the disk involving both the in-plane and out-of-plane modes and the coupling between the motions. For applications such as in railway wheels and disk brakes, for example, the disks are undoubtedly thick and the couplings between in-

plane and out-of-plane modes are quite strong. Three-dimensional models are, thus, desirable for analyses of coupled vibrations of circular disks.

Hutchinson [67] presented the first three-dimensional solution of circular disks using Bessel functions of the first kind in the radial direction and trigonometric functions in the circumferential and normal directions. The series method was used to represent the analytical solutions of annular plates [68]. So and Leissa [69-71] reported a number of studies on natural frequencies and mode shapes for thick structures including circular annular disks, through analysis of the three-dimensional models in conjunction with the Rayleigh-Ritz method. The validity of the results was demonstrated through comparisons with those reported from various thick plate models for disks with free boundary conditions. These studies suggested that selection of the origin of the radial coordinate at the middle distance between inner and outer edges would improve the convergence of the solution.

Tapered disks exhibit greater affinity in bending, which make them quite attractive in many applications. The three-dimensional vibration analysis of annular disks has been extended to study annular disks with linearly varying thickness along the radial direction by Kang and Leissa [72] and with nonlinear thickness variations by Kang [73].

The three-dimensional model has also been used by Tzou et al. [2] to investigate the vibration characteristics of a disk brake. The Rayleigh-Ritz method was used to obtain the natural frequencies of an annular thick disk with free and inner clamped boundary conditions. The effect of disk thickness on the natural frequencies and mode shapes were studied as the disk underwent continuous transition from thin disk to an annular cylinder. The results showed that several in-plane and out-of-plane modes could

be close to each other or even have identically same natural frequencies, when the disk thickness is varied. These modes could couple together in the presence of geometric asymmetry or nonlinearity.

A recent study has employed finite element method to analyze the vibration characteristics of a rotating thick plate based on Mindlin plate theory and nonlinear strain measure [74]. The governing equations were derived using Kane's method [75]. The general equations were derived in the Cartesian coordinate system for rotating rectangular disk but some results were obtained for the solid circular disks. The stiffening effect of the centrifugal forces was taken into account, which was derived from the static deflections of the rotating disk. The variations in natural frequencies with respect to different parameters such as rotational speed and thickness ratios were discussed.

Three-dimensional models, that considered the coupled in-plane and out-of-plane modes of vibrations, were essential to provide a comprehensive understanding of the modal characteristics of thick disks. Although many investigations tackled thick disk problems, it is apparent that the consideration of rotation and non-uniform support conditions is still lacking. It is, therefore, essential for a comprehensive model to take into account the coupled in-plane and out-of-plane vibrations under the effects of constraints and rotation.

1.2.4. Applications to Railway Wheel

A railway wheel can be modeled as a disk and its modes of vibration resemble those of a flat circular plate. Its interactions with the rail could excite both the in-plane and out-of-plane vibration responses. The dynamics of the railway wheels can be

21

classified based on the frequency range of interest. The low frequency responses, up to 50 Hz, concern the stability and comfort performances, where the wheel is treated as a rigid mass. The high frequency range responses, above 500 Hz, contribute to acoustic emission. The wheel dynamics in the mid frequency range concern the stress and fatigue of the wheel-rail system [45].

The high frequency vibration characteristics of the wheel are of practical interest for acoustic emission and the high frequency surface stresses [1, 12]. It has been recognized that prediction of wheel-rail noise radiation requires analyses of the sound radiation characteristics of the railway wheel [4]. Detailed high frequency models are also considered useful in establishing the validity ranges of the simplified approximate models [76].

Wheel elastic models

A number of studies have proposed different models of an elastic wheel using different approaches [45, 50, 77, 78]. Within this context, a comprehensive review of historical evolutions and recently published methods of modeling of the vehicle and track dynamic interaction problems has been given in [45]. In this reference, the theoretical importance of classical continuous models was substantiated and the adequacy of simple railway models to certain types of problems was addressed. A few studies have also investigated the vibration properties of railway wheels as thick disks. Irretier [50] developed a model to study the natural and forced flexural vibration of a railway wheel using the Mindlin's plate theory. The thickness of the disk was assumed to vary continuously in the radial direction and a linear elastic spring was introduced at the

contact point of the wheel rim and the rail in the out-of-plane direction only. The rotation of wheel was not considered and only out-of-plane characteristics were investigated.

Sakamoto et al. [78] conducted analytical and experimental studies to determine the natural frequencies of a railway wheel. The analytical model studied the in-plane and out-of-plane vibrations separately. The wheel was modeled as a circular plate with constant thickness and a ring. Good agreement was achieved between the theoretical and experimentally measured frequencies, although the natural frequencies were limited to $n \geq 2$. This was perhaps due to lack of consideration of the axle, which did not permit accurate predictions of modes corresponding to $n = 0$ and $n = 1$.

Bogacz and Dzula [79] analyzed the high-frequency forced vibration of a rolling wheelset interacting with rails by means of 3-D linear Hertzian springs. The physical model of the wheelset consisted of two elastic wheels, connected by a rigid axle shaft. The axle was considered with six degrees of freedom including three translational and three rotational motions. In the study, wheels were modeled as elastic curved beams with constant curvature. Wheels were connected to the axle by means of a distributed elastic spring.

A few studies have suggested that vibration responses of the wheels could be estimated without considering the axle, while the axle could be represented by a constraint at the inner edge of the hub. Thompson [1] estimated the natural frequencies of the wheels using a finite element model of the wheels alone. Axisymmetry of the structure was assumed with sinusoidal variations along the circumferential direction. The mode shapes were presented for several flexural and radial modes. The study concluded that for modes with $n \geq 2$, the axle could be ignored, by imposing a clamped condition at

the inner edge of the hub. This Idealization was expected to yield reasonable results for all modes, except for $n = 0$ and $n = 1$. The extension and flexure of the axle shaft, however, contributes greatly to the modes corresponding to $n = 0$ and $n = 1$[1].

Several continuum models have also been developed for analyses of the railway wheelset [45, 80, 81]. The complex geometry of the wheelset could be effectively represented by a composition of different continuous systems, often with additional masses. Wheelset models of this type differ significantly in their complexity from those summarized above. A continuous model of a flexible wheelset running on flexible track was developed by Meywerk [81] to study the dynamic behavior of the railway wheels. The axle was modeled using the Timoshenko beam theory while the wheel disk model considered the Kirchhoff's plate theory. This model, shown in see Figure 1.4, was coupled with a wear model to predict the polygonalization of the wheel and the development of out-of-roundness defects in the wheels.
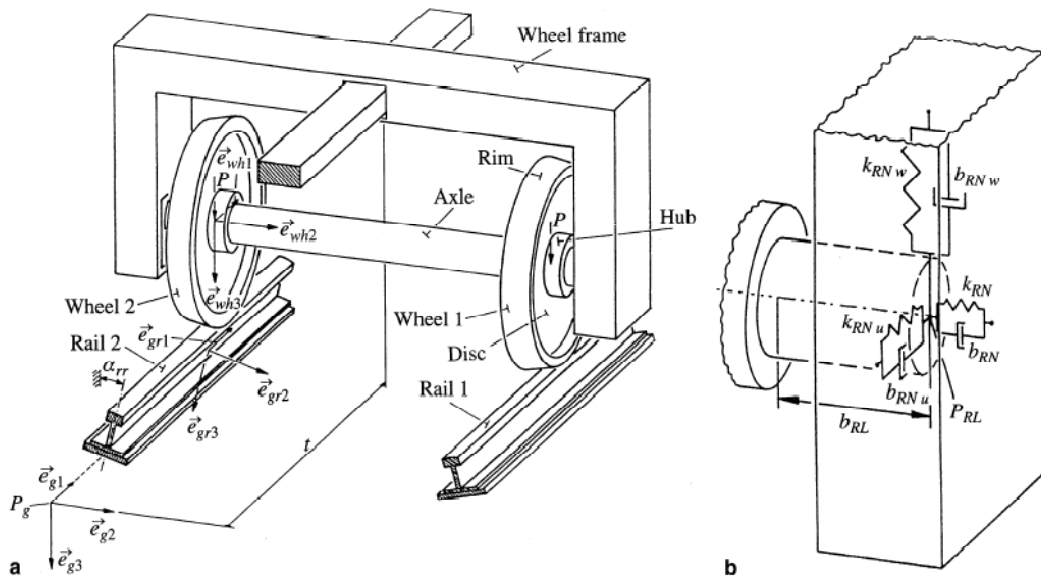
Figure 1.4: (a) Elastic wheelset/track model, and (b) primary suspension model developed by Meywerk [81].

Noise Radiation

The wheel/rail noise emission may be characterized in three primary categories, namely the rolling noise, impact noise and squeal noise. The rolling noise generally occurs on straight tracks and is predominantly caused by undulations of the wheel and the rail surfaces which induce a vertical relative vibration. Impact noise can be considered as an extreme form of rolling noise occurring at discontinuities of the wheel or rail surface, or due to wheel/rail defects. The excitation is again vertical, while the non-linearities play a greater role. The squeal noise, occurring on sharp radius curves, is usually induced by lateral excitation [3]. A review of the wheel-rail models developed to study the noise generation has been presented in a few studies [3, 12, 44]. Knothe and Grassie [12] have reviewed the evolutions in modeling of railway vehicle/track interactions with greater emphasis on the track models, while Talotte [44] presented a critical review of studies describing identifications and modeling of railway noise sources.

The frequency spectrum of the noise emitted by the wheel-rail system exhibits broad frequency content, with the highest levels occurring in the 800-2500 Hz frequency range. Figure 1.5 illustrates a typical frequency spectrum of the radiated noise [42]. The emitted noise in the frequency interval of 100–5000 Hz has been associated with rolling noise, with the highest levels occurring in the 500–2500 Hz range. At frequencies below 500 Hz, the primary contribution to the noise is radiated by the sleepers, while the rail vibration has been reported as the dominating source of noise in the 500 Hz to 1 kHz range. Stiffer rail pads tend to increase the frequency interval of the sleeper noise. The studies have suggested that wheel vibrations contribute most significantly to wheel-rail noise at frequencies above 1 kHz [82].
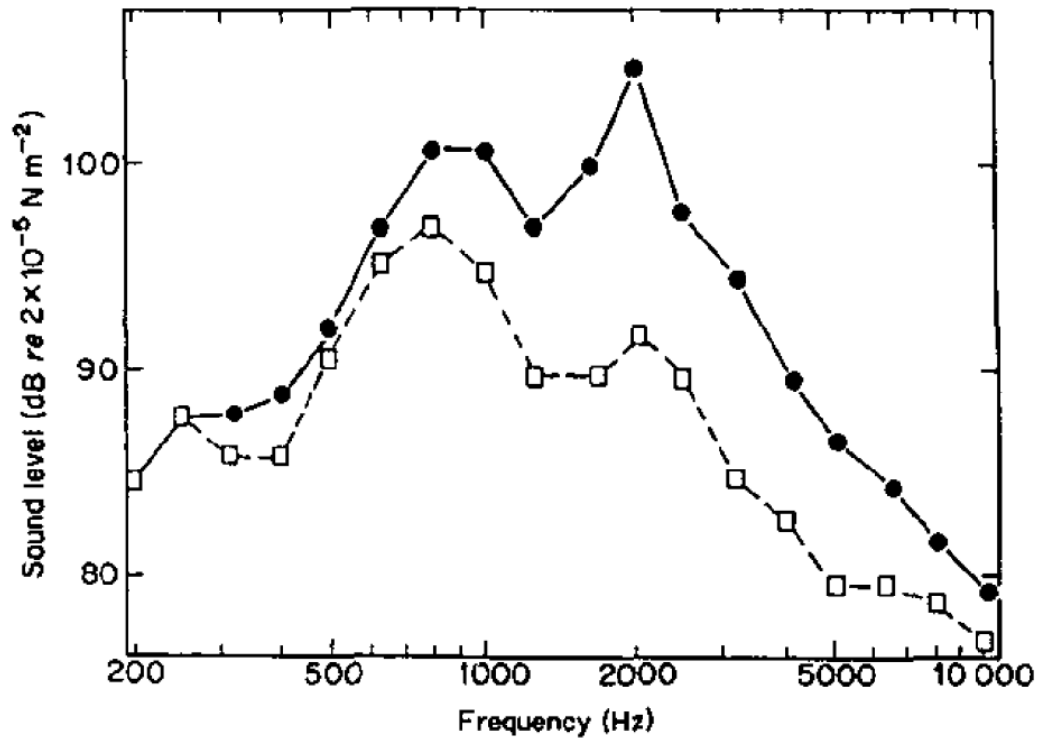
Figure 1.5: An example spectrum of the wheel-rail noise in the one-third octave bands,
————: tread-braked vehicle, — — — — — :disk-braked vehicle[42].

Fingberg [4] predicted the noise radiation from a wheel using a boundary element method with an objective to determine the squealing noise. A finite element model of the wheel was used to obtain natural frequencies and mode shapes of the wheelset. The study reported the mode shapes of a wheelset. Figure 1.6 illustrates the mode shapes corresponding to the lowest symmetric and anti-symmetric modes of the wheelset. It has been pointed that predicting the squealing noise is impossible without considering the radiation characteristics of the wheel. Wu and Thompson [43] developed a numerical model to predict the wheel/rail dynamic interaction caused by excitation due to wheel flats and the consequent noise radiation.

Symmetric	Anti-symmetric
240 Hz	238 Hz
1251 Hz	67 Hz
89 Hz	140 Hz
186 Hz	259 Hz
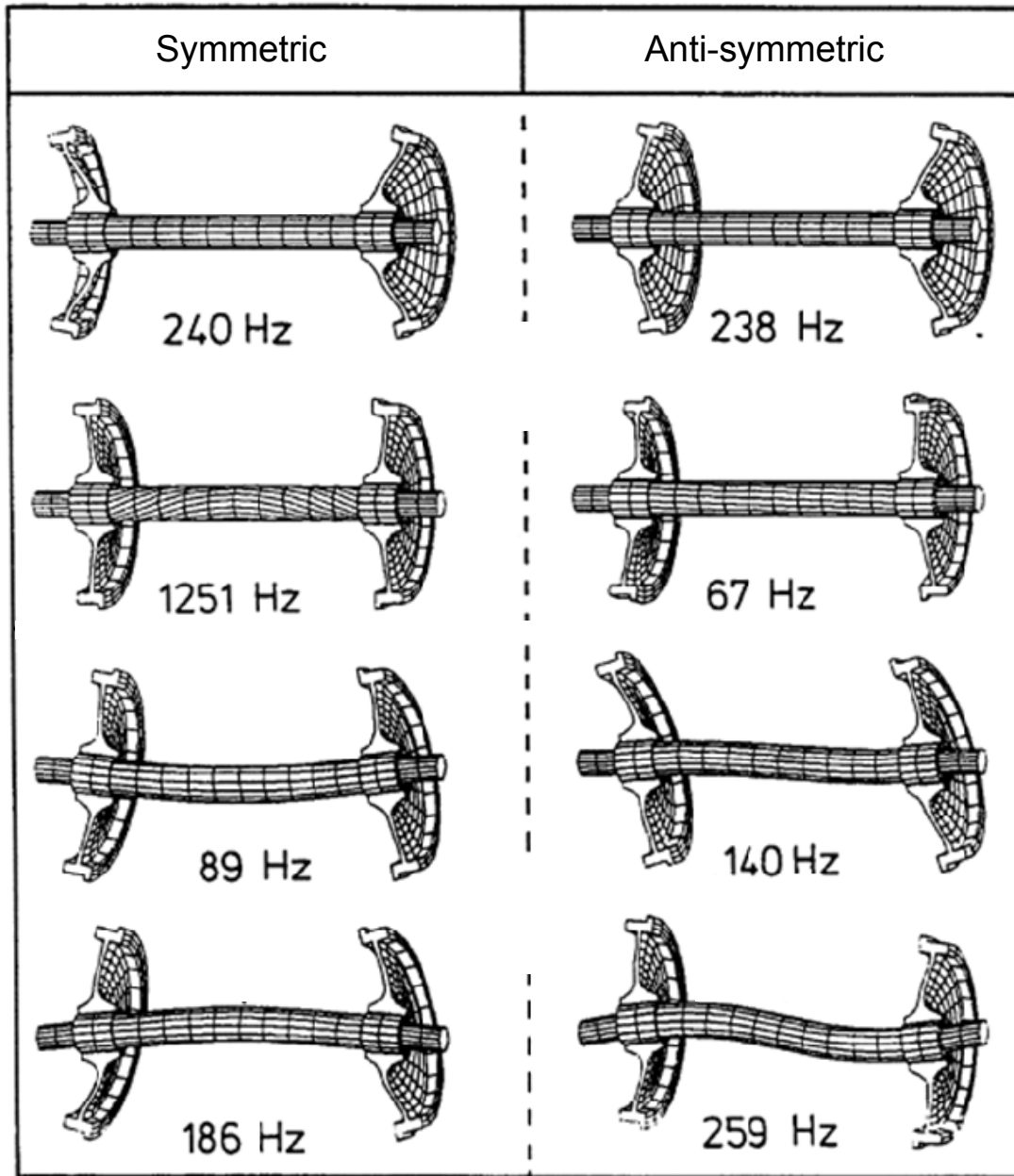
Figure 1.6: Mode shapes of an elastic wheelset [4].

1.2.5. Methods of Analysis

The reported studies on circular disks have employed widely different methods of analysis. These studies are further reviewed and briefly discussed in view of the methods used and their relative merits and limitations. For isotropic circular plates of uniform

thickness subject to the classical boundary conditions of clamped, free or simple support, exact solutions to the governing equations of motion have been obtained in terms of Bessel functions. The natural frequencies and corresponding mode shapes, thus, were derived and have been presented in [5, 6]. However, such exact solutions are limited only to special cases and are not available for the general cases involving non-uniform geometric or material properties. The vast majority of the studies have, thus, used approximate solutions of the vibration problems.

The Rayleigh-Ritz Method

The Rayleigh-Ritz method has been most commonly used to study the vibration properties of various structural components due to its accuracy and versatility. In this method, the maximum strain and kinetic energies of the system are expressed in terms of assumed deflection shapes in the form of a series of shape functions that satisfy at least geometric boundary conditions multiplied by the undetermined coefficients. These coefficients are adjusted by minimizing the frequency with respect to each of the coefficient to form an eigenvalue problem. The eigenvalues and the associated eigenvectors are subsequently obtained from the solution of the eigenvalue problem [83]. The Rayleigh-Ritz method estimates the frequencies of continuous systems with an acceptable accuracy. The accuracy of this method, however, greatly depends on the choice of the shape functions that should be differentiable half as many times as the order of the system satisfy at least the geometric boundary conditions. Several appropriate admissible functions may, thus, be used, provided they satisfy the required boundary conditions for the disks and are relatively easily determined. However, the subsequent

use of these functions in the Rayleigh-Ritz procedure would require the tedious and error-prone evaluation of integrals involving products of trigonometric and hyperbolic functions.

For problems involving multiple disks, identification of the appropriate beam functions becomes far more difficult. Bhat [84] suggested a set of boundary characteristic orthogonal polynomials for use in the Rayleigh-Ritz method as the admissible functions for dynamic and static problems of beams or plates with classical or non-classical boundary conditions. These functions exhibit a number of meritorious features such as the relative ease of generation and integration, and realization of diagonal mass matrix and diagonally dominant stiffness matrix. In these respects, the boundary characteristic orthogonal polynomials offer significant computational advantages over the beam function, particularly for the continuous disks [85].

The boundary characteristic orthogonal polynomials have been successfully employed to study the vibration characteristics of a variety of structures such as elliptical plates [86, 87], tapered beams [88] and polygonal plates [89]. Boundary characteristic orthogonal polynomials are generalized functions that are considered admissible in the Rayleigh-Ritz method for various beam and plate problems including several complicating effects. For instance, this method was used to study the flexural vibration of thin annular and circular composite plates, subject to certain complicating effects such as isotropic or polar orthotropic material, uniform or radially varying thickness and intermediate concentric ring supports [90, 87]. Similar analyses have also been performed on annular and circular, thin, sectorial plates subject to same complicating effects [90]. This illustrates the versatility and accuracy of the approach to tackle problems with a

29

variety of complicating effects whether in the material properties, boundary conditions or geometry. It has also been demonstrated that the boundary characteristic orthogonal polynomials can be used in other approximate methods such as Galerkin method [91] or Lagrangian multiplier method [92].

Boundary Conditions

The classical boundary conditions include simply supported, clamped or free end conditions. The vast majority of the reported studies in vibration of continuous systems have considered either clamped or free boundary conditions. In the Rayleigh-Ritz method, the trial functions used must satisfy at least the geometric boundary conditions, which are zero displacement and slope for the clamped conditions and zero displacement for simply-support conditions, while no geometrical boundary conditions exist for the free edges. When using the boundary characteristics orthogonal polynomials, only the starting function is selected to satisfy the geometric boundary conditions and all remaining functions are generated using the Gram-Schmidt orthogonaliztion process [84], which ensures that all the orthogonalized functions satisfy the geometric boundary conditions.

However, sometimes it is difficult to have admissible functions that satisfy the geometric boundary conditions. A circular disk clamped at a portion of the edge and free on the remaining or a disk with multiple point supports, are some of such boundary conditions. Therefore, another approach is to allow the admissible function to violate the geometric boundary conditions and then enforce the boundary conditions by using artificial springs. The artificial springs also permit the coupling of the components of

each system and simplifying the selection of trial functions or the Rayleigh-Ritz solution [93]. The principle of artificial springs can be considered as a penalty method [93], which reduces the constrained problem to an unconstrained problem by the introduction of a penalty function associated with the constraint [94]. In this approach, the error associated with the unconstrained problem is multiplied by a very large penalty parameter, which effectively reduces the emphasized error and yields a solution that satisfies the boundary conditions [95].

The approach of employing elastic springs distributed uniformly around the edge has been extensively used in problems related to out-of-plane vibrations of circular plates [96-98] and cylindrical shells [93]. Several studies have also considered the effect of partial supports and stiffness non-uniformity on the out-of-plane vibrations of plates [53-58]. Kim and Dickinson [99] studied the axisymmetrical and non-axisymmetrical vibrations of isotropic and polar orthotropic annular plates with either one or both peripheries elastically restrained against rotation and/or translation using the Rayleigh-Ritz approach.

The advantage of using this method is particularly evident when couplings between two or more elastic components are involved. Moreover, a perfectly clamped condition may not exist in practice. Flexible boundary conditions may, thus, be considered more representative of practical situations or when comparing with the experimental data. Artificial springs can also be used as a connection between different components. A rigid joint between the components can be approximated by inserting artificial springs of large stiffness, while flexible joints may be simulated by assigning the representative stiffness value for the joint [99]. Yuan and Dickenson used this method to

study the free vibration problem of systems comprised of cylindrical thin shells and thin annular circular plates [93]. The cylindrical shell was connected to the plates by means of artificial springs. In this study, the boundary characteristic orthogonal polynomials are employed in the Rayleigh-Ritz method to perform a free in-plane vibration analysis of an annular disk with uniform and non-uniform boundary conditions. Owing to its versatility, artificial springs are used to represent flexible boundary conditions at the edges.

1.3.   Scope and Objectives

Despite the extensive reported studies on the out-of-plane vibration properties of the disks, a comprehensive understanding of the in-plane vibration phenomena and its couplings with the out-of-plane modes is still lacking, particularly under non-uniform boundary conditions. A number of investigations have also tackled the modeling and analysis of in-plane vibrations, although for uniform boundary conditions [e.g. 24, 47]. These models can provide, to some degree, a qualitative insight into the in-plane vibration characteristics of disks. The review of the reported studies suggests that far more research efforts are needed for a better understanding of the in-plane modes of thick circular disks with non-uniform boundary conditions. For instance, the frequency equations for in-plane modes of disks are available only for limited boundary conditions. The effect of elastic constraint or point support on the in-plane modes has not yet been addressed. A flexible model of disk that combines the vibration theory of elastic bodies and the rotational effects is, thus, desirable which would find many applications such as in wheel-rail interactions and brake systems.

The formulation of a simple, yet credible, model that considers the in-plane modes of a rotating wheel would be desirable. Such a model could provide a reliable platform to investigate problems such as in the wheel-rail dynamics and to gain more insight into the vibration and the noise radiation of the railway vehicle. Consequently, an analytical method is developed in this dissertation research, in which a simple comprehensive approach has been put forward for the treatment of disks subject to any or all combinations of several complicating effects and having any combination of classical and non-classical boundary conditions and/or elastic supports.

The primary objective of this study is, thus, to develop a realistic mathematical model to analyze vibration characteristics of circular disks with different boundary conditions. The model is developed to accommodate various classical and non-classical boundary conditions and external excitations that may exist in many applications. The following are the specific objectives of this study:

1. To develop a generalized formulation for in-plane vibration analysis of circular annular disks under different combinations of clamped, free or flexible boundary conditions at the inner and outer edges, and derive exact frequency equations for different combinations of boundary conditions.

2. To employ the boundary characteristic orthogonal polynomials as assumed deflection functions in the Rayleigh-Ritz method in order to obtain the natural frequencies and associated mode shapes under different geometries and combinations of boundary conditions.

3. To investigate the in-plane modes of vibrations, and identify the bifurcation of frequencies, the effects of initial stress and constraint non-uniformity of rotating disks.

4. To conduct laboratory experiments on stationary and rotating circular disks under selected boundary conditions and demonstrate the validity of the analytical methods in terms of vibration and acoustic emission properties.

5. To develop an analytical model of a thick disk to evaluate its acoustic properties associated with the in-plane and out-of-plane noise radiation under free and constrained conditions, and study the coupling between the in-plane and out-of-plane vibration modes.

6. Investigate the coupled in-plane and out-of-plane modes of vibration of a thick disk in the presence of constraint non-uniformity and rotation effects using a three-dimensional model.

1.4. *Organization of the Thesis*

This dissertation is organized into seven chapters describing systematic developments in realizing the above objectives. In chapter 2, the derivation of the energy expressions is presented in polar coordinates. The corresponding equations of motion are also derived and discussed. The equations of motion are solved to obtain the exact frequency equations for the uniform boundary conditions, including flexible uniform edges. The Rayleigh-Ritz method is, then, utilized to solve the problem of in-plane vibration of circular and annular disks subject to uniform and non-uniform boundary conditions. The strain energy expressions for in the artificial springs are derived. The

model for the vibrations of rotating disks is derived based on the assumption of linear elasticity, while the effect of additional stiffening is investigated by employing nonlinear strain-displacement relation of annular disks subject to non-uniform boundary conditions. This is followed by the formulation for the in-plane acoustic properties of the circular disk.

Chapter 3 is dedicated to explore the free vibrations of stationary disks with uniform boundary conditions. The frequency parameters obtained from exact solutions are used as reference to examine the convergence property of the Rayleigh-Ritz method. The analytical results are used in a parametric study to investigate the effect of several geometric properties on the modal characteristics of annular disks. The mode shapes of disks with selected uniform boundary conditions are presented and compared with previous literature.

Chapter 4 considers the in-plane free vibrations of stationary disks with non-uniform boundary conditions. The chapter starts with a description of the finite element model and experimental setup used to validate the analytical results. Then, the convergence rate of the Rayleigh-Ritz method for problems with non-uniform boundary conditions is discussed. The frequency parameters are, then, presented for various combinations of classical and non-uniform boundary conditions. The results obtained by the current procedure are validated against the finite element results. Two-dimensional contour plots are presented for selected mode shapes to investigate the effect of the constraints on the radial and circumferential displacements. The experimental results are presented and compared with analytical results. The vibration and acoustic properties of an annular disk subject to different combinations of boundary conditions are discussed.

The focus of chapter 5 is on the analysis of in-plane vibrations of rotating disks. The rotational effects on annular disks subject to uniform boundary conditions are discussed based on the linear analysis. The variations of the travelling waves are presented with respect to rotating and fixed coordinates. Then, a rotating point-supported disk is employed to investigate the combined effect of rotation and boundary condition non-uniformity on the modal characteristics of the disk. The initial stiffening due to rotation is, then, introduced by developing a non-linear model that permits the coupling between static and dynamic problems. The general non-linear problem of an annular disk subject to non-uniform boundary conditions is investigated. Finally, the results from the experimental investigations are described.

In chapter 6, a thick disk model is proposed where the constrained and rotational effects are addressed in the context of a coupled three-dimensional model. The essential energy expressions for thick disks are derived to allow consideration of multiple disks connected by artificial spring and non-uniform point, line or area support that has variations along circumferential and normal directions. Expressions to estimate the acoustic properties from the in-plane and out-of-plane modes are also presented. The applicability of the model is demonstrated by relating it to a railway wheel while comparison with measured railway wheel data is performed to illustrate the accuracy and versatility of the developed model.

The highlights and major conclusions drawn from this study together with recommendations for the future work are finally presented in chapter 7.

2. IN-PLANE FREE VIBRATION OF ANNULAR DISKS

The out-of-plane vibration properties of circular disks have been extensively investigated under a range geometries and boundary conditions, while only limited efforts have been made to characterize the in-plane vibration characteristics. The in-plane vibration of circular disks was first attempted by Love [13] who formulated the equations of motion for a thin solid circular disk with free outer edge together with the general solution. The equations of motion were subsequently solved by Onoe [14] to obtain the exact frequency equations corresponding to different modes of a solid disk with free outer edge. Holland [15] evaluated the frequency parameters and the corresponding mode shapes for a wide range of Poisson's ratios and the vibration response to an in-plane force. The in-plane vibration characteristics of solid disks clamped at the outer edge have been investigated in a very few recent studies. Farag and Pan [16] evaluated the frequency parameters and the mode shapes of in-plane vibration of solid disks clamped at the outer edge using assumed deflection modes in terms of trigonometric and Bessel functions. Park [17] derived the exact frequency equation for the solid disk clamped at the outer edge.

The in-plane vibration analyses in the above reported studies were limited to solid disks with either free or clamped outer edge. Such analyses for the annular disks with different boundary conditions have been limited to a few studies. The variations in the in-plane vibration frequency parameters of annular disks with free edges were investigated as function of the size of the opening by Ambati et al. [18]. Another study investigated the free vibration and dynamic response characteristics of an annular disk with clamped

inner boundary and a concentrated radial force applied at the outer boundary [19]. Irie et al. [20] investigated the modal characteristics of in-plane vibration of annular disks using transfer matrix formulation while considering free and clamped inner and outer edges. The finite element technique has also been used to examine the validity of analytical methods [e.g. 16, 19]. The exact frequency equations of in-plane vibration, however, have been limited only to solid disks. Such analyses for the annular disks pose more complexities due to the presence of different combinations of boundary conditions at the inner and outer edges.

This chapter aims at generalized formulation for in-plane vibration analyses of circular annular disks under different combinations of clamped, free or flexible boundary conditions at the inner and outer edges. The primary objective of this chapter is to investigate the in-plane modal characteristics of circular and annular disks subject to general boundary conditions with relative ease and acceptable accuracy. Starting from the constitutive laws and stress-strain relations, the integral expressions for strain and kinetic energies of the disk are presented in the polar coordinates. The energy expressions are subsequently solved to determine the natural frequencies and mode shapes of annular disks. The exact frequency equations are also derived for different combinations of boundary conditions, including the flexible boundaries, for various radius ratios, while the solid disk is considered as a special case of the generalized formulation.

Moreover, the Rayleigh-Ritz method is employed to derive the eigenvalue equations. The circumferential displacement components are expressed in terms of trigonometric functions and boundary-characteristic orthogonal polynomials in the radial direction. Orthogonal polynomials are generated for the free boundary conditions of the

disk and artificial springs are used to account for any possible boundary conditions. The clamped boundary case is also analyzed with orthogonal polynomials that directly satisfy the clamped boundary conditions. The accuracy of the eigenvalues is ascertained through comparisons with the results reported in the published studies.

2.1. Equations of Motion of an Annular Circular Disk

Consider an annular disk with outer radius R_o, inner radius R_i and thickness h, as shown in Figure 2.1. It is assumed that the disk is isotropic with mass density ρ, Young's modulus E and Poisson's ratio v. The radial and circumferential displacement components of a point in the plane of the annular disk are denoted by u_r and u_θ , respectively. The expression for the strain energy of the disk in polar coordinates (r,θ) is derived from the constitutive laws and strain-displacement relations. The strain energy in polar coordinate (r,θ) can be written as:

$$\mathbb{U} = \frac{1}{2} \int_{R_i}^{R_o} \int_0^{2\pi} (\sigma_r \varepsilon_r + \sigma_\theta \varepsilon_\theta + 2\sigma_{r\theta} \varepsilon_{r\theta})\, r\, dr\, d\theta \qquad (2.1)$$

where $\mathbb{U}$ is the strain energy. In the above formulation, small strains are assumed and the Hooke's law is employed to express stress-strain relationship. For a flat disk, the plane stress conditions may be expressed by the following relations:

$$\sigma_r = \frac{E}{1-v^2}\left(\varepsilon_r + v\varepsilon_\theta\right)$$

$$\sigma_\theta = \frac{E}{1-v^2}\left(\varepsilon_\theta + v\varepsilon_r\right) \qquad (2.2)$$

$$\sigma_{r\theta} = \frac{E}{1+v}\varepsilon_{r\theta}$$

Substituting Eq. (2.2) into the strain energy expression (2.1) leads to:
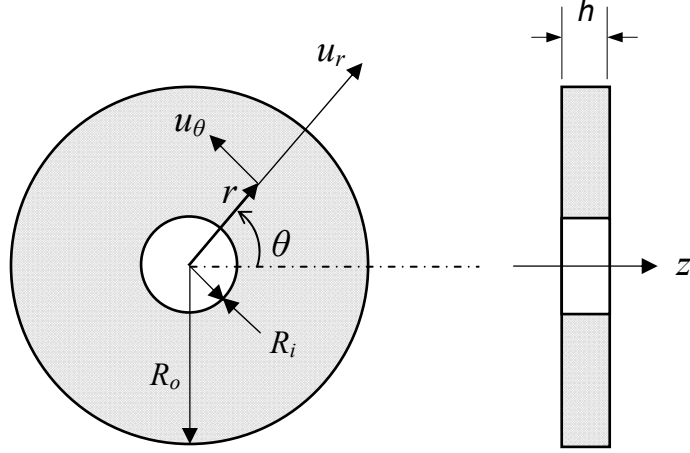
Figure 2.1: Geometry and coordinate system used for in-plane vibration analysis of an annular disk.

$$\mathbb{U} = \frac{1}{2} \int_{R_i}^{R_o} \int_0^{2\pi} \frac{E}{1-v^2} \left(\varepsilon_r^2 + 2v\varepsilon_r\varepsilon_\theta + \varepsilon_\theta^2 + 2(1-v)\varepsilon_{r\theta}^2 \right) r \, dr \, d\theta \qquad (2.3)$$

For small deformations, the strain-displacement relations are written as:

$$\varepsilon_r = \frac{\partial u_r}{\partial r}$$

$$\varepsilon_\theta = \frac{1}{r}\left(u_r + \frac{\partial u_\theta}{\partial \theta} \right) \qquad (2.4)$$

$$\varepsilon_{r\theta} = \frac{1}{2}\left(\frac{1}{r}\frac{\partial u_r}{\partial \theta} + \frac{\partial u_\theta}{\partial r} - \frac{u_\theta}{r} \right)$$

By substituting the strain-displacement relations into Eq.(2.3) and introducing the non-dimensional parameter $\xi = r/R_o$, the strain energy is expressed in terms of the displacements as:

$$\mathbb{U} = \frac{1}{2}\frac{Eh}{1-v^2} \int_0^{2\pi} \int_\beta^1 \left\{ \left(\frac{\partial u_r}{\partial \xi}\right)^2 + 2v\left(\frac{u_r}{\xi}\frac{\partial u_r}{\partial \xi} + \frac{1}{\xi}\frac{\partial u_\theta}{\partial \theta}\frac{\partial u_r}{\partial \xi}\right) + \left(\frac{u_r}{\xi}\right)^2 + 2\frac{u_r}{\xi^2}\frac{\partial u_\theta}{\partial \theta} \right. $$
$$\left. + \frac{1}{\xi^2}\left(\frac{\partial u_\theta}{\partial \theta}\right)^2 + \frac{1}{2}(1-v)\left(\frac{1}{\xi}\frac{\partial u_r}{\partial \theta} + \frac{\partial u_\theta}{\partial \xi} - \frac{u_\theta}{\xi}\right)^2 \right\} \xi d\xi d\theta \qquad (2.5)$$

where $\beta = R_i/R_o$ is the ratio of inner radius R_i to the outer radius R_o.

The kinetic energy of the disk can be expressed as:

$$T = \frac{1}{2}h\rho R_0^2 \int\limits_0^{2\pi} \int\limits_\beta^1 (\dot{u}_r^2 + \dot{u}_\theta^2)\xi d\xi d\theta \tag{2.6}$$

where T is the kinetic energy, and $\dot{u}_r$ and $\dot{u}_\theta$ are the time-derivatives of the radial and circumferential displacements, respectively.

2.1.1. Equations of Motion

The Hamilton's principle is applied to derive the equations of motion from the energy expressions, such that:

$$\delta \int\limits_{t_0}^{t_1} (T - \mathbb{U})dt = 0 \tag{2.7}$$

Performing the variations with respect to time and space results in expressions in terms of δu_r and δu_θ. Requiring the coefficient of each variation to vanish over the domain will yield the equations of motion. These equations of motion in the polar coordinate system (r,θ) are derived as:

$$\begin{aligned}
&\frac{\partial^2 u_r}{\partial t^2} - C_L^2\left[\frac{\partial^2 u_r}{\partial r^2} + \frac{1}{r}\frac{\partial u_r}{\partial r} - \frac{u_r}{r^2}\right] - \frac{C_T^2}{r^2}\frac{\partial^2 u_r}{\partial \theta^2} - C_T^2\frac{1}{r}\frac{1+v}{1-v}\frac{\partial^2 u_\theta}{\partial r\partial \theta} \\
&+ C_T^2\frac{1}{r^2}\frac{3-v}{1-v}\frac{\partial u_\theta}{\partial \theta} = 0
\end{aligned} \tag{2.8}$$

$$\begin{aligned}
&\frac{\partial^2 u_\theta}{\partial t^2} - C_T^2\left[\frac{\partial^2 u_\theta}{\partial r^2} + \frac{1}{r}\frac{\partial u_\theta}{\partial r} - \frac{u_\theta}{r^2}\right] - \frac{C_L^2}{r^2}\frac{\partial^2 u_\theta}{\partial \theta^2} - C_T^2\frac{1}{r}\frac{1+v}{1-v}\frac{\partial^2 u_r}{\partial r\partial \theta} \\
&+ C_T^2\frac{1}{r^2}\frac{3-v}{1-v}\frac{\partial u_r}{\partial \theta} = 0
\end{aligned} \tag{2.9}$$

where $C_L^2 = E/\rho(1 - v^2)$ and $C_T^2 = E/2\rho(1 + v)$.

2.2.   *Exact Frequency Equations*

Considering that the exact solutions could serve as a benchmark for all other approximate and numerical techniques, it is desirable to formulate exact frequency equations to study the in-plane vibration properties of the disk with different boundary conditions. The equations of motion, Eqs. (2.8) and (2.9), however, show strong coupling between the radial and circumferential displacements. The exact solution can be obtained for limited cases by defining variables that could produce uncoupled equations in one of the classical forms. In this section, the equations of motion are solved to obtain the exact frequency equations for the uniform boundary conditions, including flexible uniform edges. The frequency equations are subsequently used to assess the accuracy of the Rayleigh-Ritz method.

Following Love's theory [13], the radial and circumferential displacements can be expressed in terms of the Lamé Potentials $\bar{\phi}$ and $\bar{\psi}$ [100], as:

$$u_r = \left(\frac{\partial \bar{\phi}}{\partial \xi} + \frac{1}{\xi}\frac{\partial \bar{\psi}}{\partial \theta}\right)\frac{1}{R_o} \qquad (2.10)$$

$$u_\theta = \left(\frac{1}{\xi}\frac{\partial \bar{\phi}}{\partial \theta} - \frac{\partial \bar{\psi}}{\partial \xi}\right)\frac{1}{R_o} \qquad (2.11)$$

Assuming harmonic oscillations corresponding to a natural frequency ω, the potential functions $\bar{\phi}$ and $\bar{\psi}$ can be represented by:

$$\bar{\phi}(\xi, \theta, t) = \Phi(\xi)\cos n\theta \sin \omega t$$

$$\bar{\psi}(\xi, \theta, t) = \Psi(\xi)\sin n\theta \sin \omega t \qquad (2.12)$$

where *n* is the circumferential wave number or nodal diameter number. Upon substituting for u_r and u_θ in terms of ξ, Φ and Ψ from Eqs. (2.10) to (2.12), in Eqs. (2.8) and (2.9), the equations of motion reduce to the following uncoupled form:

42

$$\nabla^2 \Phi = -\lambda_1^2 \Phi$$
$$\nabla^2 \Psi = -\lambda_2^2 \Psi$$

(2.13)

where λ_1 and λ_2 are non-dimensional frequency parameters defined as

$$\lambda_1^2 = \frac{\omega^2(1-v^2)\rho R_o^2}{E}, \qquad \lambda_2^2 = \frac{2\omega^2(1+v)\rho R_o^2}{E}$$

(2.14)

and

$$\nabla^2 = \frac{\partial^2}{\partial \xi^2} + \frac{1}{\xi}\frac{\partial}{\partial \xi} - \frac{n^2}{\xi^2}$$

(2.15)

Equation (2.13) is the parametric Bessel equations and their general solutions are

expressed in terms of the Bessel functions as [101]:

$$\Phi = \{A_n J_n(\lambda_1 \xi) + B_n Y_n(\lambda_1 \xi)\}$$
$$\Psi = \{C_n J_n(\lambda_2 \xi) + D_n Y_n(\lambda_2 \xi)\}$$

(2.16)

where J_n and Y_n are the Bessel functions of the first and second kind of order n,

respectively, and A_n, B_n, C_n and D_n are the deflection coefficients.

The radial and circumferential displacements can then be expressed in terms of

the Bessel functions by substituting for Φ and Ψ in Eqs. (2.10) and (2.11). The resulting

expressions for the radial and circumferential displacements can be expressed as:

$$u_r = \frac{1}{R_o}\Big\{A_n X_n(\lambda_1 \xi) + B_n Z_n(\lambda_1 \xi)$$
$$+ \frac{n}{\xi}[C_n J_n(\lambda_2 \xi) + D_n Y_n(\lambda_2 \xi)]\Big\}\cos n\theta \sin \omega t$$

(2.17)

$$u_\theta = -\frac{1}{R_o}\Big\{C_n X_n(\lambda_2 \xi) + D_n Z_n(\lambda_2 \xi)$$
$$+ \frac{n}{\xi}[A_n J_n(\lambda_1 \xi) + B_n Y_n(\lambda_1 \xi)]\Big\}\sin n\theta \sin \omega t$$

(2.18)

where

$$X_n(\lambda_i \xi) = \frac{\partial}{\partial \xi}J_n(\lambda_i \xi) = -\frac{n}{\xi}J_n(\lambda_i \xi) + \lambda_i J_{n-1}(\lambda_i \xi),$$

$$Z_n(\lambda_i \xi) = \frac{\partial}{\partial \xi}Y_n(\lambda_i \xi) = \left(-\frac{n}{\xi}Y_n(\lambda_i \xi) + \lambda_i Y_{n-1}(\lambda_i \xi)\right) \text{ and } i = 1,2$$

(2.19)

43

2.2.1. Free and Clamped Boundary Conditions

Equations (2.17) and (2.18) represent the solutions for distributions of the radial and circumferential displacements for the general case of an annular disk. The evaluations of the natural frequencies and arbitrary deflection coefficients (A_n, B_n, C_n and D_n), however, necessitate the consideration of the in-plane free vibration response under different combinations of boundary conditions at the inner and the outer edges. For the annular disk clamped at the outer edge ($\xi = 1$), the application of boundary conditions ($u_r = 0$ and $u_\theta = 0$) to, Eqs. (2.17) and (2.18) yield:

$$A_n X_n(\lambda_1) + B_n Z_n(\lambda_1) + n[C_n J_n(\lambda_2) + D_n Y_n(\lambda_2)] = 0$$

$$C_n X_n(\lambda_2) + D_n Z_n(\lambda_2) + n[A_n J_n(\lambda_1) + B_n Y_n(\lambda_1)] = 0$$

$$(2.20)$$

In a similar manner, the solution must satisfy the following for the clamped inner edge ($\xi = \beta$):

$$A_n X_n(\lambda_1\beta) + B_n Z_n(\lambda_1\beta) + \frac{n}{\beta}[C_n J_n(\lambda_2\beta) + D_n Y_n(\lambda_2\beta)] = 0$$

$$C_n X_n(\lambda_2\beta) + D_n Z_n(\lambda_2\beta) + \frac{n}{\beta}[A_n J_n(\lambda_1\beta) + B_n Y_n(\lambda_1\beta)] = 0$$

$$(2.21)$$

The conditions at the free edges are satisfied when the radial (N_r) and circumferential ($N_{r\theta}$) in-plane forces at the edge are zero [16], such that

$$N_r = \frac{-Eh}{(1-v^2)R_o}\left[\frac{\partial u_r}{\partial \xi} + \frac{v}{\xi}\frac{\partial u_\theta}{\partial \theta} + \frac{v}{\xi}u_r\right] = 0$$

$$N_{r\theta} = \frac{-Eh}{2(1+v)R_o}\left[\frac{1}{\xi}\frac{\partial u_r}{\partial \theta} + \frac{\partial u_\theta}{\partial \xi} - \frac{u_\theta}{\xi}\right] = 0$$

$$(2.22)$$

A direct Substitution of u_r and u_θ from Eqs. (2.17) and (2.18) in the above equations would result in second derivatives of the Bessel functions. Alternatively, the above equation for the boundary conditions may be expressed in terms of Φ and Ψ

44

through direct substitution of u_r and u_θ from Eqs. (2.10) and (2.11), respectively. The boundary conditions in terms of N_r can thus be obtained as:

$$\left(\frac{\partial^2 \Phi}{\partial \xi^2} + \frac{n}{\xi}\frac{\partial \Psi}{\partial \xi} - \frac{n}{\xi^2}\Psi\right) - \frac{n^2 v}{\xi^2}\Phi - \frac{nv}{\xi}\frac{\partial \Psi}{\partial \xi} + \frac{v}{\xi}\left(\frac{\partial \Phi}{\partial \xi} + \frac{n}{\xi}\Psi\right) = 0 \qquad (2.23)$$

Rearranging Eq. (2.23) results in

$$\left(\frac{\partial^2}{\partial \xi^2} + \frac{v}{\xi}\frac{\partial}{\partial \xi} - \frac{n^2 v}{\xi^2}\right)\Phi + (1-v)\left(\frac{n}{\xi}\frac{\partial}{\partial \xi} - \frac{n}{\xi^2}\right)\Psi = 0 \qquad (2.24)$$

The second order derivative term $(\partial^2 \Phi / \partial \xi^2)$ in Eq. (2.24) can be eliminated by

adding and subtracting the term $\left(\frac{1}{\xi}\frac{\partial}{\partial \xi} - \frac{n^2}{\xi^2} + \lambda_1^2\right)\Phi$, which yields:

$$\left[\left(\frac{\partial^2}{\partial \xi^2} + \frac{1}{\xi}\frac{\partial}{\partial \xi} - \frac{n^2}{\xi^2} + \lambda_1^2\right) - \left(\frac{1}{\xi}\frac{\partial}{\partial \xi} - \frac{n^2}{\xi^2} + \lambda_1^2\right) + \frac{v}{\xi}\frac{\partial}{\partial \xi} - \frac{n^2 v}{\xi^2}\right]\Phi$$
$$+ (1-v)\left(\frac{n}{\xi}\frac{\partial}{\partial \xi} - \frac{n}{\xi^2}\right)\Psi = 0 \qquad (2.25)$$

and using Eq. (2.13), which renders the terms within the first parenthesis identically equal to zero. Equation (2.25) describing the boundary condition associated with N_r can be further simplified upon substitutions for $\lambda_1^2 = \lambda_2^2 (1-v)/2$, which yields

$$\left(\frac{n^2}{\xi^2} - \frac{1}{\xi}\frac{\partial}{\partial \xi} - \frac{1}{2}\lambda_2^2\right)\Phi + n\left(\frac{1}{\xi}\frac{\partial}{\partial \xi} - \frac{1}{\xi^2}\right)\Psi = 0 \qquad (2.26)$$

Similarly, the boundary condition equation associated with $N_{r\theta}$, Eq.(2.22), can be simplified as:

$$\frac{2n}{\xi}\left(-\frac{\partial}{\partial \xi} + \frac{1}{\xi}\right)\Phi + \left(\frac{2}{\xi}\frac{\partial}{\partial \xi} - \frac{2n^2}{\xi^2} + \lambda_2^2\right)\Psi = 0 \qquad (2.27)$$

Upon substituting for Φ and Ψ from Eqs. (2.16) in Eqs. (2.26) and (2.27), the boundary condition equations for the free edges are obtained, which involve only first derivatives of the Bessel functions. For an annular disk with free inner and outer edges,

45

Eqs. (2.26) and (2.27) represent the conditions at both the inner and the outer boundaries ($\xi = 1$ and $\xi = \beta$). The equations for the free edge boundary conditions can be expressed in the matrix form in the four deflection coefficients, as:

$$
\begin{bmatrix}
\left(n^2 - \frac{\lambda_2^2}{2}\right)J_n(\lambda_1) - X_n(\lambda_1) & \left(n^2 - \frac{\lambda_2^2}{2}\right)Y_n(\lambda_1) - Z_n(\lambda_1) \\
2nJ_n(\lambda_1) - 2nX_n(\lambda_1) & 2nY_n(\lambda_1) - 2nZ_n(\lambda_1) \\
\left(\frac{n^2}{\beta^2} - \frac{\lambda_2^2}{2}\right)J_n(\lambda_1\beta) - \frac{1}{\beta}X_n(\lambda_1\beta) & \left(\frac{n^2}{\beta^2} - \frac{\lambda_2^2}{2}\right)Y_n(\lambda_1\beta) - \frac{1}{\beta}Z_n(\lambda_1\beta) \\
\frac{2n}{\beta^2}J_n(\lambda_1\beta) - \frac{2n}{\beta}X_n(\lambda_1\beta) & \frac{2n}{\beta^2}Y_n(\lambda_1\beta) - \frac{2n}{\beta}Z_n(\lambda_1\beta)
\end{bmatrix}
$$

$$
\left.
\begin{matrix}
nX_n(\lambda_2) - nJ_n(\lambda_2) & nZ_n(\lambda_2) - nY_n(\lambda_2) \\
2X_n(\lambda_2) - (2n^2 - \lambda_2^2)J_n(\lambda_2) & 2Z_n(\lambda_2) - (2n^2 - \lambda_2^2)Y_n(\lambda_2) \\
\frac{n}{\beta}X_n(\lambda_2\beta) - \frac{n}{\beta^2}J_n(\lambda_2\beta) & \frac{n}{\beta}Z_n(\lambda_2\beta) - \frac{n}{\beta^2}Y_n(\lambda_2\beta) \\
\frac{2}{\beta}X_n(\lambda_2\beta) - \left(\frac{2n^2}{\beta^2} - \lambda_2^2\right)J_n(\lambda_2\beta) & \frac{2}{\beta}Z_n(\lambda_2\beta) - \left(\frac{2n^2}{\beta^2} - \lambda_2^2\right)Y_n(\lambda_2\beta)
\end{matrix}
\right]
\begin{Bmatrix}
A_n \\ B_n \\ C_n \\ D_n
\end{Bmatrix} = \{0\}
$$

(2.28)

The determinant of the above matrix yields the frequency equation for the annular disk with free inner and outer edge conditions.

For the clamped inner and outer edges, the equations for the boundary conditions can be obtained directly from Eqs. (2.20) and (2.21), such that

$$
\begin{bmatrix}
X_n(\lambda_1) & Z_n(\lambda_1) & nJ_n(\lambda_2) & nY_n(\lambda_2) \\
nJ_n(\lambda_1) & nY_n(\lambda_1) & X_n(\lambda_2) & Z_n(\lambda_2) \\
X_n(\lambda_1\beta) & Z_n(\lambda_1\beta) & \frac{n}{\beta}J_n(\lambda_2\beta) & \frac{n}{\beta}Y_n(\lambda_2\beta) \\
\frac{n}{\beta}J_n(\lambda_1\beta) & \frac{n}{\beta}Y_n(\lambda_1\beta) & X_n(\lambda_2\beta) & Z_n(\lambda_2\beta)
\end{bmatrix}
\begin{Bmatrix}
A_n \\ B_n \\ C_n \\ D_n
\end{Bmatrix} = \{0\}
\qquad (2.29)
$$

In the above equations, the first two rows describe the boundary condition at the outer edge, while the last two rows are associated with those at the inner edge. The equations for the boundary conditions involving combinations of free and clamped edges can thus be directly obtained from the above two equations. For the free inner edge and clamped outer edge, denoted as 'free-clamped' condition, the matrix equation comprises the first two rows of the matrix in Eq.(2.29) and the lower two rows from Eq.(2.28). For

46

the clamped inner edge and free outer edge, denoted as 'Clamped-Free' condition, the matrix equation is formulated in a similar manner using the lower and upper two rows from Eqs. (2.29) and (2.28), respectively.

The in-plane vibration analysis of a solid disk can be shown as a special case of the above generalized formulations. Upon eliminating the coefficients associated with Bessel function of the second kind, Eqs. (2.28) and (2.29) reduce to those reported by Onoe [14] for free solid disk and by Park [17] for the clamped solid disk. The frequency equation corresponding to different values of n for the solid disks involving the two boundary conditions are summarized in Table 2.1, where $X_n(\lambda_1)$ is the derivative of the Bessel function J_n evaluated at the outer edge ($\xi = 1$). For annular disks, a simplified frequency eqautaions can be obtained for the axisymmetric modes. These equations are expressed in Table 2.2 for the four combinations of boundary conditions.

Table 2.1: Frequency equations for the solid disks corresponding to free and clamped edge conditions.

Boundary conditions at $\xi = 1$		clamped	Free
$n=0$	Radial	$J_1(\lambda_1)=0$	$\lambda_1 J_0(\lambda_1) = (1 - v)J_1(\lambda_1)$
	Circumferential	$J_1(\lambda_2)=0$	$\lambda_2 J_0(\lambda_2) = 2J_1(\lambda_2)$
$n=1$		$X_n(\lambda_1)X_n(\lambda_2) = n^2 J_n(\lambda_1)J_n(\lambda_2)$	$[X_1(\lambda_2)J_1(\lambda_1)] + [X_1(\lambda_1)J_1(\lambda_2)] = \left(2 - \frac{\lambda_2^2}{2}\right)J_1(\lambda_2)J_1(\lambda_1)$
$n>1$			$[X_n(\lambda_2) - QJ_n(\lambda_2)][X_n(\lambda_1) - QJ_n(\lambda_1)] = n^2(Q - 1)^2$ where $Q = \lambda_2^2/2(n^2 - 1)$

Table 2.2: Frequency equations of axisymmetric modes for annular disks

Boundary conditions		radial	Circumferential
inner	outer		
Clamped	Clamped	$J_1(\lambda_1)Y_1(\lambda_1\beta) - J_1(\lambda_1\beta)Y_1(\lambda_1) = 0$	$J_1(\lambda_2)Y_1(\lambda_2\beta) - J_1(\lambda_2\beta)Y_1(\lambda_2) = 0$
Free	Free	$\left[\left(-\frac{\lambda_1}{(1-v)}\right)J_0(\lambda_1) + J_1(\lambda_1)\right]\left[\left(-\frac{\lambda_1}{(1-v)}\right)Y_0(\lambda_1\beta)\right.$ $\left. + \frac{1}{\beta}Y_1(\lambda_1\beta)\right] - \left[\frac{-\lambda_1}{(1-v)}Y_0(\lambda_1)\right.$ $\left. + Y_1(\lambda_1)\right]\left[\left(-\frac{\lambda_1}{(1-v)}\right)J_0(\lambda_1\beta)\right.$ $\left. + \frac{1}{\beta}J_1(\lambda_1\beta)\right] = 0$	$\left[-2J_1(\lambda_2) + \lambda_2 J_0(\lambda_2)\right]\left[-\frac{2}{\beta}Y_1(\lambda_2\beta)\right.$ $\left. + \lambda_2 Y_0(\lambda_2\beta)\right]$ $- \left[-\frac{2}{\beta}J_1(\lambda_2\beta)\right.$ $\left. + \lambda_2 J_0(\lambda_2\beta)\right]\left[-2\,Y_1(\lambda_2)\right.$ $\left. + \lambda_2 Y_0(\lambda_2)\right] = 0$
Clamped	Free	$\left[\left(\frac{\lambda_1}{(1-v)}\right)J_0(\lambda_1) - J_1(\lambda_1)\right]Y_1(\lambda_1\beta)$ $- J_1(\lambda_1\beta)\left[\left(\frac{\lambda_1}{(1-v)}\right)Y_0(\lambda_1)\right.$ $\left. - Y_1(\lambda_1)\right] = 0$	$[2J_1(\lambda_2) - \lambda_2 J_0(\lambda_2)]Y_1(\lambda_2\beta)$ $- J_1(\lambda_2\beta)[2\,Y_1(\lambda_2)$ $- \lambda_2 Y_0(\lambda_2)] = 0$
Free	Clamped	$J_1(\lambda_1)\left[\left(-\frac{\lambda_1}{(1-v)}\right)Y_0(\lambda_1\beta) + \frac{1}{\beta}Y_1(\lambda_1\beta)\right]$ $+ \left[\left(-\frac{\lambda_1}{(1-v)}\right)J_0(\lambda_1\beta)\right.$ $\left. + \frac{1}{\beta}J_1(\lambda_1\beta)\right]Y_1(\lambda_1) = 0$	$J_1(\lambda_2)\left[-\frac{2}{\beta}Y_1(\lambda_2\beta) + \lambda_2 Y_0(\lambda_2\beta)\right]$ $- \left[-\frac{2}{\beta}J_1(\lambda_2\beta)\right.$ $\left. + \lambda_2 J_0(\lambda_2\beta)\right]Y_1(\lambda_2) = 0$

2.2.2. Flexible Boundary Conditions

In the above formulations, the boundary conditions considered are either clamped or free. However, flexible boundary conditions may be considered more representative of many practical situations. The proposed formulations can be further employed to study the in-plane vibration of solid as well as annular disks with flexible boundary conditions. Artificial springs may be applied to describe the flexible boundary conditions at the inner or the outer edge of an annular disk. A number of studies on the analysis of out-of-plane vibration characteristics of circular plates and cylindrical shells have employed uniformly distributed artificial springs around the edge to represent a flexible boundary conditions or a flexible joint [96-99].

Artificial springs, distributed along the radial and circumferential directions at the free outer and/or inner edges, were considered to simulate the flexible boundary conditions, as shown in Figure 2.2. The exact solution of the frequency equations for the disk with flexible supports can be attained from Eqs. (2.17) and (2.18) together with the consideration of the flexible boundary conditions. The conditions involving flexible edge supports at the inner and outer edges are satisfied when the radial (N_r) and circumferential ($N_{r\theta}$) in-plane forces at the edges are equal to the respective radial and circumferential spring forces, such that

$$N_r = \frac{-Eh}{(1-v^2)R_o}\left[\frac{\partial u_r}{\partial \xi} + \frac{v}{\xi}\frac{\partial u_\theta}{\partial \theta} + \frac{v}{\xi}u_r\right] = K_r u_r(\xi,\theta) \tag{2.30}$$

$$N_{r\theta} = \frac{-Eh}{2(1+v)R_o}\left[\frac{1}{\xi}\frac{\partial u_r}{\partial \theta} + \frac{\partial u_\theta}{\partial \xi} - \frac{u_\theta}{\xi}\right] = K_\theta u_\theta(\xi,\theta) \tag{2.31}$$

where K_r and K_θ are the radial and circumferential stiffness coefficients, respectively. Introducing the non-dimensional stiffness parameters, $\bar{K}_r = K_r R_o(1-v^2)/Eh$ and $\bar{K}_\theta = K_\theta R_o(1+v)/Eh$, Eqs. (2.30) and (2.31) can be written as

$$\left(\frac{n^2}{\xi^2} - \frac{1}{\xi}\frac{\partial}{\partial \xi} - \frac{1}{2}\lambda_2^2 + \bar{K}_r\frac{\partial}{\partial \xi}\right)\Phi + n\left(\frac{1}{\xi}\frac{\partial}{\partial \xi} - \frac{1}{\xi^2} + \frac{1}{\xi}\bar{K}_r\right)\Psi = 0 \tag{2.32}$$

$$n\left(\frac{1}{\xi}\frac{\partial}{\partial \xi} - \frac{1}{\xi^2} - \frac{1}{\xi}\bar{K}_\theta\right)\Phi + \left(\frac{n^2}{\xi^2} - \frac{1}{\xi}\frac{\partial}{\partial \xi} - \frac{1}{2}\lambda_2^2 - \bar{K}_\theta\frac{\partial}{\partial \xi}\right)\Psi = 0 \tag{2.33}$$

The application of the above conditions yields the matrix equations for the disk with flexible supports at the inner and outer edges, similar to Eq. (2.28). The frequency parameters are subsequently obtained through solution of the matrix equations. The above boundary equations reduce to those in Eqs. (2.26) and (2.27) for the free edge conditions by letting $\bar{K}_r = 0$ and $\bar{K}_\theta = 0$. Furthermore, the clamped edge condition can

49

be represented by considering infinite values of $\overline{K}_r$ and $\overline{K}_\theta$. Equations (2.32) and (2.33) further show that the flexible edge support conditions involve combinations of the free and clamped edge conditions.

2.3.   Analyses Using Rayleigh-Ritz Method

Exact analysis of a vibrating system with several complicating effects is generally difficult. Therefore, several approximate methods have been developed to solve the vibration problems with acceptable and reliable accuracy [83, 88]. The Rayleigh-Ritz method is one of the most popular methods that have been used to obtain the natural frequencies and mode shapes of a wide range of vibration problems. In this section, the Rayleigh-Ritz method is utilized to solve the problem of in-plane vibration of circular and annular disks, described in Eqs. (2.5) and (2.6).

For harmonic vibration with time dependence, the free in-plane vibration response is assumed to have a sinusoidal variation around the disk, and may be expressed in the form:

$$u_r(\xi,\theta,t) = \sum_{n}^{\infty} U_n(\xi)\cos(n\theta)e^{-j\omega t} \tag{2.34}$$

$$u_\theta(\xi,\theta,t) = \sum_{n}^{\infty} V_n(\xi)\sin(n\theta)e^{-j\omega t} \tag{2.35}$$

where U_n and V_n are radial and circumferential deflection functions, respectively. The above assumed solutions are substituted in the energy expression, the energy Eqs. (2.5) and (2.6), which are then integrated with respect to θ (0, 2π), The Integrals of the trigonometric functions are expressed by the relations:

50

$$\int_0^{2\pi} \cos(n\theta)\sin(n'\theta)d\theta = 0$$

$$\int_0^{2\pi} \cos(n\theta)\cos(n'\theta)d\theta = \begin{cases} 0 & for \quad n \neq n' \\ \pi & for \quad n = n' \end{cases}$$

$$\int_0^{2\pi} \sin(n\theta)\sin(n'\theta)d\theta = \begin{cases} 0 & for \quad n \neq n' \\ \pi & for \quad n = n' \end{cases}$$

The substations of the above integrals in the energy expressions yields the following expressions for maximum strain energy, $\mathbb{U}_{max}$, and kinetic energy, T_{max}:

$$\mathbb{U}_{max} = \frac{\pi}{2}\frac{Eh}{1-v^2}\int_\beta^1 \left\{ (U_n')^2 + 2vU_n'\left(\frac{U_n}{\xi} + \frac{nV_n}{\xi}\right) + \left(\frac{U_n}{\xi} + \frac{nV_n}{\xi}\right)^2 \right.$$

$$\left. + \frac{1}{2}(1-v)\left(-\frac{nU_n}{\xi} + V_n' - \frac{V_n}{\xi}\right)^2 \right\}\xi d\xi \qquad (2.36)$$

$$T_{max} = \frac{\pi}{2}\omega^2 h\rho R_0^2 \int_\beta^1 (U_n^2 + V_n^2)\xi d\xi \qquad (2.37)$$

where " ' " represent the derivative with respect to ξ. Employing the condition $\mathbb{U}_{max} = T_{max}$, the Rayleigh's quotient can be written as:

$$\lambda^2 = \frac{\int_\beta^1 \left\{ (U_n')^2 + 2vU_n'\left(\frac{U_n}{\xi} + \frac{nV_n}{\xi}\right) + \left(\frac{U_n}{\xi} + \frac{nV_n}{\xi}\right)^2 + \frac{1}{2}(1-v)\left(-\frac{nU_n}{\xi} + V_n' - \frac{V_n}{\xi}\right)^2 \right\}\xi d\xi}{\int_\beta^1 (U_n^2 + V_n^2)\,\xi d\xi} \qquad (2.38)$$

where $\lambda^2 = \rho\omega^2 R_o^2(1-v^2)\big/E$.

2.3.1. Boundary Characteristic Orthogonal Polynomials

The displacements $U_n(\xi)$ and $V_n(\xi)$ of the circular disks can be expressed as a linear combination of the assumed deflection shapes in the form of the boundary characteristic orthogonal polynomial (BCOP) set $(\phi_1, \phi_2, \ldots.. \phi_n)$, first proposed by Bhat

[84]. A brief discussion about the properties of the boundary characteristic orthogonal polynomials is given here in order to better understand their versatility. The first property of these polynomials is the "Orthogonality", which helps simplifying the analysis and eliminates the problem of matrix ill-conditioning. The definitions of orthogonality can be described as [101, 102]:

Functions $y_1(x)$, $y_2(x)$, ... defined on some interval $a \leq x \leq b$ are called **Orthogonal** with respect to a weight function $p(x) > 0$ if

$$\int_a^b p(x) y_k(x) y_l(x) dx \begin{cases} = 0 & \text{for } k \neq l \\ \neq 0 & \text{for } k = l \end{cases} \qquad (2.39)$$

The norm $\|y_k\|$ of y_k is defined by

$$\|y_k\| = \sqrt{\int_a^b p(x) y_k^2(x) dx} = 0 \qquad (2.40)$$

If a set of functions $y(x)$ are orthogonal and all have norm of unity, they are called orthonormal functions. The orthogonal polynomials are related to each other using the following recurrence formula:

$$y_{k+1}(x) = (x - b_k) y_k(x) - c_k y_{k-1}(x) \qquad \text{for } k = 1,2,3 \ldots \qquad (2.41)$$

where b_k and c_k are constants to be defined and $y_0(x) = 0$. Multiplying both sides of Eq. (2.41) by $p(x) y_k(x)$ and integrating over the interval $a \leq x \leq b$ yields:

$$\int_a^b p(x) y_{k+1}(x) y_k(x) dx = \int_a^b p(x) x y_k^2(x) dx - b_k \int_a^b p(x) y_k^2(x) dx$$
$$- c_k \int_a^b p(x) y_{k-1}(x) y_k(x) dx \qquad (2.42)$$

52

Due to the orthogonal property, the first and last terms in Eq. (2.42) vanish. The coefficients b_k are thus obtained as:

$$b_k = \int_a^b p(x) x y_k^2(x) dx \Bigg/ \int_a^b p(x) y_k^2(x) dx \qquad (2.43)$$

Similarly, multiplying both sides of Eq. (2.41) by $p(x) y_{k-1}(x)$ yields the expression for constant c_k as:

$$c_k = \int_a^b p(x) x y_k(x) y_{k-1}(x) dx \Bigg/ \int_a^b p(x) y_{k-1}^2(x) dx \qquad (2.44)$$

The set of polynomials generated using the above formulations for b_k and c_k maintains the orthogonal properties for the entire set. There are two properties of the BCOP that are useful in the Rayleigh-Ritz method [85]: (*i*) when the value of the first function $y_1(x)$ and its derivatives are equal to zero at x_p in the interval $a \leq x_p \leq b$, then, all the generated polynomials and their derivatives will be identically zero at $x = x_p$; (*ii*) if the first polynomial is symmetrical or anti-symmetrical around an axis, then all the functions will hold the same symmetric or anti-symmetric property around the same axis. These two properties are necessary to ensure that the generated polynomials satisfy the boundary conditions at the edges or at any intermediate positions and preserve the symmetry of the system. The proofs for these properties have been reported in [85] together with detailed descriptions of the BCOP.

In this analysis, the BCOP are used as admissible functions for the variations in the radial displacements, $U_n(\xi)$ and $V_n(\xi)$, with the weighting function $p(\xi) = \xi$. A

starting function $\phi_1(\xi)$ is constructed as the polynomial of the lowest degree that satisfies the geometric boundary conditions, such that:

$$\begin{aligned}\phi_1(\xi) &= (1-\xi^2)^2; \quad \text{for clamped conditions} \\ &= 1 \quad ; \qquad \text{for free conditions}\end{aligned} \tag{2.45}$$

The successive polynomials are generated using the recurrence relation

$$\begin{aligned}\phi_2(\xi) &= (\xi - b_1)\phi_1(\xi), \\ \phi_{k+1}(\xi) &= (\xi - b_k)\phi_k(\xi) - c_k\phi_{k-1}(\xi), \quad k \geq 2,\end{aligned} \tag{2.46}$$

where

$$\begin{aligned}b_k &= \int_\beta^1 \xi^2 \phi_k^2(\xi)d\xi \bigg/ \int_0^1 \xi\,\phi_k^2(\xi)d\xi, \quad k \geq 1 \\ c_k &= \int_\beta^1 \xi^2 \phi_k(\xi)\phi_{k-1}(\xi)d\xi \bigg/ \int_0^1 \xi\,\phi_{k-1}^2(\xi)d\xi, \quad k \geq 2\end{aligned} \tag{2.47}$$

The displacement responses are subsequently derived from:

$$U_n(\xi) = \sum_m \bar{U}_{mn}\phi(\xi) \tag{2.48}$$

$$V_n(\xi) = \sum_m \bar{V}_{mn}\phi(\xi) \tag{2.49}$$

Substituting Eqs. (2.48) and (2.49) into Eq. (2.38) and applying the condition of stationarity of λ^2 with respect to the arbitrary coefficients $\bar{U}_{mn}$ and $\bar{V}_{mn}$:

$$\begin{aligned}\frac{\partial \lambda^2}{\partial \bar{U}_{mn}} &= 0 \\ \frac{\partial \lambda^2}{\partial \bar{V}_{mn}} &= 0\end{aligned} \tag{2.50}$$

results in the eigenvalue problem:

$$\left([K] - \lambda^2 [M]\right)\begin{Bmatrix}\overline{U}_{mn} \\ \overline{V}_{mn}\end{Bmatrix} = \{0\}. \tag{2.51}$$

The stiffness matrix $[K]$ is given by:

$$[K] = \begin{bmatrix} [UU] & [UV] \\ [VU] & [VV] \end{bmatrix}$$

where

$$(UU)_{ij} = \int_{\beta}^{1}\left(\begin{array}{c}\xi\phi_i'\phi_j' + v(\phi_i'\phi_j + \phi_i\phi_j') \\ + \dfrac{\phi_i\,\phi_j}{\xi} + \dfrac{1-v}{2}\dfrac{n^2}{\xi}\phi_i\,\phi_j\end{array}\right)d\xi; \quad (VV)_{ij} = \int_{\beta}^{1}\left(\begin{array}{c}\dfrac{n^2}{\xi}\phi_i\phi_j + \dfrac{1-v}{2}\xi\phi_i'\phi_j' \\ + \dfrac{v-1}{2}(\phi_i'\phi_j + \phi_i\phi_j') + \dfrac{1-v}{2}\dfrac{\phi_i\,\phi_j}{\xi}\end{array}\right)d\xi$$

$$(UV)_{ij} = \int_{\beta}^{1}\left(\begin{array}{c}\dfrac{n}{\xi}\phi_i\phi_j + vn\phi_i'\phi_j \\ + \dfrac{v-1}{2}n\phi_i\phi_j' + \dfrac{1-v}{2}n\dfrac{\phi_i\,\phi_j}{\xi}\end{array}\right)d\xi;$$

$$(VU)_{ij} = \int_{\beta}^{1}\left(\begin{array}{c}\dfrac{n}{\xi}\phi_i\phi_j + vn\phi_i\phi_j' \\ + \dfrac{v-1}{2}n\phi_i'\phi_j + \dfrac{1-v}{2}n\dfrac{\phi_i\,\phi_j}{\xi}\end{array}\right)d\xi; \quad i=1,\ldots,mn; \text{ and } j=1,\ldots,mn$$

and $\phi_i' = \dfrac{d\phi}{d\xi}$.

In the eigenvalue problem, Eq.(2.51) , $[M]$ is the mass matrix and is given by:

$$[M] = \begin{bmatrix} [m_{ii}] & [0] \\ [0] & [m_{ii}] \end{bmatrix} \quad \text{where } m_{ii} = \int_{\beta}^{1}\phi_i^2\,\xi\,d\xi.$$

The mass matrix is diagonal due to the orthogonal property of the assumed deflection modes. The frequency parameters are obtained by solving the eigenvalues problem, Eq. (2.51).

The above formulation can be applied to obtain the natural frequencies of annular disks under different combinations of boundary conditions at the inner and outer edges. A

55

polynomial of degree four is used to define the starting function in the orthogonal set, such that:

$$\phi_1(\xi) = \sum_{i=0}^{4} a_{i+1}\xi^i \qquad (2.52)$$

The constant coefficients, a_{i+1}, of the assumed starting function under different combinations of boundary conditions are presented in Table 2.3. In the table, the boundary conditions C-C and F-F refer to the clamped (inner edge) – clamped (outer edge) and free (inner edge) – free (outer edge), conditions, respectively. Similarly C-F and F-C refer to the clamped (inner edge) – free (outer edge) and free (inner edge) – clamped (outer edge), conditions, respectively. It should be noted that for a solid disk ($\beta = 0$) the starting function will be identical to Eq. (2.45).

Alternatively, the natural frequencies of the disk with clamped boundary conditions can be obtained using artificial springs with admissible functions that satisfy the free boundary conditions. The natural frequencies would approach those of the disk with clamped conditions, when the stiffness due to artificial stiffness is significantly greater than that of the disk. This approach is particularly advantageous when two or more elastic components need to be connected. Rigid joint between the two components can be approximated by increasing the stiffness due to the artificial springs to a very high value. Flexible joints can be simulated by assigning the appropriate values of the stiffness due to the joint [99]. This method is also beneficial in verification of the analytical approach on the basis of the laboratory measured data since it is quite difficult to simulate a perfectly clamped condition at the boundary in the experimental setup.

56

Table 2.3: Coefficients of starting functions satisfying geometrical boundary conditions for annular disk. (F= Free, C= Clamped).

Coefficients	Boundary Conditions			
	C-C	C-F	F-C	F-F
a_1	$-\beta^2$	$-\dfrac{2\beta^2+2\beta^3-3\beta^4+\beta^5}{(\beta-1)^3}$	$-\dfrac{1-3\beta+\beta^2-3\beta^3+3\beta^4-\beta^5}{(\beta-1)^3}$	1
a_2	$2(\beta+\beta^2)$	$-\dfrac{2(-2\beta-2\beta^2+2\beta^4-\beta^5)}{(\beta-1)^3}$	$-\dfrac{2(2\beta+2\beta^2-2\beta^4+\beta^5)}{(\beta-1)^3}$	0
a_3	$-1-4\beta-\beta^2$	$-\dfrac{2+2\beta+8\beta^2-8\beta^3+\beta^4+\beta^5}{(\beta-1)^3}$	$-\dfrac{-2-2\beta-8\beta^2+8\beta^3-\beta^4-\beta^5}{(\beta-1)^3}$	0
a_4	$2(1+\beta)$	$-\dfrac{2(-2\beta+2\beta^3-\beta^4)}{(\beta-1)^3}$	$-\dfrac{2(2\beta-2\beta^3+\beta^4)}{(\beta-1)^3}$	0
a_5	-1	-1	1	0

In this study, artificial springs, distributed in the radial and circumferential direction on both the inner and outer edges of the disk, are employed (Figure 2.2). The maximum strain energy stored in the artificial springs is computed from: $\mathbb{U}$

$$\mathbb{U}_d = \frac{1}{2}h\left[\int_0^{2\pi} K_{ro}[u_r(R_o,\theta,t))]^2 R_o d\theta + \int_0^{2\pi} K_{ri}[u_r(R_i,\theta,t))]^2 R_i d\theta \right.$$
$$\left. + \int_0^{2\pi} K_{\theta o}[u_\theta(R_o,\theta,t))]^2 R_o d\theta + \int_0^{2\pi} K_{\theta i}[u_\theta(R_i,\theta,t))]^2 R_i d\theta \right] \tag{2.53}$$

where K represents the stiffness per unit length, subscripts r and θ represent the radial and circumferential directions, respectively, and the subscripts i and o refer to the inner and outer radii of the disk. The total strain energy of the disk is then obtained by adding Eq. (2.53) to that presented in Eq. (2.36). Following the same aforementioned procedure and assuming the polynomial functions that satisfy the free conditions, the eigenvalue problem is formulated and solved to determine the natural frequencies of the disk with clamped condition at the inner and/or outer boundary. For instance a C-F, boundary

condition (clamped inner and free outer edges) is simulated by selecting high stiffness value for the inner boundary springs, and zero stiffness for outer edge artificial springs.

2.4.   *Boundary Conditions Non-uniformity*

The disks in various applications may have non-uniform boundary conditions such as disks supported on a point or over a partial edge. Furthermore the support stiffness at an edge may vary along the support. Several studies have considered the effects of such partial supports and stiffness non-uniformity on the out-of plane vibration properties of the plates [56-62]. The studies have shown that partial supports cause the frequency parameters to split into symmetric and anti-symmetric frequencies corresponding to each mode [56], as was illustrated in Figure 1.3. These frequency parameters, however, converged to identical values when uniform boundary conditions were considered.

The studies on in-plane vibration of disks, however, have not yet considered the effects of partial supports. Consideration of circular disks with either a point or a patch constraint would be more practical for analyses of in-plane vibration in many situations such as automobile wheel/tire assembly and railway wheels. The dynamic railway wheel and track interactions in the presence of wheel flat defects would be of particular interest in the context of in-plane railway wheel vibration, which may contribute to dynamic wheel impact loads and noise emission [12]. The effects of partial supports and flexible boundary conditions on the in-plane free vibration of circular disks are thus investigated using the methodology presented in the previous section. The boundary characteristic orthogonal polynomials are employed as assumed deflection functions in the Rayleigh-

Ritz method to obtain the natural frequencies and associated mode shapes. Unlike the disk with uniform constraints, the partial support is characterized by defining artificial spring coefficients as functions of the angular coordinate. The strain and kinetic energy for the disk are identical to those presented in Eqs. (2.5) and (2.6), respectively, while partial support condition is achieved by introducing artificial springs along the concerned portion of the free edge.

The free in-plane vibration of the disk is assumed to exhibit sinusoidal variations along the circumferential direction, and may be expressed in the form:

$$u_r(\xi,\theta,t) = \sum_{n=0}^{\infty} U_{c,n}(\xi,t)\cos(n\theta) + U_{s,n}(\xi,t)\sin(n\theta), \tag{2.54}$$

$$u_\theta(\xi,\theta,t) = \sum_{n=0}^{\infty} V_{c,n}(\xi,t)\cos(n\theta) + V_{s,n}(\xi,t)\sin(n\theta), \tag{2.55}$$

where $n = 0, 1, 2, ...$, is the circumferential wave number or nodal diameter number, and U and V are radial and circumferential deflection functions, respectively, expressed as linear combinations of assumed deflection modes in the form of boundary characteristic orthogonal polynomials, such that:

$$U_{c,n}(\xi,t) = \sum_{m=1}^{\infty} \phi_m(\xi)\overline{U}_{c,mn}(t), \qquad U_{s,n}(\xi,t) = \sum_{m=1}^{\infty} \phi_m(\xi)\overline{U}_{s,mn}(t), \tag{2.56}$$

$$V_{c,n}(\xi,t) = \sum_{m=1}^{\infty} \phi_m(\xi)\overline{V}_{c,mn}(t), \qquad V_{s,n}(\xi,t) = \sum_{m=1}^{\infty} \phi_m(\xi)\overline{V}_{s,mn}(t), \tag{2.57}$$

where the first subscripts of functions U and V, c and s, respectively, refer to cosine and sine components of the deflections, $\overline{U}$ and $\overline{V}$ are the deflection coefficients, and $\phi_m(\xi)$ is the assumed deflection shape corresponding to mode m. It should be noted that the radial and circumferential displacement for the disk with uniform boundary conditions,

presented in Eqs. (2.34) and (2.35), include only the cosine and sine components of Eqs. (2.54) and (2.55), respectively. This will be discussed in more details in a subsequent section.

Substituting the displacement functions from Eqs. (2.54) and (2.55) into the energy expressions, Eqs. (2.5) and (2.6), and equating the maximum kinetic and potential energies yields the Rayleigh's quotient λ^2, where $\lambda^2 = \rho\omega^2 R_o^2(1-v^2)/E$, as formulated in the previous section. Application of the condition of stationarity with respect to the arbitrary coefficients, $\bar{U}_{c,mn}$, $\bar{U}_{s,mn}$ $\bar{V}_{c,mn}$ and $\bar{V}_{s,mn}$ yields:

$$\frac{\partial \lambda^2}{\partial \bar{U}_{c,mn}} = 0 \; ; \; \frac{\partial \lambda^2}{\partial \bar{U}_{s,mn}} = 0$$

$$\frac{\partial \lambda^2}{\partial \bar{V}_{c,mn}} = 0 \; ; \; \frac{\partial \lambda^2}{\partial \bar{V}_{s,mn}} = 0,$$

(2.58)

and the following eigenvalue problem:

$$\left([K] - \lambda^2[M]\right) \begin{Bmatrix} \bar{U}_{c,mn} \\ \bar{U}_{s,mn} \\ \bar{V}_{c,mn} \\ \bar{V}_{s,mn} \end{Bmatrix} = \{0\}.$$

(2.59)

The eigenvectors in the above formulation include both the cosine and sine components of the radial and circumferential displacements, where $[K]$ and $[M]$ are $(4 \times m \times n)$ nondimesional stiffness and mass matrices, respectively. Due to the nature of couplings between the modes of non-rotating disks, the system of equations could be decomposed into two subsets, each of size $(2 \times m \times n)$. The solution of Eq. (2.59) revealed that the radial cosine components, $\bar{U}_{c,mn}$, are coupled with the corresponding circumferential sine components, $\bar{V}_{s,mn}$ only. The radial sine components, $\bar{U}_{s,mn}$, on the other hand, are coupled with the circumferential cosine components, $\bar{V}_{c,mn}$ only. The

couplings between the various modes and their effects are described in the subsequent sections. The formulations of the stiffness and mass matrices are thus presented considering only one subset of equations. Furthermore, the subscripts *c* and *s* corresponding to the cosine and sine components are omitted for the purpose of brevity. The stiffness and mass matrices for each subsystem are defined in a manner similar to that presented in section 2.3.

2.4.1. Boundary Conditions

A set of artificial springs are introduced at the free outer and inner edges to simulate the clamped and flexible boundary conditions. A significantly higher spring stiffness could be chosen to represent a clamped boundary condition. The artificial springs are distributed in the radial and circumferential directions on both the inner and outer edges of the disk, as shown in Figure 2.2. The artificial springs may also be applied only to a portion of the edges along the circumferential direction to realize a partial support or a point support condition. The maximum strain energy stored in the distributed artificial springs at the inner and outer edges, $\mathbb{U}_d$ can be obtained as:

$$\mathbb{U}_d = \frac{1}{2}h\left[\int_0^{2\pi} K_{ro}(\theta)[u_r(R_o,\theta,t))]^2 R_o d\theta + \int_0^{2\pi} K_{ri}(\theta)[u_r(R_i,\theta,t))]^2 R_i d\theta \right.$$
$$\left. + \int_0^{2\pi} K_{\theta o}(\theta)[u_\theta(R_o,\theta,t))]^2 R_o d\theta + \int_0^{2\pi} K_{\theta i}(\theta)[u_\theta(R_i,\theta,t))]^2 R_i d\theta \right] \quad (2.60)$$

where $K(\theta)$ represents radial and circumferential stiffness per unit length of the disk, subscripts r_o and r_i denote radial springs at the outer and inner edges, respectively, and subscripts θ_o and θ_i represent the respective springs along the circumferential directions.

It is assumed that the artificial springs are symmetric about $\theta = 0$. The spring stiffness $K(\theta)$ may thus be expressed by a Fourier cosine series, as:

$$K(\theta) = \frac{a_0}{2} + \sum_{l=1}^{\infty} a_l \cos(l\theta) \tag{2.61}$$

where

$$a_l = \frac{1}{\pi} \int_0^{2\pi} K(\theta) \cos(l\theta)\, d\theta \qquad (l = 0,1,2,\dots) \tag{2.62}$$
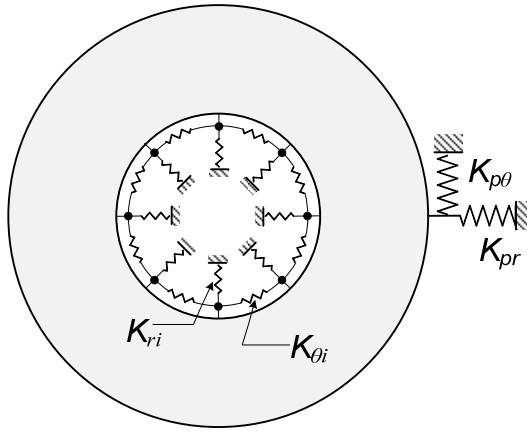
Figure 2.2: Annular disk with an elastic point support at the outer edge; and uniformly clamped at the inner edge

A clamped boundary condition may be realized by assuming $K(\theta)$ as a constant in Eq. (2.60) and by selecting nearly infinite stiffness values. For a disk supported at a point on the outer edge, the maximum potential energy $\mathbb{U}_p$ can be derived as:

$$\mathbb{U}_p = \frac{1}{2} K_{pr} h[u_r(R_o, \theta_0, t)]^2 + \frac{1}{2} K_{p\theta} h[u_\theta(R_o, \theta_0, t)]^2 \tag{2.63}$$

where K_{pr} and $K_{p\theta}$ are the stiffness per unit length due to the point elastic support in the radial and circumferential directions, respectively, and θ_0 is the circumferential coordinate of the point support.

The total strain energy is obtained by adding either Eq. (2.60) or (2.63) to Eq. (2.5), depending upon the constraint. The solution of the resulting eigenvalue

problem then yields the frequency parameters for the in-plane vibration of the annular disk subject to selected boundary and constraint conditions at the two free edges. For example, a clamped condition at the inner boundary and a free outer boundary (C-F) can be realized by letting $K_{ri}, K_{\theta i} \to \infty$ and $K_{ro}, K_{\theta o} \to 0$.

2.4.2. Nature of Couplings

The in-plane vibration modes exhibit complex couplings among them, which further depend upon the boundary conditions. The solutions of the eigenvalue problems for different boundary conditions can provide significant insight into the nature of couplings between different modes and the effects of boundary conditions on the in-plane vibration properties. It should be noted that the mass matrix is diagonal due to the orthogonal property of the assumed deflection shapes. The stiffness matrix, however, is non-diagonal due to the presence of derivatives of the assumed deflection shapes and non-uniform constraint conditions. The couplings among different modes can thus be solely attributed to the stiffness matrix. As discussed earlier, the system of equations can be represented by those of two independent subsystems, associated with coupled radial cosine and circumferential sine, and radial sine and circumferential cosine modes, respectively. In the following discussion, these are referred to as even and odd subsystems with respect to the radial displacement. It should also be noted that the even radial displacement is coupled with the odd circumferential displacement only. The odd and even subsystems, however, would be coupled in the case of rotating disks, which is considered in section 2.5.

For different combinations of classical boundary conditions, the following observations related to mode couplings could be made through examination of the stiffness matrix:

- The modes with different nodal diameter number (n) are uncoupled. The coupling exists between modes with different nodal circles (m) within the same nodal diameter number (n). Consequently, each set of modes corresponding to the same n can be studied independently.

- For modes with zero nodal diameter number, $n = 0$, the modes are either purely radial or purely circumferential. The even subsystem would yield radial expansion modes, while the odd subsystem gives the torsional modes. Since the variation of displacements along the circumferential direction is zero, these modes are considered as axisymmetric modes.

- For $n \geq 1$, the radial and circumferential displacements are coupled within the same nodal diameter number n. The frequency parameters of the odd subsystem are identical to those obtained for the even subsystem. The modes of the odd subsystem, however, exhibit a phase shift of $\pi/(2n)$ with respect to their counterpart. It would thus be sufficient to compute the frequency parameters of one of the subsystems.

For a disk with non-uniform boundary conditions, nature of coupling between the modes would differ from those observed under classical boundary conditions, specifically:

- The modes associated with different nodal diameter number n are coupled, and thus cannot be studied independently. Although the two subsystems could still be

treated independently assuming symmetry about $\theta = 0$, the resulting modes will be coupled within each subsystem.

- For axisymmetric modes, $n = 0$, the odd subsystem yields free vibration responses that are different from those of the even subsystem. However, the modes are no longer purely radial or purely circumferential due to the effect of partial supports.

- Although the even and odd subsystems remain uncoupled, they yield different values of the frequency parameters. The effect of partial elastic support can be considered similar to the gyroscopic effect due to rotation in which the natural frequencies split into two different values. Similar effect has been reported by Narita and Leissa [57] and Eastep and Hemmig [61] for the case of out-of-plane vibrations.

The frequency parameters are tabulated and the mode shapes of the in-plane free vibration of circular disks are presented and discussed in the next chapter. The results obtained are compared with those reported and those obtained from the finite element analysis in order to illustrate the validity of the present method.

2.5. *Rotational Effects*

The problems of in-plane vibration of rotating disks have been addressed in only a few studies, although the rotating disks are of extreme importance in many engineering applications. Bhuta and Jones [26] provided a solution to the symmetric in-plane vibrations of a thin rotating circular full disk and determined natural frequencies for some specific modes. Burdess et al. [27] presented generalized formulation by implementing

Lame's potentials to consider asymmetric in-plane vibrations and discussed the effect of rotational speed on the forward and backward traveling waves of a two nodal diameter mode. Chen and Jhu [25, 28] extended the analysis to study the divergence instability of spinning annular disks clamped at the inner edge and free at the outer boundary. The effect of radius ratio on the natural frequencies and critical speeds of the disk was also investigated. Hamidzadeh [30, 31] analyzed the same problem with a different formulation. In these studies, the critical speeds were determined using the classical theory of linear elasticity, while the boundary conditions were limited to a free outer edge.

Many engineering applications involve rotating disks with point or patch contact such as railway wheel-rail contact and disk brake-friction pad contact. The effect of flexible partial or point supports on the in-plane vibration of rotating circular disks, however, have not been investigated. In this study, the boundary characteristic orthogonal polynomials are employed as assumed deflection functions in the Lagrange's equation to obtain the natural frequencies for various rotating speeds with different sets of boundary conditions. The formulations are also applied to study the combined effects of rotation and constraint non-uniformity on the natural frequencies.

2.5.1. Linear Model Formulation

Consider a disk rotating at constant speed Ω. In order to describe the system of rotating disk, two coordinate systems are needed, as shown in Figure 2.3. The first coordinate system (r,θ) is the rotating frame where θ is the circumferential coordinate

attached to the rotating disk. The second coordinate system (r, η) is a fixed frame, where η is the circumferential coordinate referenced to the inertial frame.

The expression for strain energy of the disk is identical to that derived for the stationary disk which comprises the strain energy due to the elastic properties of the free disk, as described in Eq. (2.5), and the strain energy due to boundary constraints, as described in Eq. (2.60) or Eq. (2.63). The expression for the kinetic energy of the disk is
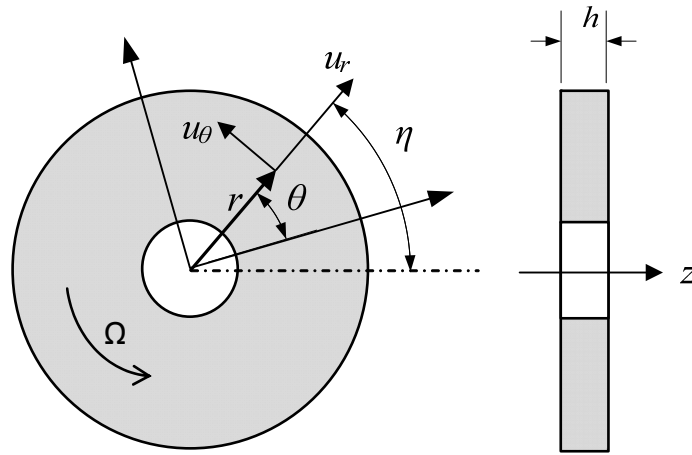
Figure 2.3: Geometry and coordinate system used for in-plane vibration analysis of a rotating disk

formulated upon considering the effects of centrifugal and coriolis forces arising from the disk rotation. Let r_0 denote the undeformed location of a particle in the disk and $\bar{u}$ be the corresponding displacement vector. The instantaneous position of the particle can thus be described as $\bar{r} = r_0 + \bar{u}$, and the corresponding velocity as $\partial \bar{r} / \partial t$. Let $\bar{e}_r$ and $\bar{e}_\theta$ be the unit vectors in the radial and circumferential directions, respectively, and $\bar{e}_z$ be perpendicular to the plane containing $\bar{e}_r$ and $\bar{e}_\theta$. The position vector can be expressed as:

$$\bar{u} = (r + u_r)\bar{e}_r + u_\theta \bar{e}_\theta \qquad (2.64)$$

The angular velocity vector, $\vec{\Omega}$, can be expressed in terms of the angular speed, Ω as:

$$\vec{\Omega} = \Omega \bar{e}_z$$

The velocity vector is subsequently derived as:

$$\vec{v} = (\dot{u}_r - \Omega u_\theta)\bar{e}_r + (\dot{u}_\theta + \Omega u_r)\bar{e}_\theta$$

The kinetic energy of the rotating disk in the rotating coordinate system (r,θ) is derived as:

$$T = \frac{1}{2}h\rho R_0^2 \int\limits_0^{2\pi} \int\limits_\beta^1 \left((\dot{u}_r - \Omega u_\theta)^2 + (\dot{u}_\theta + \Omega u_r)^2 \right) \xi \, d\xi \, d\theta \tag{2.65}$$

In the above formulation, the displacement functions (u_r, u_θ) are identical to those derived in Eqs. (2.54) and (2.55). Substituting the assumed solutions into the energy expressions, Eqs. (2.5) and (2.6), yields the expressions for the strain and kinetic energy in terms of the displacement functions. The strain energy of the disk can be written in matrix form as:

$$\mathbb{U} = \frac{1}{2}\{q\}^T [K]\{q\} \tag{2.66}$$

where $\{q\} = \{\bar{U}_{c,m} \quad \bar{U}_{s,m} \quad \bar{V}_{c,m} \quad \bar{V}_{s,m}\}^T$ and the stiffness matrix $[K]$ is given by:

$$[K] = \begin{bmatrix} [UU] & [0] & [0] & [UV] \\ [0] & [UU] & [UV] & [0] \\ [0] & [VU] & [VV] & [0] \\ [VU] & [0] & [0] & [VV] \end{bmatrix}$$

The elements of the above stiffness matrix have been defined in section 2.3.

The kinetic energy of the rotating disk can also be expressed in matrix form as:

$$T = \frac{1}{2}\{\dot{q}\}^T [M]\{\dot{q}\} + \frac{1}{2}\Omega^2 \{q\}^T [M]\{q\} + \Omega\{q\}^T [G]\{\dot{q}\} \tag{2.67}$$

where $[M]$ is the mass matrix formulated as:

$$[M] = \begin{bmatrix} [m_{ii}] & [0] & [0] & [0] \\ [0] & [m_{ii}] & [0] & [0] \\ [0] & [0] & [m_{ii}] & [0] \\ [0] & [0] & [0] & [m_{ii}] \end{bmatrix}$$

And m_{ii} is the generalized mass, derived from:

$$m_{ii} = \int_0^1 \phi_i \phi_i \xi d\xi$$

The mass matrix is diagonal because of the orthogonal property of the assumed polynomial functions. The second term in Eq. (2.67) is attributed to the centrifugal force and is a function of the rotational speed. The third term includes the skew-symmetric gyroscopic matrix $[G]$, derived as:

$$[G] = \begin{bmatrix} [0] & [0] & [-2m_{ii}] & [0] \\ [0] & [0] & [0] & [-2m_{ii}] \\ [2m_{ii}] & [0] & [0] & [0] \\ [0] & [2m_{ii}] & [0] & [0] \end{bmatrix}$$

The energy expressions are subsequently used to derive the equations of motion for the rotating disk in the fixed coordinate system, and the eigenvalue problem. The differential equations of motion for the rotating disk are obtained using the Lagrange equation, and expressed as:

$$[M]\{\ddot{q}\} + \Omega[G]\{\dot{q}\} + [K]\{q\} = \{0\} \tag{2.68}$$

An eigenvalue problem is formulated and solved to determine the natural frequencies of the in-plane vibration of the disk subject to different combinations of boundary conditions, including the flexible and partial supports.

The coupling between the in-plane vibration modes depends upon the boundary conditions and the rotation of the disk. As discussed in section2.4.2, non-uniform

boundary conditions produce coupling between modes with different nodal diameter number, n, while rotation of the disk is responsible for the coupling between modes within the same nodal diameter number. Hence, for a disk subject to uniform boundary conditions (stationary or rotating), modes with different nodal diameter number, n, are uncoupled and can be studied separately. Moreover, for a stationary disk, two uncoupled subsystems exists for each nodal diameter number, the first subsystem constitutes the radial cosine modes coupled with the circumferential sine modes (referred to as even subsystem) while the second subsystem has the radial sine modes coupled with the circumferential cosine modes within the same nodal diameter number (referred to as odd subsystem). Both the subsystems yield identical values of the frequency parameters except for the axisymmetric modes. Rotation of the disk produces coupling between these two subsystems through the gyroscopic matrix. The modes with different nodal diameter, however, remain uncoupled for the disk with uniform edge conditions, which suggest that the summation over n could be omitted in Eqs. (2.54) and (2.55) describing the displacement response, while the eigenvalue problem could be significantly simplified.

The non-uniformity of the boundary conditions, however, causes the radial and the circumferential modes to couple with radial and circumferential modes with different nodal diameter numbers, respectively. The system may be decomposed into even and odd subsystems, which could be studied independently for the stationary disks. Each subsystem would yield distinct frequency parameters due to the coupling between modes with different nodal diameter number. For the rotating disks with non-uniform boundary conditions, all the modes are derived from Eq. (2.68) and need to be solved simultaneously to determine the deflection coefficients.

2.5.2. Formulation of the Nonlinear Rotational Effects

When a circular disk rotates at a constant speed, the disk undergoes an initial deformation resulting from the centrifugal forces. This initial deformation can be obtained by solving the static problem associated with the abovementioned energy expressions. The linear in-plane vibration analysis, however, assumes this initial deformation to be small and thereby neglects the stiffening effect of this deformation. The static deformation, however, is directly proportional to the rotational speed and may not be of the same order as the amplitude of the in-plane oscillations. This static deformation is also known as the axisymmetric radial expansion of the disk or the steady state solution. The effect of the initial deformation could be incorporated in the analysis by consideration of the stiffening effect through nonlinear strain-displacement relations. A number of studies have investigated the effect of this additional stiffening on the out-of-plane vibration of different structures such as rings, beams and plates (out-of-plane) [e.g. 32, 33].

The effects on the in-plane vibration, however, have been explored in a single study by Deshpande and Mote who studied the in-plane stability of a spinning thin disk using a nonlinear strain measure in order to account for the stiffening of the disk due to rotation [36]. The study did not observe any critical speed in the range of rotational speed considered for modes with two or less nodal diameters. An upper limit of the rotational speed was identified where the assumption of linear strain measure would be applicable. The study considered free edge boundary conditions. In this study a nonlinear formulation is realized to study the effect of additional stiffening on the vibration of an annular disk subject to non-uniform boundary conditions, using the nonlinear strain-

displacement relation. The stress-strain relation, however, is assumed to be linear (plane stress conditions). The disk is assumed to rotate at a constant speed until it reaches its equilibrium position, with no in-plane vibration. The radial expansion is subsequently calculated and added as an additional stiffness to the governing equations of motion. This is achieved by employing the strain-displacement relations written as:

$$\varepsilon_r = \frac{\partial u_r}{\partial r} + \frac{1}{2}\left[\left(\frac{\partial u_r}{\partial r}\right)^2 + \left(\frac{\partial u_\theta}{\partial r}\right)^2\right]$$

$$\varepsilon_\theta = \frac{u_r}{r} + \frac{1}{r}\left(1+\frac{u_r}{r}\right)\frac{\partial u_\theta}{\partial \theta} - \frac{u_\theta}{r^2}\frac{\partial u_r}{\partial \theta} + \frac{1}{2r^2}\left[u_r^2 + u_\theta^2 + \left(\frac{\partial u_r}{\partial \theta}\right)^2 + \left(\frac{\partial u_\theta}{\partial \theta}\right)^2\right]. \tag{2.69}$$

$$\varepsilon_{r\theta} = \frac{1}{2r}\left(\frac{\partial u_r}{\partial \theta} + r\frac{\partial u_\theta}{\partial r} - u_\theta + \frac{\partial u_r}{\partial r}\frac{\partial u_r}{\partial \theta} - u_\theta\frac{\partial u_r}{\partial r} + u_r\frac{\partial u_\theta}{\partial r} + \frac{\partial u_\theta}{\partial r}\frac{\partial u_\theta}{\partial \theta}\right)$$

By substituting the above strain-displacement relations into the strain energy expressions, Eq. (2.3), and introducing the non-dimensional parameter $\xi = r/R_o$, the strain energy can be expressed in terms of the displacements. Substituting the assumed solutions, Eqs. (2.54) and (2.55), in the strain energy expression yields the nonlinear strain energy expression in terms of displacement functions. The resulting strain energy expression contains both the linear terms (squared displacement function shown in Eq. (2.5)) and nonlinear terms (cubic and fourth order displacement terms) and can be written in matrix form as:

$$\mathbb{U} = \frac{1}{2}\{q\}^T([K] + [\bar{K}_q] + [\bar{\bar{K}}_{qq}])\{q\} \tag{2.70}$$

where $\{q\} = \{\bar{U}_{c,m} \quad \bar{U}_{s,m} \quad \bar{V}_{c,m} \quad \bar{V}_{s,m}\}^T$ and $[K]$ is the linear stiffness matrix obtained from the linear strain relation. The nonlinear stiffness matrices $[\bar{K}_q]$ and $[\bar{\bar{K}}_{qq}]$, obtained from the cubic and fourth order terms, respectively, are dependent on the generalized

72

coordinates $\{q\}$. In this study, only the contributions of $[K]$ and $[\overline{K}_q]$ associated with linear and nonlinear cubic terms, are retained in the strain energy, assuming relatively small contribution due to higher order terms. This leads to a simplified strain energy expression, written as:

$$\mathbb{U} = \frac{1}{2}\{q\}^T([K] + [\overline{K}_q])\{q\} \tag{2.71}$$

The linear component of the above strain energy expression can be used to obtain the static deformation. The resulting strain energy expression is presented in Eq. (2.5) for a disk rotating at a constant speed with negligible in-plane oscillation; only radial deformation of the disk is present, which is function of r alone. This suggests that all circumferential displacements and variations with respect to θ could be disregarded. The linear strain energy expression then reduces to:

$$\mathbb{U} = \frac{1}{2}\frac{Eh}{1-v^2}\int_0^{2\pi}\int_\beta^1 \left\{\left(\frac{\partial u_r}{\partial \xi}\right)^2 + 2v\left(\frac{u_r}{\xi}\frac{\partial u_r}{\partial \xi}\right) + \left(\frac{u_r}{\xi}\right)^2\right\}\xi d\xi d\theta \tag{2.72}$$

The kinetic energy expression can also be derived from:

$$T = \frac{1}{2}h\rho R_0^2 \int_0^{2\pi}\int_\beta^1 (\Omega(\xi + u_r))^2 \xi d\xi d\theta \tag{2.73}$$

The equation of equilibrium of the disk can be subsequently derived from Eqs. (2.72) and (2.73) as:

$$\frac{\partial^2 u_r}{\partial \xi^2} + \frac{1}{\xi}\frac{\partial u_r}{\partial \xi} - \frac{u_r}{\xi^2} + \frac{\rho(1-v^2)}{E}\Omega^2(\xi + u_r) = 0 \tag{2.74}$$

The solution of the above equation can be expanded in terms of Bessel function, as:

$$u_r = -\xi + A_1 J_1(\alpha\xi) + B_1 Y_1(\alpha\xi) \tag{2.75}$$

where $\alpha^2 = \frac{\rho(1-\nu^2)}{E}\Omega^2$, and A_1 and B_1 are the arbitrary coefficients that can be solved by applying the boundary conditions.

The equilibrium equation (2.74) is valid only for uniform boundary conditions in the rotating coordinate system. For a boundary condition involving single point support or an edge support, the expansion due to rotation is not axisymmetric and the solution (2.75) cannot be considered valid. The static deformation thus describes the steady state solution obtained from the original strain and kinetic energy expressions, Eq. (2.5) and Eq. (2.73). The static displacement is derived from the solution of the governing equation of the total deformation (including static deformation and the in-plane oscillation):

$$[M]\{\ddot{q}\} + \Omega[G]\{\dot{q}\} + \big([K]+[\overline{K}_q]\big)\{q\} = \{F_s\} \tag{2.76}$$

where F_s is the force due to rotation. Let us define an initial configuration where the disk is subject to static deformation alone. All the terms in Eq. (2.76) will vanish except for the stiffness and force terms, resulting in:

$$\big([K]+[\overline{K}_{qs}]\big)\{q_s\} = \{F_s\} \tag{2.77}$$

The above equation is solved to determine the vector $\{q_s\}$, which contains the coefficients associated with the initial deflection. It can also be noted that for a linear in-plane analysis, the nonlinear stiffness matrix will vanish and the disk will undergo radial expansion only. Equation (2.77) can be reduced to a set of linear algebraic equations to yield:

74

$$\{q_s\} = [K]^{-1}\{F_s\} \tag{2.78}$$

The above solution is identical to that obtained from Eq. (2.75), when the disk is subject to uniform boundary conditions. For non-uniform boundary condition, the nonlinear or linear formulations, Eqs. (2.77) and (2.78) can be solved for the nonlinear analysis and linear analysis, respectively.

For the dynamic analysis, an alternate dynamic vector $\{q_d\}$ relative to the static displacement vector $\{q_s\}$ is defined as:

$$\{q_d\} = \{q\} - \{q_s\} \tag{2.79}$$

Replacing the vector $\{q\}$ by $\{q_d\} + \{q_s\}$ in Eq. (2.76) yields:

$$[M]\{\ddot{q}_d\} + \Omega[G]\{\dot{q}_d\} + ([K] + [\bar{K}_{qs}])\{q_d\} + [\bar{K}_{qd}]\{q_s\} + [\bar{K}_{qd}]\{q_d\}$$
$$+ ([K] + [\bar{K}_{qs}])\{q_s\} = \{F_s\} \tag{2.80}$$

The last terms in Eq. (2.80) is identical to Eq. (2.77) obtained from the static analysis and could be eliminated. Equation (2.80) thus reduces to the dynamic displacement vector $\{q_d\}$ alone. The free vibration analysis of the rotating disk is subsequently performed by neglecting the nonlinear matrix that depends on the dynamic displacement vector, $[\bar{K}_{qd}]\{q_d\}$. Equation (2.80) is thus written as:

$$[M]\{\ddot{q}_d\} + \Omega[G]\{\dot{q}_d\} + [K]\{q_d\} + [\bar{K}_{qd}]\{q_s\} + [\bar{K}_{qs}]\{q_d\} = 0 \tag{2.81}$$

Equation (2.81) is the governing equation of motion of a rotating disk subject to initial deformation due to its rotation and uniform as well as non-uniform boundary conditions.

2.5.3. Formulations in the Fixed Coordinate System

For rotating disks, it may be convenient to transform the energy expressions to the inertial frame, particularly when an external non-rotating force or constraint is applied as in the case of a rotating railway wheel. Energy expressions are transformed from the rotating coordinate system (r, θ) to the fixed coordinate system (r, η) by using the following transformations:

$$\dot{u}_r(r,\theta) = \left(\frac{\partial}{\partial t} + \Omega\frac{\partial}{\partial \eta}\right)u_r(r,\eta)$$
$$\dot{u}_\theta(r,\theta) = \left(\frac{\partial}{\partial t} + \Omega\frac{\partial}{\partial \eta}\right)u_\eta(r,\eta)$$

(2.82)

where

$$\eta = \theta + \Omega t$$

(2.83)

While the resulting strain energy is similar to that presented in Eq. (2.5) for the linear analysis with u_θ replaced by u_η, the kinetic energy with respect to the fixed coordinate system is derived as:

$$T = \frac{1}{2}h\rho R_0^2 \int_0^{2\pi} \int_\beta^1 \left(\left(\dot{u}_r + \Omega\frac{\partial u_r}{\partial \eta} - \Omega u_\eta\right)^2 + \left(\dot{u}_\eta + \Omega\frac{\partial u_\eta}{\partial \eta} + \Omega u_r\right)^2\right)\xi d\xi d\theta$$

(2.84)
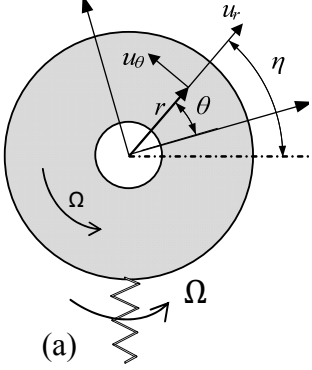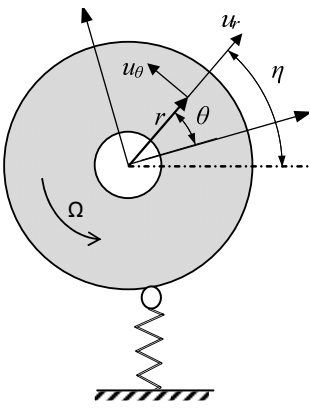
In a similar manner, the non-linear problem can also be transformed to the inertial frame by using transformations described in Eq. (2.82). The effect due to additional static deformation is included by neglecting the time derivative terms from Eq. (2.84), which yields:

$$T = \frac{1}{2}h\rho R_0^2 \int_0^{2\pi} \int_\beta^1 \left(\left(\Omega\frac{\partial u_r}{\partial \eta} - \Omega u_\eta\right)^2 + \left(\Omega\frac{\partial u_\eta}{\partial \eta} + \Omega(\xi + u_r)\right)^2\right)\xi d\xi d\theta$$

(2.85)

The static deformation coefficients vector $\{q_s\}$ in the fixed frame is derived using the approach described in section (2.5.4) involving solutions of Eqs. (2.77) and (2.78). The dynamic deflection coefficient vector $\{q_d\}$ in the fixed-frame is subsequently obtained using $\{q_s\}$ and the governing equations of motion as described above.

There are two particular problems that are of practical importance for the rotating disks. The first problem concerns rotating disk with non-rotating boundary conditions such as in a rotating railway wheel with a non-rotating constraint, which is the rail contact. In this case, the constraint is applied after transforming the expressions to the fixed coordinate system. This differs from the problem involving rotations of both the disk and the constraints, which could represent a rotating disk bolted at certain points to a shaft. Both the problems are presented in Table 2.4 together with the corresponding energy expressions.

Table 2.4: Rotating disk with (a) rotating constraint, (b) non-rotating constraint.

Strain Energy: Eq (2.5)	Strain Energy: Eq. (2.5)
Spring energy: $\frac{1}{2}K_{pr}h[u_r(R_o,\theta_0,t)]^2$	Spring energy: $\frac{1}{2}K_{pr}h[u_r(R_o,\eta_0,t)]^2$
Kinetic energy: Rotating coordinate	Kinetic energy: Fixed coordinate

| frame, Eq. (2.6) | frame, Eq. (2.84) |

2.6. *Formulation of the Acoustic Model*

The noise radiation from both out-of-plane and in-plane modes of circular disks are important in many applications. In this section, an acoustic model of the circular disk involving in-plane vibration model is formulated to study the noise radiation characteristics. The model is derived using the formulation presented by Junger and Feit [103], William [104] and Lee and Singh [24].

2.6.1. *Sound Radiations Associated with In-plane Modes*

Lee and Singh [24] presented two different approaches to calculate the sound pressure associated with in-plane modes. The first approach involved the Rayleigh integral in a manner similar to that employed in the out-of-plane analysis. The second approach treated the outer and inner edges of an annular disk as two separate cylindrical sound radiators. In this study, the formulations are derived on the basis of the second approach, since it is considered to yield more accurate analysis of the in-plane noise radiation [24].

The sound radiation due to radial displacement of the disk can be obtained by solving the Helmholtz equation. The Helmholtz pressure equation can be written in terms of the Fourier transform of the sound pressure $\tilde{P}$, as [104]:

$$\left(\frac{\partial^2}{\partial r^2} + \frac{1}{r}\frac{\partial}{\partial r} + k^2 - k_z^2 + \frac{1}{r^2}\frac{\partial^2}{\partial \theta^2}\right)\tilde{P}(r,\theta,k_z) = 0 \qquad (2.86)$$

where k is the acoustic wave number and k_z is structural wave number in the z direction. The solution of the above equation is assumed to be of the form:

78

$$\tilde{P}(r, \theta, k_z) = AH_n^1\left[r\sqrt{(k^2 - k_z^2)}\right]\cos n\theta \qquad (2.87)$$

where H_n^1 is the Hankel function of order n. The coefficient A in this equation can be obtained from the boundary conditions at the edge of the disk, as:

$$\frac{\partial \tilde{P}(r, \theta, k_z)}{\partial r} = -\rho_0\ddot{u}(r, \theta, k_z); \text{ at } r = R_o \qquad (2.88)$$

where ρ_0 is mass density of air. The acceleration of the disk surface can be obtained from the vibration analysis of the disk, which can be expressed as:

$$\ddot{u}(\theta, z) = |\ddot{U}|Z(z)\cos n\theta \qquad (2.89)$$

where $Z(z)$ is the acceleration distribution function in the z direction. Equations (2.88) and (2.89) yield the following:

$$\frac{\partial \tilde{P}(r, \theta, k_z)}{\partial r} = -\rho_0|\ddot{U}|\tilde{Z}(k_z)\cos n\theta, \qquad \text{at } r = R_0 \qquad (2.90)$$

where

$$\tilde{Z}(z) = \int_{-h/2}^{h/2} Z(z)e^{ik_z z}dz \qquad (2.91)$$

The constant A in Eq. (2.87) can be obtained from Eq. (2.90), as:

$$A = \frac{-\rho_0|\ddot{U}|\tilde{Z}(k_z)}{\sqrt{(k^2 - k_z^2)}H_n^1\left[R_0\sqrt{(k^2 - k_z^2)}\right]} \qquad (2.92)$$

After taking the inverse Fourier transform and simplifying the expression for the sound pressure, the sound pressure from the outer surface P_o and from the inner surface P_i can be expressed, respectively, as:

$$P_{o,n}(R,\theta,\phi) = \frac{\rho_0 e^{ik_n R}}{\pi k_n R \sin\phi} |\ddot{u}_n| h \frac{Sinc(k_n \sin\phi\, h/2)(-i)^{n+1}}{H_n^{1'}(k_n R_0 \sin\phi)} \cos(n\theta) \qquad (2.93)$$

$$P_{i,n}(R,\theta,\phi) = \frac{\rho_0 e^{ik_n R}}{\pi k_n R \sin\phi} |\ddot{u}_n| h \frac{Sinc(k_n \sin\phi\, h/2)(-i)^{n+1}}{H_n^{2'}(k_n R_i \sin\phi)} \cos(n\theta) \qquad (2.94)$$

where H_n^1 is Hankel functions of the first kind of order n and ' is the derivative with respect to the argument of the Hankel function and R is the distance between the receiver and the center of the disk. The total modal sound pressure P_n is the sum of the sound pressures from two radial edges, such that:

$$P_n(R,\theta,\phi) = P_{o,n}(R,\theta,\phi) + P_{i,n}(R,\theta,\phi) \qquad (2.95)$$

The modal directivity function $D_n(\theta,\phi)$ can be written as:

$$D_n(\theta,\phi) = RP_n(R,\theta,\phi)e^{ik_n R} \qquad (2.96)$$

The modal sound power can be expressed as:

$$\Pi_n = \frac{1}{2} \int\limits_0^{2\pi}\int\limits_0^{\pi} \frac{P_n^2}{\rho_0 c_0} \sin(\phi)d\theta d\phi \qquad (2.97)$$

where c_0 is the speed of sound. The modal radiation efficiency can be calculated using the following equation:

$$\sigma_n = \frac{\Pi_n}{\langle|\dot{u}_{mn}|^2\rangle}$$

where

$$\langle|\dot{u}_n|^2\rangle = \frac{1}{2\pi(R_i^2 - R_o^2)} \int\limits_{R_i}^{R_0}\int\limits_0^{2\pi} \dot{U}_n^2 \, d\phi dr$$

$$(2.98)$$

The above formulations have been widely used to determine the sound radiation from disks with free boundary conditions [24, 104], and could also be applied for disks subject to non-uniform conditions. The primary difference between the two sets of

80

boundary conditions lies only in the expression of the arbitrary coefficient A in Eq. (2.92). These are thus derived considering the non-uniform boundary conditions. The radial acceleration of the disk subject to a non-uniform boundary condition can be derived as:

$$\ddot{u}(a,\theta,z) = Z(z) \sum_{n=0}^{\infty} \left[\left| \ddot{U}_{c,n} \right| \cos(n\theta) + \left| \ddot{U}_{s,n} \right| \sin(n\theta) \right] \tag{2.99}$$

For a stationary disk, it has been shown that the cosine and sine components are uncoupled (see section 2.4.2) which yield identical natural frequencies for the uniform boundary conditions. For the partially supported disk, they remain uncoupled but yield different values for the natural frequencies. The radial acceleration of the disk is thus rewritten in terms of components for the even and odd systems, such that:

$$\ddot{u}_c(a,\theta,z) = Z(z) \sum_{n=0}^{\infty} \left| \ddot{U}_{c,n} \right| \cos(n\theta) ; \quad \text{even system} \tag{2.100}$$

for the even system, and

$$\ddot{u}_s(a,\theta,z) = Z(z) \sum_{n=0}^{\infty} \left| \ddot{U}_{s,n} \right| \sin(n\theta) ; \quad \text{odd system} \tag{2.101}$$

for the odd system. The application of the boundary conditions to Eq. (2.88) yields:

$$\frac{\partial \tilde{P}\left(r,\theta,k_z\right)}{\partial r} = \sum A_n H_n^{1\prime} \left[r\sqrt{(k^2 - k_z^2)} \right] \cos n\theta$$

$$= -\rho_0 \tilde{Z}(k_z) \sum_{n=0}^{\infty} \left| \ddot{U}_{c,n} \right| \cos(n\theta) \tag{2.102}$$

Multiplying both sides by $\cos(\bar{n}\theta)$ and integrating from zero to 2π, yields following expression for the coefficients A_n:

$$A_n = \begin{cases} \dfrac{-\rho_0 |\ddot{U}_{c,n}| \tilde{Z}(k_z)}{\sqrt{(k^2 - k_z^2)} H_n^1 \left[a\sqrt{(k^2 - k_z^2)} \right]}, & n = \bar{n} \\ 0 & n \neq \bar{n} \end{cases} \tag{2.103}$$

The above is identical to expression (2.92) obtained for the free boundary conditions. The same term could also be obtained for the sine component, when sine expression for the odd system is employed instead of cosine term for the even system in Eq.(2.87), in solution of the Helmholtz equation.

The displacement functions in the above equations were obtained from the harmonic response due to a point harmonic force, which can be calculated as:

$$u(r, \theta) = -\frac{F}{\rho h} \omega_n^2 \sum_n^N \frac{U_n(r_f, \theta_f) U_n^T(r, \theta)}{(\omega^2 - \omega_n^2) + i2\varsigma_n(\omega/\omega_n)} \tag{2.104}$$

where U_n is the eigenfunction, r_f and θ_f are the radial and circumferential location of the excitation harmonic force and ς_n is the modal damping ratio.

2.7. Summary

This chapter presented the systematic formulations of the mathematical models for the in-plane vibration characteristics and acoustic properties of annular disks. The frequency parameters were obtained using exact solutions of the equations of motion and the Rayleigh-Ritz method for disks subject to free, clamped and flexible boundary conditions. The Rayleigh-Ritz method is extended to include the effect of boundary condition non-uniformity by employing distributed artificial springs along the circumferential direction. It has been observed that non-uniformity in the boundary conditions introduced additional coupling between modes with different nodal diameter

numbers, which in turn increased the degree of complexity in the system. The coupling effects would yield different solutions for the eigenvalue problems of the even and odd subsystems which caused the split of frequency parameters.

For rotating disks, the equations of motion were derived with respect to rotating and inertial frames. The presented formulation allowed the inclusion of non-uniform support and initial stiffening in the analysis. Rotational effects introduced coupling between even and odd systems and need to be solved simultaneously. Finally, the expressions for the acoustic properties of annular disks subject to non-uniform boundary conditions were derived. In the following chapters, the obtained results are presented and discussed.

3. IN-PLANE VIBRATIONS OF STATIONARY DISKS

The accuracy and applicability of the proposed methodologies in predicting the in-plane modal characteristics of annular disks are investigated in this chapter. The free vibration properties of the stationary annular disks with uniform boundary conditions, including flexible boundaries, are explored using the method described in the previous chapter. The validity of the method is demonstrated by comparing the results with the data reported in the literature. However, the reported studies on exact solutions have been limited to in-plane frequency analysis of the solid disks alone [15, 17]. The frequency parameters obtained from the exact frequency equations are subsequently used as a reference to examine the convergence property of the Rayleigh-Ritz method. The modal in-plane characteristics of annular disks are expected to be strongly influenced by various geometric properties, although the effects have been explored only in a few studies [2, 18].

In this study the Rayleigh-Ritz method is applied to study the effects of several geometric properties on the modal characteristics of annular disks. The model validity is further examined by comparing the mode shapes of disks with selected uniform boundary conditions with the reported model characteristics. It needs to be emphasized that the in-plane model characteristics of annular disks with non-uniform boundary conditions are not found in published literature. The discussions in this chapter are thus devoted to disks with uniform boundary conditions only, while the non-uniform support conditions are investigated in the subsequent chapter.

3.1.   Model Validations

The frequency equations derived for the annular disks with arbitrary radius ratios in section 2.2 could be evaluated to obtain the modal characteristics of the disks. The analytical models of the stationary disks subject to uniform boundary conditions, however, have been formulated using a number of simplifying assumptions. It is, thus, essential to verify the validity of the analytical model in predicting the in-plane vibration responses of the disks. The verification of the analytical formulations is generally performed through comparisons with a reference response that may be obtained from different methods or experimentally. The exact solutions for the in-plane vibration modes, however, have been obtained only for solid disks, while exact frequency parameters for annular disks could not be found in the published studies. Therefore, the exact frequency equations, derived in section 2.2, are evaluated numerically and compared with those reported for the solid disks with free or clamped outer edge. The validity of the exact solutions obtained for the annular disks is examined through comparisons of the exact solutions with those reported in the published studies on the basis of alternate approximate or numerical methods. The exact solutions were obtained from the Bessel's functions, as described in section 2.2. The resulting exact solutions of the frequency equations are then considered to serve as benchmark for verification of the solutions obtained using the approximate techniques for all the uniform boundary conditions, including the flexible boundaries.

In this section, the frequency parameters derived for different combinations of boundary conditions are compared with those reported in different studies for the solid disks to demonstrate the validity of the proposed formulation. For this purpose, the

85

frequency parameters of a solid disk with free and clamped outer edge are initially evaluated and compared with those reported by Holland [15] and Park [17], respectively. Tables 3.1 and 3.2 and summarize the frequency parameters of a solid disk with free and clamped outer edge conditions, respectively, derived from the exact solutions. The tables illustrate the results corresponding to a few selected modes. The obtained results were found to be identical to those reported in [15] and [17] for solid disks suggesting the validity of the solution methodology.

The exact frequency parameters for the annular disks were subsequently obtained under different combinations of boundary conditions at the inner and outer edges. The edge conditions are presented for the inner edge followed by that of the outer edge. For instance, a 'Free-Clamped' condition refers to free inner edge and clamped outer edge. The solutions obtained for conditions involving free and clamped edges ('Free-Free', 'Free-Clamped', ' Clamped-Clamped' and 'Clamped-Free') are compared with those reported by Irie et al. [20] in Tables 3.3 to 3.6, respectively. The simulation results were obtained for two different values of the radial ratios ($\beta = 0.2$ and 0.4), and $v = 0.3$. The results show excellent agreements of the values obtained in the present study with those reported in [20], irrespective of the boundary condition and radius ratio considered. It must be noted that for the solid disk with free edge and for free-free annular disk that natural frequencies for $n = 2$ case are lower than those for $n = 1$. The results suggest that the proposed frequency equations could serve as the reference for approximate methods on in-plane vibration characteristics of annular disks with different combinations of edge conditions.

Table 3.1: Exact frequency parameters of in-plane vibration of a solid disk with free edge ($v = 0.3$).

Mode	$n = 1$	$n = 2$	$n = 3$	$n = 4$
1	1.6176	1.3876	2.1304	2.7740
2	3.5291	2.5112	3.4517	4.4008
3	4.0474	4.5208	5.3492	6.1396
4	5.8861	5.2029	6.3695	7.4633
5	6.9113	6.7549	7.6186	8.5007
6	7.7980	8.2639	9.3470	10.2350
7	9.6594	8.7342	9.8366	11.0551

Table 3.2: Exact frequency parameters of in-plane vibration of a solid disk with clamped edge ($v = 0.33$).

Mode	$n = 1$	$n = 2$	$n = 3$	$n = 4$
1	1.9441	3.0185	3.0185	4.7021
2	3.1126	4.0127	4.0127	5.8985
3	4.9104	5.7398	5.7398	7.3648
4	5.3570	6.7079	6.7079	8.9816
5	6.7763	7.6442	7.6442	9.5296
6	8.4938	9.4356	9.4356	11.1087
7	8.6458	9.9894	9.9894	12.5940

Table 3.3: Frequency parameters of in-plane vibration of an annular disk with 'Free-Free' conditions ($v = 0.3$).

radius ratio	$n = 1$		$n = 2$		$n = 3$		$n = 4$	
	Reference [20]	present study	Reference [20]	present study	Reference [20]	present study	Reference [20]	present study
0.2	1.652	1.651	1.110	1.110	2.071	2.071	2.767	2.766
	3.842	3.842	2.403	2.402	3.401	3.400	4.389	4.388
0.4	1.683	1.682	0.721	0.721	1.618	1.619	2.482	2.482
	4.044	4.044	2.451	2.450	3.346	3.346	4.227	4.226

Table 3.4: Frequency parameters of in-plane vibration of an annular disk with 'Free-Clamped' conditions ($v = 0.3$).

radius ratio	$n = 1$		$n = 2$		$n = 3$		$n = 4$	
	Reference [20]	present study	Reference [20]	present study	Reference [20]	present study	Reference [20]	present study
0.2	2.104	2.103	2.553	2.553	3.688	3.688	4.712	4.711
	3.303	3.302	3.948	3.948	4.859	4.858	5.894	5.893
0.4	2.517	2.517	2.721	2.721	3.214	3.214	3.955	3.956
	3.508	3.508	4.147	4.147	4.998	4.998	5.874	5.873

Table 3.5: Frequency parameters of in-plane vibration of an annular disk with 'Clamped-Clamped' conditions ($v = 0.3$).

radius ratio	$n = 1$ Reference [20]	present study	$n = 2$ Reference [20]	present study	$n = 3$ Reference [20]	present study	$n = 4$ Reference [20]	present study
0.2	2.783	2.783	3.378	3.378	4.066	4.065	4.802	4.800
	4.060	4.060	4.360	4.359	5.104	5.103	6.003	6.001
0.4	3.429	3.429	4.023	4.022	4.707	4.707	5.287	5.286
	5.306	5.306	5.311	5.311	5.619	5.619	6.289	6.288

Table 3.6: Frequency parameters of in-plane vibration of an annular disk with 'Clamped-Free' conditions ($v = 0.3$).

radius ratio	n=1 Reference [20]	present study	n=2 Reference [20]	present study	n=3 Reference [20]	present study	n=4 Reference [20]	present study
0.2	0.919	0.919	1.542	1.541	2.157	2.157	2.778	2.777
	2.121	2.121	2.605	2.604	3.473	3.472	4.408	4.406
0.4	1.281	1.281	1.965	1.964	2.445	2.445	2.911	2.911
	2.691	2.691	2.908	2.907	3.604	3.603	4.492	4.491

It should be noted that the reported results were obtained using the exact frequency equations, which are applicable only for uniform boundary conditions. In this study, the Rayleigh-Ritz method formulation has been extended to study the modal behavior of annular disks subject to non-uniform boundary conditions. The accuracy and convergence properties of the Rayleigh-Ritz method are evaluated, although the analyses are limited to uniform boundary conditions only in this chapter.

3.2. Convergence Property of the Rayleigh-Ritz Method

The convergence of the frequencies obtained using the Rayleigh-Ritz method to the corresponding exacts values strongly relies upon three primary factors. These include the number of boundary characteristic orthogonal polynomials (BCOP) used in the analysis, and number of terms considered in the solutions for non-uniformities. The

stiffness parameters chosen to simulate a clamped boundary condition may also influence the accuracy of the convergence and the computational efficiency. In order to investigate the accuracy of the Rayleigh-Ritz method, a convergence study is conducted by considering different number of polynomials. The results are used to assess the accuracy of the solutions and the required number of the BCOP to be used in the model. The convergence of the frequency parameters with spring stiffness parameters varying from zero (free condition) to infinity (clamped conditions) is further investigated.

3.2.1. Effects of Number of Polynomials

The effect of number of polynomials (M) on the solutions in terms of the frequency parameter is investigated by considering a few lower modes. The solutions were initially obtained for $M = 2$ and the number of polynomials was increased in a sequential manner until the solution converged to the exact reported value within four significant figures. As an example, Tables 3.7 and 3.8 illustrate the frequency parameters corresponding to the lower modes of a solid disk with fixed and clamped outer edge, respectively, for different values of (M). The clamped boundary condition is applied through selection of a first polynomial that satisfies the zero deflection at the outer edge. The last row in both the tables show the exact values obtained from the frequency equations.

The results suggest that accurate frequency parameters of in-plane vibration of solid disks could be obtained by considering M in the order of 3 to 4. Tables 3.9 and 3.10 show the convergence of the frequency parameters of annular disks with radius ratios of 0.2 and 0.6, respectively, with free boundaries. The results were obtained for M ranging

from 2 to 10 in case of the $\beta = 0.2$ and from 2 to 6 for $\beta = 0.6$. The simulations revealed numerically stable solutions for the ranges of M considered. The lower frequency parameters tend to converge more rapidly than those of the higher modes. A larger number of polynomials is thus required in order to assure the convergence of the first five modes to four significant figures. Based upon these results, ten polynomials were used in the subsequent calculations, unless otherwise specified.

Table 3.7: Influence of number of polynomials on the convergence of the frequency parameters of a solid disk with free outer edge ($v = 0.3$).

M	(0,2)	(1,1)	(0,0)r	(0,3)	(1,2)
2	1.3915	1.6599	2.0519	2.3015	2.6210
3	1.3883	1.6177	2.0490	2.1332	2.5285
4	1.3876	1.6176	2.0488	2.1312	2.5117
5	1.3876	1.6176	2.0488	2.1304	2.5112
6	1.3876	1.6176	2.0488	2.1304	2.5112
7	1.3876	1.6176	2.0488	2.1304	2.5112
Exact	1.3876	1.6176	2.0488	2.1304	2.5112

r: pure radial mode;

Table 3.8: Influence of number of polynomials on the convergence of the frequency parameters of a solid disk with clamped outer edge ($v = 0.33$).

M	(0,1)	(0,0)θ	(0,2)	(1,1)	(0,0)r
2	1.9442	2.2290	3.0367	3.1956	3.8508
3	1.9442	2.2178	3.0213	3.1154	3.8318
4	1.9441	2.2178	3.0185	3.1136	3.8317
5	1.9441	2.2178	3.0185	3.1130	3.8317
6	1.9441	2.2178	3.0185	3.1130	3.8317
Exact	1.9441	2.2178	3.0185	3.113	3.8317

r: pure radial mode; θ: pure circumferential mode.

Table 3.9: Influence of number of polynomials on the convergence of the frequency parameters of an annular disk with free edges ($\beta = 0.2; v = 0.3$).

M	(0,2)	(1,1)	(0,0)r	(0,3)	(1,2)
2	1.1493	1.6778	1.8211	2.1481	2.4455
3	1.1273	1.6513	1.8063	2.0847	2.4093
4	1.1169	1.6512	1.8025	2.0754	2.4047
5	1.1126	1.6512	1.8017	2.0731	2.4030
6	1.1108	1.6512	1.8015	2.0717	2.4026
7	1.1102	1.6512	1.8015	2.0711	2.4025
8	1.1100	1.6512	1.8015	2.0708	2.4024
9	1.1100	1.6512	1.8015	2.0708	2.4024
10	1.1100	1.6512	1.8015	2.0707	2.4024
Exact	1.11	1.6512	1.8015	2.0707	2.4024

r: pure radial mode;

Table 3.10: Influence of number of polynomials on the convergence of the frequency parameters of an annular disk with free edges ($\beta = 0.6; v = 0.3$).

M	(0,2)	(0,3)	(0,0)r	(1,1)	(0,4)
2	0.4253	1.0687	1.2201	1.6196	1.8055
3	0.4186	1.0451	1.2197	1.6179	1.7573
4	0.4182	1.0431	1.2197	1.6178	1.7524
5	0.4181	1.0430	1.2197	1.6178	1.7520
6	0.4181	1.0430	1.2197	1.6178	1.7519
Exact	0.4181	1.0430	1.2197	1.6178	1.7519

r : pure radial mode.

3.2.2. Effect of Stiffness Parameters

The rate of convergence of the frequency parameters of an annular disk with artificial springs distributed uniformly along the inner or outer edges is strongly dependent upon the chosen stiffness parameters. Higher values of the stiffness parameter

yield higher frequency parameters and approach those of a disk with a clamped edge. For the current analysis, the stiffness parameters along radial and circumferential directions are assumed to be equal. The variations in the frequency parameters with unequal stiffness parameters will be discussed in the next section. The influence of variations in the stiffness parameters on the in-plane vibration frequency parameters are investigated for both the solid and the annular disk with uniformly distributed artificial springs along the outer edge.

The influences of variations in the stiffness parameter on the frequency parameters corresponding to selected models of a solid disk elastically constrained along the outer edge are shown in Table 3.11. Table 3.12 presents the convergence rate of an annular disk with artificial springs along the inner edge for different values of the stiffness parameters. The tables also list the exact frequency parameters of the disks with free and clamped edge. The results suggest that a stiffness value exceeding 10^5 would be sufficient to simulate the clamped boundary with estimated frequency precision to four significant figures. The first two frequency parameters of the solid disk (0,0) and (0,1)θ represent the rigid body modes under a free boundary condition. The values of these frequency parameters increase with increasing stiffness parameters and approach those of a clamped disk as the stiffness exceeds 10^5. The frequency parameters of the annular disk (Table 3.12) also exhibits similar tendency. From the results, it can be concluded that the convergence can be achieved relatively rapidly with increasing stiffness parameters and the number of polynomials.

Table 3.11: Convergence of the frequency parameters of a solid disk with artificial springs uniformly distributed along the outer edge as the spring parameters increase $(v = 0.33)$.

(m,n)	(0,1)	(0,0)θ	(0,2)	(1,1)	(0,0)r	(0,3)	(1,2)
Free	0	0	1.3579	1.5945	2.0674	2.0863	2.4776
10^{-1}	0.4318	0.6169	1.4321	1.7140	2.1266	2.1465	2.5771
10^{0}	1.1104	1.5805	1.8812	2.3538	2.5312	2.5614	3.1437
10^{1}	1.7750	2.1426	2.7458	3.0056	3.4898	3.5663	3.8550
10^{2}	1.9256	2.2103	2.9886	3.1022	3.7937	3.8749	3.9960
10^{3}	1.9423	2.2170	3.0154	3.1119	3.8279	3.9080	4.0115
10^{4}	1.9440	2.2177	3.0181	3.1129	3.8313	3.9112	4.0125
10^{5}	1.9441	2.2178	3.0184	3.1130	3.8317	3.9116	4.0126
10^{6}	1.9441	2.2178	3.0185	3.1130	3.8317	3.9116	4.0127
Clamped	1.9441	2.2178	3.0185	3.1130	3.8317	3.9116	4.0127

r: pure radial mode; θ: pure circumferential mode.

Table 3.12: Convergence of the frequency parameters of an annular disk with artificial springs uniformly distributed along the inner edge as the spring parameters increase $(\beta = 0.6; v = 0.3)$.

(m,n)	(0,0)θ	(0,1)	(0,2)	(0,3)	(0,0)r	(1,1)	(0,4)
Free	0	0	0.4181	1.0430	1.2197	1.6178	1.7519
10^{-1}	0.3959	0.5444	0.7557	1.2292	1.3579	1.6833	1.8687
10^{0}	1.0267	1.3608	1.7765	2.0905	2.1102	2.1883	2.5165
10^{1}	1.5462	1.8527	2.5178	3.1254	3.4504	3.4527	3.4828
10^{2}	1.6496	1.9411	2.5984	3.2782	3.8683	3.8583	3.6972
10^{3}	1.6610	1.9509	2.6067	3.2921	3.9181	3.9065	3.7198
10^{4}	1.6622	1.9518	2.6076	3.2934	3.9232	3.9114	3.7220
10^{5}	1.6623	1.9519	2.6077	3.2936	3.9237	3.9119	3.7223
10^{6}	1.6623	1.9519	2.6077	3.2936	3.9237	3.9119	3.7223
Clamped	1.6623	1.9519	2.6077	3.2936	3.9237	3.9119	3.7223

r: pure radial mode; θ: pure circumferential mode.

3.2.3. Influences of Boundary Conditions

The results presented in Tables 3.1 to 3.12 demonstrate the effectiveness of the Rayleigh-Ritz method in predicting the modal characteristics of annular disks with good accuracy. The frequency parameters of the annular disk are further investigated for boundary conditions involving different combinations of free, clamped and elastic edges. The solutions corresponding to selected modes are obtained for the 'Elastic-Free', 'Elastic-Clamped', 'Elastic-Elastic', 'Free-Elastic' and 'Clamped-Elastic' conditions. The results obtained for these boundary conditions are presented in Table 3.13. The results were obtained for $\beta = 0.2$ and $v = 0.3$, while the non-dimensional radial and circumferential stiffness parameters were chosen as , $\overline{K}_r = 1$ and $\overline{K}_\theta = 1$. The results presented for a few lower modes are compared with those obtained from the exact solution. The comparisons reveal very good agreement between the exact and the approximate results irrespective of the boundary condition considered, further verifying the effectiveness of the proposed method.

Table 3.13: Frequency parameters of in-plane vibration of an annular disk with flexible boundary conditions.

Boundary conditions	$n = 1$		$n = 2$		$n = 3$		$n = 4$	
	Rayleigh-Ritz	Exact	Rayleigh-Ritz	Exact	Rayleigh-Ritz	Exact	Rayleigh-Ritz	Exact
Elastic-Free	0.771	0.771	1.408	1.408	2.121	2.121	2.772	2.772
	1.906	1.906	2.524	2.524	3.444	3.444	4.397	4.397
Elastic-Clamped	2.590	2.590	3.117	3.116	3.928	3.926	4.759	4.760
	3.625	3.625	4.134	4.136	5.000	5.001	5.957	5.957
Elastic-Elastic	1.494	1.492	1.815	1.813	2.474	2.472	3.123	3.120
	2.603	2.601	3.209	3.207	4.004	4.002	4.859	4.857
Free-Elastic	1.040	1.046	1.505	1.504	2.414	2.416	3.114	3.116
	2.432	2.432	3.018	3.018	3.895	3.896	4.833	4.834
Clamped-Elastic	1.686	1.686	1.960	1.959	2.514	2.512	3.129	3.127
	2.764	2.765	3.319	3.317	4.061	4.060	4.879	4.877

3.3. Factors Affecting In-Plane Vibration of Annular Disks

The frequency parameters of an annular disk are strongly affected by the geometry and the boundary conditions of the disk. This section is devoted to investigate the relation between the frequency parameters and several geometric and boundary conditions parameters.

3.3.1. Influence of the Constraints Stiffness

The stiffness parameters of the artificial springs introduced at the boundary further affect the frequency parameters, as illustrated in Tables 3.11 and 3.12. The effects of variations in the stiffness parameters along each direction (radial and circumferential) on the frequency parameters are also investigated. For this purpose, the artificial springs are introduced along the radial and the circumferential directions on the outer edge of an annular disk ($\beta = 0.2$; v=0.3).The inner edge of the disk, however, is assumed to be free.

Figure 3.1 illustrates the influence of spring stiffness at the outer edge on the frequency parameters for selected modes. The figures illustrate the influences of different combinations of non-dimensional spring stiffness parameters along the radial direction, $\overline{K}_r = K_r R(1 - v^2)/Eh$ and along the circumferential direction, $\overline{K}_\theta = K_\theta R(1 - v^2)/Eh$, on the frequency parameter. The frequency parameters are expressed by the frequency ratio, $\bar{\lambda}_{m,n} = \lambda_{m,n}/(\lambda_f)_{m,n}$, where $(\lambda_f)_{m,n}$ is the frequency parameter corresponding to the disk with free edge, shown in Table 3.3. The results suggest that the frequency increase with increase in $\overline{K}_r$ and $\overline{K}_\theta$. The frequency corresponding to the lower modes increases more significantly with increase in $\overline{K}_r$ than $\overline{K}_\theta$. For higher modes, the effect of

$\overline{K}_\theta$ becomes more significant, although the influence of spring constant becomes less significant as *m* and *n* increase. These suggest that the lower modes are significantly influenced by $\overline{K}_r$, while $\overline{K}_\theta$ affects frequencies of the higher modes. The variations in the frequency parameters are rapid at lower stiffness values for all modes. The figure also shows the frequency parameters of the disk constrained by the radial springs alone in the X-Z plane ($\overline{K}_\theta = 0$) or by the circumferential springs alone in the Y-Z plane ($\overline{K}_\theta = 0$). These boundary conditions are similar to those reported for rectangular disks where the normal displacement is constrained while the tangential displacement remains free or vice-versa, referred to as "simply-supported" boundary condition [106].

From the formulations, presented in section 2.3, it is evident that the frequency parameters would be affected by a number of geometric parameters, namely, the thickness, radius ratio and the outer radius of the annular disk. The effect of radius ratio on the frequency parameters has been discussed by Ambati et al. [18] for an annular disk with free boundary conditions only. In this study, the effects of each parameter on the natural frequencies of the disk are investigated, for the general boundary conditions at the inner and outer edges.

3.3.2. Influence of Radius Ratio

The effect of radius ratio of the annular disk on the frequency parameters are illustrated in figures 3.2 to 3.7 for different boundary conditions. The frequency parameters follow different trends as the radius ratio varies between zero (solid disk) and unity (thin ring). For a disk with free boundary conditions, three different trends are observed. The first trend is for modes with nodal diameters but no nodal circles (*m*=0).

These frequency parameters approach zero as the radius ratio approaches unity as shown

in Figure 3.2. The figure shows the variations in frequency parameters for free disk with

Poisson's ratio of 0.3. In addition to the modes shown, there exist two rigid body modes

with zero values for the free disk, irrespective of the radius ratios. These include the body

translation $(0,1)$ and body rotation $(0,0)\theta$.
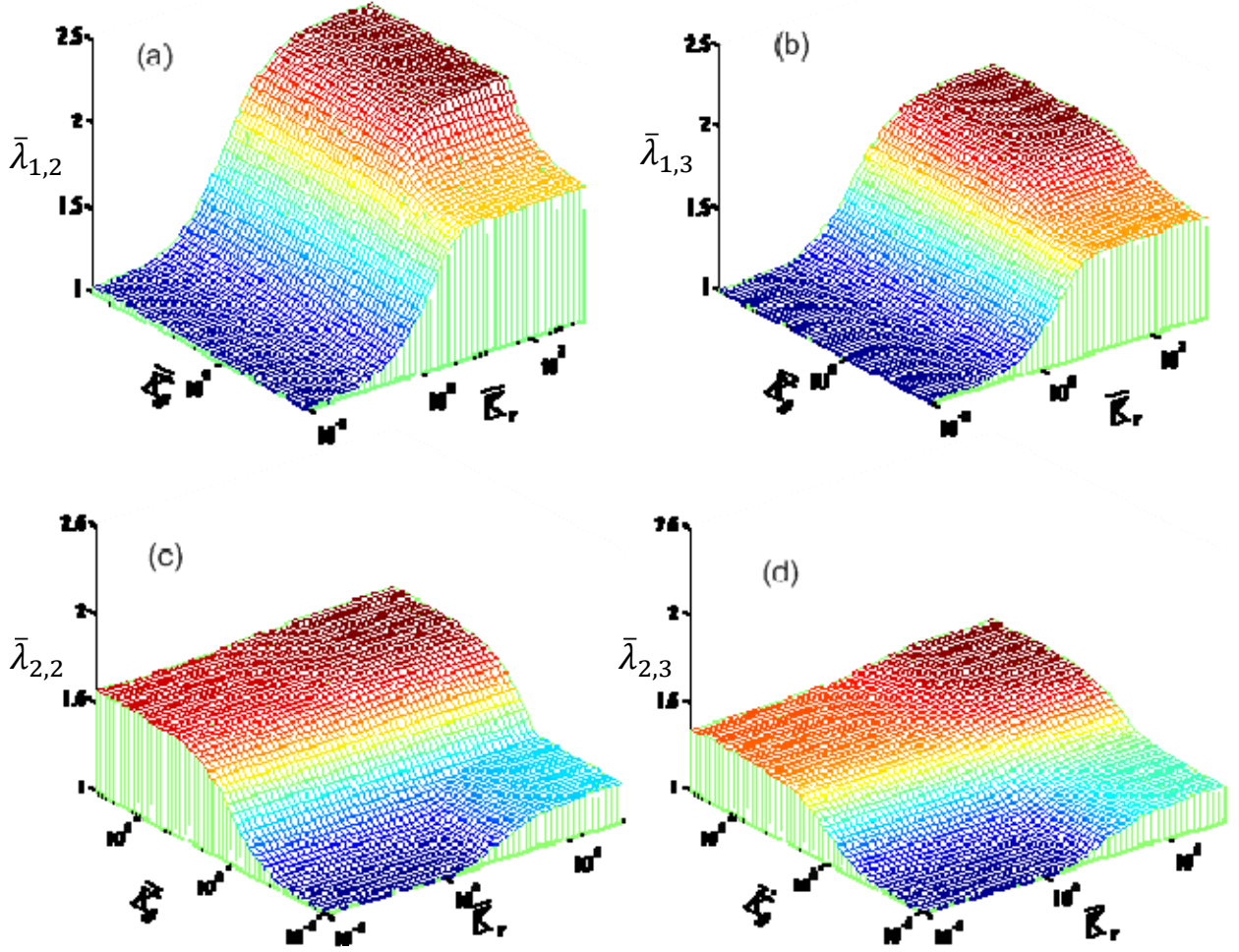
Figure 3.1: Influences of variations in the non-dimensional radial $(\bar{K}_r)$ and circumferential stiffness $(\bar{K}_\theta)$ at the outer edge of the disk on the normalized frequency parameters $\left(\bar{\lambda}_{m,n} = \lambda_{m,n}/(\lambda_f)_{m,n}\right)$; $v = 0.3; \beta = 0.2.$

The second group of modes is those where the frequency parameters approach

finite values for the thin rings as increasing the radius ratio. These frequency parameters

97

are shown in Figure 3.3. The mode $(0,0)r$ is the pure radial mode, which approaches the mode that is referred to as the "breathing mode" of thin rings ($\beta \approx 1$). All the remaining modes in Figure 3.3 have one nodal circle number m and approach the extensional ring modes with increasing radius ratio. It should be noted that the frequency parameter of the $(0,0)r$ mode is greater than that of $(1,1)$ mode for low radius ratios but it becomes lower than that of the $(1,1)$ mode as the radius ratio exceeds 0.3. The third group of modes includes all the remaining modes that approach infinity as the radius ratio approaches unity. This group includes modes with nodal circle number $m \geq 2$ as shown in Figure 3.4. Modes with same nodal circles number used to group with each other and follow the same path to infinity, as shown in the figure. These modes exhibit different behavior in the middle range of radius ratios. At radius ratios $\beta = 0.3$ to 0.5, for instance, several modes become close to each other and cross over. Pure torsional or radial modes join the nearest group of m and follow their path to infinity as shown in the figure.
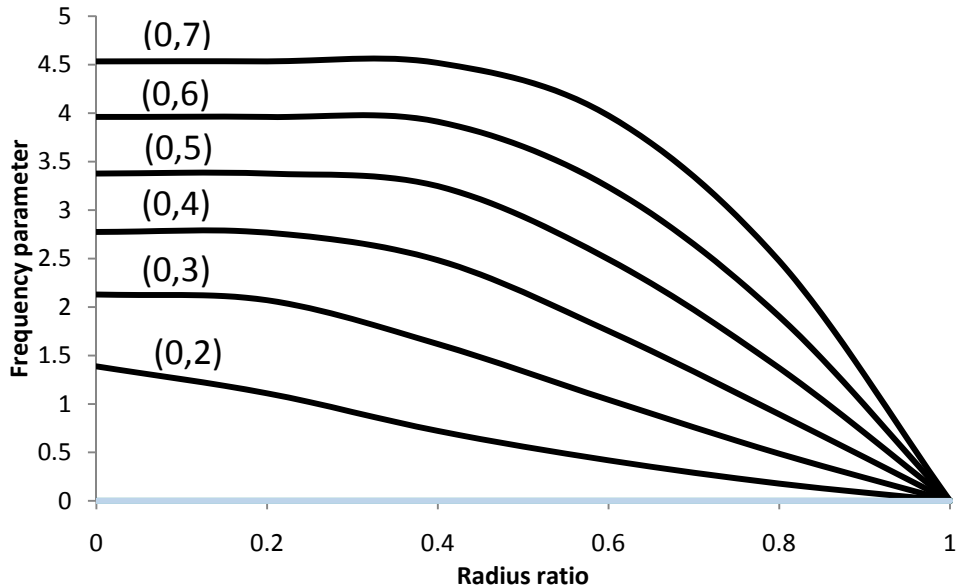
Figure 3.2: Variations in frequency parameters of modes with zero nodal circle as a function of the radius ratio ($v = 0.3$); free boundary conditions.
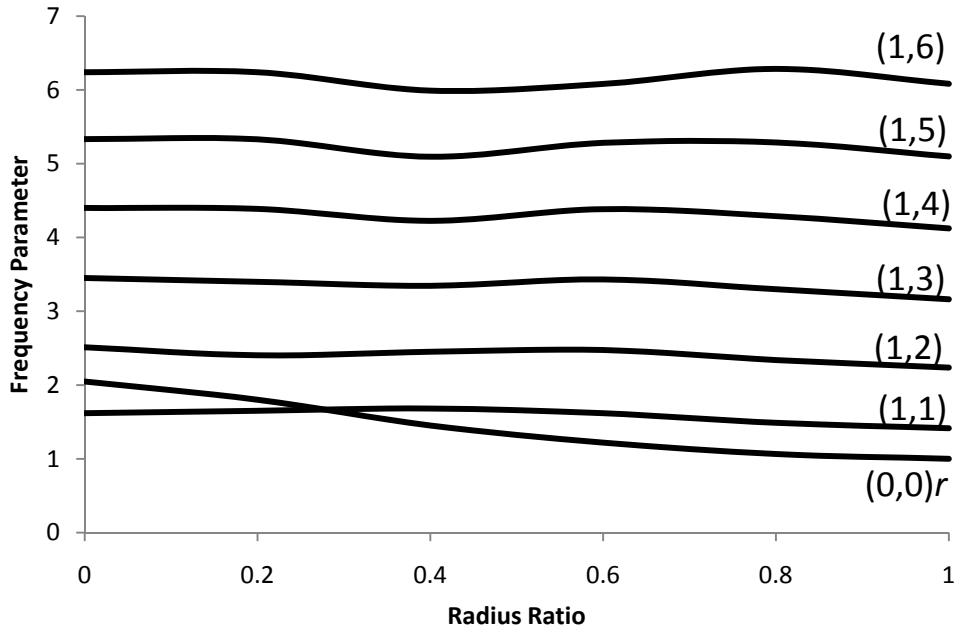
Figure 3.3: Variations in the frequency parameters of the finite modes as a function of the $(v = 0.3)$; free boundary conditions.
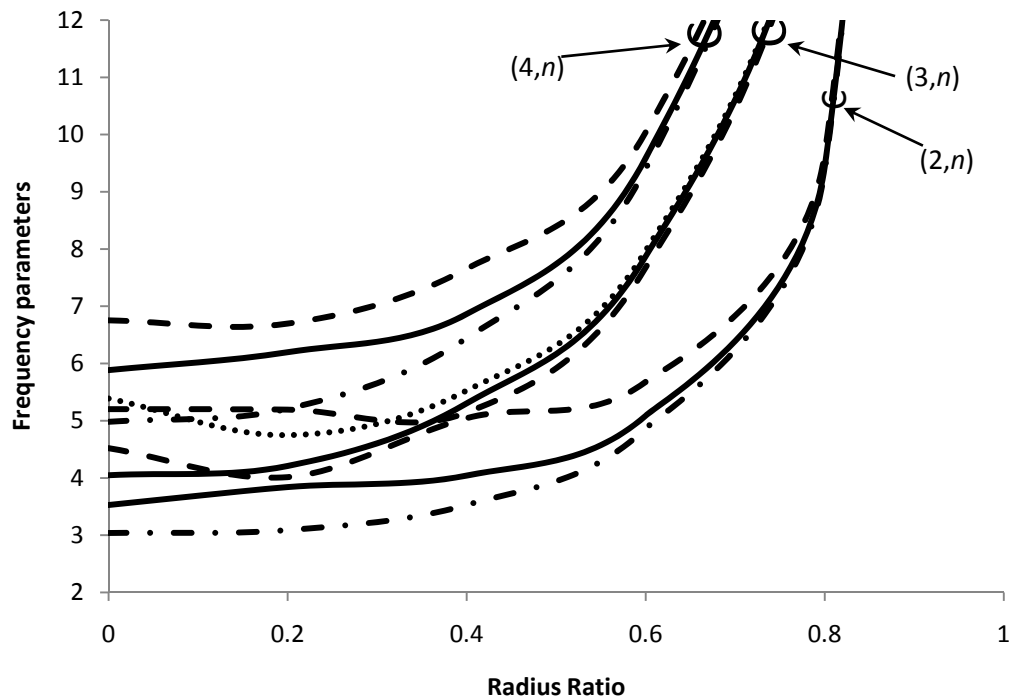
Figure 3.4: Variations in the frequency of parameters of the infinite modes versus radius ratio $(v = 0.3)$ for free boundary conditions, ———$n = 1$, – – – – – $n = 2$, ⋯⋯⋯⋯ radial modes, — . — . — torsional modes.

For an annular disk with uniformly clamped inner edge, as the radius ratio increases, the degrees of freedom of the resulting ring are constrained by the clamped edge, which yields extremely rigid constraints. The frequency parameters corresponding to all of the modes thus approach infinity as the radius ratio approaches unity as shown in Figure 3.5. It is, however, important to examine the trends in frequency parameters of different modes in the middle range of radius ratios, which could permit the grouping of the modes or changing their order with variations in the radius ratio. Figure 3.5 shows variations in the frequency parameters of the lowest four nodal circle number (m) as a function of the radius ratio.

It is apparent that frequency parameters of modes with same m tend to group together as they approach infinity with increasing value of β. As the nodal circle number increases, the frequency parameters approach infinite more rapidly. For a solid disk ($\beta = 0$), although the inner edge is clamped, there exists a rigid body rotational mode. This is due to the fact that the torsional stiffness at the inner radius becomes very small when the radius ratio approaches zero. At radius ratios close to unity, some ill-conditioning was observed in the numerical evaluations since the annular disk reduces to a rigid thin ring.

3.3.3. Influence of Disk Diameter

The in-plane vibration properties of the annular disks are evaluated in terms of non-dimensional frequency parameters, for different the radius ratios. In order to study the effect of disk diameter on the in-plane vibration properties, the natural frequencies in Hertz are obtained from the frequency parameters. This may be of particular importance

100

in the design stages and has been used to specify the dimensions of the disks used in the experimental part of this dissertation research. The effect of variations in the diameter is investigated for different radius ratios, while the material properties are the same as those specified in experimental investigations, see Table 4.5 in the next chapter.
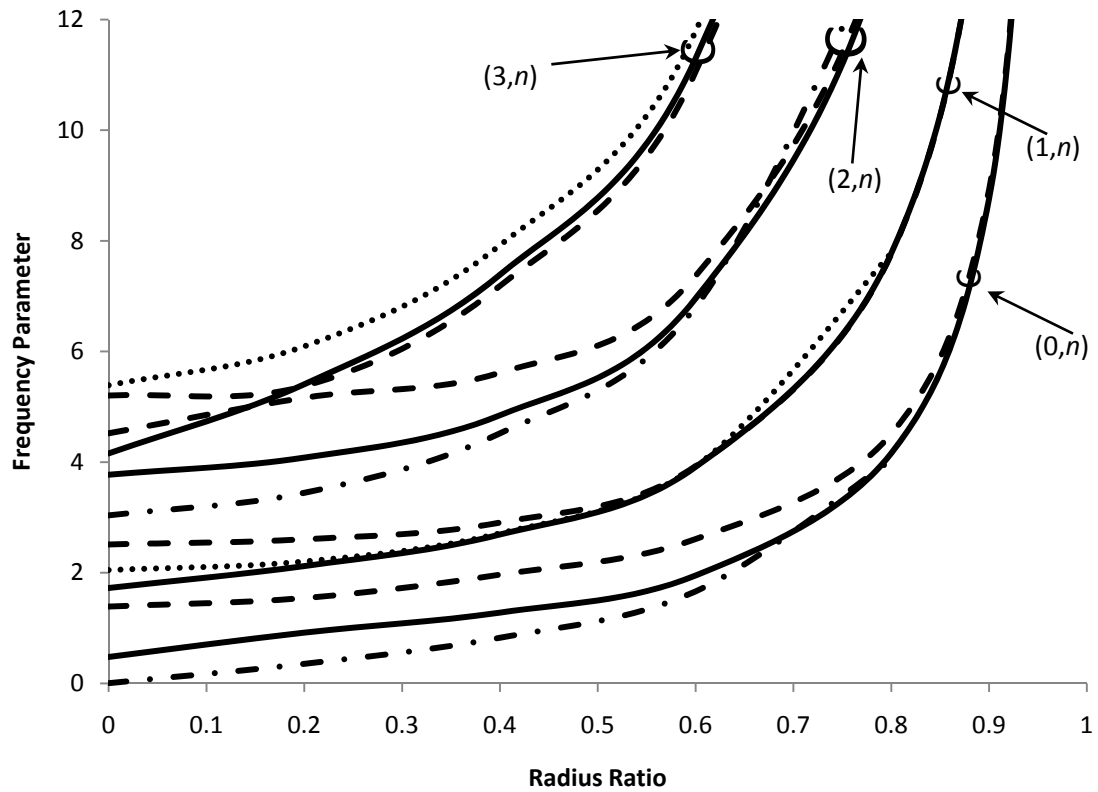
Figure 3.5: Variations in frequency parameters as a function of the radius ratio for a disk with inner clamped edge ($v = 0.3$), ————$n = 1$, – – – – – $n = 2$, ················ radial modes, — · — · — torsional modes.

Generally, the natural frequency is inversely proportional to the outer radius, as it can be deduced from Eq. (2.38). The effect of radius on the natural frequency, however, would be different for each mode depending on the radius ratio. The effect of variations in the outer radius of an annular disk is thus evaluated for four different radius ratio

(β = 0.2, 0.4, 0.6 and 0.8). The analysis is performed for frequencies corresponding to various modes, while the results are presented for four modes: (0,2)θ, (1,1), (0,3) and (1,0), in Figure 3.6, for the disk with free-free boundary conditions. The presented four modes belong to different groups with respect to their variations with the radius ratio as described above. The results are presented for different values of outer radius, ranging from 0.05m to 0.35m. The results show that the natural frequencies decrease with increasing diameter, irrespective of β. The decrease in frequency with increasing diameter is more significant for lower value of β, as it would be expected. Figure 3.6 (a) and (c) are the two modes that converge to zero as the radius ratio approaches unity, see Figure 3.2.

For this group the range of variation of natural frequencies is the largest for solid disks and decreases as the radius increases. Figure 3.6 (b) is the mode that converges to a finite ring mode, see Figure 3.3, which is nearly unaffected by the change in the radius ratio. The third type of modes are those for which natural frequencies increase as the radius ratio increases, which are shown in Figure 3.6 (d). These modes have opposite trend to the first group, Figure 3.6 (a) and (c). The lowest natural frequencies are for solid disks while it increases as the radius ratio increases.

Similarly, Figure 3.7 shows the variation for an annular disk with clamped inner edge. Since all modes approach infinity as the radius ratio increases, they all follow same trend as in Figure 3.6 (d). The disk in Figure 3.7 (a) has a rigid body mode for solid disk and is always zero.
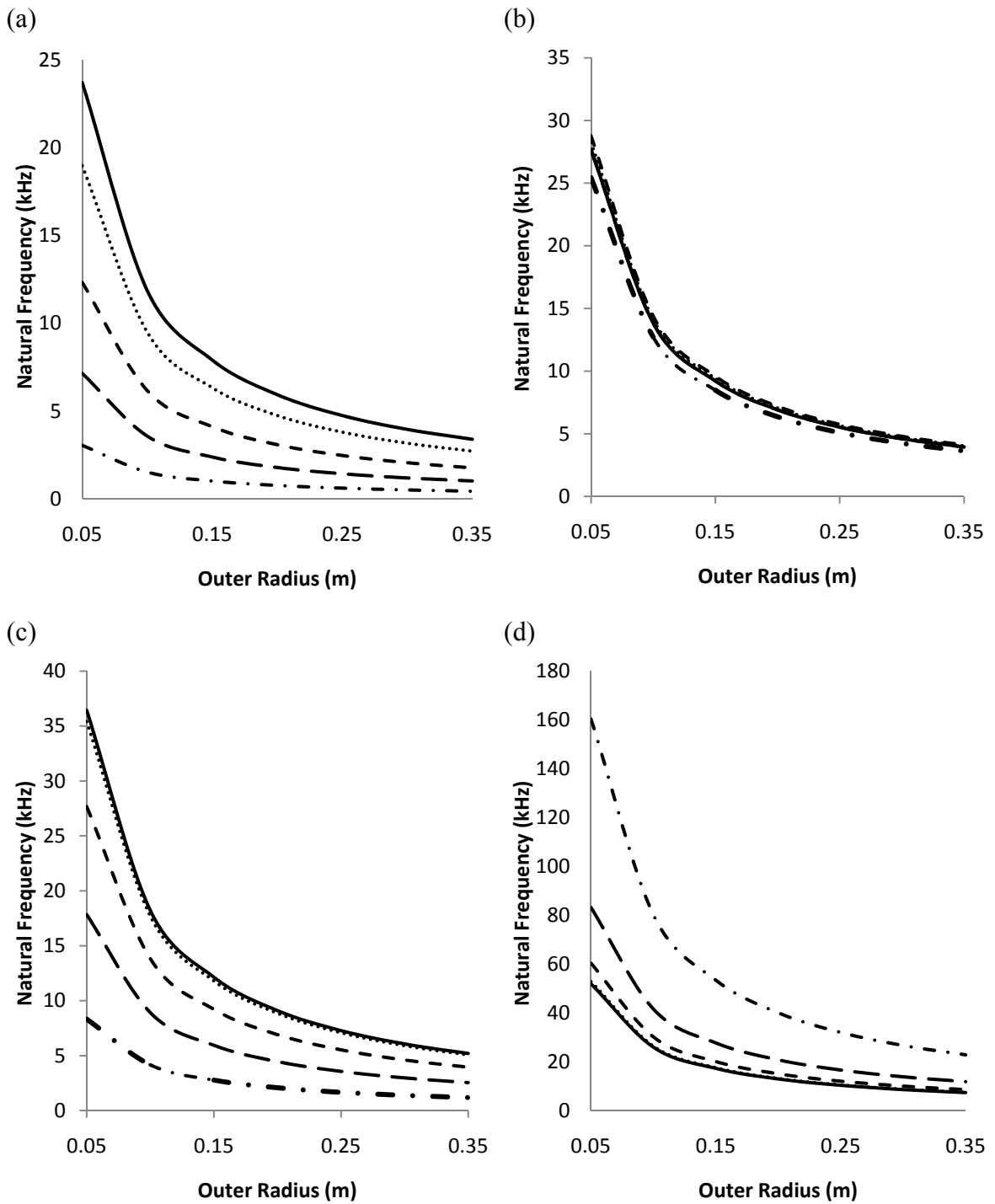
Figure 3.6: Variation in the natural frequencies of disk with free edges with respect to the outer radius: (a) mode (0,2), (b) mode (1,1), (c) mode (0,3) and (d) mode (1,0)θ. ——— $\beta = 0$, ··················· $\beta = 0.2$, – – – – – $\beta = 0.4$, — — — · $\beta = 0.6$, — · — · — $\beta = 0.8$.

103

(a)

(b)

(c)

(d)
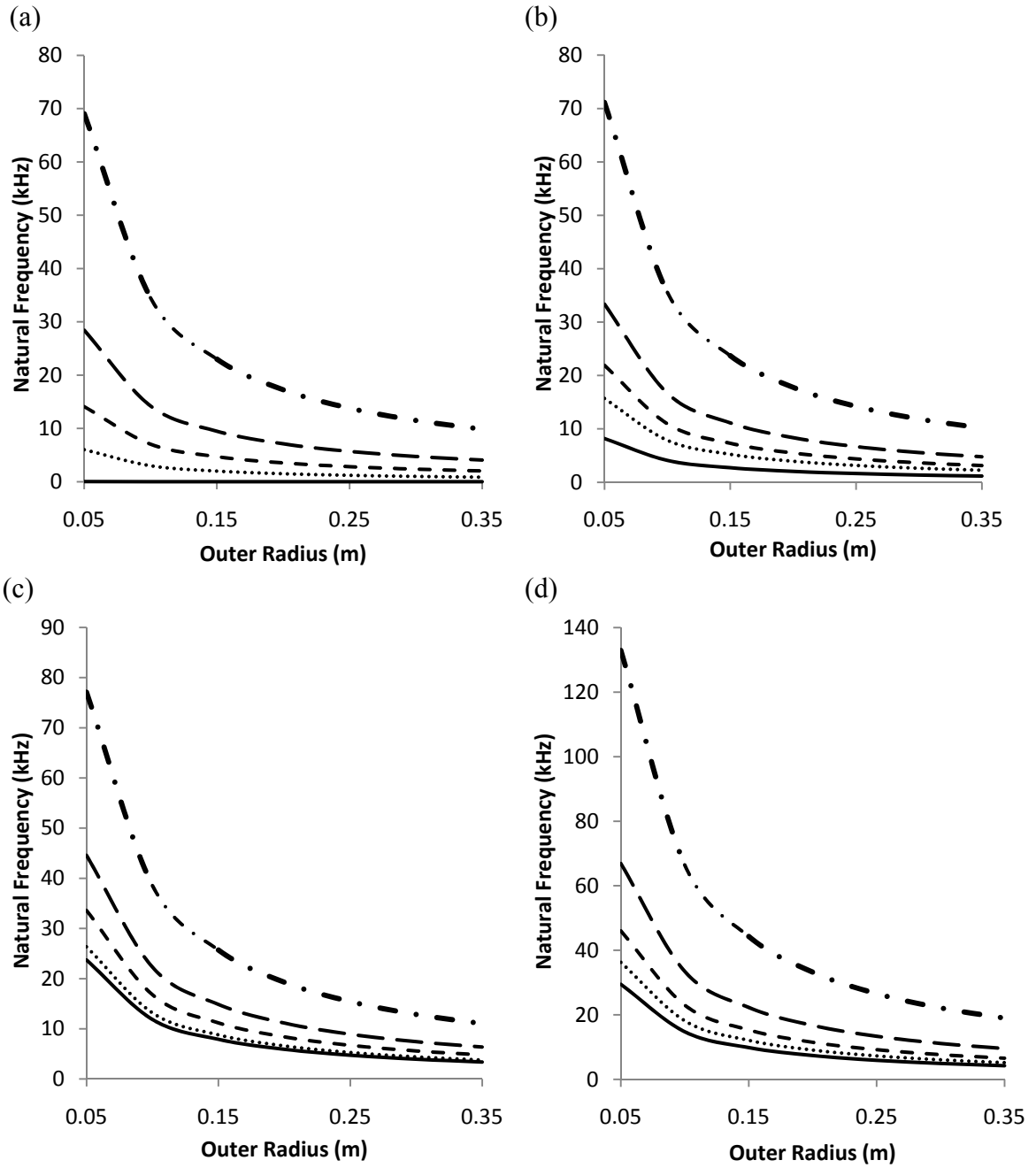
Figure 3.7: Variation of the natural frequencies of disk with clamped inner edge with respect to the outer radius: (a) mode $(1,0)\theta$, (b) mode $(1,1)$, (c) mode $(1,2)$, (d) mode $(2,1)$. ——— $\beta = 0$, ... $\beta = 0.2$, – – – – – $\beta = 0.4$, — — — . $\beta = 0.6$, — . — . — $\beta = 0.8$.

104

3.3.4. Influence of Disk Thickness

The third geometric parameter that is considered in the free in-plane vibration problems is the thickness of the disk. Several studies have investigated the effect of the thickness on the frequency parameters [2, 16, 36]. Equation (2.38) shows that the thickness of the disk can be eliminated from the formulations which suggests that the frequency parameters are unaffected by the thickness of the disk. This assumption is valid only for thin disks. Kane and Mindlin [107] suggested that the effect of thickness can be neglected for circular disks with thickness to radius ratios less than 0.2. Therefore, the thickness effect on the in-plane modes of vibration has to be studied for thick disks only on the basis of three-dimensional thick disks models. The variations of the radial and circumferential displacements along the normal direction have to be considered which will result in symmetric and anti-symmetric modes along the normal direction.

3.4.   Mode Shapes

Radial distributions of the modal deflections are depicted in Figure 3.8 for a few selected modes for a solid disk with clamped outer edge. The mode shapes exhibit harmonic distributions of the circumferential variations. The mode shapes clearly show that the center of the disk is always a nodal point with zero deflection for all the modes. This was evident for all the boundary conditions considered, except for modes with $n = 1$. This can attributed to the fact that, for any mode that corresponds to $n \neq 1$, a displacement component of the center at an angle θ is offset by an equal displacement in the opposite direction, $\theta+\pi$. For $n = 1$, the component of the displacement at $\theta+\pi$ is added to the response at θ due to the change of the sine and cosine functions when the

105

angle is increased by π [16]. This concludes that modes with $n = 1$ are the only group of modes that involve movement of the center. Therefore, the disk can be decoupled from any other components, i.e. the shafts, when calculating the modes other than n=1 modes. The motion of the center, however, needs to be specified for modes with n=1. This is probably the reason that Thompson [1] included the axle in his finite element model involving the one-nodal diameter modes of a railway wheel and excluded it from the vibrations corresponding to other modes.

The mode shapes of an annular disk ($\beta = 0.2$) with free inner and outer edges are shown in Figure 3.9 for the first five modes. The figure shows the radial variations in the circumferential and radial displacements in the left column and a two-dimensional contour plot of the deformed shape of the disk, which can be obtained by a vector sum of both displacements in the right column. The dashed line in deformed shape represents the initial shape of the inner and outer edges of the disk. Darker shadings in the contour plots represent zero displacements, while the regions of maximum displacements are represented by lighter shadings. The nodal diameters are clearly shown as dark shadings along the disk. The nodal circle of the first torsional mode (0,1) is shown in the figure, while the nodal circle for mode (1,1) is not clearly shown in the deformed shapes since it appears on the circumferential displacement only.

3.5.   Summary

This chapter discussed the free vibrations of in-plane modes of annular disk subject to uniform boundary conditions. The accuracy of the results is demonstrated by comparison of the results with the data reported in the literature. The exact frequency

equations were used to assess the convergence property of the Rayleigh-Ritz method. The effect of stiffness parameter, radius ratio and outer radius on the natural frequencies of the disk is investigated. The frequency parameters follow different trends as the radius ratio increases for free disks, while they all approach infinity for disks with clamped edge. The mode shapes of solid disks illustrated that modes with $n = 1$ are the only group of modes that involve movement of the center of the disk, while other modes have zero displacement at the center regardless of the boundary conditions. This chapter was devoted to the discussion of stationary disks subject to uniform boundary conditions, while disks subject to non-uniform supports are investigated in the subsequent chapter.
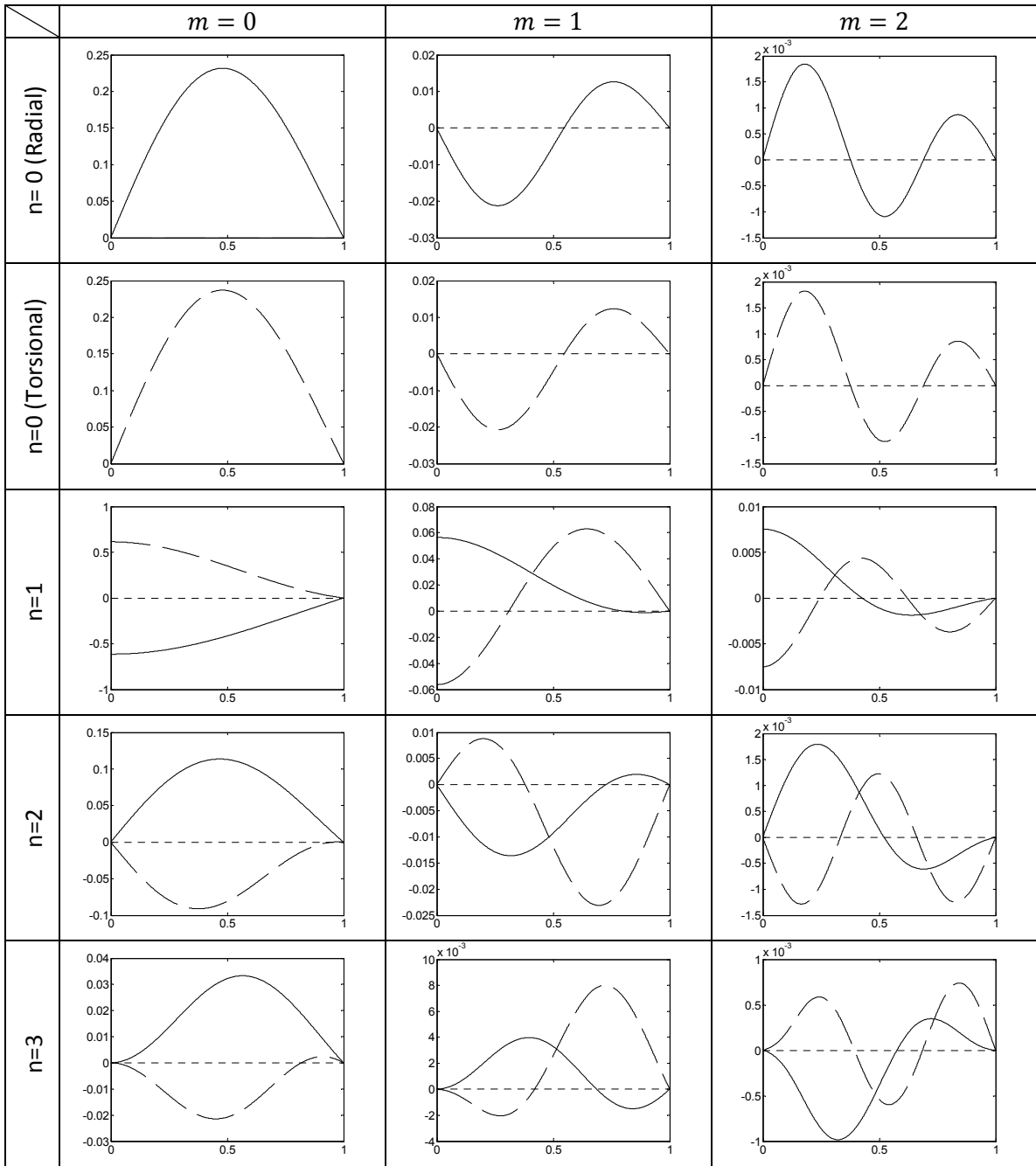
Figure 3.8: Radial and circumferential mode shapes for a solid disk clamped at the outer edge, (horizontal axis is the radial variation; ⎯⎯⎯ radial displacement, ⎯ ⎯ ⎯ ⎯ circumferential displacement).
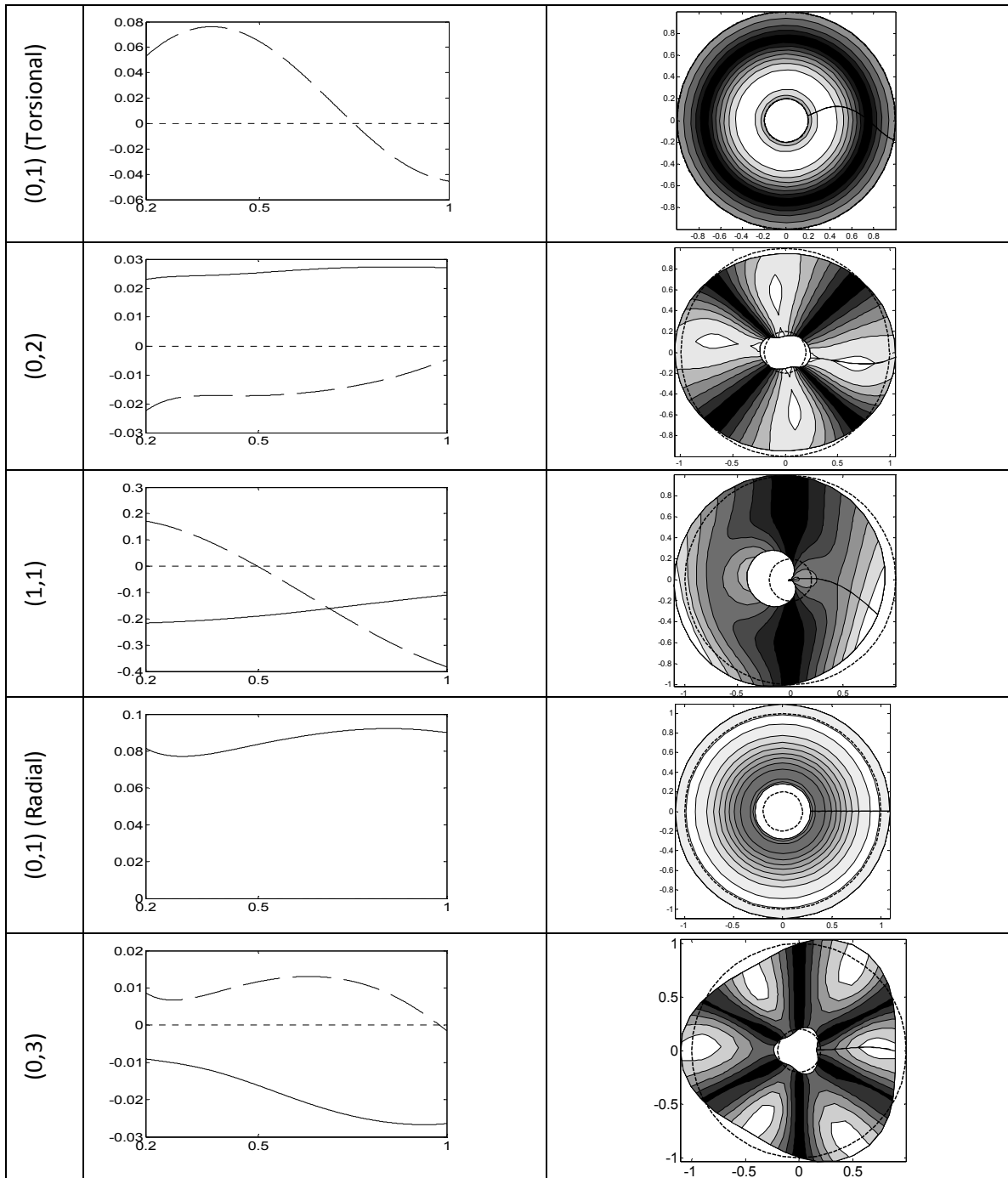
Figure 3.9: Radial and circumferential mode shapes and deformed shapes of an annular disk with free inner and outer edges; ———— radial displacement, _ _ _ _ _ circumferential displacement.

4. IN-PLANE VIBRATIONS OF ANNULAR DISKS WITH NON-UNIFORM BOUNDARY CONDITIONS

4.1.   Introduction

In the previous chapter, in-plane vibration properties of annular disks were investigated under boundary conditions with uniform distribution along the circumferential direction. In this case, the admissible functions could be easily selected to satisfy the geometric boundary conditions at both the inner and outer edges of the annular disks. The uniformity of the boundary conditions simplified the analysis and reduced the required computational effort for solving the vibration problem. In many applications, the disks may involve discrete supports at a given point or over a partial circumference of the disks or have a contact with some other components that constrain only a partition of the edge. The methodology presented in section 2.4 could be employed to investigate the in-plane modal characteristics of solid and annular disks subject to different types of non-uniform boundary conditions.

The validity of the proposed method is examined in this chapter. For this purpose, a finite element model of the disk is formulated and analyzed and laboratory experiments are performed to obtain frequency parameters under selected boundary conditions. Both the numerical results and the experimental data are used to demonstrate the validity of the proposed method. The convergence of the Rayleigh-Ritz method for solutions of problems with non-uniform boundary conditions is investigated and discussed.

The solutions are obtained for both the odd and even subsystems for evaluations of the frequency parameters and the mode shapes, for various combinations of classical and non-uniform boundary conditions. Two-dimensional contour plots of the mode shapes are presented for selected modes to evaluate the effect of the constraints on the radial and circumferential displacements. Both the vibration and acoustic properties of an annular disk subject to different combinations of boundary conditions are discussed for the stationary disks, while those of a rotating disk are discussed in the next chapter.

4.2.   *Stiffness Due to Non-uniform Constraints*

The strain energy expressions for the non-uniform boundary conditions have been expressed in Eq.(2.60). The variations in the stiffness parameters representing the boundary along circumferential direction are modified in order to characterize single, multiple points or line support conditions. The circumferential variations of the stiffness parameter $K(\theta)$ can be expressed by its Fourier series expansion to allow simplified representation of complex variations.   Figure 4.1 shows the Fourier expansion of the stiffness parameter corresponding to a number of support conditions that are used in the following computation analyses of in-plane vibration properties of disks under non-uniform conditions. The stiffness parameters should have constant values at the angular positions of the support and zero otherwise. A uniform clamped condition can be considered as the limiting case, when the stiffness parameter is distributed uniformly along the entire periphery. Finer distributions can be achieved by increasing the number of terms (l) in Eq. (2.61), which will reduce the undesired negative stiffness values that appear at some of the angular positions. The stiffness for different support conditions,

shown in Figure 4.1, have axis of symmetry about $\theta = 0$, in order to decouple the system

into odd and even subsystems as described in section 2.4.2.
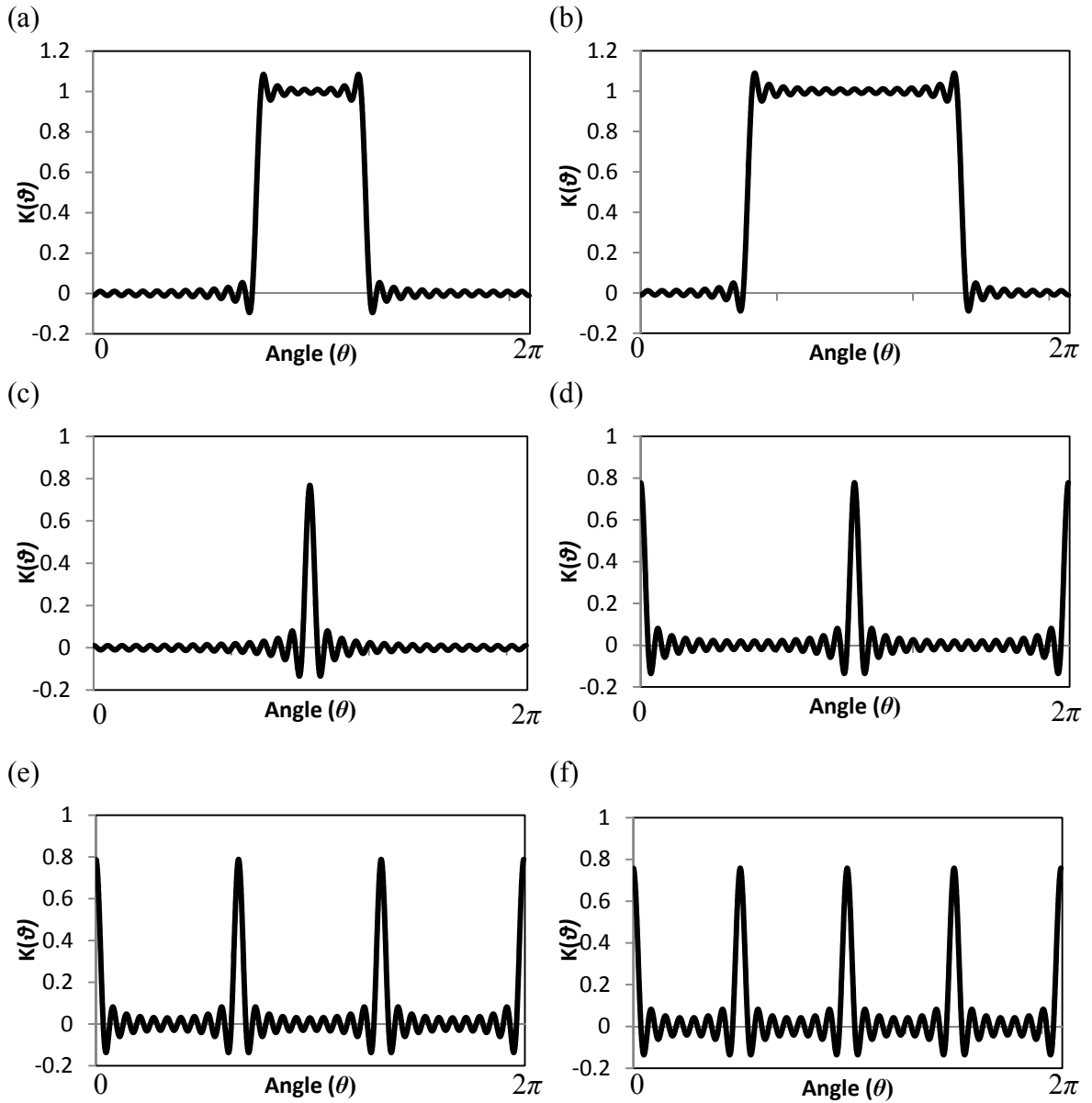
Figure 4.1: Fourier expansion of the stiffness parameter $K(\theta)$ for different support conditions: (a) clamped, $\theta = \pi/2$; (b) clamped, $\theta = \pi$; (c) point support; (d) two point support; (e) three point support; and (f) four point support.

Alternatively, Eq. (2.63) can be used to constrain the disk at the single or multiple points. It should be noted that the radial and circumferential stiffness parameters are assumed to have the same variation along the circumferential direction, irrespective of the type of constraint considered. In this chapter, the variations in the frequency parameters are obtained for the odd and even subsystems, for different stiffness parameters and the angular positions of the constrained portion. The effect of different orientations of multiple point supports on the frequency parameters and mode shapes are also discussed. Although the results are restricted for supports at the boundaries, the formulation can be equally used to represent support conditions at points located at different positions on the disk.

4.3.   Validation Methods

The validation of analytical models is vital to assure the reliability of the model in evaluating and solving the vibration problems. A number of studies have derived exact solutions under limited types of boundary conditions, which could serve as the reference response [13-15, 17]. The exact solutions for the in-plane vibration modes, however, are available only for solid disks with uniform boundary conditions. From the review of the published studies, it became evident that the free vibration responses of the annular disks have been mostly obtained using numerical approaches, which are also limited for the uniform boundary conditions, namely free or clamped edges [20]. Therefore, alternate methods are required for verification of vibration responses of annular disks with non-uniform boundary conditions. These may include laboratory experiments or numerical approximate methods that could serve as the reference responses.

113

In the previous chapter, the reported data have been used to examine the validity of the proposed models under uniform boundary conditions. The exact frequency equations are, then, considered as the benchmark for evaluating the accuracy of the Rayleigh-Ritz method for uniform boundaries. In this chapter, finite-element model of the disks with non-uniform boundary conditions are formulated and solved to provide the reference data under such conditions. Furthermore, simple laboratory experiments are performed to verify the frequency parameters of the disks under selected conditions.

4.3.1. Finite Element Analysis

Considering that the natural frequencies of in-plane modes of circular disks with non-uniform boundary conditions have not yet been reported in the literature, the finite-element method is used to obtain free vibration properties for examining the validity of the analytical results. In the finite element models, the modal analyses were performed to obtain the natural frequencies and the mode shapes of an annular disk subject to different types of boundary conditions at the inner and outer edges. Figure 4.2 illustrates the two-dimensional finite-element model used to study the in-plane vibration characteristics of annular disks. The model was formulated using four node shell elements (SHELL63), which are considered to yield more accurate results in the context of linear modal analyses [105]. Each element possesses six degrees-of-freedom (DOF) at each node including three in translation and three in rotation. Quadrilateral element shapes were used, instead of the triangular elements, for mesh generation which is known to give more accurate results as recommended in the ANSYS manual [105]. The distribution of elements was controlled by specifying the number of elements along the radial and

circumferential directions. The mesh distribution is depicted in Figure 4.2. The number of elements as well as that of the nodes was permitted to vary for each case due to differences in the radius ratios.
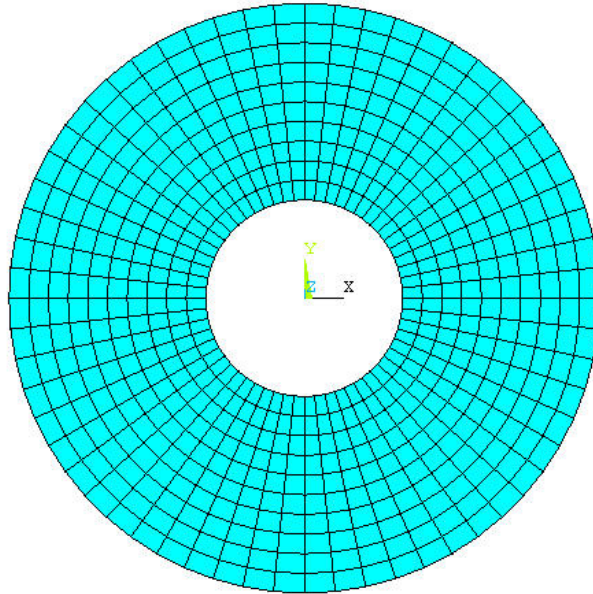
Figure 4.2: Finite-element model of an annular disk used in the modal analysis.

The modal extraction analysis was used to solve for the natural frequencies and mode shapes for the annular disk subject to different boundary conditions. The rigid body mode option was also selected in order to identify the rigid body modes that may exist especially for the totally free disks. The clamped boundary conditions were applied by enforcing the nodes at the particular edge to have zero displacements and rotations. The point or partial boundary constraints were enforced by constraining single or multiple adjacent nodes on the edge. The finite-element model can yield both the in-plane and out-of-plane modes of vibrations. In order to obtain the in-plane modes only, all other nodal displacement and rotational DOF were constrained to have zero displacements. Similarly,

the in-plane DOF of all the nodes were constrained to have zero displacements in order to extract the out-of-plane modes of vibrations.

The material properties and dimensions of the disk used were selected to be identical to those employed in the reported studies [e.g. 23], when model verifications were sought on the basis of the reported data. In cases involving verifications against the experimental data, the properties and dimensions were selected as those of the disk used in the experimental investigation, which will be described in the next section. Furthermore, the comparisons of the modal responses with either reported or measured data are presented in terms of the non-dimensional frequency parameters. Table 4.1summerizes the properties of the disks used in this study.

Table 4.1: Properties of the annular disk used in this study [23].

material properties	density (ρ)	7905.9 kg/m^3
	Modulus of elasticity (E)	218 x 10^9 N/m^2
	Poisson's ratio (v)	0.305
Geometrical properties	Thickness (h)	31.5 mm
	Outside diameter (R_o)	151.5 mm
	Inside diameter (R_i)	87.5 mm

The validity of the finite-element model is initially established by comparing the resulting in-plane frequency parameters with those reported in the literature. The reported results, however, are limited only to the uniform boundary conditions. Table 4.2 encompasses the frequency parameters of selected in-plane vibration of an annular disk clamped at the inner edge and with free outer boundary, referred to as 'Clamped-Free', derived from the analytical method and the finite element model, with those reported in

116

[20]. The comparisons revealed very good agreements between the analytical, finite element model and the reported results, suggesting the validity of the finite element and the analytical models in predicting the in-plane vibration properties under classical boundary conditions.

Owing to the lack of published results on the in-plane free vibration of disks under partial or point supports, the validity of the finite element model under such constraints could only be established on the basis of the out-of-plane free vibration responses. The frequency parameters reported by Narita and Leissa [57] for the out-of-plane vibration of point-simply supported and point-clamped solid disks are considered, and compared with those obtained from the finite element model (Table 4.3). The comparisons suggest reasonably good agreements between the reported and finite element model results under both types of point support conditions. From the reasonably good agreements observed in Tables 4.2 and 4.3, it is deduced that the finite element model can be considered to yield reasonably accurate in-plane free vibration characteristics of the annular disk subject to constraints involving point, partial or full supports.

Table 4.2: Comparisons of frequency parameters λ of in-plane vibration of an annular disk clamped at the inner edge ($v = 0.3$, $\beta = 0.2$).

(m,n)	Reference [20]	present study	FE Model
$(1,0)^{\theta}$	0.352	0.3526	0.3524
$(1,1)$	0.919	0.9193	0.9193
$(1,2)$	1.542	1.5416	1.5414
$(2,1)$	2.121	2.1208	2.1208
$(1,3)$	2.157	2.1570	2.1568
$(1,0)^{r}$	2.204	2.2040	2.2039

r: pure radial mode; θ: pure circumferential mode.

Table 4.3: Comparisons of frequency parameters λ of out-of-plane vibration of a solid disk ($\nu =0.3$).

(m,n)	Solid disk with point clamped		Solid disk with point simply-supported	
	Reference [57]	FE Model	Reference [57]	FE Model
(0,0)	0.737	0.714	0	0
(0,1)	1.943	1.932	1.816	1.815
(0,2)	2.904	2.896	2.795	2.793
(1,0)	3.227	3.236	3.200	3.200
(0,3)	3.630	3.627	4.052	4.052

4.3.2. Laboratory Measurements

The vibration characteristics of circular disks were also investigated in the laboratory under limited boundary conditions to further examine the validity of the analytical results. It needs to be emphasized that only a few studies have experimentally investigated the in-plane modes of vibrations of annular disks with uniform boundary conditions [18, 22, 108]. In the present study, an experiment is designed to measure the in-plane free-vibration properties of a non-rotating annular disk with free and point support conditions using an accelerometer and a microphone. The measured data are also used to characterize the acoustic radiation properties of disks.

Figure 4.3 shows the schematic of the experimental setup. The disk is excited along the radial direction by an impulse hammer, while an accelerometer is mounted radially to capture the acceleration in the radial direction. In order to assure that the captured frequencies are due to in-plane motion and not due to out-of-plane vibrations, the measurements are also taken by exciting the out-of-plane modes. The experiment design thus permitted the measurements of in-plane and the out-of-plane vibration due to both in-plane and out-of-plane excitations, as shown in Table 4.4.
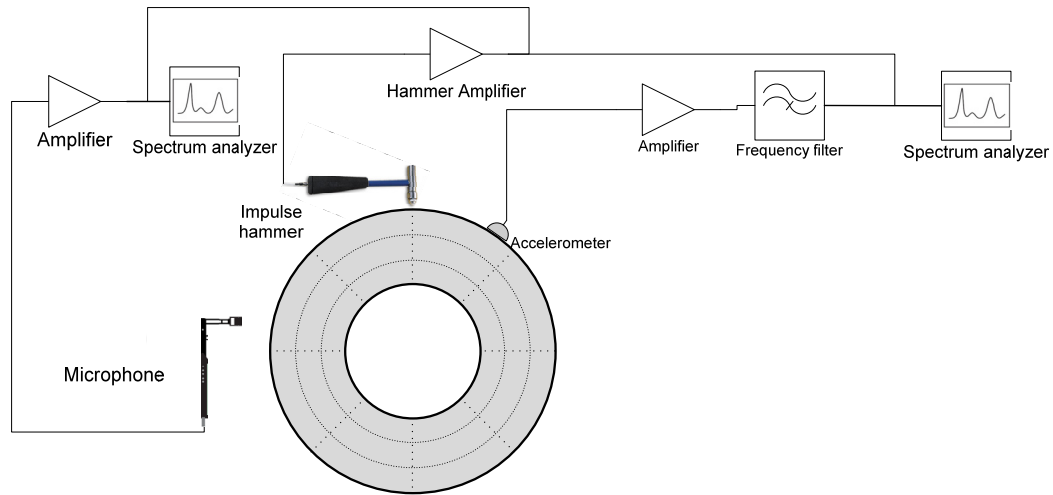
Figure 4.3: Schematic of the experimental set up.

Table 4.4: Schematic showing positions of the impulse hammer excitation and the accelerometers on the surface of circular disk for capturing in-plane and out-of-plane vibration frequencies: Accelerometer: ⟶ , Hammer: ⟹.

Out-of-plane	
In-plane	
Out-of-plane due to in-plane Excitation	

The impulse hammer used in this study is equipped with a force sensor (KISTLER 9722A500). A high frequency IEPE miniature accelerometer with built-in pre-amplifiers was used to measure the acceleration (Bruel and Kjaer 4508B). The sound pressure measurements were also conducted using a Bruel and Kjaer 4181 microphone combined with pre-amplifier, which was mounted close to the position of the accelerometer to capture the radiated acoustic signal (Figure 4.3). The acceleration, force and sound signals were acquired in a multi-channel signal analyzer (PULSE) and analyzed to obtain the frequency spectra of vibration and sound pressure. The analyses

119

were performed over the bandwidth of 12 kHz, which encompassed the lowest four in-plane vibration modes.

From the results presented in the previous chapter, it was observed that the first and third natural frequencies decrease with increasing radius ratio, while the second mode frequency is independent of the radius ratio. This observation was used to determine the dimensions of the disks used in the experiments. Two annular disks of different radius ratios were used in the experiment to observe the natural frequency behavior for different radius ratios. The geometric and material properties of both disks are shown in Table 4.5. The measurements were performed for the disks with different sets of boundary conditions. The natural frequencies of the disks were initially identified by placing the disk on a soft cushion to resemble free boundary conditions. Each disk was subsequently mounted vertically with a portion of its outer edge clamped in a vice-grip to represent a point support condition. A C-clamp was further used to simulate the disk supported at two points. The measured data were acquired for each experimental condition shown in Table 4.4 for the boundary conditions described above.

Table 4.5: Geometric and material properties of annular disks used in the experiments.

	Disk I	Disk II
Outer radius, R_o	0.15 m	
Inner radius, R_i	0.05 m	0.09 m
Thickness, h	0.01 m	
Material	1018 Carbon Steel	
Density, ρ	7850 kg/m^3	
Modulus of elasticity, E	210 x 10^9 N/m^2	
Poisson's ratio, v	0.3	

4.4. Convergence Study

In the previous chapter, a convergence study of the proposed analytical method was presented for uniform boundary conditions. It was deduced that the number of polynomials used in the formulation and the stiffness parameters could affect both the accuracy and the convergence of the results. It is reasonable to expect that these parameters would play an important role in the accuracy of the analysis for the non-uniform boundary conditions in a similar manner. It was further shown that the modes with different nodal diameter number (n) are uncoupled for the uniform boundary conditions. The coupling, however, was observed between modes with different nodal circles (m) within the same nodal diameter number (n). For disks with non-uniform boundary conditions, the modes associated with different nodal diameter number n are coupled and cannot be studied independently. Therefore, the number of terms (N), which is the maximum number of modes used along the circumferential direction, would form an additional important parameter to be considered for the convergence study.

The formulations presented in section 2.4 were solved to determine the frequency parameters for solid and annular disks with different combinations of boundary conditions. Figures 4.4 and 4.5 illustrate variations in frequency parameters corresponding to the first few odd and even modes of solid and an annular disk ($\beta = 0.6$) for different number of terms (N) under single-point and line support condition, respectively. The results are presented for (N) ranging from 5 to 200. The results were obtained using a fixed number of polynomials along the radial direction and constant stiffness parameters that were determined from the results of the convergence study presented in the previous chapter. Figure 4.4(a) and (b) present the variations in the

121

frequency parameters for an annular disk ($\beta = 0.6$) obtained from the even and odd analyses, respectively, while those for solid disks are presented in Figure 4.4 (c) and (d). The point support at the outer edge is taken at $\theta = 0$ as shown in Figure 4.4, while the line support condition refers to clamped condition along one-quarter of the outer edge as in Figure 4.5. It can be noticed that some of the frequency parameters do not vary with the number of terms for the point support condition. This is attributed to the location of the point support being on a nodal diameter of that specific mode. Both, the solid and annular disks, exhibit the first rigid body mode in translation, derived from the odd mode with nodal diameter at the location of the support. A detailed discussion of the nodal diameters is presented in the subsequent sections describing the deformed shapes.

The results attained for the annular disk with $\beta = 0.6$, free at the inner edge and clamped along one-quarter of its outer edge are illustrated in Figure 4.5. The Fourier expansion of the stiffness parameter is same as the one shown in Figure 4.1(a). The variations in the even and odd frequency parameters with varying (N) are shown in Figure 4.5(a) and (b), respectively for annular disk, while those for the solid disk that its partly clamped at the outer edge are shown in Figure 4.5 (c) and (d). Unlike the point support conditions, the convergence of frequency parameters for all modes seems to be affected by the number of terms (N) used, which is attributed to the more severe influence of the line support constraint. All the frequency parameters exhibit converging behavior with increasing number of terms while the rate of convergence differs for different modes. The figures show considerable variations in the frequency parameters until N approaches 50, although a greater N may be required for some of the modes. Based upon these results, subsequent calculations in this chapter are carried out using $N = 50$,
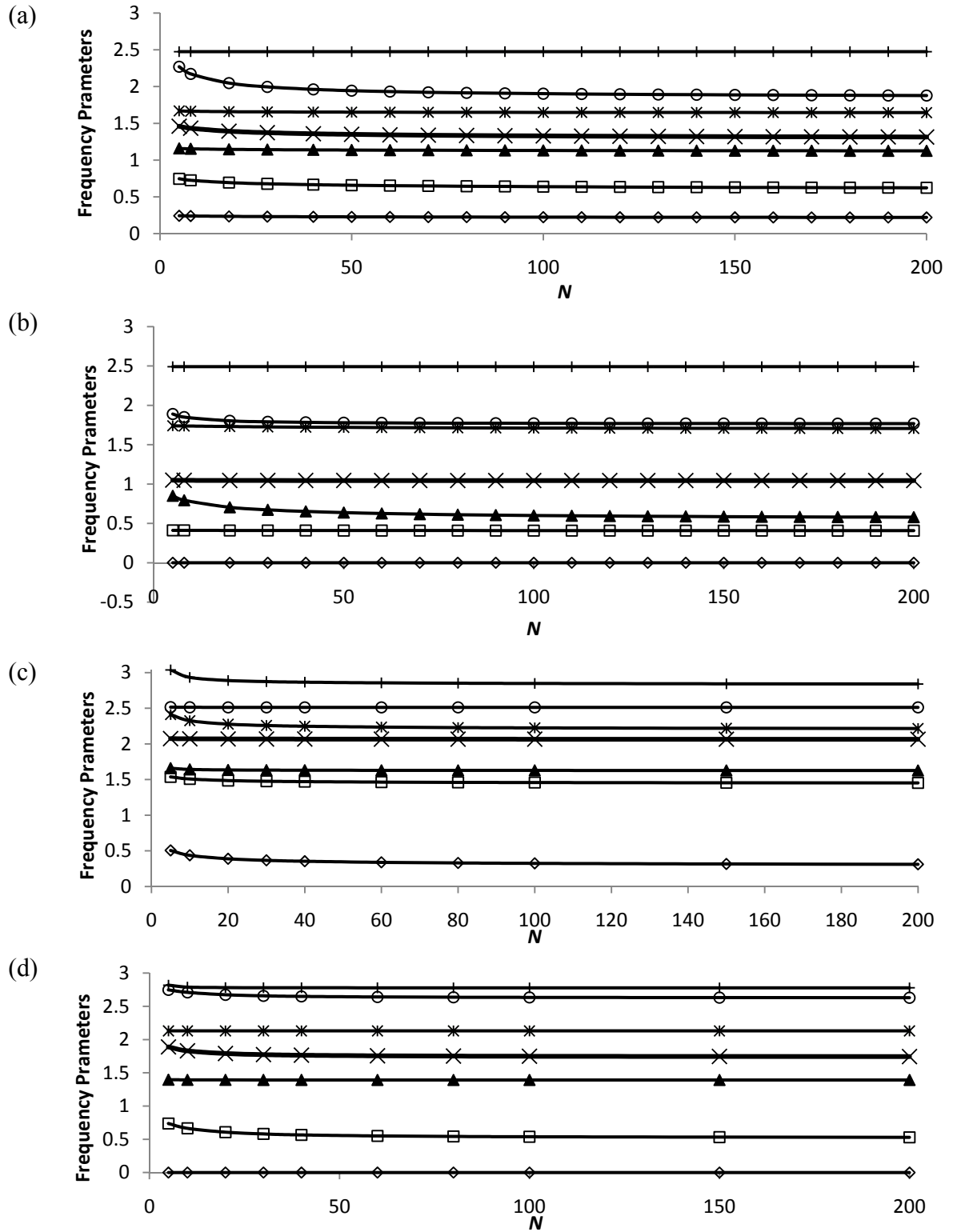
Figure 4.4: Variations in the frequency parameters of disks with single point support for different number of terms (*N*) used in the formulations: (a) annular-even; (b) annular-odd; (c) solid-even; (d) solid-odd.

123
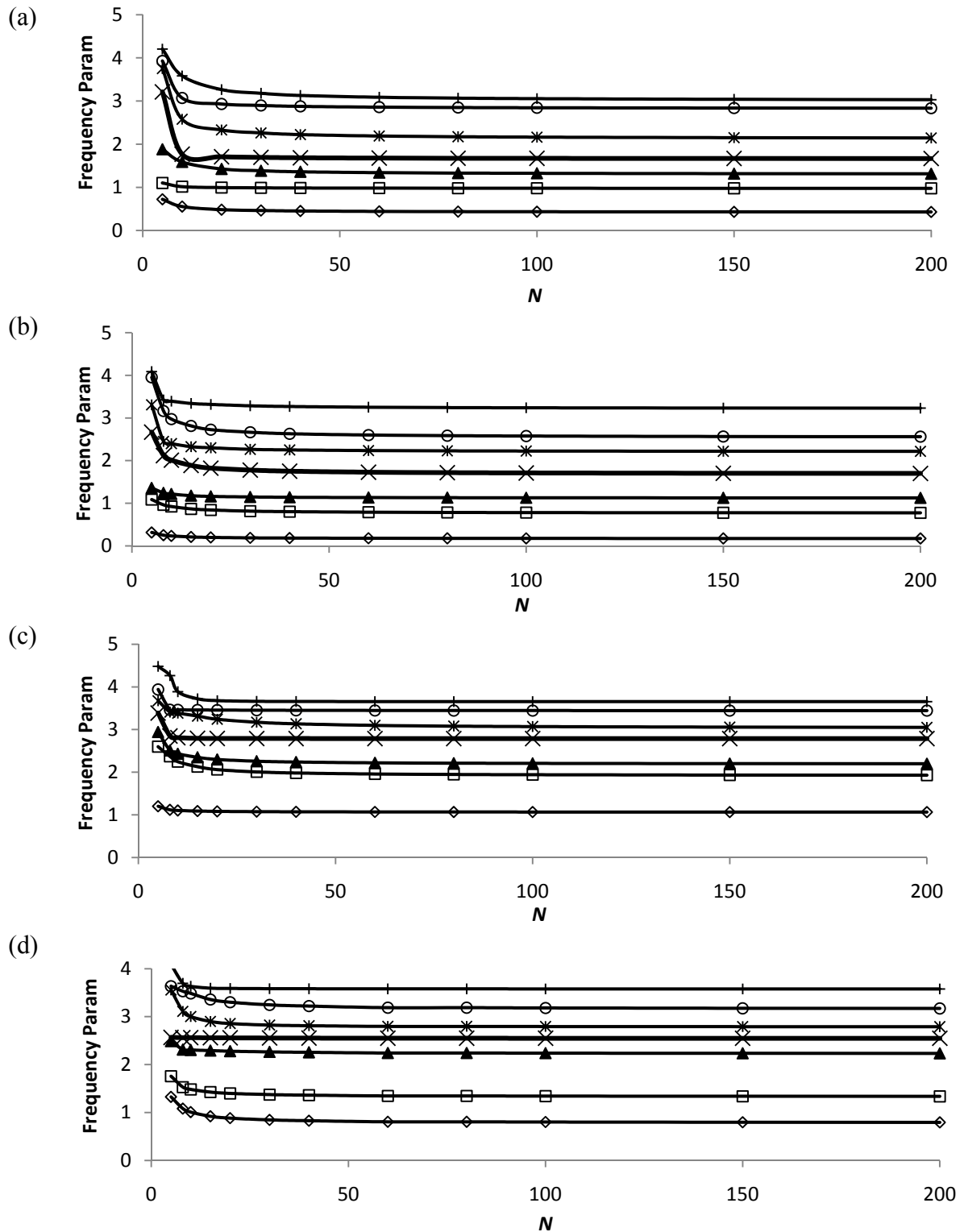
Figure 4.5: Variations in the frequency parameters of disks with single point support for different number of terms (*N*) used in the formulations: (a) annular-even; (b) annular-odd; (c) solid-even; (d) solid-odd.

and $\overline{K}_r = \overline{K}_\theta = 10^5$ except for the situations where the influences of support stiffness on the variations of the frequency parameters are investigated.

4.5. *In-plane Vibration Analysis of Annular Disks with Single Point Support*

The frequency parameters and the corresponding mode shapes of annular disks with different edge constraints are obtained by solving the eigenvalue problem, defined in Eq.(2.59). This section is devoted to discuss the effects of additional point supports on the frequency parameters and mode shapes of annular disks. The effect of multiple point supports with different orientations and line support will be discussed in the following section.

The frequency parameters and mode shapes for the in-plane free vibration of the annular disk were obtained under four different support conditions: (i) Clamped inner edge with point clamp support at the outer edge, referred to as 'Clamped-Point Clamped' condition; (ii) Point-clamped support at the inner edge with clamped outer edge, referred to as 'Point Clamped -Clamped' condition; (iii) Point clamp support at inner edge with free outer edge, referred to as 'Point Clamped -Free' condition; and (iv) Free inner edge with point-clamp support at the outer edge, referred to as 'Free-Point Clamped ' condition. A point-constraint within the annular disk is realized by introducing a two-dimensional point spring, as was illustrated in Figure 2.2. The analyses were performed to obtain frequency parameters of the even (coupled radial cosine and circumferential sine modes) and odd (coupled radial sine and circumferential cosine modes) subsystems corresponding to the selected modes, which are presented in Tables 4.6 and 4.7,

respectively. It can be noted from Tables 4.6 and 4.7 that the even and odd subsystems yield distinctly different frequency parameters.

It is important to note that the label (*m,n*) in Tables 4.6 and 4.7 does not reflect the nodal diameter and the nodal circle number, since the modes are coupled within each subsystem. The label (*m,n*) for the 'Clamped-Point Clamped' support condition, however, can be directly related to those reported in Table 4.2, when the point support constraint is relaxed at the free edge. The results presented in Tables 4.2, 4.6 and 4.7 suggest that the frequency parameters of the disk with an outer edge point support are higher than those of the disk with the free outer edge.

Table 4.6: Even frequency parameters λ of selected modes of In-plane vibration of the annular disk ($v = 0.3, \beta = 0.2$).

Constraint	Clamped-Point Clamped		Point Clamped-Clamped		Free-Point Clamped		Point Clamped-Free	
	Present study	FE Model	Present study	FE Model	Present study	FE Model	Present study	FE Model
(*m,n*)								
(0,1)	0.9561	0.9548	2.1618	2.1576	0.3073	0.3031	0.3040	0.2808
(0,2)	1.605	1.5999	2.6399	2.6334	1.1868	1.1883	1.1633	1.1584
(1,1)	2.1349	2.135	3.3025	3.3055	1.6589	1.6645	1.6851	1.6850
(0,3)	2.1882	2.1882	3.7375	3.7351	1.8327	1.8304	1.8355	1.8284
(0,0)	2.3097	2.2999	3.3944	3.3847	2.145	2.1471	2.0793	2.0845

Table 4.7: Odd frequency parameters λ of selected modes of In-plane vibration of the annular disk ($v = 0.3, \beta = 0.2$).

Constraint	Clamped-Point Clamped		Point Clamped-Clamped		Free-Point Clamped		Point Clamped-Free	
	Present study	FE Model	Present study	FE Model	Present study	FE Model	Present study	FE Model
(*m,n*)								
(0,0)	0.5148	0.5142	2.1712	2.1702	0	0	0	0
(0,1)	1.0773	1.0636	2.3021	2.3054	0.5202	0.5266	0.3251	0.3331
(0,2)	1.5554	1.556	2.6812	2.6685	1.1122	1.1125	1.1712	1.1732
(0,3)	2.1568	2.1616	3.7300	3.7360	2.0721	2.0738	2.0791	2.0836
(1,1)	2.1754	2.1753	3.3219	3.3249	1.7643	1.7693	1.6807	1.6849

The effect of the point support is further investigated by varying the support stiffness on the frequency parameter, and the corresponding mode. The radial and circumferential stiffness parameters of the point support are varied from zero (free

126

condition) to very large values (nearly clamped) condition. Figure 4.6 illustrates the variations in the frequency parameters corresponding to selected modes with variations in the normalized stiffness parameters in the radial, $\bar{K}_{pr} = K_{pr}(1 - v^2)/E$ and circumferential, $\bar{K}_{p\theta} = K_{p\theta}(1 - v^2)/E$, directions. The figure illustrates the frequency parameters of the selected odd and even modes, denoted by 'O' and 'Ev', respectively. The results clearly show considerable deviation in the frequency parameters corresponding to the even and odd modes when the stiffness parameters of the point support are increased. The two, however, converge to values identical to those in Table 4.2, when the point support stiffness diminishes to free outer edge condition. This tendency was observed for all the four constraint conditions considered. As an additional example, Figure 4.7 illustrates the variations in frequency parameters of selected modes of the annular disk with free inner edge but point-supported outer edge with varying support stiffness.

The results in Figure 4.6 further show a change in the order of the modes with increasing support stiffness. For the annular disk clamped at the inner edge, the frequency parameter of the (1, 1) odd mode becomes greater than that of the (0, 3) odd mode, while the order of these modes is opposite when the support stiffness is relatively small. This trend is not observed for the 'Free-Point Clamped' condition as seen in Figure 4.7.

The in-plane vibration of the disk with different support conditions were further evaluated using the two-dimensional deformation plots, obtained from Eqs. (2.54) and (2.55). The results, however, were presented for the clamped inner edge and point supported outer edge only in order to illustrate the effect of point clamped support on the in-plane vibration modes. Deformation contour plots for selected modes of the 'Clamped-Point Clamped' disk were presented and compared with those of the 'Clamped-Free' disk.

127
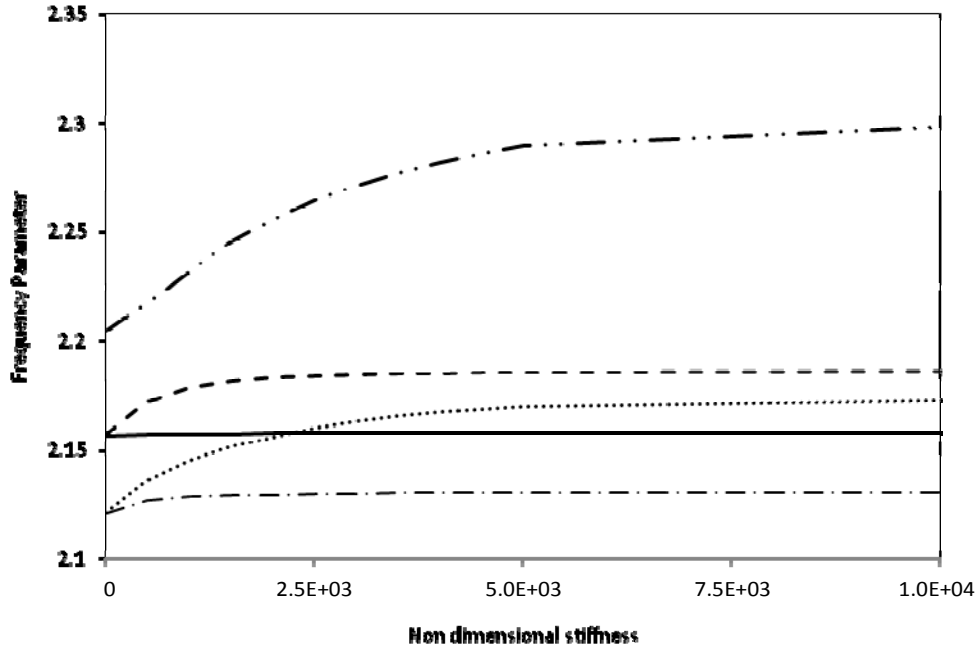
Figure 4.6: Variation in the frequency parameters of selected modes with varying normalized point support stiffness at the outer edge of an annular disk clamped at the inner edge ($v = 0.3, \beta = 0.2$), $\_ . . \_ . \_ . .$ (1,1)Ev, ... (1,1)O, ———— (0,3)O, $\_ \_ \_ \_ \_$ (0,3)Ev, $\_ . . \_ \_ . .$ (0,0)Ev.
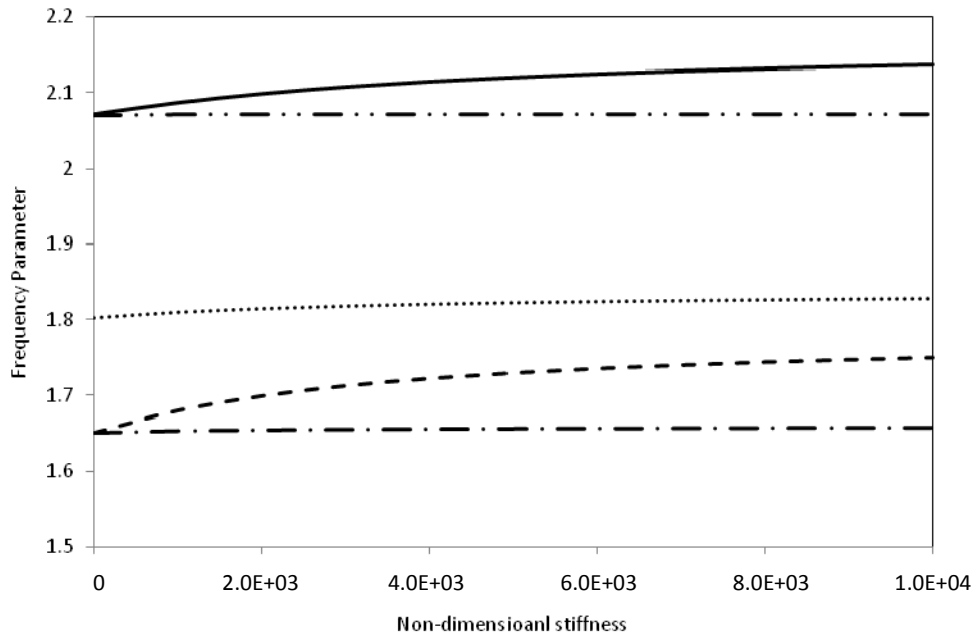
Figure 4.7: Variation in the frequency parameters of selected modes with varying normalized point support stiffness at the outer edge of an annular disk clamped at the inner edge ($v = 0.3, \beta = 0.2$), $\_ . \_ . \_ . .$ (1,1)Ev, $\_ \_ \_ \_ \_$ (1,1)O, ... (0,0)Ev, $\_ . . \_ . .$ (0,3)Ev, ———— (0,3)O.

128

Figure 4.8 illustrates the deformed shape corresponding to the lowest mode of the 'Clamped-Free' disk (mode (0,0)θ in Table 4.2) obtained analytically and from the finite element analysis. This mode is purely circumferential obtained from the odd subsystem.

(a) (b)
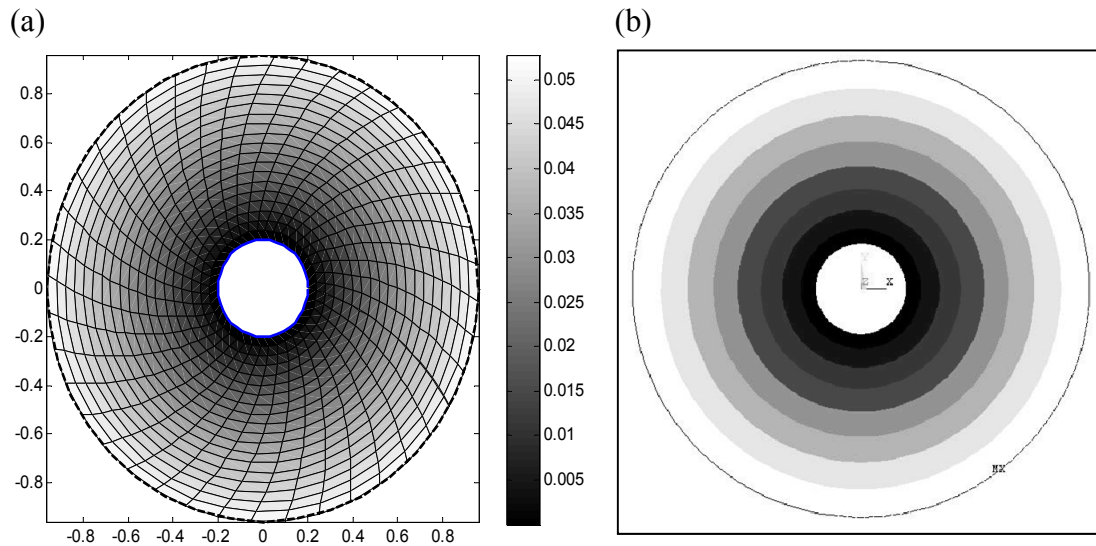
Figure 4.8: Contour deformation plots of the purely circumferential mode (0,0)θ for a 'Clamped-Point Clamped' disk: (a) present analysis; and (b) finite element model.

The effect of additional point clamped support at the outer edge on this mode is illustrated in Figure 4.9. The figure illustrates the mode shapes with predominant radial and circumferential deformation, as shown in Figure 4.9 (a) and (b), respectively, that are obtained through solution of the odd subsystem. The figure also shows the resultant deformation mode obtained from vector summation of the radial and circumferential displacements together with the deformed shape obtained from the finite element analysis, as seen in Figure 4.9 (c) and (d), respectively. The results show that the addition of the point clamped support yields radial displacement apart from the circumferential deformation, which makes the mode neither purely circumferential nor axisymmetric. The results also show that the resultant deformation contours corresponding to mode

129

$(0,0)\theta$ are quite comparable with those obtained from the finite element analysis. The odd subsystem mode shapes, shown in Figure 4.9(a) and (b), thus exhibit predominantly circumferential deformation and relatively small radial displacement.

(a)

(b)

(c)

(d)

Figure 4.9: Contour deformation plots of mode (1,0) for a 'Clamped-Point Clamped' disk: (a) radial displacement; (b) circumferential displacement, (c) vector sum of displacements; (d) deformed shape from finite element model, ◁ : point clamped support , - - - - undeformed edge.

Unlike the mode $(0,0)\theta$, the even and odd frequency parameters corresponding to non-axisymmetric modes of the 'Clamped-Free' disk are identical. The predominantly radial and circumferential deformation modes $(0,1)$ of the 'Clamped-Free' disk are illustrated in Figure 4.10 (a) and (b), respectively. These also clearly show the nodal diameter in both the radial and circumferential deformation shapes. It should be noted that both the even and odd subsystems also yield identical mode shapes, except for the $\pi/2$ radians shift. The figure also shows the resultant deformation contours obtained from the vector summation of the radial and circumferential displacements and the finite element analysis, respectively. The addition of the outer-edge point clamped support yields a split between the odd and even frequencies, as observed in Figure 4.6. The corresponding deformation modes obtained from the even and odd subsystems also differ, as seen in Figures 4.11 and 4.12 for mode $(0,1)$, respectively.

Each figure illustrates predominantly radial and circumferential deformation shapes together with the resultant deformation contours. The resultant displacement contours are quite similar to those obtained from the finite element analysis in both the cases. A comparison of Figures 4.10 and 4.11 suggests that the addition of the point clamped support does not affect the predominantly circumferential mode of the even subsystem. In a similar manner, the predominantly radial mode of the odd subsystem is insensitive to the point clamped support. This can also be deduced from Eqs. (2.54), (2.55) and (2.63), which show that the even subsystem is affected only by the radial stiffness constant of the point spring support at $\theta_0 = 0$, while the odd subsystem is influenced only by the circumferential stiffness of the point spring. The resultant even and odd subsystems of in-plane vibration modes of the 'Clamped-Point Clamped' disk are

131

affected by the radial and circumferential stiffness property of the point-support, respectively.
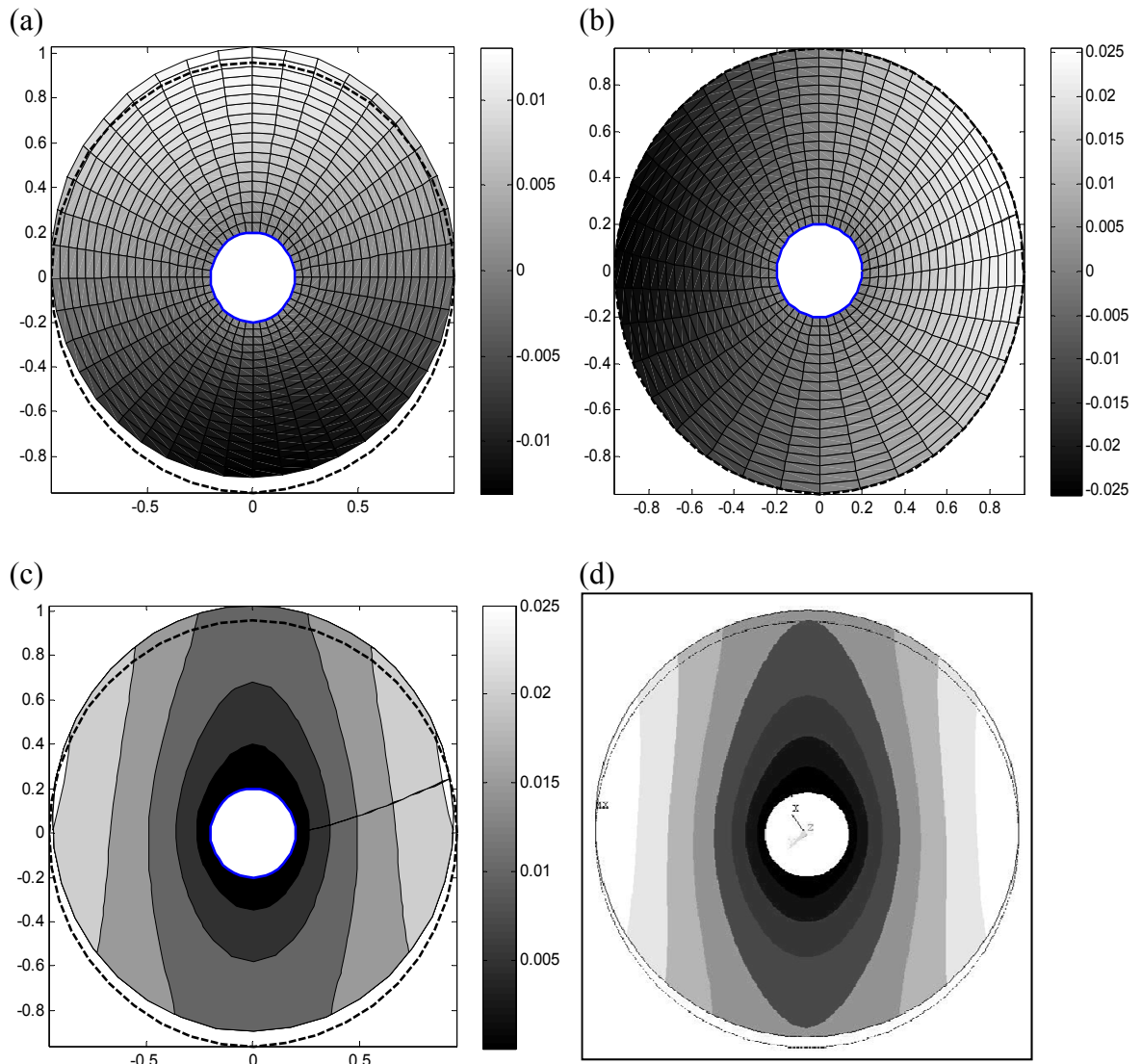
Figure 4.10: Contour deformation plots of mode (0,1) for a 'Clamped-Free' disk: (a) radial displacement; (b) circumferential displacement, (c) vector sum of displacements; and (d) deformed shape from finite element model.
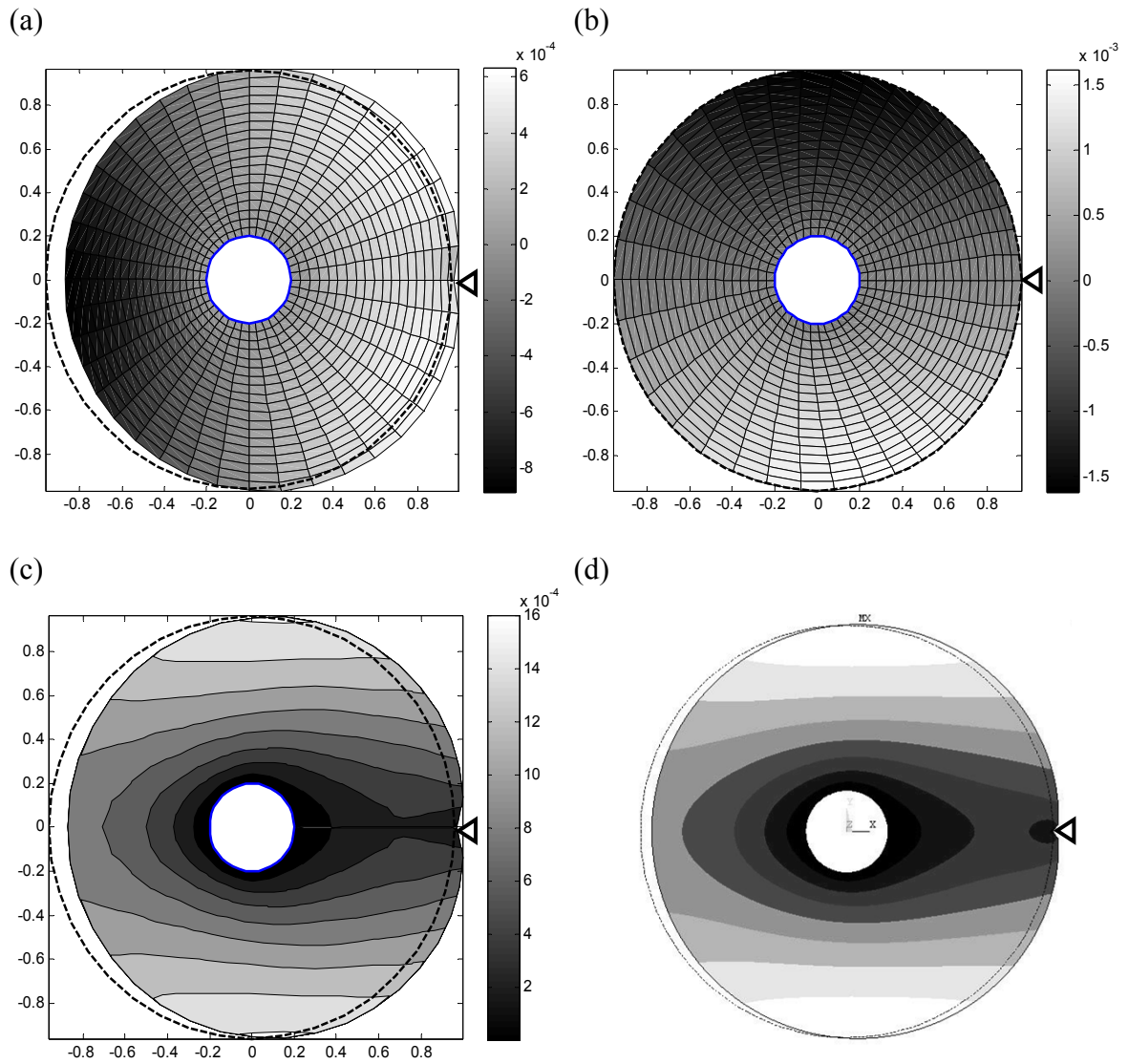
Figure 4.11: Contour deformation plots of the even mode (0,1) for a 'Clamped-Point Clamped' disk: (a) radial displacement; (b) circumferential displacement, (c) vector sum of displacements; and (d) deformed shape from finite element model, ◁ : point clamped support , – – – – undeformed edge.
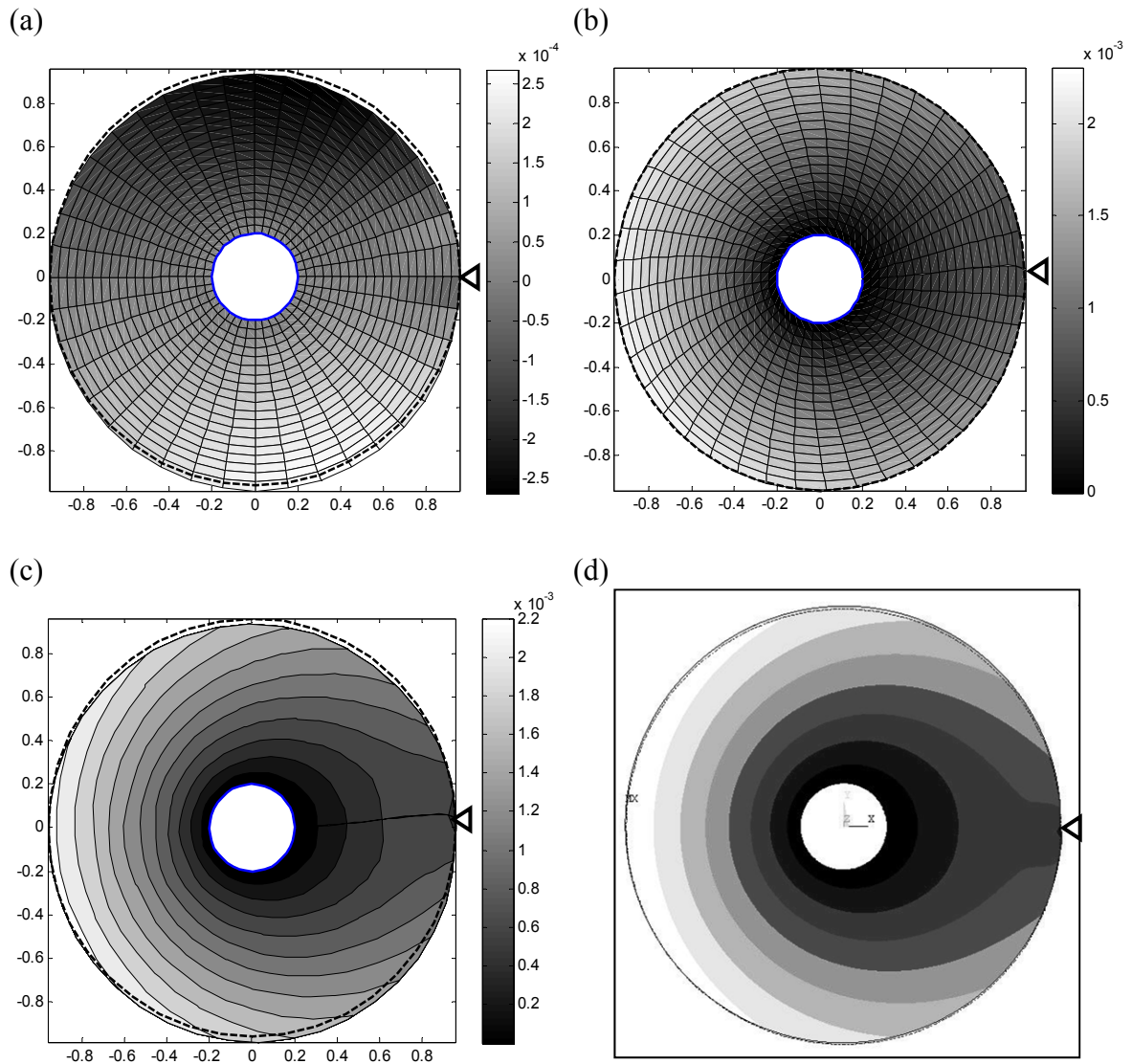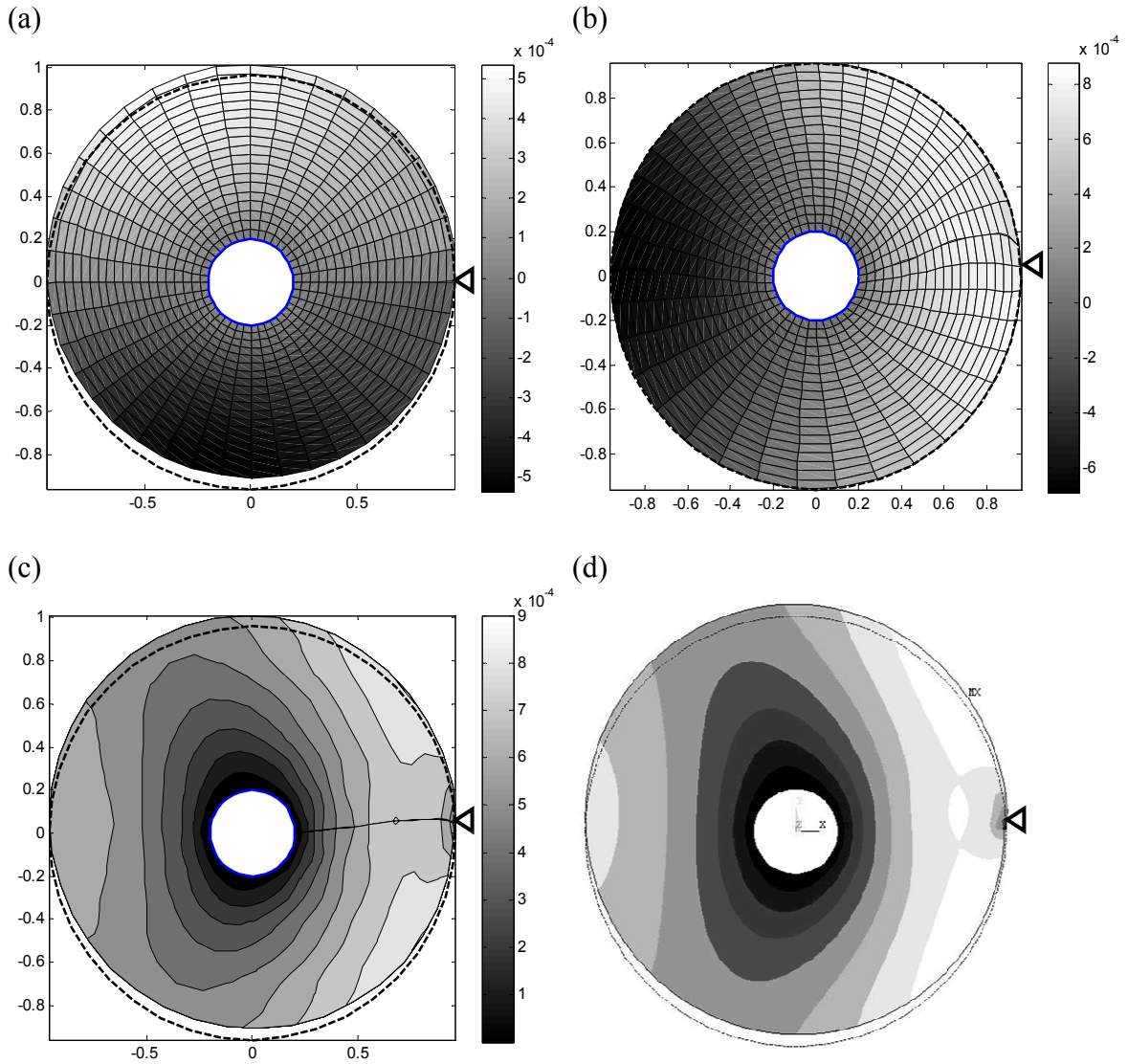
Figure 4.12: Contour deformation plots of the odd mode (0,1) for a 'Clamped-Point Clamped' disk: (a) radial displacement; (b) circumferential displacement, (c) vector sum of displacements; and (d) deformed shape from Finite element model, ◁ : point clamped support , - - - - undeformed edge.

4.6.   Vibration of Disks with Multiple and Distributed Support

The effect of partial supports on the in-plane frequency parameters and modes of vibration are investigated for a solid disk, subject to partial supports. The length of the clamped support is varied by varying the arc angle from 0 to 2π radians, where the extreme angles, 0 and 2π radians, represent the single-point support and the uniformly clamped edge, respectively. Figure 4.13 illustrates variations in the frequency parameters of the disk corresponding to a few selected modes with variations in the constraint length. The stiffness coefficients were considered to be constant over the clamped portion along the circumferential direction. The results suggest that a point support causes the odd and even modes to split into two different values except for the modes with $n = 0$. Odd and even frequency parameters follow different trends as the angle of the clamped edge increases from 0 to 2π radians. As the clamped portion approaches a totally clamped edge, even and odd frequency parameters converge to identical values, which are indicated on the right of Figure 4.13. These values correspond to the frequency parameters for the annular disk subject to clamped conditions at the inner and outer edges. The nodal diameter number (*n*) and nodal circles (*m*) are also shown for next to their corresponding frequency parameter.

Similarly, Figure 4.14 shows the variation in the frequency parameters of a solid disk with variations in the arc length of the clamped support. It is clear in both figures that, for even and odd modes that approach identical values, there might be change of orders as the clamping angle increases. Even and odd modes do not intersect with other modes of the same group, although even modes may intersect with one or more odd modes and vice versa.

135
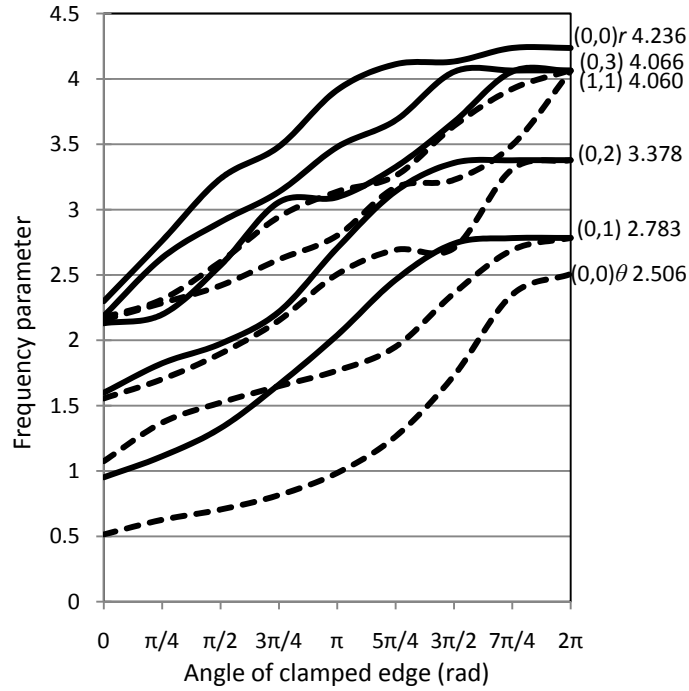
Figure 4.13: Variations in frequency parameters of in-plane vibration of an annular disk clamped at the inner edge and with varying length of the constraint at the outer edge ($\beta = 0.2, v = 0.3$).
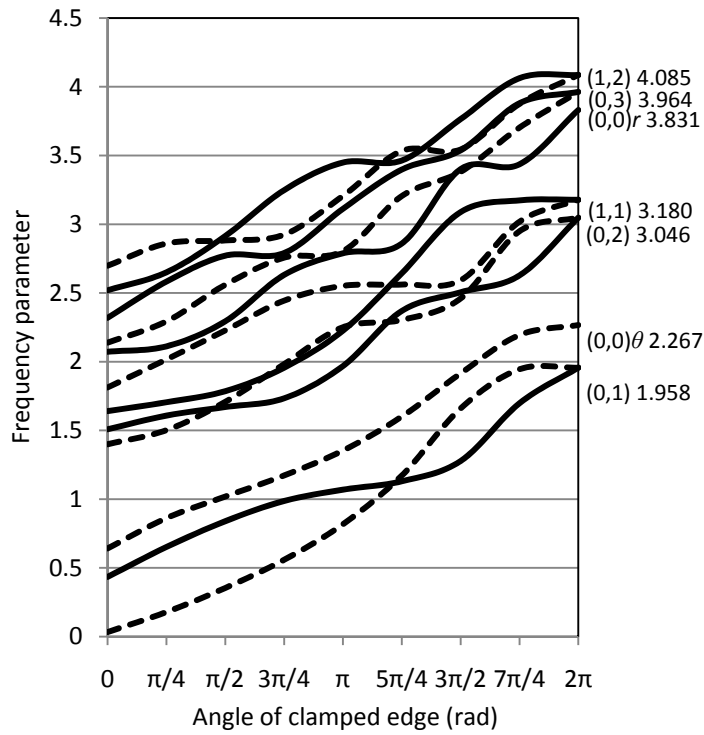
Figure 4.14: Variations in frequency parameters of in-plane vibration of a solid disk with varying length of the constraint at the outer edge ($v = 0.3$).

The in-plane vibration characteristics of an annular disk bolted at multiple points, more representative of many engineering applications, are subsequently investigated. Increasing the number of supports would increase the natural frequencies in a manner similar to that shown in Figure 4.13 for increasing constraints length. Different orientations of the same number of point supports, however, may exhibit different effects on the natural frequencies and the mode shapes. An annular disk clamped at two points is considered to illustrate the effect of support location on the natural frequencies and mode shapes. The analysis is performed for four different combinations of two point supports at the inner or the outer edges, as illustrated in Figure 4.15.

The lowest frequency parameters, for each condition, obtained from the even and the odd subsystems are summarized in Tables 4.8 and 4.9, respectively. The labels shown in the first row of both tables describe the location of the two point supports. For example, the $(0, \beta)$ represents a point support at $\theta = 0$ and $\xi = \beta$, where $(\pi, 1)$ is the point support located at $\theta = \pi$ and $\xi = 1$. Both tables show that the frequency parameters differ considerably with changes in the orientation of the point supports.

Table 4.8: Variations in frequency parameters of in-plane vibration of an annular disk $(\beta = 0.2, v = 0.3)$ with two point supports derived from the even subsystem.

Constraint	(0,1) (π,1)	(0,β) (π, β)	(0,β) (π,1)	(π, β) (π,1)
1	0.439	0.462	0.451	0.398
2	1.205	1.250	1.227	1.229
3	1.727	1.668	1.695	1.688
4	1.852	1.873	1.861	1.866
5	2.087	2.208	2.148	2.168

Figure 4.15: Contour plots of the first even mode of the annular disk clamped at two points: (a) radial displacement; (b) circumferential displacement, (c) vector sum of displacements◁ : point clamped support, ----- undeformed edge.

Table 4.9: Variations in frequency parameters of in-plane vibration of an annular disk
($\beta = 0.2, v = 0.3$) with two point supports derived from the odd subsystem.

Constraint	(0,1) (π,1)	(0,β) (π, β)	(0,β) (π,1)	(π, β) (π,1)
1	0.122	0.417	0.299	0.180
2	0.478	0.619	0.550	0.606
3	1.225	1.116	1.171	1.186
4	1.707	1.894	1.797	1.777
5	2.089	2.071	2.080	2.078

Figure 4.15 shows the contour plots of the first mode obtained from the even subsystem for different point support configurations. For each support condition, the figure illustrates the mode shapes with predominant radial and circumferential deformation in the second and third columns, respectively. The deformed shapes obtained from the vector summation of the radial and circumferential displacements are illustrated in the fourth column, while the dashed line represents the undeformed edges of the annular disk. Darker shadings in the contour plots represent zero displacements, while the regions of maximum displacements are represented by lighter shadings. As shown in Figure 4.15, the deformed shapes differ considerably for the four constraint cases considered, although they are all supported at two points. The nodal diameter of this mode is horizontal in the circumferential mode shape and vertical in the radial mode shape. The circumferential mode shapes corresponding to all the four support conditions are thus almost similar, since all the points are located at the nodal diameter of this mode.

The radial mode shape, however, is strongly affected by the locations of the point supports. The first two support cases, the disk supported at two points at the outer edge and the disk supported at two points at the inner edge, are symmetric about the vertical nodal diameter causing the nodal diameter to remain vertical. The nodal diameters
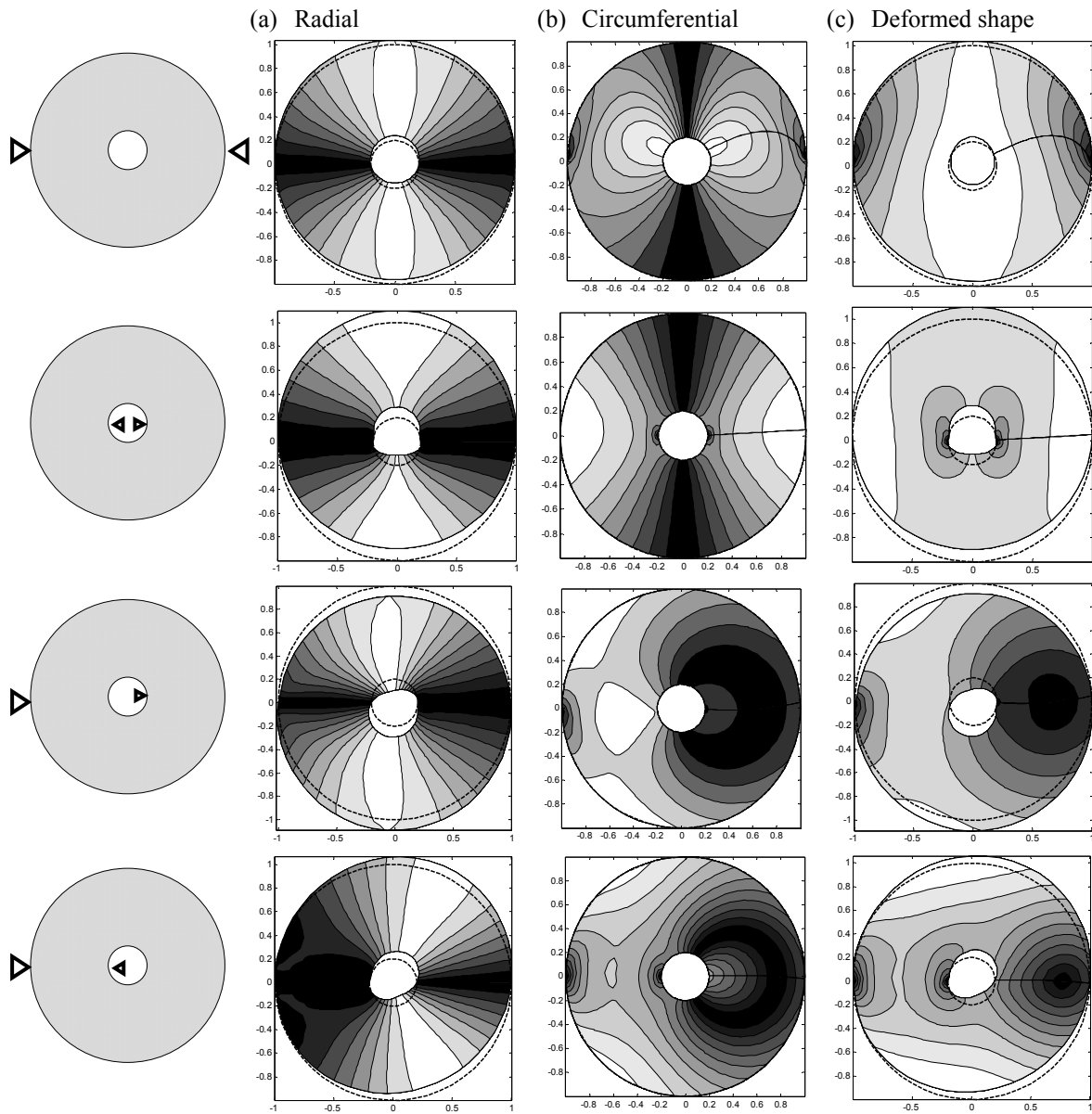
Figure 4.16: Contour plots of the first odd mode of the annular disk clamped at two points: (a) radial displacement; (b) circumferential displacement, (c) vector sum of displacements ◁ : point clamped support, ---- undeformed edge.

corresponding to the third and fourth conditions, however, are not vertical due to the orientation of the clamped points. For the fourth case, there exists a short nodal line passing through the two points. For the same mode of vibration, the mode shapes obtained from the odd subsystem are illustrated in Figure 4.16 for the same four clamped

conditions considered in Figure 4.15. The contour plots suggest that the radial displacement mode shape has a horizontal nodal diameter and the clamped points yield only insignificant effect on the mode shape. The mode shape of circumferential displacement is considerably affected by the clamped points especially for the last two conditions where the clamped points are not symmetric about the vertical line. Therefore, locating the point supports on the nodal diameter of the mode minimizes the effect of the support on that particular mode. Moreover, the symmetry of point supports about the nodal diameter reduces the effect on the mode shapes.

(a) Radial   (b) Circumferential   (c) Deformed shape

Even Modes
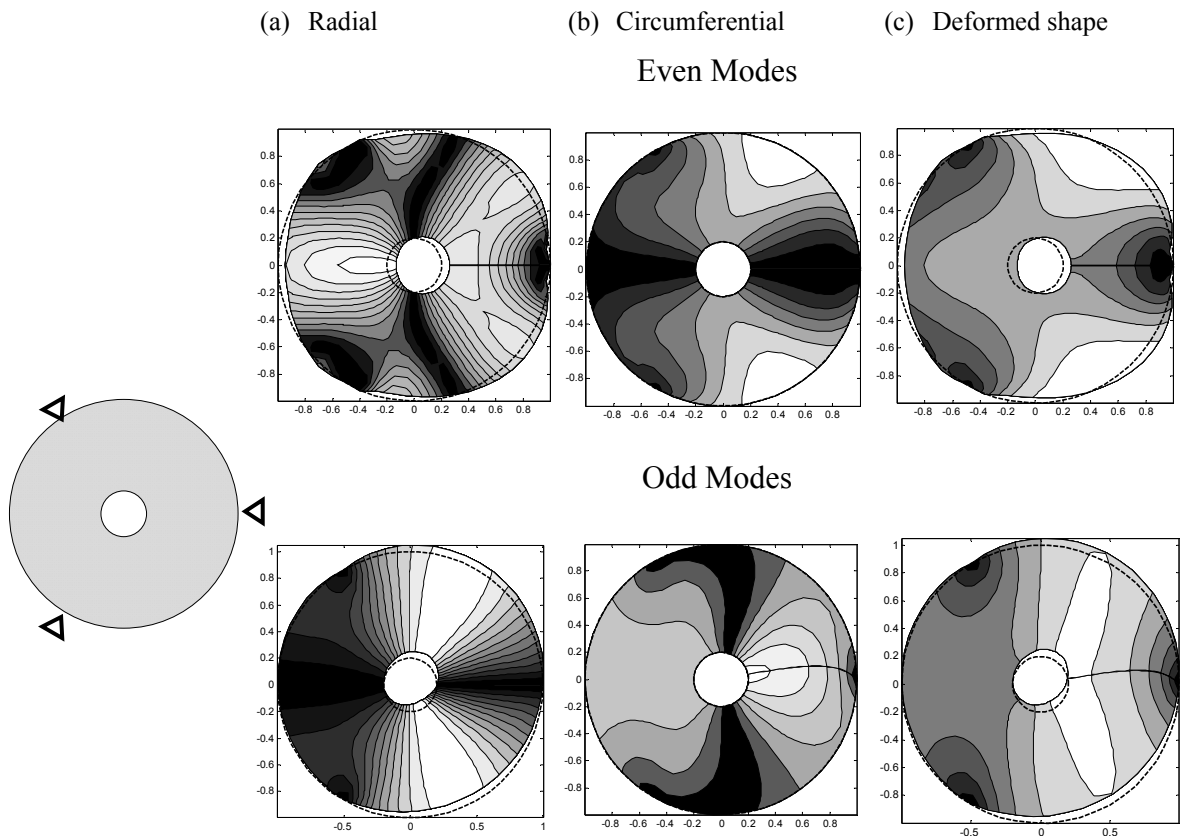
Odd Modes

Figure 4.17: Contour plots of the first even and odd modes of the annular disk clamped at three points: (a) radial displacement; (b) circumferential displacement, (c) vector sum of displacements◁ : point clamped support, - - - - · undeformed edge.

The same deflection mode is also investigated under the conditions of three and four point supports and the resulting contour plots are presented in figures 4.17 and 4.18, respectively. Each figure illustrates the results obtained from the even and odd subsystems. In the circumferential mode shape shown in Figure 4.17, the nodal diameter expands towards the point supports for both the odd and even modes. The results show that the number of bolts and their locations would have considerable effect on the frequency parameters and mode shapes.

(a) Radial   (b) Circumferential   (c) Deformed shape
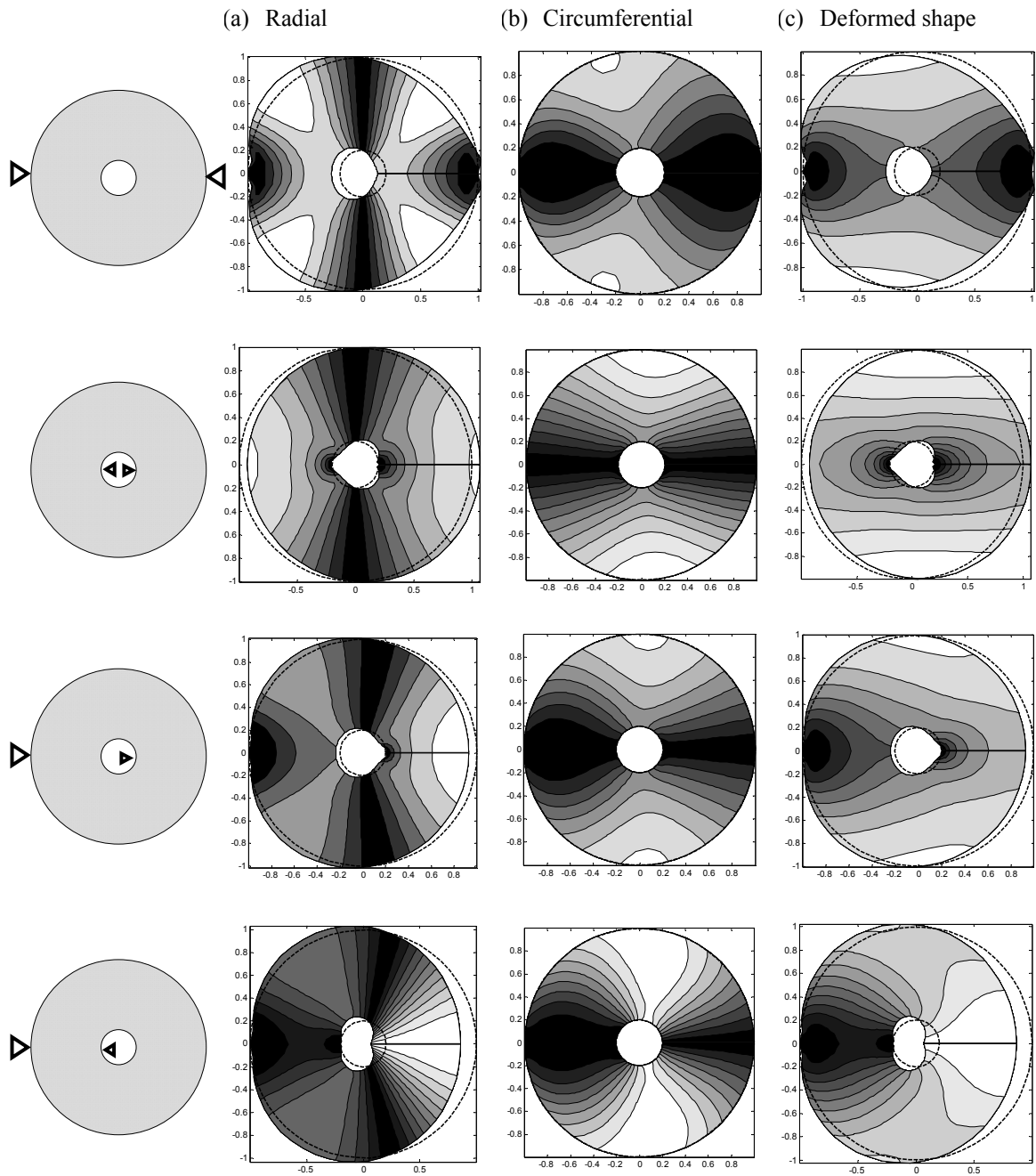
Even Modes
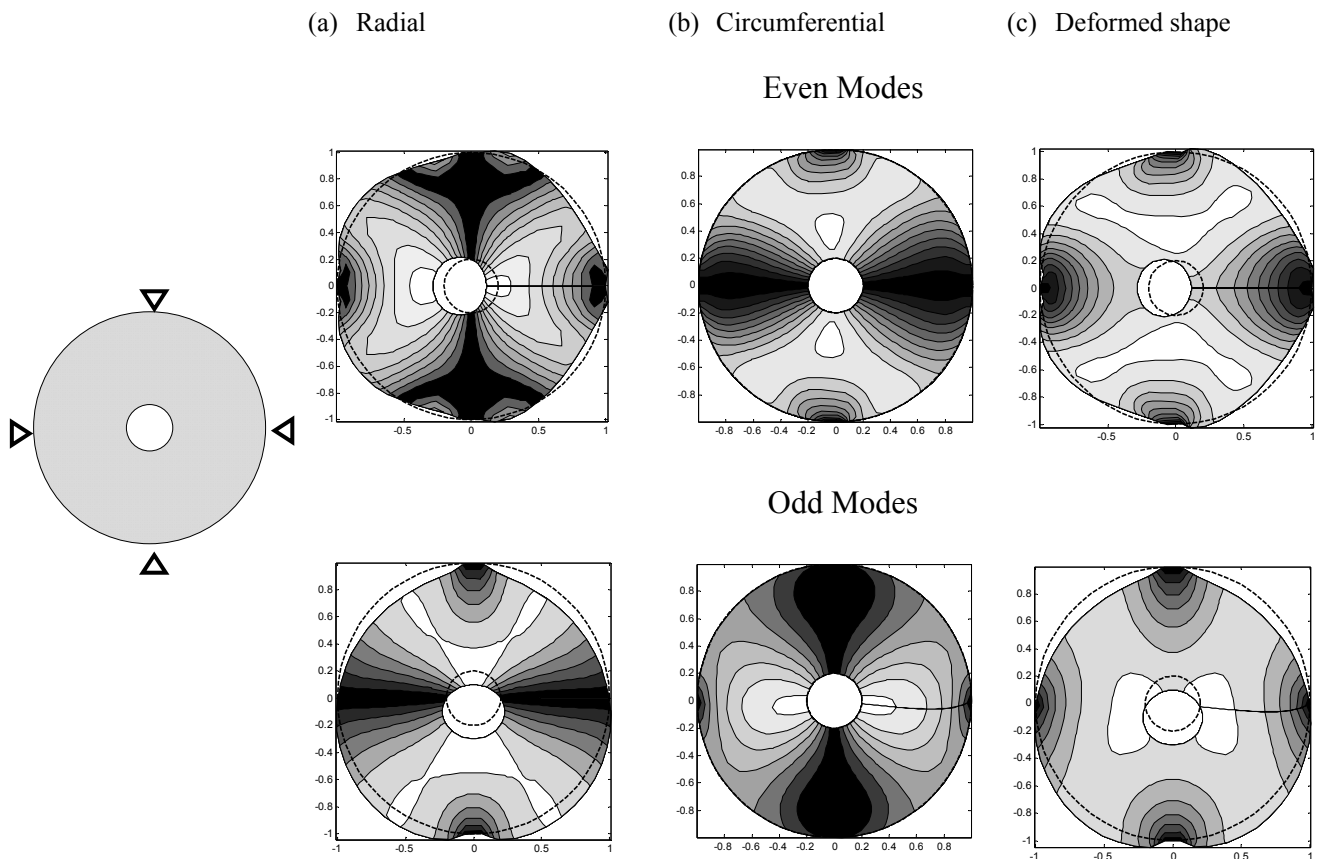
Odd Modes

Figure 4.18: Contour plots of the first even and odd modes of the annular disk clamped at four points: (a) radial displacement; (b) circumferential displacement, (c) vector sum of displacements◁ : point clamped support,   ----· undeformed edge.

142

4.7. Experimental Results

In this section, the results obtained from the experimental investigations on annular disks are presented, and discussed to illustrate the effects of non-uniformity of the support on the modal characteristics of the disks. The results obtained from the laboratory measurements are also compared with those obtained from the analytical model.

4.7.1. Disks with Free Boundary Conditions

Table 4.10 compares the first four in-plane natural frequencies of the annular disk (DISK I) with free edges obtained from the analytical model and experimental measurements. Figure 4.19 further presents the frequency spectrum of the measured in-plane vibrations of the disk. The measured and computed out-of-plane natural frequencies of the same disk are presented in Table 4.11, while the frequency spectrum of the vibration in the 12 kHz range is shown in Figure 4.20. Comparisons of the spectra presented in Figures 4.19 and 4.20 suggest that none of the out-of-plane modes occur in the proximity of the in-plane modes. The first in-plane mode occurs at 4848 Hz, while none of the out-of-plane modes seem to be present near this frequency. Similarly, none of the out-of-plane modes exist between the 8486 and 10460 Hz frequency range, where the next three in-plane modes are observed. It is thus concluded that the measurements acquired along the radial direction can accurately describe the in-plane modes of vibration with negligible coupling effects of the in-plane and out-of-plane modes. Tables 4.10 and 4.11 show good agreements between the analytical and experimentally observed natural frequencies of in-plane and out-of-plane vibration of the disk suggesting

143

the validity of the analytical model in predicting the natural frequencies of annular disks

with free edges.

Table 4.10: Compariosn of in-plane natural frequencies of the annular disk with free edges (DISK I) identified from the experiment with those derived from the analytical model.

(m,n)	(0,2)	(1,1)	(0,0)r	(0,3)
Experimental (Hz)	4848	8952	9720	10450
Analytical (Hz)	4821	8865	9602	10332
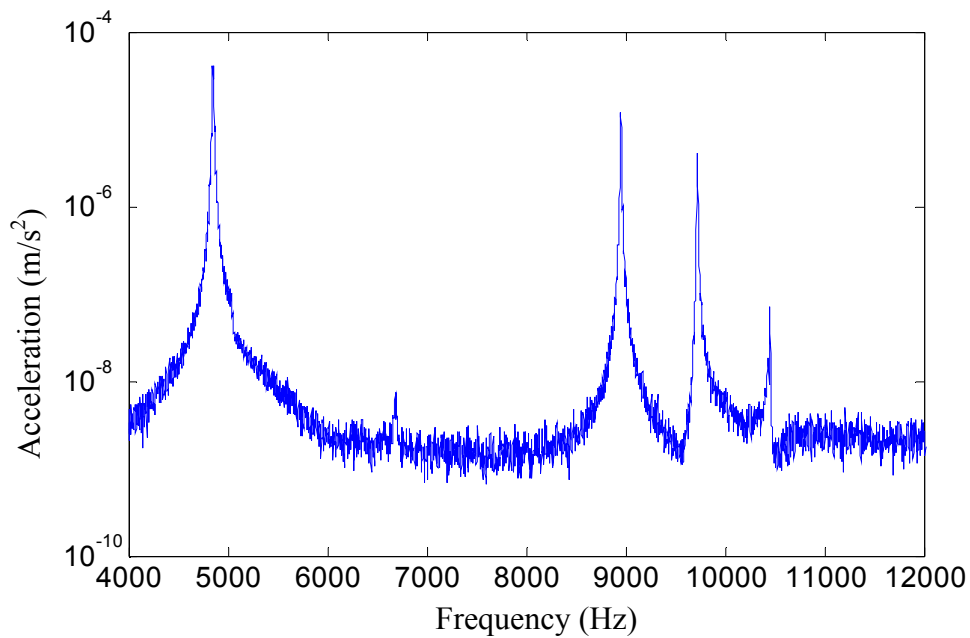
Figure 4.19: Frequency spectrum of measured in-plane vibration for an annular disk with free edges (DISK I).

Table 4.11: Compariosn of out-of-plane natural frequencies of the annular disk with free edges (DISK I) identified from the experiment with those derived from the analytical model.

Experimental (Hz)	522	936	1326	1908	2354	3486	3598	5036
Analytical (Hz)	528	922	1337	1965	2388	3572	3678	5211
Experimental (Hz)	5348	5854	6504	6676	7502	8220	8486	10460
Analytical (Hz)	5520	5990	6788	6988	7848	8801	9009	10476

144
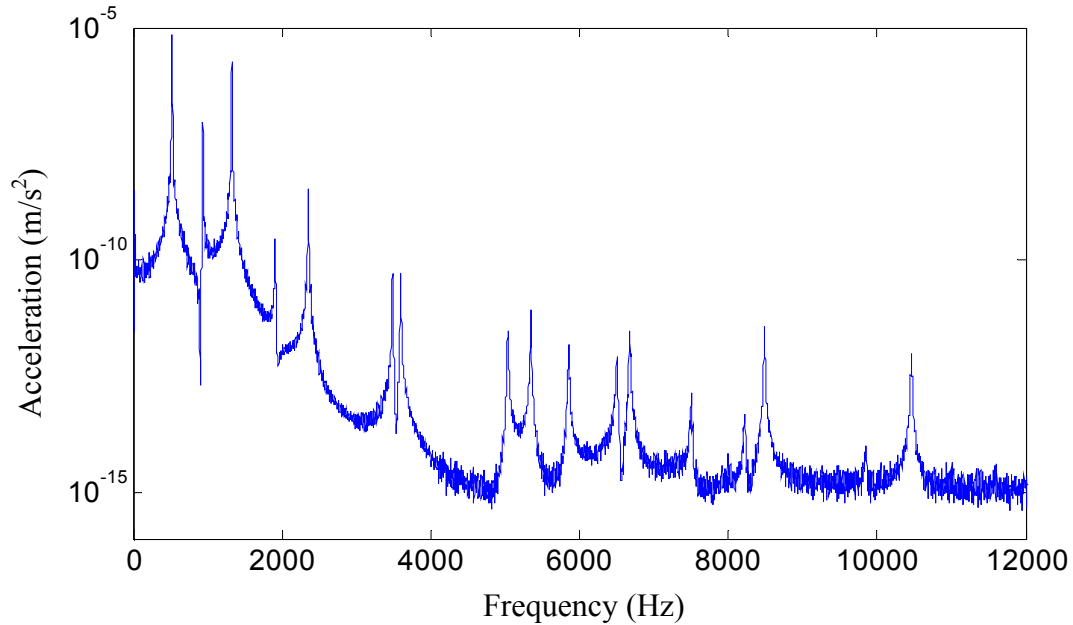
Figure 4.20: Frequency spectrum of measured out-of-plane vibration of an annular disk with free edges (DISK I).

Table 4.12 compares the in-plane natural frequencies of the annular disk (DISK II, R_i = 0.09 m) with free edges obtained from the measurements and the analytical model. Figure 4.21 illustrates the spectrum of measured in-plane vibration of the disk. Comparison of the in-plane natural frequencies of DISK I (Table 4.10) and DISK II (Table 4.12) show the effect of variation in the radius ratio on the natural frequencies. The results were also observed to be in close agreement with those reported by Ambati [18] for disks with free edges. The modes with zero nodal circles ($m = 0$) exhibit the lowest values for DISK II, which confirms that these modes approach zero frequencies as the radius ratio increases. The mode (0, 3) tends to decrease from around 10 kHz for DISK I to nearly 6 kHz for DISK II, as the radius ratio increases. The radial mode $(0, 0)r$ and the mode (1,1) change their order but their values do not decrease dramatically. The mode (0,4) is an additional mode shown within the range of interest in the DISK II

response which was higher than the range of interest for the low radius ratio disk (DISK I).

Table 4.12: Compariosn of in-plane natural frequencies of the annular disk with free edges (DISK II) identified from the experiment with those derived from the analytical model.

(*m,n*)	(0,2)	(0,3)	(0,0)r	(1,1)	(0,4)
Experimental (Hz)	2432	6064	7040	9344	10160
Analytical (Hz)	2439	6018	6951	9243	10065
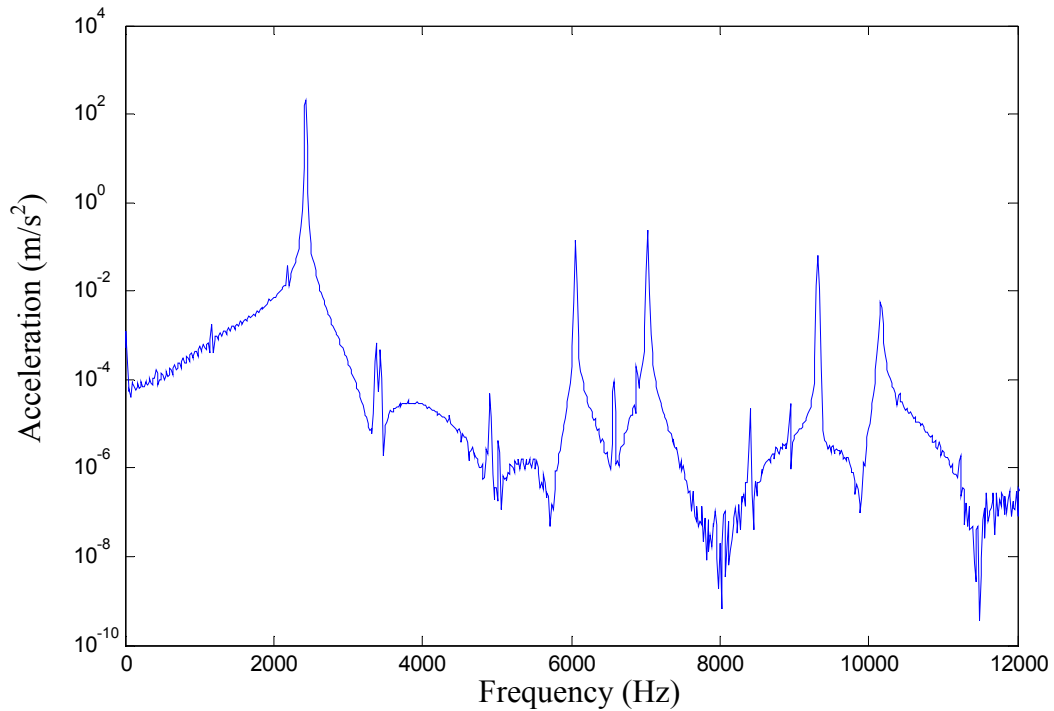
Figure 4.21: Frequency spectrum of measured in-plane vibration for an annular disk with free edges (DISK II).

4.7.2. Non-uniform Support Conditions

Since a perfectly clamped condition at a point or edge cannot be achieved in practice, all of the reported experimental works on in-plane vibrations have been conducted with disks with free edges. While the primary purpose of the experiments in this study was to obtain the frequency distributions for disks with point support

146

conditions, the results could not be compared with analytical results for circular disks with such clamped points. The measured data obtained for point-clamped disks are thus compared with those obtained for the disks with free edges in order to examine the frequency responses in a qualitative sense. The frequency distribution is compared with that of the disk without supports to study the effects of additional supports on the natural frequencies. The results obtained from the analytical model for disks with a point support are used to facilitate the interpretation of the experimental results. It is also important to note that the experimentally observed frequencies would be higher than those derived from the model since the clamped support used in the experiment cannot be characterized by a point support that is considered in the model. Furthermore, the measured data could be affected by several other factors such as the location of the accelerometer relative to the support location. The location of the accelerometer at or near the nodal diameter of some of the modes would significantly influence the measurements. Furthermore, in order to limit the contribution of the in-plane modes, the analysis of the effects of point supports on the out-of-plane modes has been limited to frequency range of 5 kHz.

Out-of-plane Modes

Figure 4.22 shows the frequency spectrum of the out-of-plane vibration response of the point-supported disk. The figure illustrates the spectra of the measurements taken at two different points relative to the support. Comparisons of the spectra with that of the disk with free edges (Figure 4.20) show significant effect of the support on the frequency distribution. For example, the free disk mode located at 1908 Hz (Figure 4.20) splits into two distinct peaks for the point-supported disk at 1918 Hz and 2230 Hz (Figure 4.22(a)).

147

The observed results agree very well with the analytical results. Moreover, Figure 4.22(b) shows two distinct peaks at 2538 and 3170 Hz, which could not be observed from the previous figures. The results obtained from the analytical model, however, revealed these two peaks to be the odd and even natural frequencies of the 2356 Hz mode observed in Figure 4.20. In Figure 4.22 (a) and (b), the peak observed near 4604 Hz is not evident in the response of the disk with free edges (Figure 4.20). This peak, however, corresponds to the 3598 Hz mode in Figure 4.20, which suggests that the corresponding frequency increases by nearly 1.0 kHz due to the additional support.
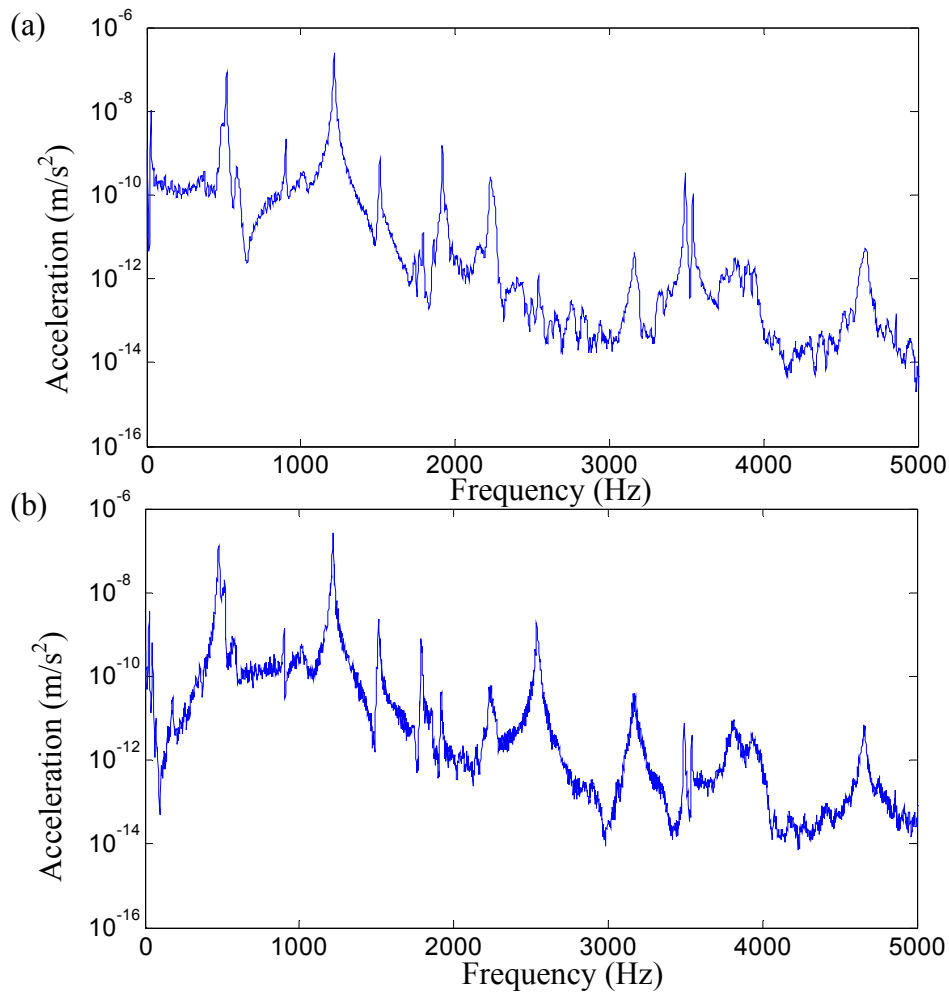
Figure 4.22: Out-of-plane frequency spectrum for an annular disk with point support (DISK I): angular position of the accelerometer relative to the support (a) $\pi/2$, (b) π.

148

The frequency spectrum of the out-of-plane vibration measured under an excitation along the radial direction is shown in Figure 4.23. The pairs of frequencies described in Figure 4.22 are also clearly observed from Figure 4.23. The first in-plane mode is also observed at 4848 Hz, which was not evident in the spectra (Figure 4.22) obtained under out-of-plane excitations alone. This figure demonstrates a strong relation between the out-of-plane and in-plane modes of vibration, and that the in-plane excitations could excite the out-of-plane modes in a manner similar to that caused by excitations along the out-of-plane direction.
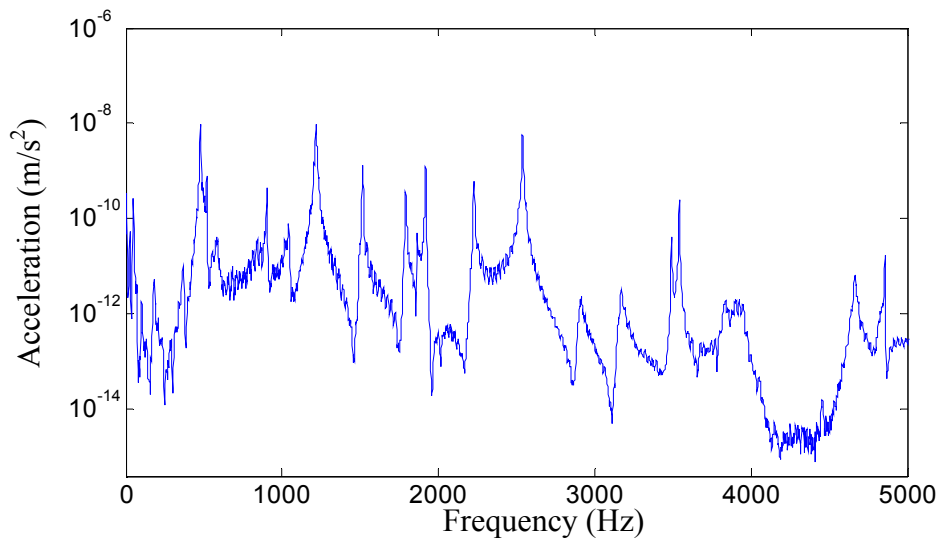
Figure 4.23: Out-of-plane frequency spectrum for an annular disk with point support (DISK I) due to in-plane excitation.

In-plane Modes

The effect of point supports on the in-plane modes of vibration is illustrated by examining the frequency spectrum of in-plane vibration of the point-supported disk, as shown in Figure 4.24. Comparison with the frequency spectrum of the disk with free edges (Figure 4.19) suggests the presence of five peaks in the 8.5 to 11.0 kHz range instead of the three peaks observed for the free disk. This is attributed to the splitting of

149

the two modes into two distinct frequencies, while the third one was a purely radial mode whose frequency increased slightly with the point-support. The first in-plane mode at 4848 Hz (Figure 4.19) also increased slightly due to the point support but did not split into two values although it belongs to the group of modes that are expected to yield such a behavior. This could be explained by the fact that this mode is (0, 2), where both the odd and even components have nodal points at the support locations which are not affected by the additional support. In this situation, the acceleration measurement at the outer edge could not detect the predominant circumferential modes. The measurements could thus capture the radial displacement only. Furthermore, the circumferential modes are also difficult to excite, as reported in a previous study [14].

Figure 4.25 illustrates the frequency spectrum of in-plane vibration of the annular disk (DISK II) supported using a C-clamp to simulate two points supports. The orientation of the support is similar to the last condition shown in Figure 4.15. A comparison of the spectrum of the disk with that of the free disk (Figure 4.21) and the frequencies in Table 4.12, shows the significant effect of the additional support on the natural frequencies. A split of the first mode (0,2) to odd and even values could not be observed, which is most likely attributed to the factors discussed in the response of DISK I (Figure 4.24). The second mode (0,3), however, splits into two values, where the first value is same as that of the free disk while the second value corresponds to an additional peak near 6.4 kHz. The third mode is a purely radial mode and its frequency increased from 7.0 kHz to 7.3 kHz, as it would be expected. The spectrum also exhibits several smaller peaks above the first radial modes; a definite association with the out-of-plane or in-plane modes could not be established.

150
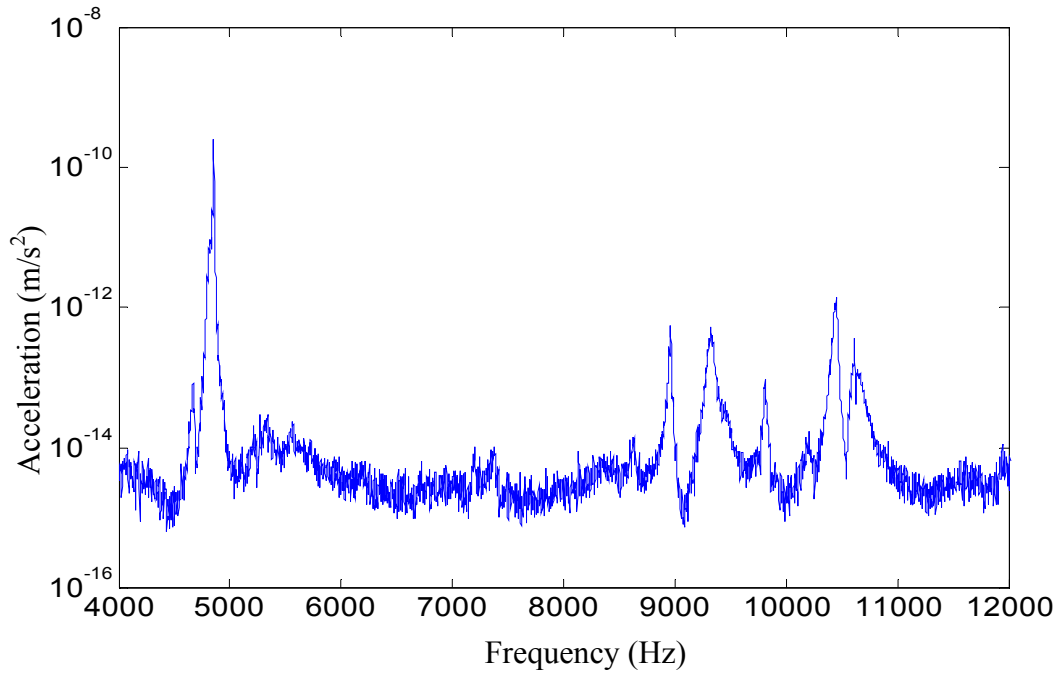
Figure 4.24: In-plane frequency spectrum for an annular disk with point support (DISK I) due to in-plane excitation.
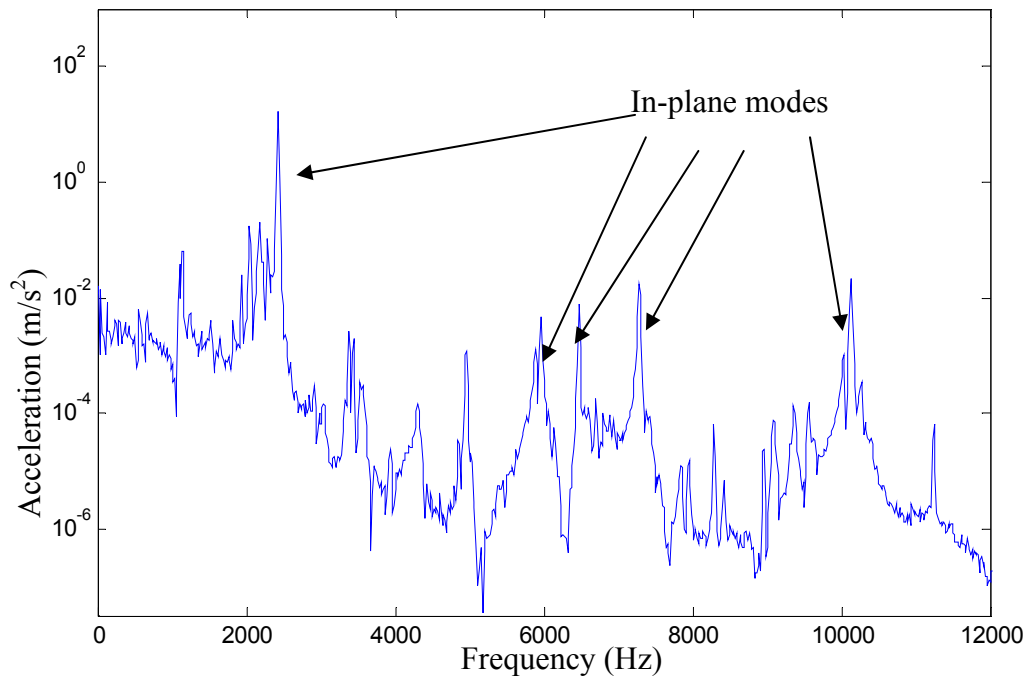
Figure 4.25: In-plane frequency spectrum for an annular disk with two-point support (DISK II) due to in-plane excitation.

The results obtained from the accelerometer are also compared with those from the microphone to confirm that in-plane modes contribute to the total noise

151

radiations. Figure 4.26 shows the frequency spectrum of the acoustic signal measured at the out-of-plane position. A comparison with the frequency spectrum obtained from the accelerometer along the radial direction in Figure 4.19 shows that the in-plane modes are effectively detected by the microphone and the magnitudes of the observed peeks are comparable to those corresponding to the out-of-plane modes. Figure 4.27 shows the sound pressure spectrum when the microphone is placed along the radial direction. The results suggest stronger contributions of the in-plane modes compared to the out-of-plane modes over the same range. It should be noted that the results are presented in the 4000 Hz to 12000Hz frequency range, since the first in-plane mode is observed 4848 Hz for DISK I. These results confirm that the in-plane modes of vibration are an important contributor to the total noise radiation if they fall in the range of interest for the particular application.

The signals obtained from the accelerometer are also compared with those from the microphone to illustrate the contributions of the in-plane modes to the total noise radiations. A comparison of the frequency spectrum of the measured in-plane vibration of the free disk excited along the radial direction with that of (Figure 4.19) the sound pressure signal measured at an out-of-plane position (Figure 4.26) shows that the in-plane modes could also be detected from the microphone signal. Furthermore, the magnitudes of the observed peaks are comparable to those of the out-of-plane vibration peaks in the vicinity. When the microphone is placed along the radial direction, the frequency distribution in Figure 4.27 shows more important contributions of the in-plane modes than the out-of-plane modes in the same range.
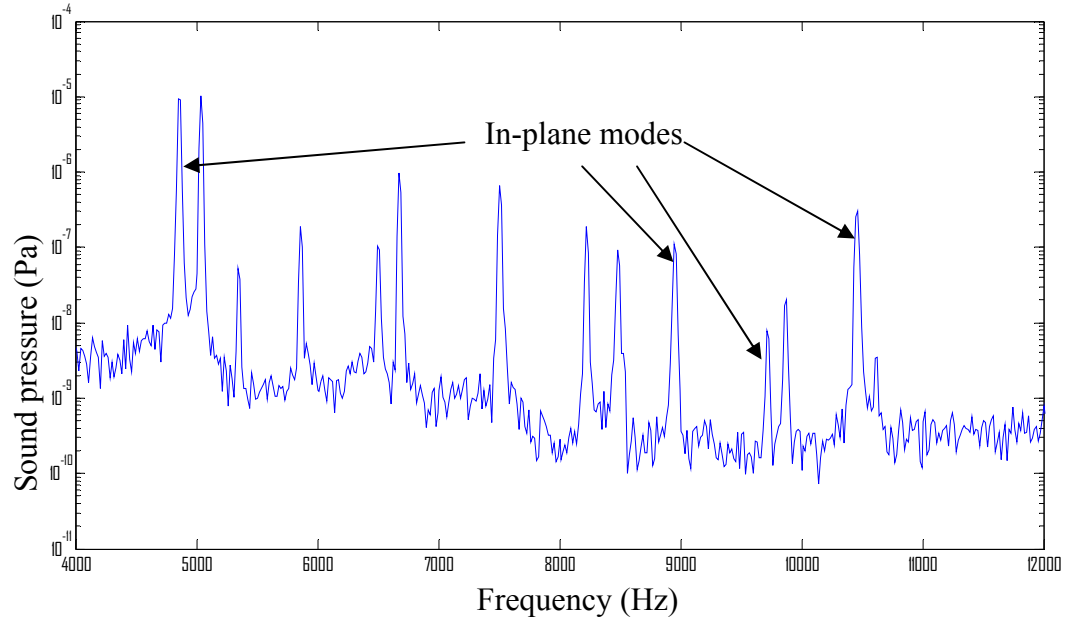
Figure 4.26: Frequency spectrum of the microphone signal at the out-of-plane position.
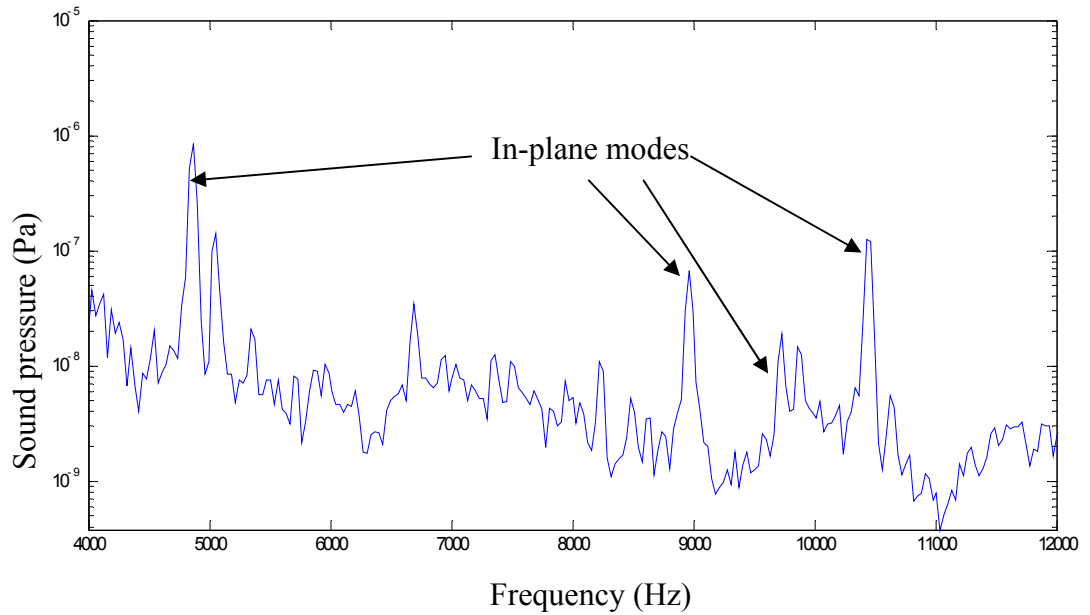
Figure 4.27: Frequency spectrum of the microphone signal at the in-plane position.

The experimental results also confirm the analytical results that some modes split into two distinct values when non-uniform boundary conditions are introduced. The results show that in-plane modes contribute to the total noise radiation and cannot be ignored. Experimental investigations also showed that in-plane modes can be detected

153

along the out-of-plane direction suggesting a strong coupling between in-plane and out-of-plane modes even though the thickness to radius ratio is relatively low.

4.8. *Analysis of Acoustic Responses*

Acoustic properties of annular disks such as sound pressure, directivity and sound power could also be obtained from the analytical approach described in section 2.6. The effects of non-uniformity of the boundary conditions on the acoustic properties of the disk could thus be investigated in a similar manner. The results are compared with those obtained by Lee and Singh [24] for the free edges conditions to examine the validity of the analytical approach. The effects of an additional point support are, then, investigated and discussed. The geometric and material properties of the annular disk used in the current analysis are same as that used by Lee and Singh [24] (R_o= 151.5 mm, R_i = 87.5 mm, h = 31.5 mm, ρ = 7905.9 kg/m^3, E = 218 × 10^9 N/m^2 and v = 0.305. In order to obtain an estimate of the acoustic properties, the frequency response characteristics of the disk are computed to determine the relative amplitudes of radial displacements of the inner and outer edges. For this purpose, a reduced order model is formulated for the annular disks with the specified boundary conditions. For this purpose, the modal properties of the disk are obtained by solving the associated eigenvalue problem. A modal transformation is then invoked to formulate the system in terms of a reduced set of modal DOF representing the significant modes. Equation (2.104) is subsequently solved to determine the frequency response characteristics of the radial displacement due to a unit harmonic force applied at the outer edge.

Figure 4.28 shows the frequency response characteristics of the annular disk with free and point support boundary conditions used in the analysis. The solid line represents the frequency response of the disk with free edges, while the dashed and dotted lines represent the frequency response of the disk supported at a single point obtained from the even and the odd systems, respectively. The peaks shown in the frequency responses correspond to modes (0,2), (0,3) and (0,0)r. It is evident that the odd part of the mode (0,3) is hardly affected by the additional support, suggesting that the support is located at a nodal diameter of this specific mode. The acoustic radiations associated with the first two in-plane modes are evaluated and discussed below.
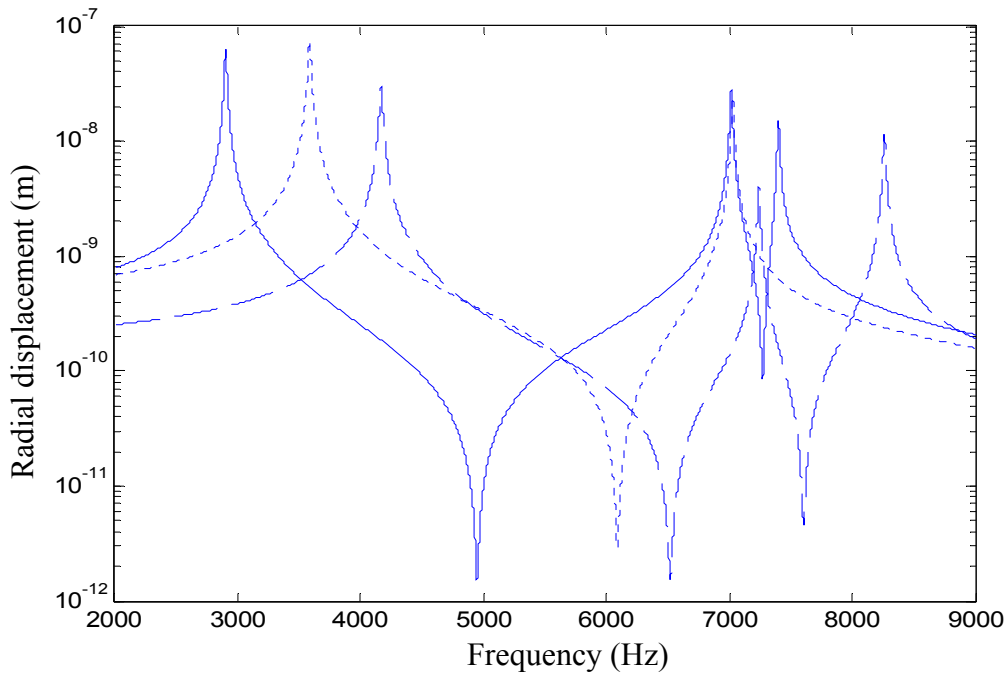
Figure 4.28: Frequency response characteristics of the annular disk with different boundary conditions: ——— free, – – – – point support (even system), ················ point support (odd).

The deflection modes of the radial displacements associated with the first two in-plane modes of the disk with free edges are shown in Figure 4.29. The far-field sound pressure is then obtained from Eq. (2.93) through (2.95) assuming that the sound pressure

is only due to the in-plane velocities of the inner and outer surfaces. The sound pressure expressions are evaluated at several points on a sphere of 303 mm radius with center coinciding with the center of the disk. The variations in the directivity patterns $D(\theta, \phi)$ are obtained along the θ and ϕ directions. Figure 4.30 shows the directivity patterns for the first two modes along θ directions for a disk with free boundary conditions obtained from the even subsystem with $\phi = \pi/2$, while Figure 4.31 shows the directivity along θ direction with $\theta = 0$. The results are presented in terms of normalized pressure, which is the sound pressure normalized by the maximum pressure value. The results in both the figures agree very well with those presented by Lee [108].

(a)   (b)
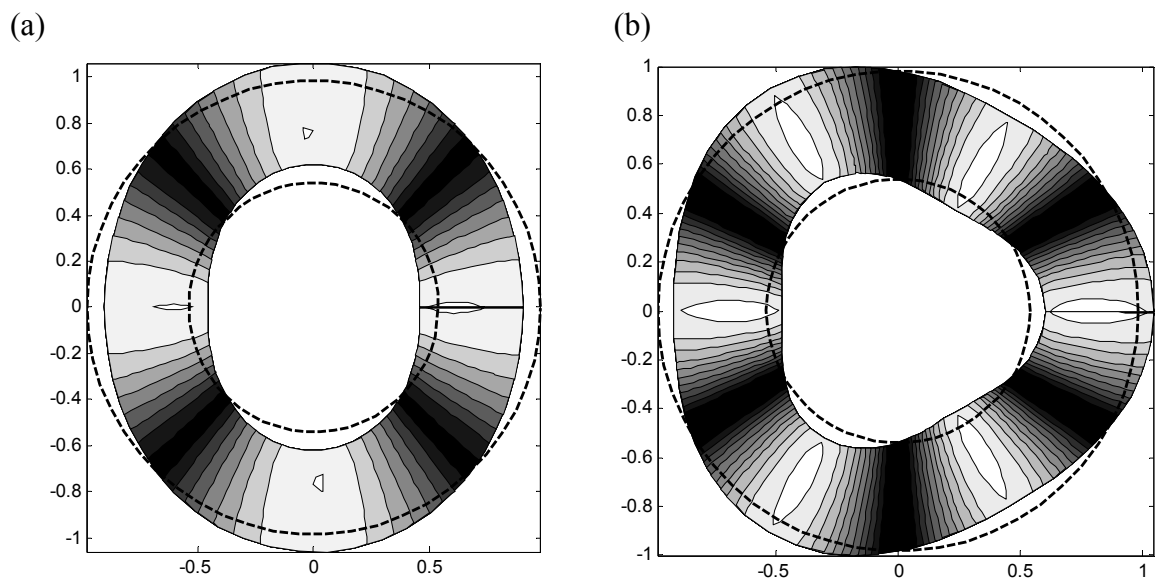
Figure 4.29: The radial deflection plots of the annular disk with free edges: (a) mode (0,2); and (b) mode (0,3).

Considering the symmetry of the patterns, the directivity is plotted in the 0 to 90^0 span. The directivity pattern of the free disk obtained from the odd subsystem along the θ directions with $\phi = \pi/2$ is illustrated in Figure 4.32 for the first two modes. The variations along the θ direction show harmonic patterns similar to the variation observed

156

in the structural radial displacement in Figure 4.29, while the directivity of the odd subsystem exhibit a phase shift of $\pi/(2n)$ with respect to the counterpart from the even subsystem. The variation along ϕ direction for the odd subsystem is identical to that of the even subsystem, as shown in Figure 4.31.

(a)

(b)
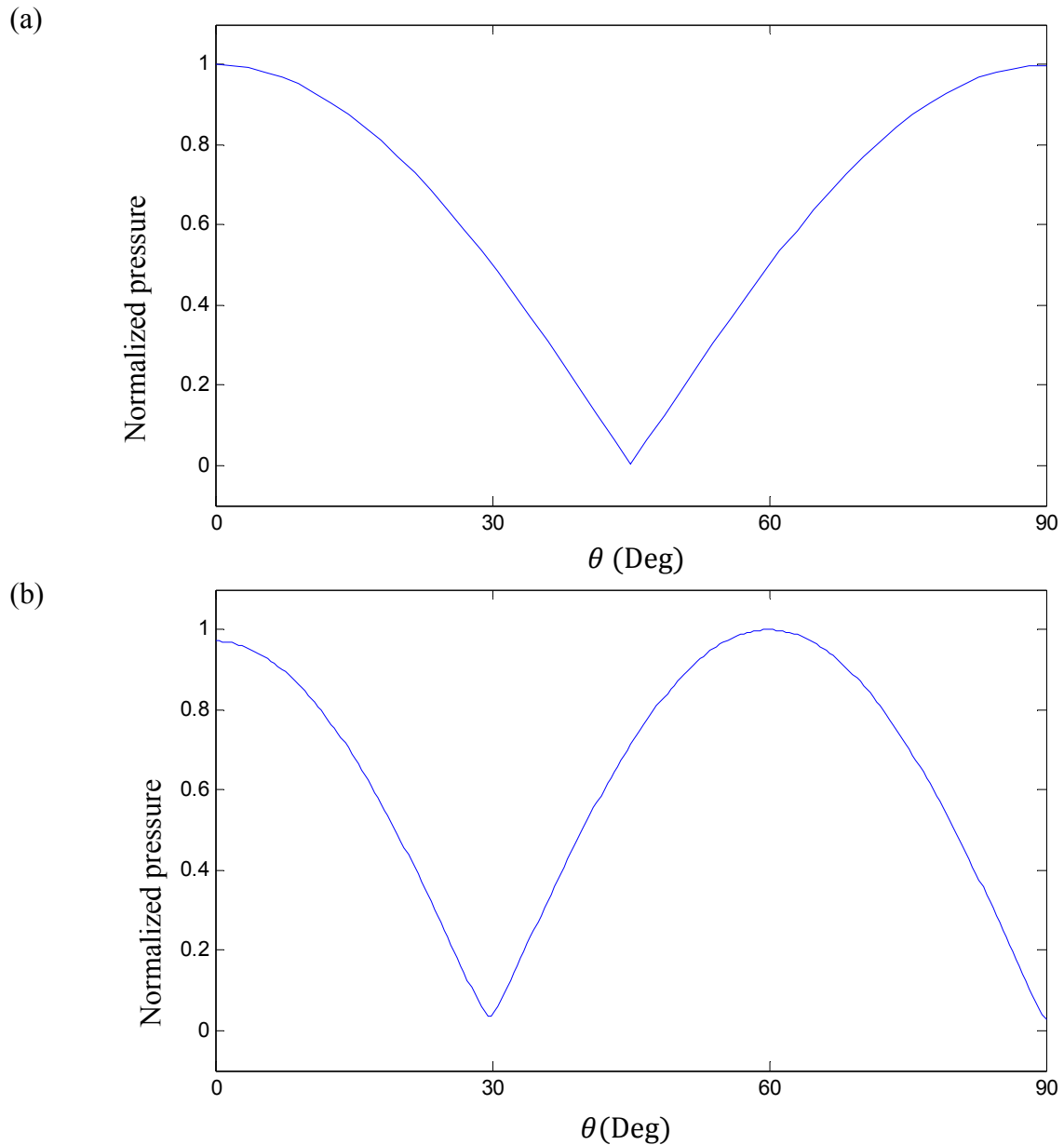
Figure 4.30: Directivity pattern of the annular disk with free edges along θ direction for even subsystem: a) mode (0,2); b) mode (0,3).

(a)

ϕ(Deg)

(b)

ϕ(Deg)
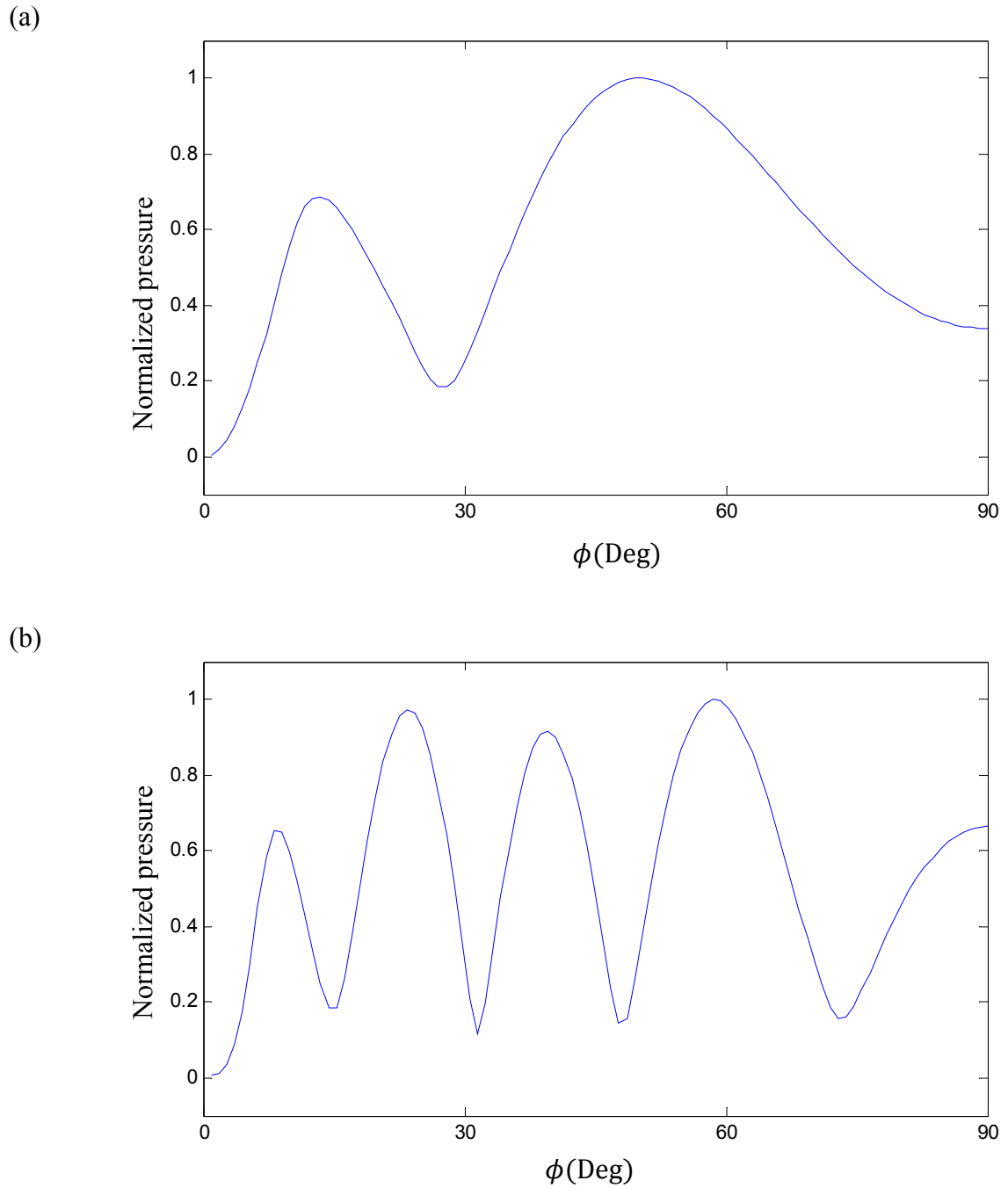
Figure 4.31: Directivity pattern of the annular disk with free edges along ϕ direction for even subsystem: (a) mode (0,2); (b) mode (0,3).

(a)

(b)
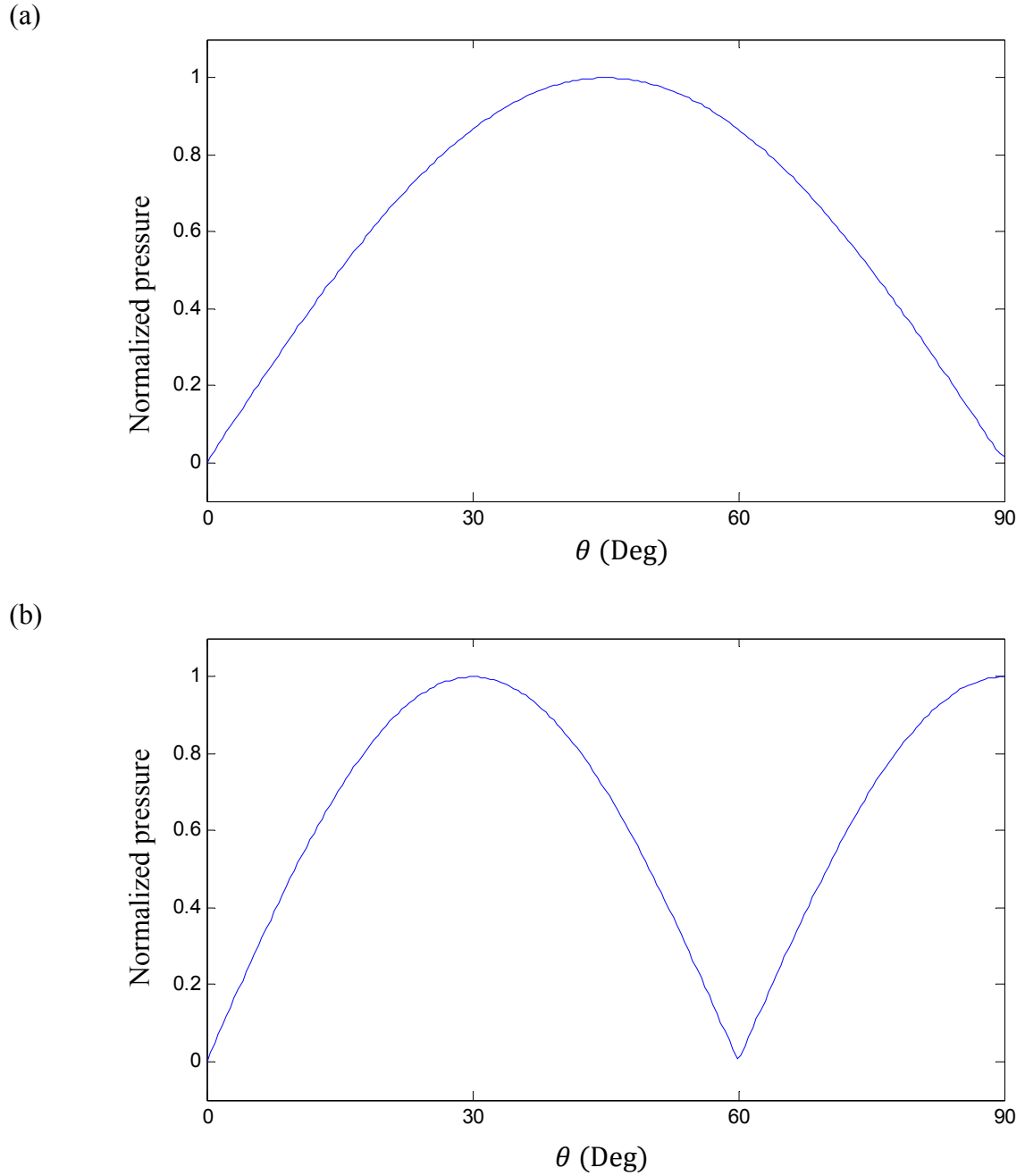
Figure 4.32: Directivity pattern of the annular disk with free edges along θ direction for odd subsystem: (a) mode (0,2); (b) mode (0,3).

Figure 4.33 illustrates the directivity of the first two modes of the disk with a point support at the outer edge along the θ direction obtained from the even subsystem. Unlike the free conditions, the sound pressure does not reach zero at the nodal line

159

location which can be attributed to the coupling with other modes. The directivity pattern is affected by the support although similar primary trend can be observed. The variation in the sound pressure along ϕ direction is shown in Figure 4.34. The directivity patterns obtained from the odd subsystem along the θ and ϕ directions are depicted in Figures 4.35 and 4.36, respectively. Comparisons of results show that the directivity patterns of the odd and even subsystems for the point-supported disk are quite different. Figures 4.35(b) and 4.36(b) show that the directivity pattern corresponding of mode (0,3), obtained from the odd subsystem, are identical to those obtained for the free disk. This is attributable to the fact that the point support is located along the nodal diameter of this specific mode and does not affect the modal and acoustic characteristics. This was also observed from the frequency response of the free disk in Figure 4.28 where the second peak derived from the odd subsystem coincides with the peak corresponding to mode (0,3).

The modal sound power Π_{mn} and radiation efficiency σ_{mn} are further obtained and compared with the reported numerical results obtained using boundary element method (BEM) and measured data [108]. Tables 4.13 and 4.14 present comparisons of the computed modal sound power and the radiation efficiency, respectively, with the reported numerical and measured values. The results show reasonably good agreements between the model and the reported the results, suggesting that the analytical model can predict acoustic properties of the annular disks with sufficient accuracy. Table 4.15 summarizes the sound power and radiation efficiency for the even and odd subsystems of the same annular disk with a point support. For the even sub system, the sound power Π_{mn} of mode (0,2) increases due to the substantial increase in the natural frequency of the point-

160
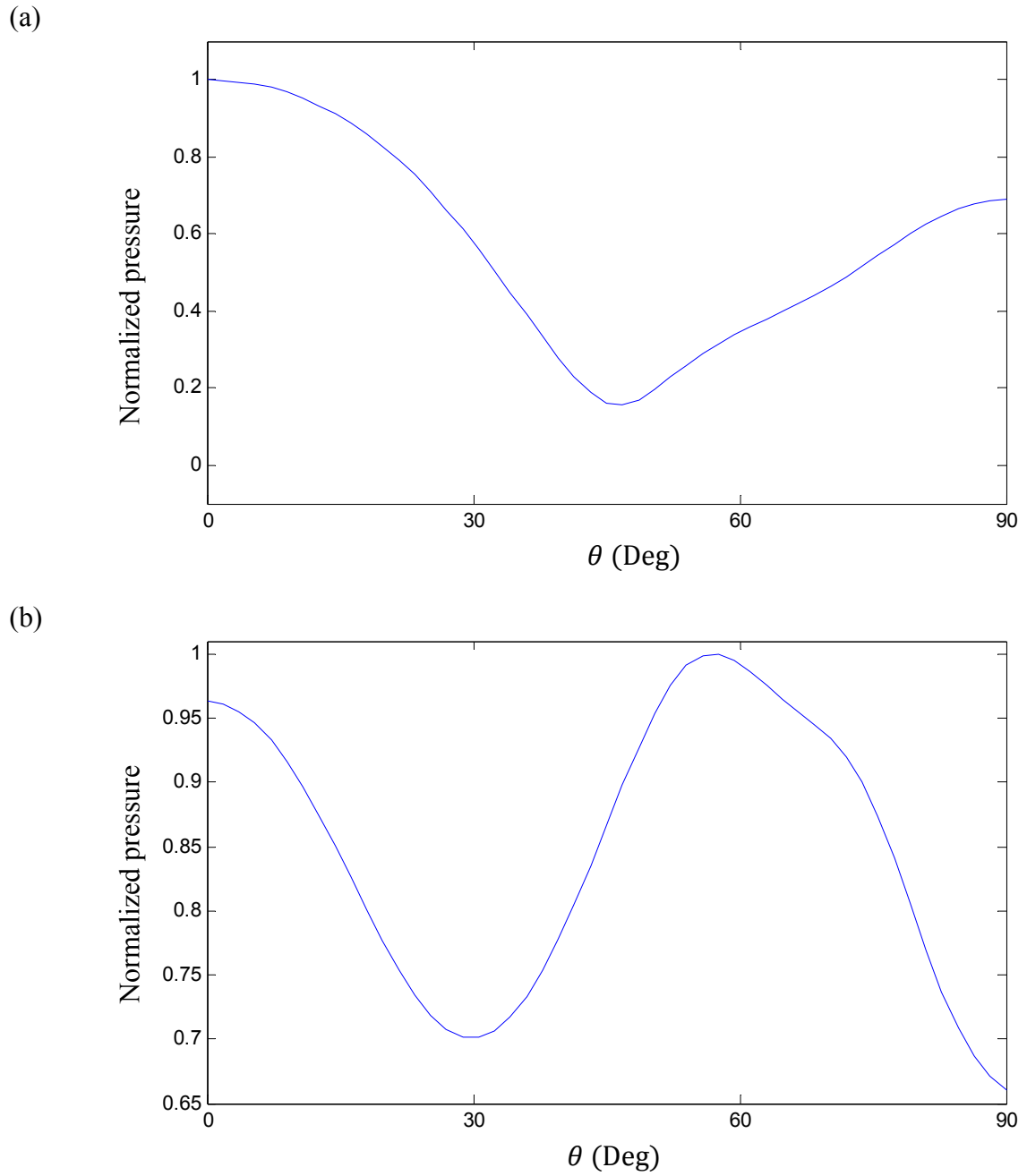
Figure 4.33: Directivity pattern of the point-supported annular disk along θ direction for even subsystem: (a) mode (0,2); (b) mode (0,3).

(a)

ϕ(Deg)

(b)

ϕ (Deg)
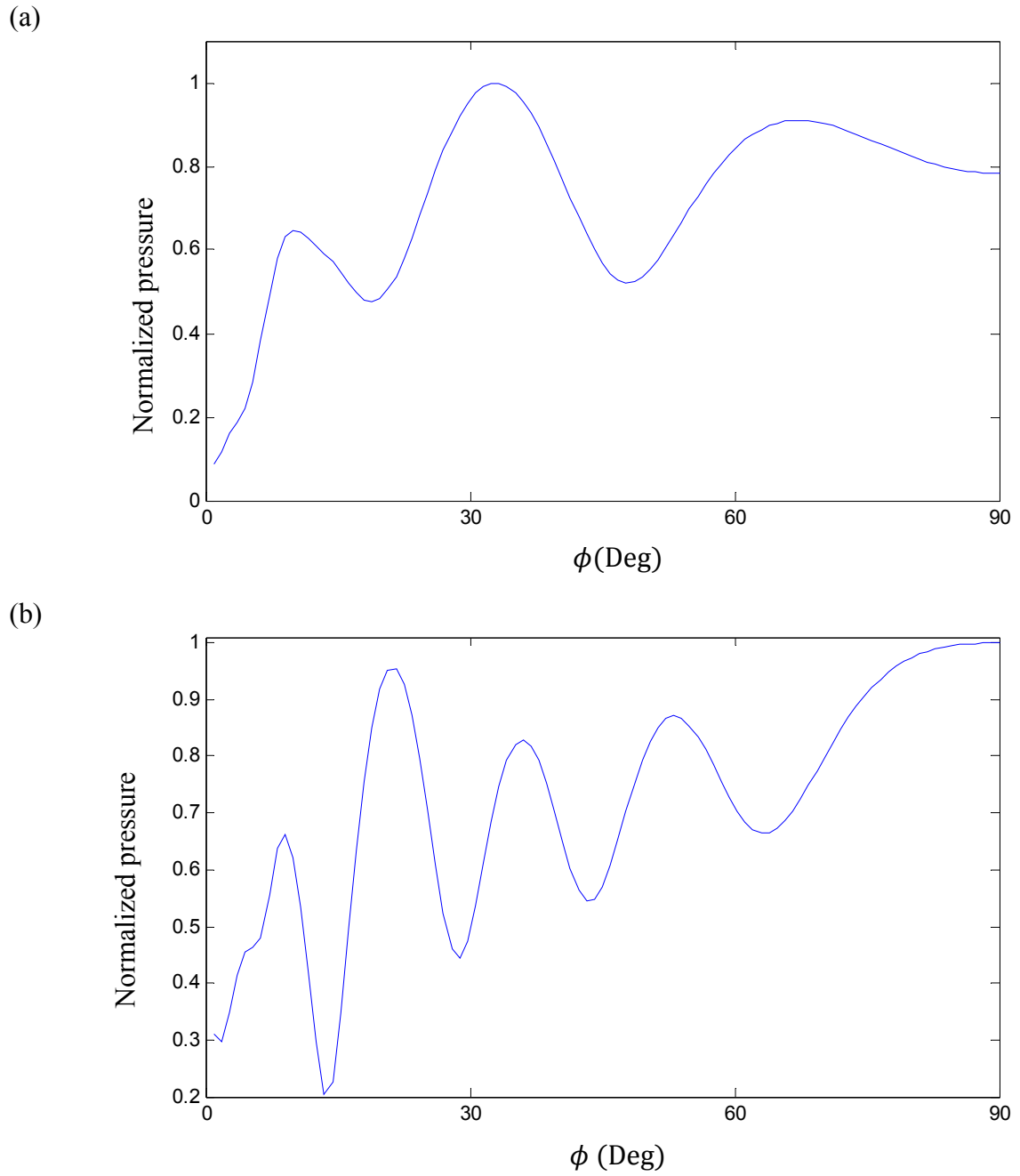
Figure 4.34: Directivity pattern of the point-supported annular disk along ϕ direction derived from even subsystem: (a) mode (0,2); (b) mode (0,3).

(a)

(b)
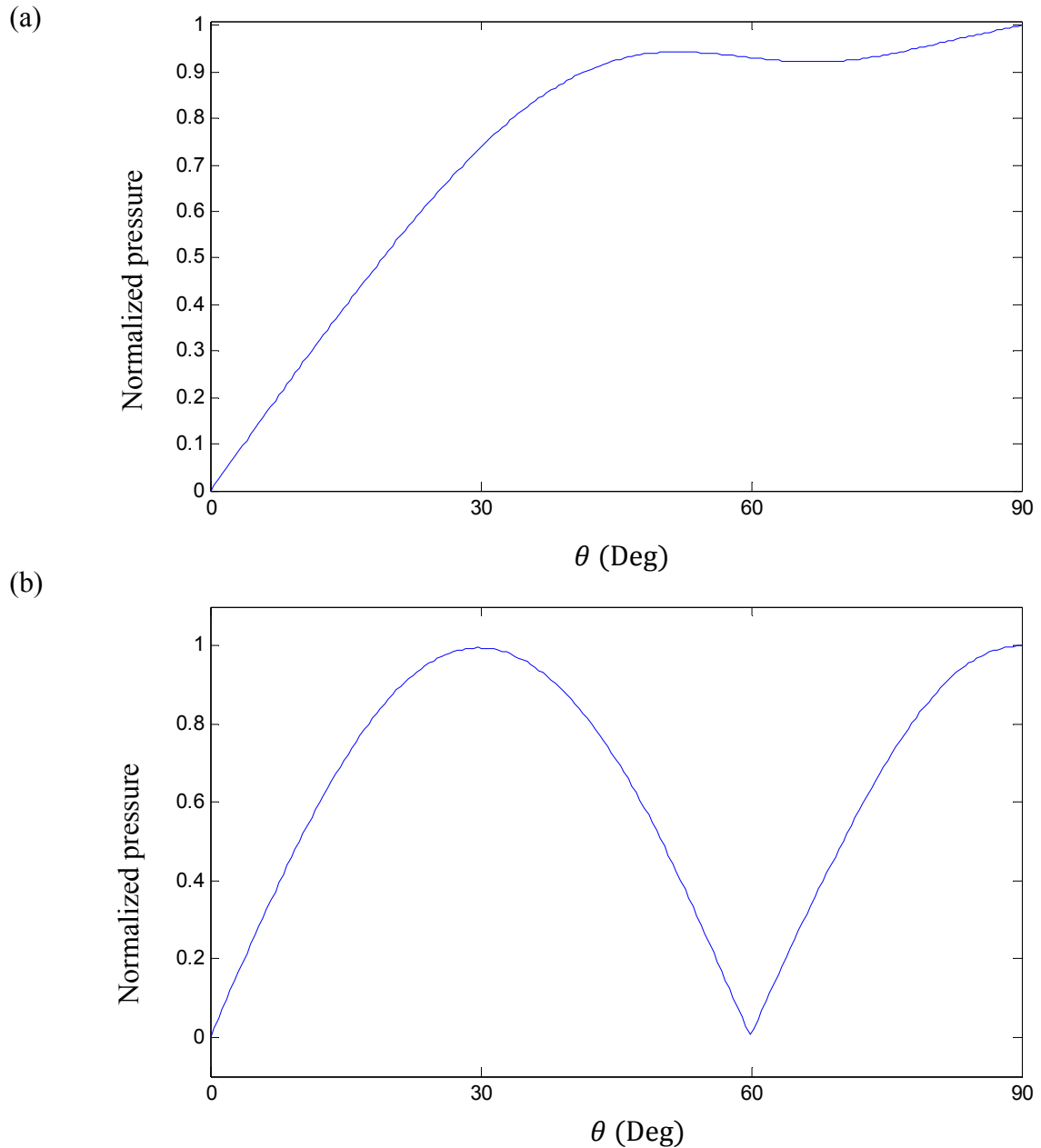
Figure 4.35: Directivity pattern of the point-supported annular disk along θ direction derived from odd subsystem: (a) mode (0,2); (b) mode (0,3).

supported disks as shown in Figure 4.28. The sound power corresponding to mode (0,3) decreases as a result of the decrease in the magnitude of the even part of the mode (0,3), although the natural frequency increases slightly. The radiation efficiency increases in both the modes due to increase in the natural frequency. The sound power and radiation

163

efficiency of the odd subsystems increase for mode (0,2) due to increase in the natural frequency while they do not change for mode (0,3) since it is not affected by the point support.

(a)

(b)
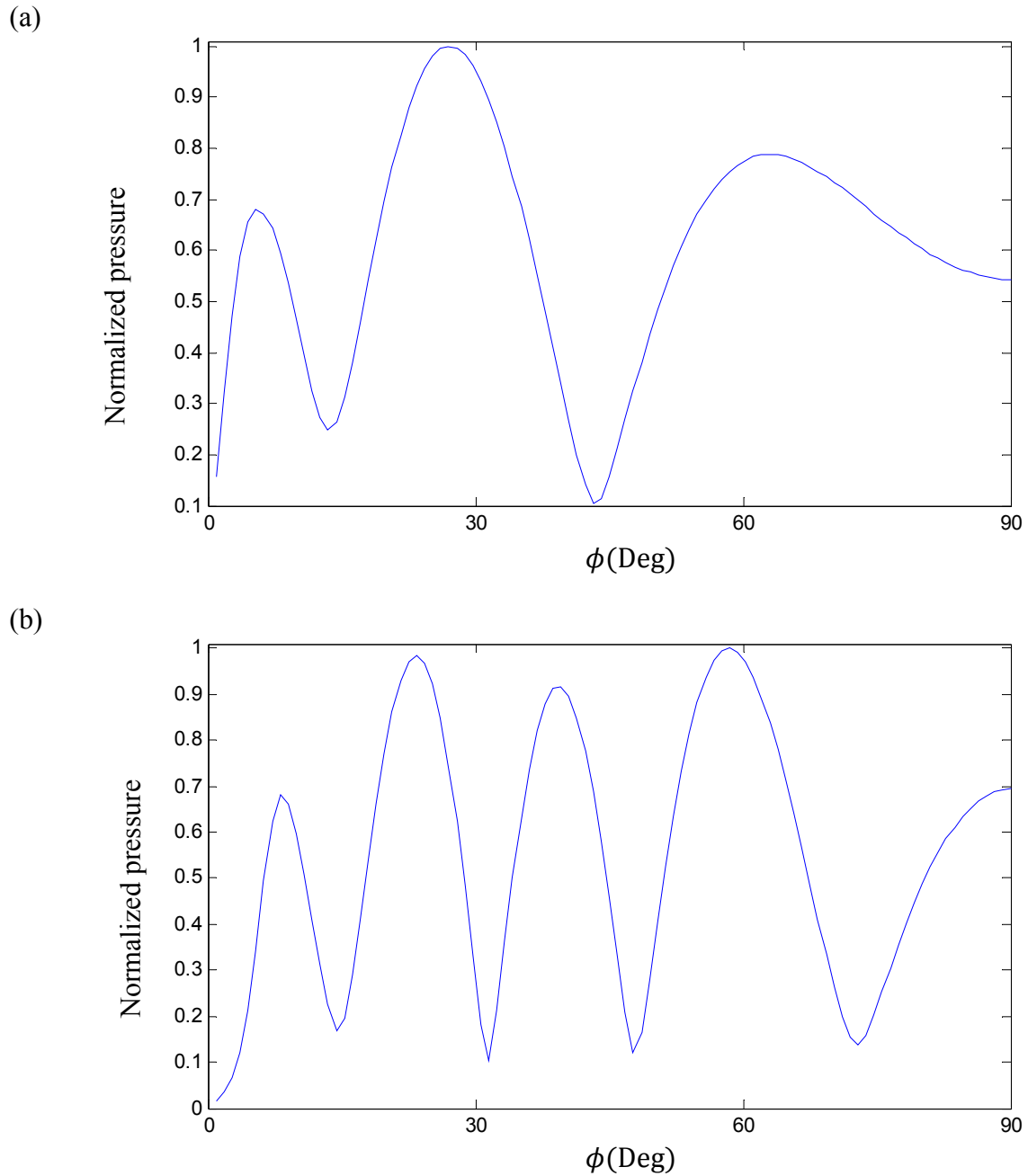
Figure 4.36: Directivity pattern of the point-supported annular disk along ϕ direction for even subsystem: (a) mode (0,2); (b) mode (0,3).

4.9.   Summary

The presented results show the capability of the analytical method in performing modal and acoustic analysis with acceptable accuracy. The analysis was performed with no restrictions on the boundary conditions. It has been shown that the non-uniformity in the boundary conditions affect the modal and acoustic characteristics of the disk. The current chapter discussed the properties of stationary disks while the rotational effect will be explored in the next chapter.

Table 4.13: Comparison of modal sound power Π_{mn} (dB re 1pW) for an annular disk with free edges.

mode (m,n)	Measured [108]	BEM [108]	Present study
(0,2)	66.5	66.5	64.9
(0,3)	68.0	67.5	68.4

Table 4.14: Comparison of modal radiation efficiency σ_{mn} (dB re 1).

mode (m,n)	Measured [108]	BEM [108]	Present study
(0,2)	-3.5	-4.0	-3.3
(0,3)	-1.5	-1.0	-1.0

Table 4.15: Acoustic properties of a point-supported disk.

mode (m,n)	Even subsystem		Odd subsystem	
	Π_{mn}	σ_{mn}	Π_{mn}	σ_{mn}
(0,2)	66.9	-0.68	66.1	-0.8
(0,3)	65.6	0.47	68.4	-1.0

5. IN-PLANE FREE VIBRATIONS OF ROTATING DISKS

5.1. *Introduction*

The in-plane vibration characteristics of stationary annular disks subject to different combinations of boundary conditions, including flexible and non-uniform supports, have been evaluated analytically and experimentally, and discussed in chapters 3 and 4. The majority of the applications where in-plane modes of vibration would be of practical importance, however, involve rotating disks. It is, thus vital to investigate the modal characteristics of disks under rotational effects.

The in-plane vibration analysis of circular disks, however, has been emphasized in the past few years, which reflect its importance in various practical applications [2, 11, 40]. A solution to the symmetric in-plane vibrations of a thin rotating solid circular disk was provided by Bhuta and Jones [26] who also determined natural frequencies for some specific modes. Burdess et al. [27] presented generalized formulation to consider asymmetric in-plane vibrations, while the effect of rotational speed on forward and backward traveling waves of a two nodal diameter mode was discussed. Chen and Jhu [25, 28] extended the analysis to study the divergence instability of spinning annular disks clamped at the inner edge and free at the outer boundary. The effect of radius ratio on the natural frequencies and critical speeds of the disk was also investigated. Hamidzadeh [30, 31] analyzed the same problem with a different formulation. In these studies, the critical speeds where determined using the classical theory of linear elasticity. Deshpande and Mote [36] studied the stability of spinning thin

disk using a nonlinear strain measure in order to account for the stiffening of the disk due to rotation. The study did not observe a critical speed in the range of rotational speed considered for modes with two or less nodal diameters. An upper limit for the rotational speed was identified where the assumption of linear strain measure would be applicable. The effect of flexible partial or point supports on the in-plane vibration of rotating circular disks, however, have not been investigated.

The in-plane vibration properties of disks would be strongly influenced by the coriolis and centrifugal effects due to rotation. The mathematical formulations were presented, based on the linear theory, in section 2.5.1. The first section describes the rotational effects on annular disks subject to uniform boundary conditions. The variations of the travelling waves are presented with respect to rotating and fixed coordinate. Then, a rotating point-supported disk is implemented to investigate the combined effect of rotation and boundary conditions non-uniformity on the modal characteristics of the disk. This problem involves stationary disk with rotating support and a rotating disk with stationary support. The later condition is relevant to the application of railway wheel with rail contact or a disk brake with friction pad. The initial stiffening due to rotation is, then, introduced by developing a non-linear model that permits the coupling between static and dynamic problems. The general non-linear problem of an annular disk subject to non-uniform boundary conditions is explored. Finally, the results from the experimental investigations are described.

5.2.   *Linear In-plane Vibration Analysis*

The vibration properties of a rotating disk subject to uniform boundary conditions could be conveniently evaluated using linear theory of elasticity, assuming small displacements around the equilibrium condition. The non-homogenous terms associated with the rotation could thus be decoupled from the equations of motion of the disk. For uniform boundary conditions along the circumferential direction, the coupling would then be limited to modes within the same nodal diameter number. The vibration analysis of the rotating disk can thus be reduced to *n* sets of uncoupled subsystems as discussed in section 2.5. The uncoupled subsystems are solved assuming a constant angular velocity of the disk. The solutions, however, are obtained for various constant angular speeds. The frequency parameters of in-plane vibration are also compared with those reported in the published studies for stationary disks by letting the speed as zero, as well as the rotating disks when available.

For the rotating disks, two distinct values of the frequency parameters of the in-plane vibration are obtained irrespective of the angular speed, which represents the forward and backward frequencies. As an example, Figure 5.1 illustrates the frequency parameters corresponding to mode (0,2) as a function of the rotating speed for a solid disk with free boundary condition with respect to the rotating coordinate. The figure illustrates the variations in the frequency parameters with the non-dimensional rational speed defined as $\bar{\Omega} = \Omega R_o \sqrt{\rho(1 - v^2)/E}$. The results show considerable differences in the frequency parameters corresponding to the forward and backward waves. The parameter of the forward wave decreases from 1.39 at $\bar{\Omega} = 0$ to zero at $\bar{\Omega} \approx 1.35$. The

direction of the wave reverses thereafter and can be interpreted as a backward traveling wave. For the backward wave, the magnitude of the frequency parameter increases slightly from its initial value of -1.39 at $\bar{\Omega} = 0$ towards a maximum value of -1.7 near $\bar{\Omega} = 0.5$. A further increase in the rotating speed causes a reduction in the magnitude of the frequency parameter. The parameters of the two waves (forward and backward) converge as speed increases. This point of convergence is considered as the dynamic stability limit, where the roots approach imaginary values. The results shown in Figure 5.1 agreed very well with those reported in a previous study [27].
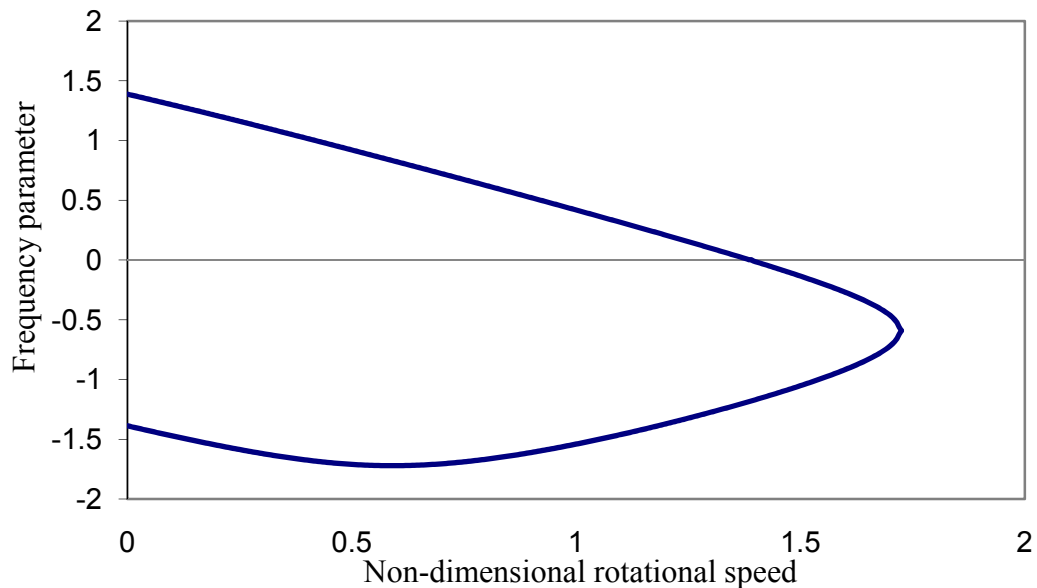
Figure 5.1: Variations in frequencies parameters of in-plane vibration of a free solid disk corresponding to mode (0, 2) with respect to the rotating coordinate.

The results in Figure 5.1 show the variations in frequency parameters with respect to the rotating coordinate system. Alternatively, the variations in the frequency parameters of in-plane vibration with the rotational speed can also be obtained with respect to the fixed coordinate system (η, r) shown in Figure 2.3. The variations in the

frequency parameters corresponding to forward and backward traveling waves for an annular disk with respect to fixed frame are illustrated in Figure 5.2 for a few selected modes. The results are obtained for the clamped inner edge and free outer edge conditions with $\beta = 0.2$. The label (m, n) refers to the mode with m nodal circle and n nodal diameter, while the letters f and b denote the forward and backward waves, respectively. The results show that the frequencies corresponding to forward and backward waves are identical for the stationary disk, when uniform boundary conditions are considered. Due to the rotational effects involved, the odd and even subsystems are coupled and the forward and backward waves comprise the predominant cosine and sine modes, respectively, of the coupled system. In Figure 5.2, the mode (0,0) is the pure torsional mode as the speed increases which does not split into forward and backward directions and is the first vanishing mode as speed increases. The frequencies corresponding to backward waves of the other selected modes also diminish to zero as the rotational speed increases and approaches the critical speed. The backward wave is reflected back to a forward travelling wave as the speed increases beyond the critical speed, which is referred to as the "reflected waves" and denoted by rw in Figure 5.2. Similarly, Figure 5.3 shows the variations in the natural frequency of a free-free annular disk as a function of the rotational speed. The slope of the forward and backward waves increases as n increases. The results obtained for the annular disk subject to uniform clamped-free and free-free conditions (Figures 5.2 and 5.3) are found identical to those reported in [28, 31], while the analyses of in-plane vibration of disks with the non-uniform boundary conditions are discussed in the next sections.
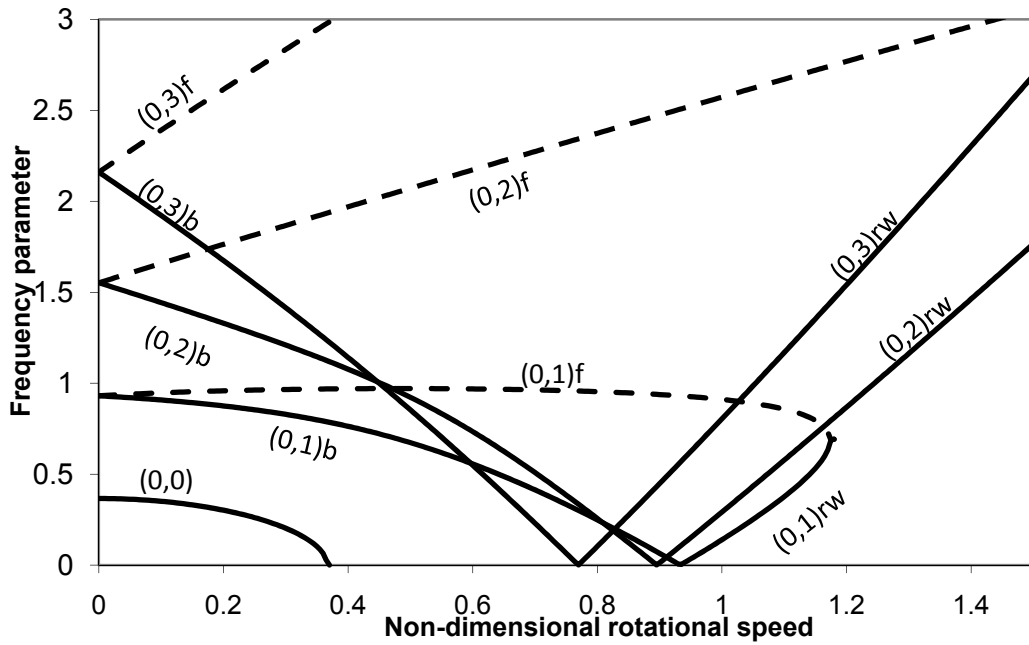
Figure 5.2: Variations in frequency parameter of a rotating clamped-free annular disk ($\beta = 0.2$) with respect to the fixed coordinate; ———— : backward waves, and _ _ _ _ _ :forward waves.
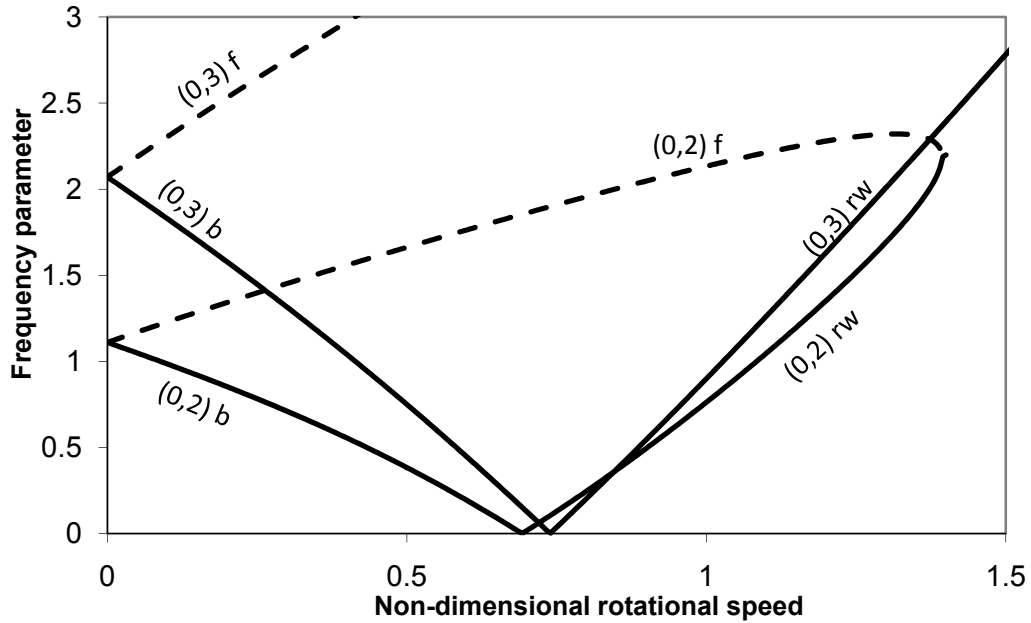
Figure 5.3: Variations in frequency parameter of a rotating free-free annular disk ($\beta = 0.2$) with respect to the fixed coordinate; ———— : backward waves, and _ _ _ _ _ :forward waves.

5.3. In-plane Vibration Analysis of a Rotating Point-Supported Disk

The variations in frequency parameters of in-plane vibration of solid and annular disks with partial or point supports are investigated as a function of the rotational speed. Unlike the disks with uniform boundary conditions, the partial supports cause the frequencies to further split into two different values. This effect is added to the split caused by the gyroscopic effect of the rotating disk as observed in the results presented for the uniform boundary conditions (Figures 5.2 and 5.3). Figure 5.4 illustrates variations in the natural frequencies with rotational speed of a solid disk with free edge and a point support for mode (0,2). The addition of a point support yields two different values of the natural frequency even when the disk is stationary, as observed in the figure. Furthermore, both the values tend to be higher than the natural frequency of the free disk.

With increasing rotational speed, the variations in the forward and backward frequencies exhibit the same trend, irrespective of the support condition considered. The results further show critical speed of the disk with a point support is greater than that of the free disk. Moreover, the reflected wave does not reflect at the same speed. It should be noted that Figure 5.4 illustrates the variations in the frequency parameters corresponding to mode (0, 2) alone, while the veering in the frequency curve in the presence of the other mode frequencies was suppressed in order to clearly illustrate the effect of the point support. The variations in the frequency parameters of the point-support rotating disk show the veering in frequency corresponding to each mode. While this effect has been shown in many studies on the out-of-plane vibration of rotating disk [109, 110], the effects on in-plane modes have not been illustrated.

172
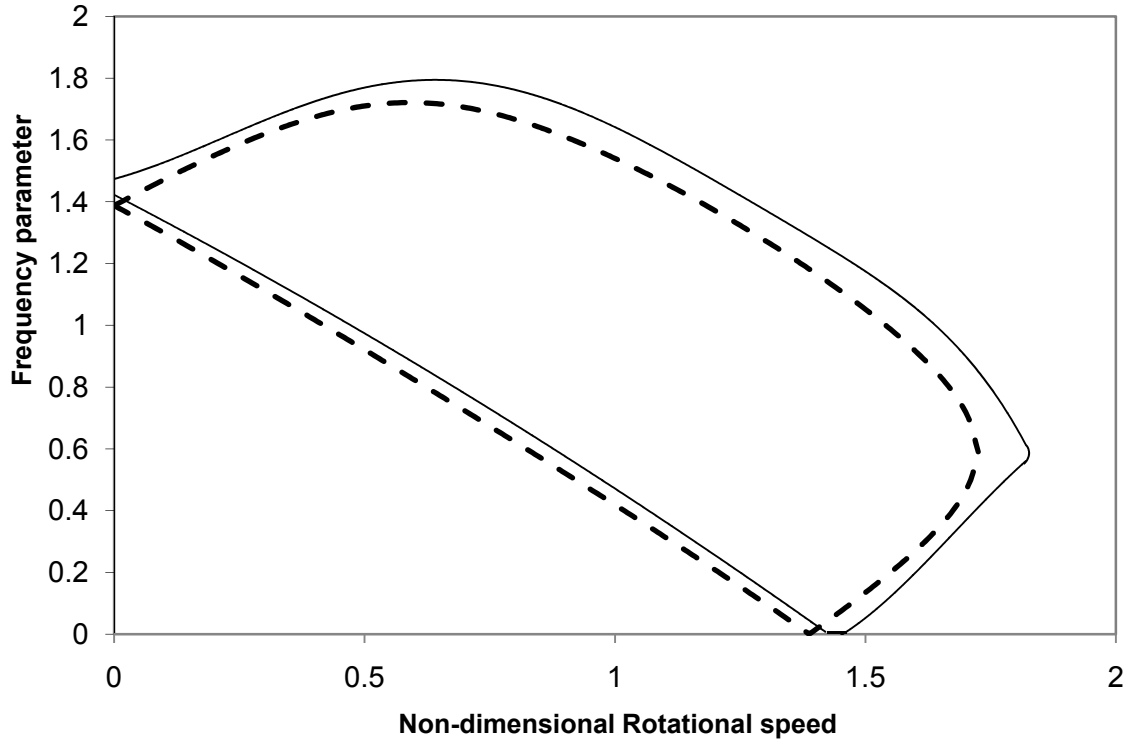
Figure 5.4: Effect of rotational speed on the variation in natural frequency corresponding to mode (0,2) of a solid disk with respect to the rotating coordinate system: , ‒ ‒ ‒ ‒ ‒ Free disk; and ────point-supported disk .

Figure 5.5 illustrates variations in frequency parameters corresponding to the forward and backward waves of an annular disk clamped at the inner edge for a few coupled modes in the rotating coordinate system. The solid lines in the figure show the variations for the uniform clamped-free condition, while those in dotted lines illustrate the variations for the clamped-point supported disk.

Figure 5.6 illustrates the variations in the forward, backward and reflected waves of the selected modes of the annular disk with the same support conditions in the fixed coordinate system. The results in Figures 5.5 and 5.6 are obtained for a low stiffness of the point $\overline{K}_r = \overline{K}_\theta = 1$, in order to compare them with those of the free disk. From the results, it is observed that, for each mode, the backward wave does not reflect at the

173
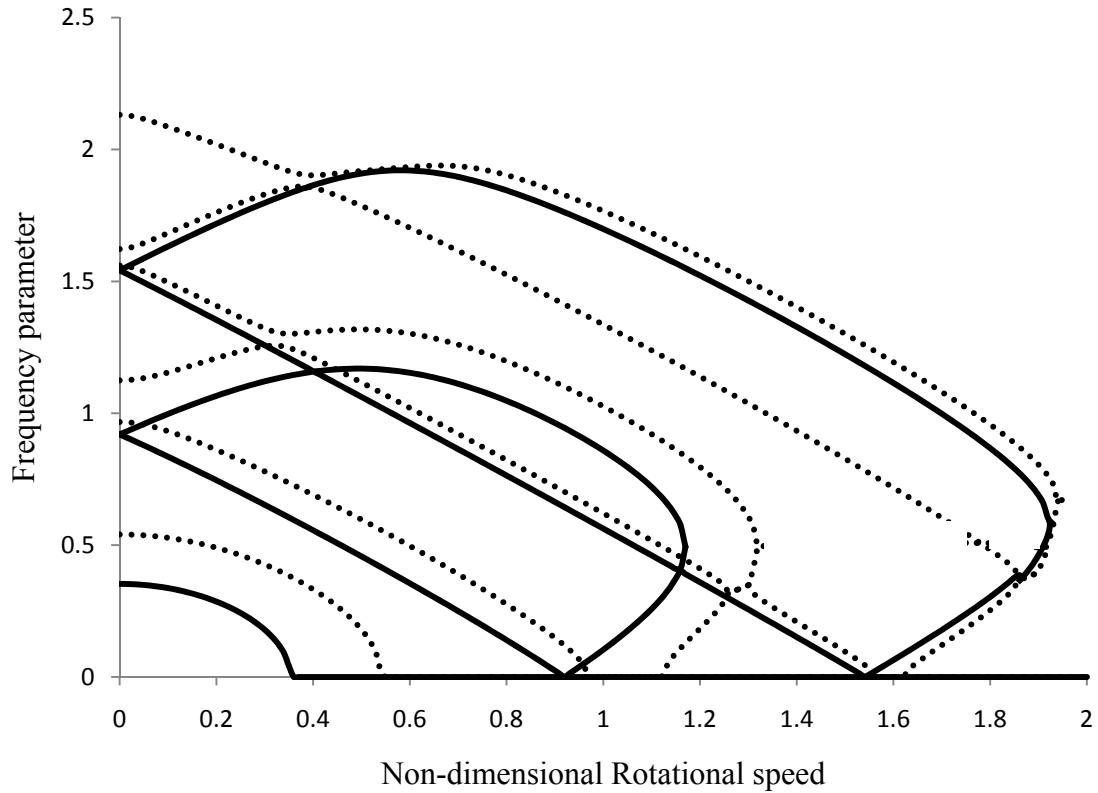
Figure 5.5: Effect of rotational speed on variations in the natural frequencies corresponding to selected modes of an annular disk ($\beta = 0.2$) with respect to the rotating coordinate system: ————— : clamped-free; and _ _ _ _ _ : clamped-point support.

same critical speed. This is illustrated in the detailed view of the critical speed region Figure 5.6 (b). This region of zero frequencies has been referred to as the divergence type instability [111] or stationary instability [112]. The length of the instability region of each mode shows the severity of the point support on that specific mode. For example, Figure 5.6 (b) illustrates that mode (0,1) is strongly affected by the support conditions, while the effect on modes (0,2) and (0,3) is relatively smaller. Due to the additional coupling introduced by the non-uniform support, the forward, backward and the reflected waves tend to merge or separate from each other at different rotational speeds, as seen in Figure 5.6 (a). These trends are not evident from the results obtained

174

for free outer edge condition, which is also clearly seen in Figure 5.2. For this uniform boundary condition, the frequencies of modes simply cross over, as seen in the figure. It is observed that the frequency curve corresponding to a particular mode of a point-supported disk veers away from that of another mode as it approaches the frequency of the other mode. For example, the backward branch of mode (1,2) and the forward branch of mode (0,1) veer away from each other as they approach comparable values near $\bar{\Omega} = 0.75$. This is a well-known phenomenon, which is called "curve veering" and has been observed in many discrete and continuous systems [109, 110]. The results obtained in this study revealed that not all modes veer away from each other. The frequency variations in some of the modes approach each other and merge before they split again. Mode (1,1)b, for example, merges with mode (0,3)rw before they separate and each one continues its original path. This is known as flutter instability [111] or merged type instability [112] of rotating disks. It can be noted that when frequencies corresponding to two modes approach comparable values, they tend to merge if one of these relates to a reflected wave; otherwise they tend to veer away from each other.

The observed veering and merger tendencies of the frequencies corresponding to all the modes are strongly influenced by the stiffness parameter of the point support stiffness. Figure 5.7, as an example, illustrates the variations in frequency parameters of the (0,1) and (0,2) in the fixed coordinate system for the clamped-point supported disk with nominal support stiffness ($\bar{K}_r = \bar{K}_\theta = 10^5$). Comparisons of the results shown in Figures 5.6 and 5.7 clearly show the effect of support stiffness parameter on the speeds at which the veering and merging of frequencies of the two modes could be observed.
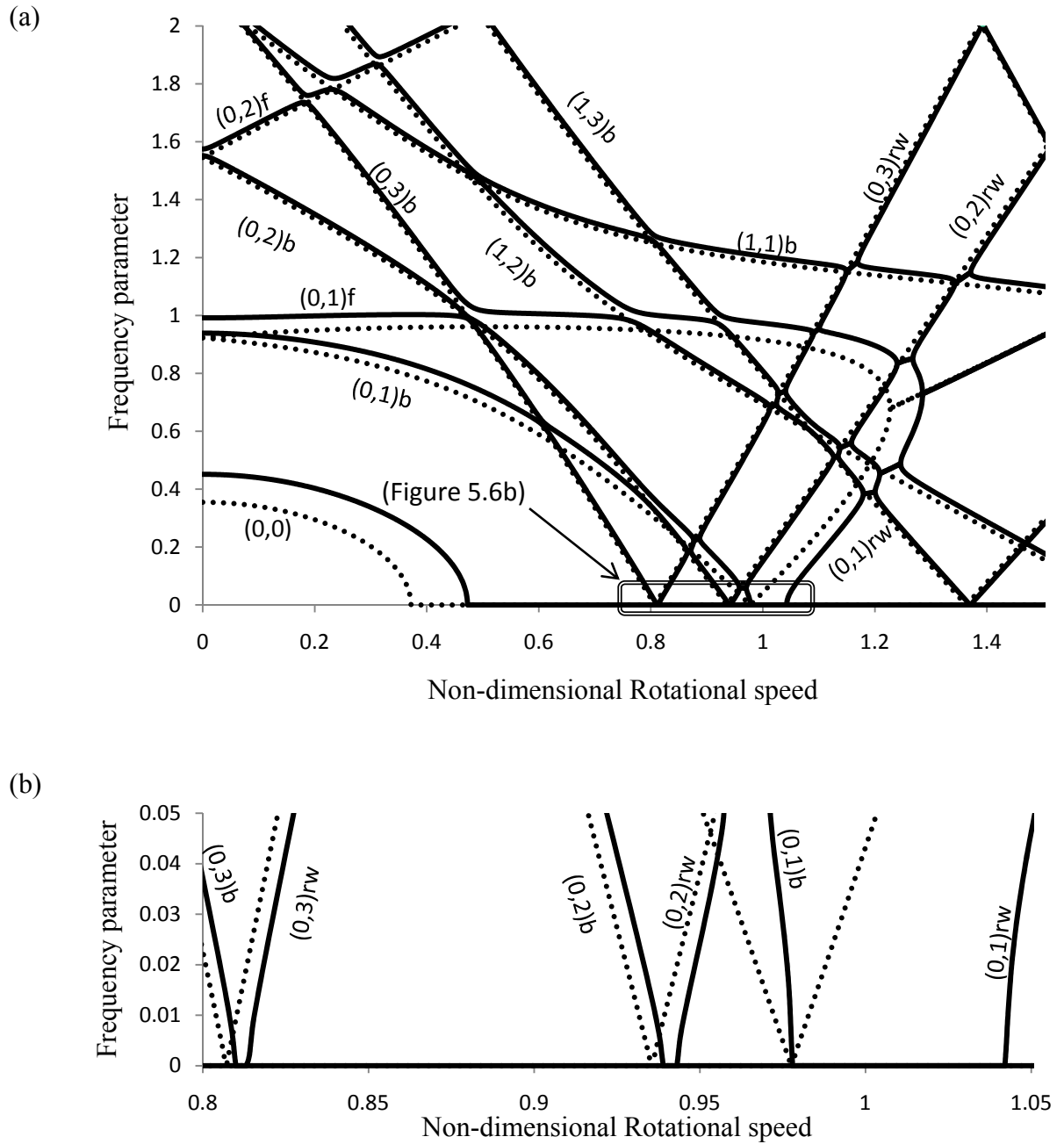
Figure 5.6: (a) Variation of non-dimensional natural frequencies of an annular disk ($\beta = 0.2$) with respect to the fixed coordinate; $-\,-\,-\,-\,-$: clamped-free, $\rule{1cm}{0.4pt}$: clamped-point support, point-support stiffness $\bar{K}_r = \bar{K}_\theta = 1$, (b) detailed view of the critical speed region.
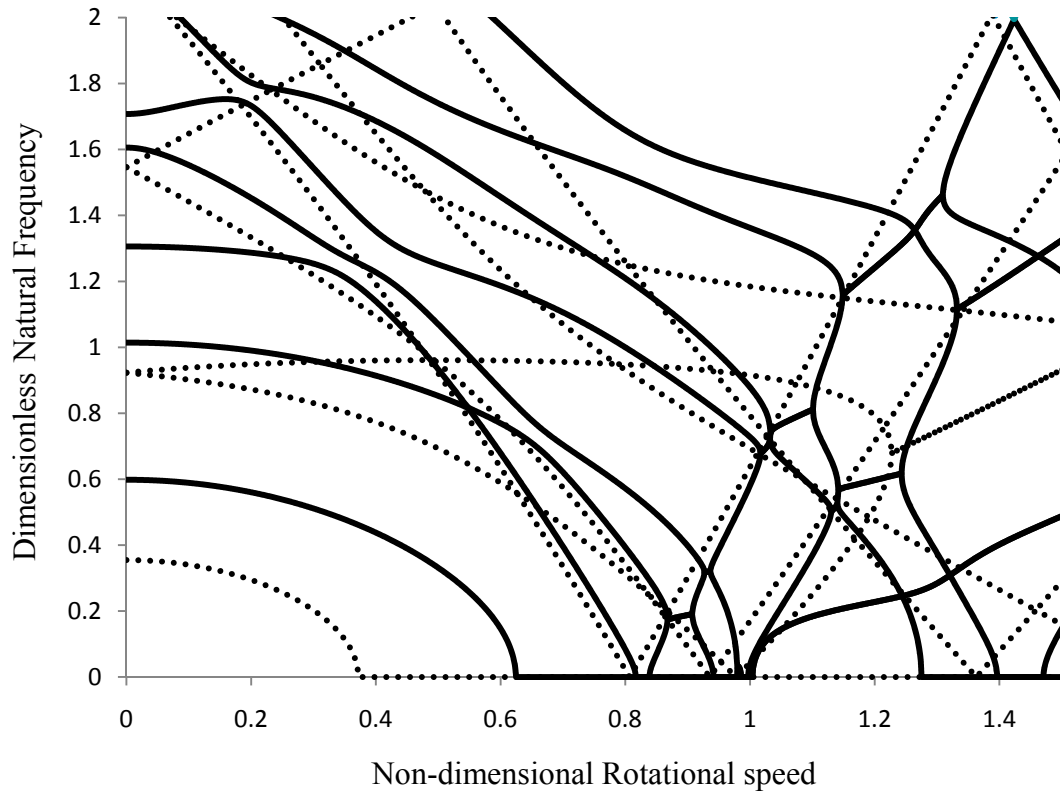
Figure 5.7: Variation of non-dimensional natural frequencies of an annular disk ($\beta = 0.2$) with respect to the fixed coordinate; $\_\,\_\,\_\,\_\,\_$: clamped-free, $\underline{\quad\quad}$: clamped-point support.

5.4. Rotational Stiffening Effect

A rotating disk undergoes initial deflection which causes additional stiffening effect, as described in section 2.5.2. The linear analysis based on the linear strain measure, however, cannot account for this stiffening effect. The stationary instability regions observed in Figures 5.6 and 5.7 are mostly attributed to the use of linear strain measure or lack of consideration of the stiffening due to rotation. It is thus important to consider this stiffening effect for disks especially when the disk is rotating at high speeds. The effect of this stiffening has been considered for disks with uniform boundary conditions only recently [36]. In the reported study, the radial displacement was assumed

to be axisymmetric with no circumferential displacements. This assumption simplifies the equation of equilibrium to Eq. (2.74), which can be solved to yield a closed form relation of Eq.(2.75). This solution, however, is applicable to disks with uniform boundary conditions, only. The generalized formulation, developed in this study, can be applied for analysis of the static displacements due to rotation of an annular disk with non-uniform boundary conditions. This formulation has been presented in Eq. (2.78). The radial expansion of Eq. (2.78) would be identical to that obtained from Eq.(2.75) for uniform boundary conditions. The solutions are obtained for uniform boundary conditions and the resulting coefficients of the static vector $\{q_s\}$ are examined, which reveal all the coefficients as zero, except for those associated with the axisymmetric displacement $(n = 0)$.

For a disk with non-uniform boundary conditions, Eq. (2.74) would be invalid since the circumferential displacements and their variations along the circumferential coordinate are neglected. In this case, radial expansion would be obtained through solution of Eq. (2.78) only. The resulting displacements are not axisymmetric due to variations in the boundary conditions along the circumferential direction $\left(\frac{\partial}{\partial \theta} \neq 0\right)$. This makes the coefficients associated with $(n > 0)$ in the static vector $\{q_s\}$ to have nonzero values and contribute to the radial displacement responses. Figure 5.8(*a*) and (*b*) show the radial expansions of the outer edge of the disk with free and point-supported outer edge, respectively. The undeformed shape of the disk without the rotational effects is shown by the dashed line. From Figure 5.8(a), it is evident that the radial expansion is axisymmetric, while the point support enforces zero displacement that disturbs the

axisymmetry of the expansion. The expansion, shown in Figure 5.8(b), is identical for a rotating or fixed point support relative to the disk. The two cases are shown in Table 2.4. For a rotating disk with a rotating support, the radial expansion also exhibits rotation at the same speed. For the rotating disk with a stationary support, the shape in Figure 5.8(b) is be non-rotating, while the disk itself is rotating.
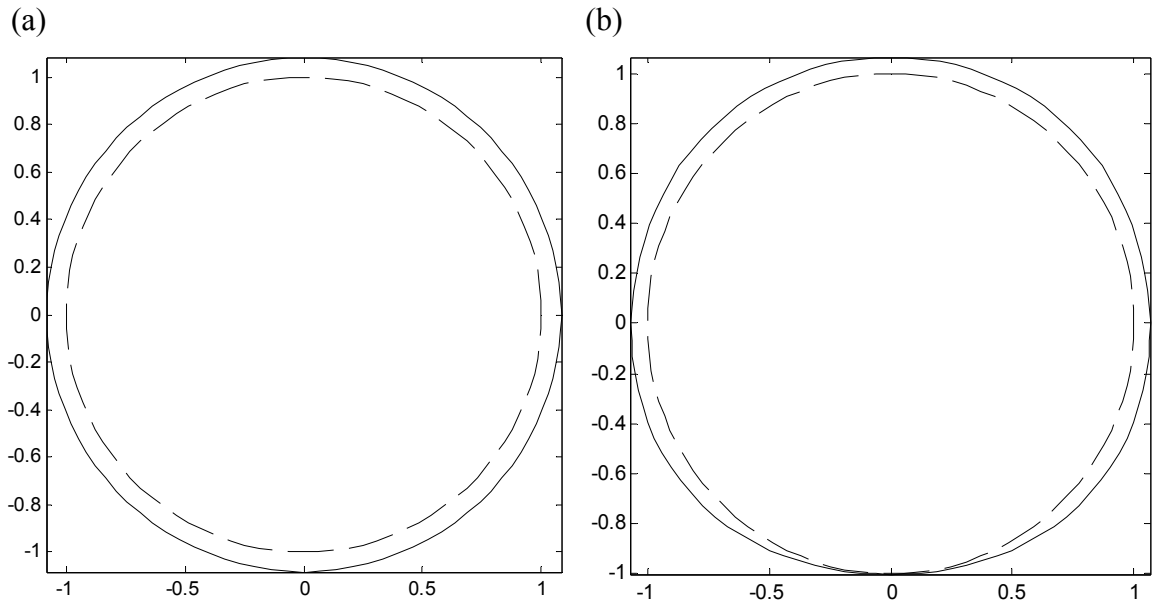
Figure 5.8: Radial expansion due to rotation for the outer edge of a disk: (a) with free boundary conditions, (b) with a point support at the outer edge. _____ deformed edge, _ _ _ _ _ undeformed edge .

In order to obtain the modal characteristics of a rotating disk with consideration of rotational stiffening effect, it is essential to solve for vector $\{q_s\}$ associated with initial deformation of the disk, which is a function of the rotational speed. Equation (2.81) is then solved for the dynamic displacement vector $\{q_d\}$, which yields the modal characteristics of the rotating disk. Figure 5.9 compares the frequency parameters of a rotating annular disk with clamped-free boundary conditions and $\beta = 0.2$, with and without the consideration of the rotational stiffening effect. The figure shows the

179

variations in the frequency parameters corresponding to a few selected modes, where the solid lines represent the variation without considering the stiffening effects, while the dashed lines show the variations under the effect of additional stiffening. The results clearly show the absence of critical speeds when the rotational stiffening is considered. Moreover, the rotational stiffening does not introduce any additional coupling between the modes and the variations exhibit only simple crossover of frequencies corresponding to different modes, as they approach comparable values.

The effect of additional stiffening is further explored on the in-plane vibration properties of disks with non-uniform support conditions. The variations in the frequency parameters and the traveling waves of an annular disk clamped at the inner edge and point-supported at the outer edge are shown in Figure 5.10. The results are presented for a few selected modes; which do not show the presence of a critical speed in the speed range considered. The results thus suggest that merged type or stationary instabilities do not occur when the additional rotational stiffness effect is considered. This instability, however, is evident in the results obtained without the additional stiffness at speeds above the critical speed. The only phenomenon that can be observed in Figure 5.10 is the curve veering, which occurs regardless of the consideration of the stiffening effects. From the results it can be concluded that the additional stiffening due to rotation needs to be incorporated in the analysis in order to accurately predict the dynamic response of the disk, particularly for applications involving high rotational speeds.
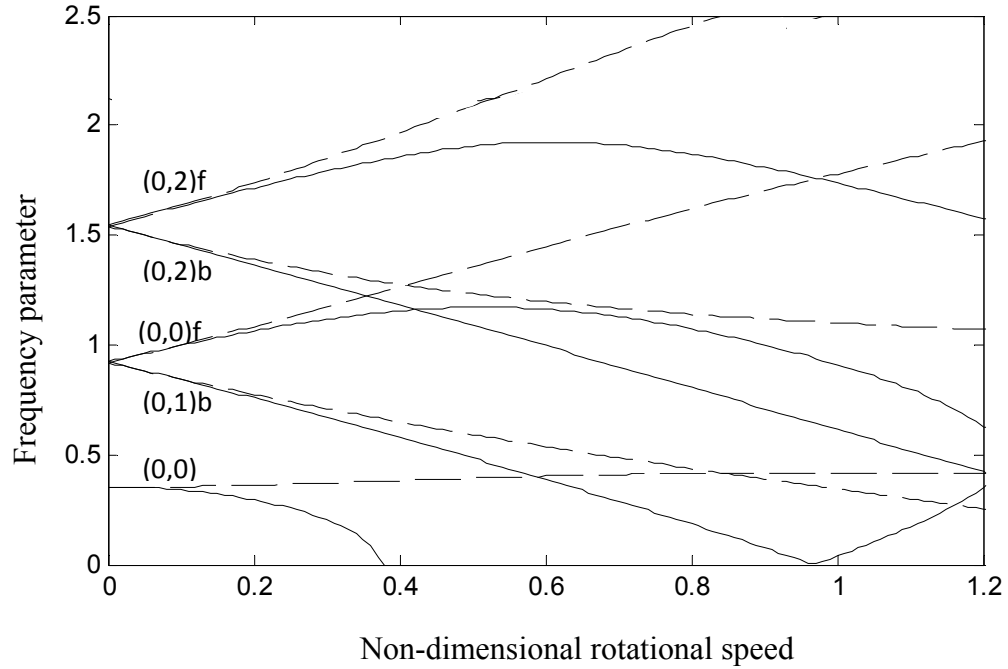
Figure 5.9: Variations in the frequency parameter of a clamped-free annular disk ($\beta = 0.2$) with the rotational speed, ——— : without stiffening effect, ----- : with stiffening effect.
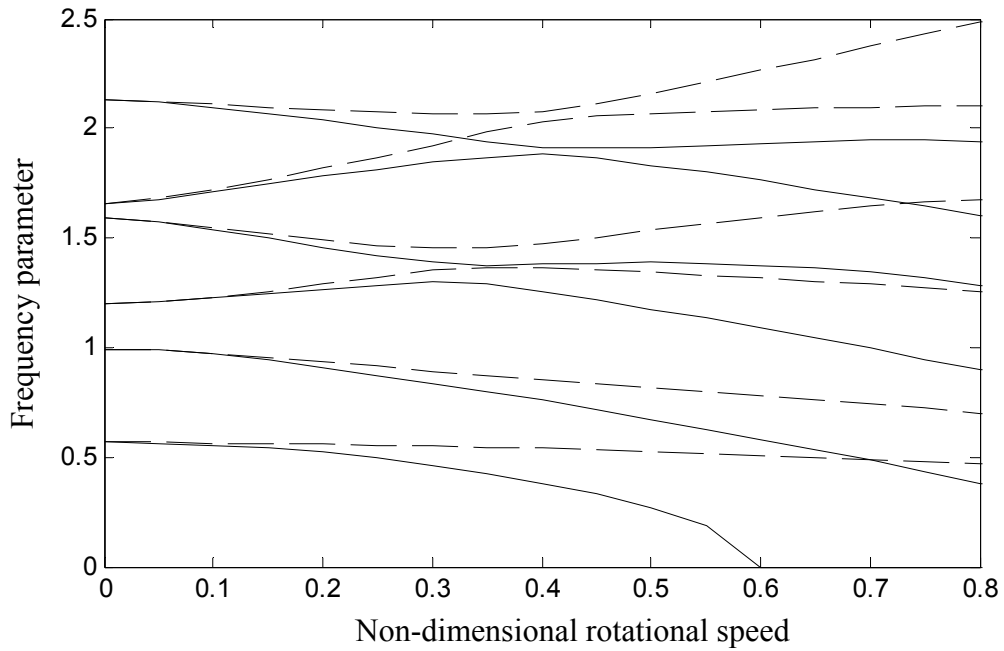
Figure 5.10: Variations in the non-dimensional natural frequencies of a clamped-point supported annular disk ($\beta = 0.2$) with the rotational speed, ——— : without stiffening effect, ----- : with stiffening effect.

5.5.   *Laboratory Measurements*

Laboratory experiments were performed to study the effects of rotation and the supports on the modal characteristics of the disks. The primary goal of the experimental study was to confirm the split in natural frequencies of the disk that was observed in the analytical results under both rotation and support non-uniformity.   While the effects of the supports on the natural frequencies were investigated experimentally and discussed in section 4.7 for stationary disks, additional experiments were performed to measure the effect of disk-rotation on its in-plane modes under uniform and point-support boundary conditions.

5.5.1. *Experimental Setup*

The experimental setup consisted of an aluminum disk mounted on a uniform 2.5 cm diameter steel shaft that was supported by a number of bearings and driven by a variable speed DC motor. The motor could be operated in the 0 to 3000 rpm, using the speed controller. Figure 5.11 illustrates schematic and a pictorial view of the shaft disk assembly and the experimental setup. The disk is mounted near the free end of the shaft in order to reduce the contribution of the motor noise to an extent. The shaft was supported by three bearings; two of these were located close to the disk in order to minimize its deflection due to shaft rotation, as seen in Figure 5.11. An aluminum disk was used, instead of the steel disk, in order to reduce the magnitude of the centrifugal forces due to rotation of the disk. The properties of the disk used were: $R_o = 0.15$m, $R_i i = 0.02$m, $h = 0.01$m, $\rho = 2680$ kg/m^3, $E = 15 \times 10^9$ N/m^2 and $v = 0.33$. The measurements were initially performed on the stationary disk using the microphone, the

accelerometer and the impulse hammer, as described earlier in section 4.3.2. The accelerometer was used to identify both the in-plane and out-of-plane modes of vibration of the stationary disk. A plexiglass guard was placed around the rotating disk to ensure the safety of those working there. The motor was operated at different speeds, and a microphone was positioned on the guard close to the disk in order to measure the radiated sound pressure. From the preliminary measurements, it was concluded that the in-plane modes of the disk could not be adequately excited by the rotation of the disk. A steel stick was thus placed between the guard and the disk that maintained a contact with the outer edge of the disk and thus served as a source of continuous excitation to the disk along the radial direction.

The measured signals, however, revealed significant contributions due to several undesired noise sources such as motor, bearings, and vibrations of the supporting table. In order to account for contributions due to these sources, the measurements were taken at each speed of interest with the disk rotating freely in the absence of the in-plane excitation through the steel stick. This served as the reference signal that was applied to signals acquired from the disk subjected to in-plane excitation. A point-support was subsequently introduced in order to resemble fixed point contact with the disk. The point support assembly consisted of a bearing with a hard urethane rubber casing on its outer edge. The bearing was attached to a pin, as shown in Figure 5.11. The support assembly was designed to achieve adjustable height, which permitted variations in the support force imposed on to the disk.
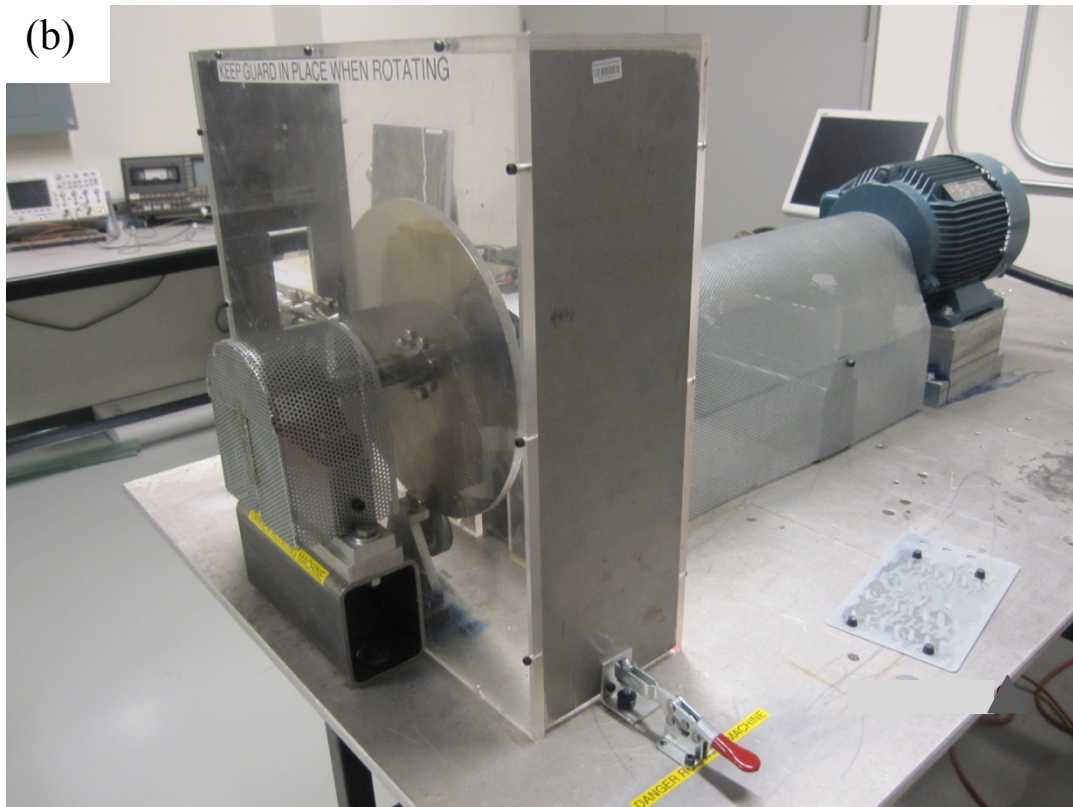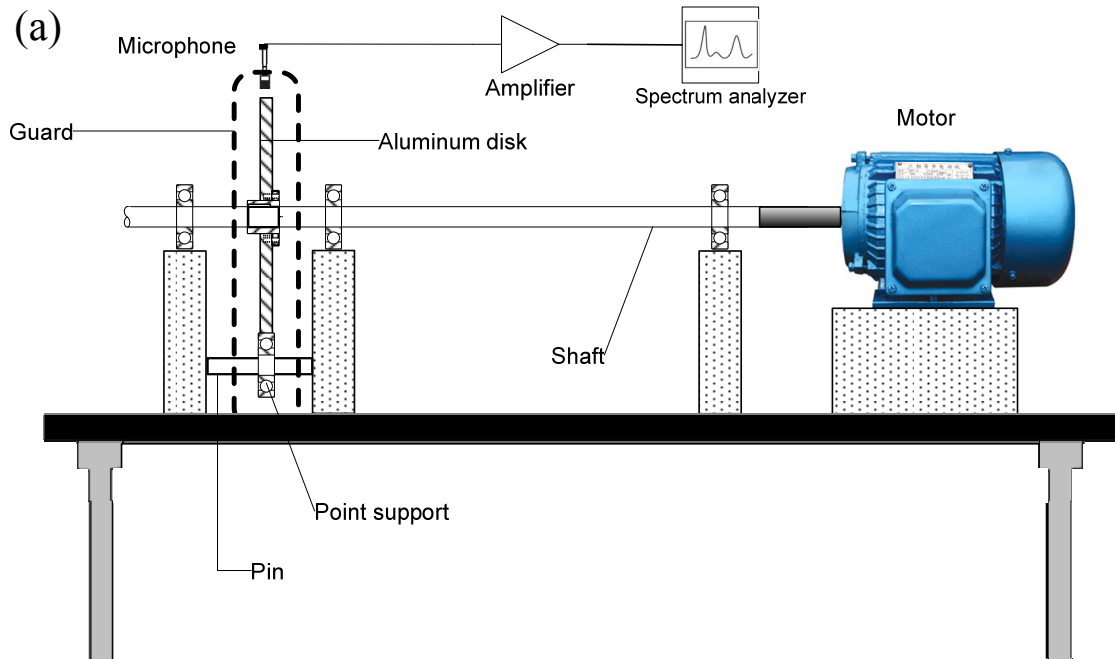
Figure 5.11: (a) Schematic of experimental set up for rotating disk, and (b) pictorial view.

5.5.2. Experimental Results

The experiment design used in the study posed several challenges in measurements and identifications of in-plane modes of vibration of the rotating disks. The primary challenge arose from characterizations of the boundary conditions at the inner edge of the disk. In the experiment, the disk was coupled to the shaft through a flange using eight bolts. This boundary condition could be assumed to be uniform along the circumferential direction at the inner edge, although this would not simulate a perfectly clamped conditions, which is quite complex to realize in practice. This boundary condition, however, was considered to be better described by a flexible inner edge boundary condition, while the stiffness due to the constraint would be an unknown. The simulations were performed to compute the in-plane natural frequencies of the disk with both free and perfectly clamped inner edge. The results obtained for the two extreme boundary conditions, free and clamped inner edge, were considered as the lower and upper bounds of the natural frequencies of the disk. Since the disk has a low radius ratio, the differences between the upper and lower bounds were found to be relatively small.

The experiments were initially conducted on the stationary disk excited along the radial direction, while the response was measured at the outer edge using the accelerometer and the microphone. Similarly, the measurements were also performed to acquire the out-of-plane vibration response in order to identify the out-of-plane modes that might be detected along the radial direction due to the coupling effects. Comparison between the analytical and experimental values provided guidance for selecting the inner edge support stiffness. A stiffness parameter value of $\overline{K}_r = \overline{K}_\theta = 1/4$ was considered adequate for the purpose of comparisons with the study of rotational effect. Table 5.1

shows the comparisons between the experimental measurements and the results obtained from analytical formulation, for a few lower modes, when the inner edge is considered to be supported by chosen stiffness parameters. The results show good agreements between the measured and model results. The peak error is in the order of 1%.

Table 5.1: In-plane natural frequencies of an aluminum disk with flexible inner edges condition.

	Natural frequency (Hz)		
Experimental (Hz)	7680	9984	11820
Analytical (Hz)	7700	10100	11900

Apart from the above, the disk could be operated only at relatively low speeds partly due to speed limit of the motor and in-part due to the safety concerns. The in-plane natural frequencies of the disk, however, were relatively high due to the low radius ratio and small outer radius of the disk. The rotational speed that would allow the disk to reach instability was thus significantly high and could not be attempted in the experiments. Furthermore the aerodynamic forces/ moments tend to be quite significant at higher speeds and would yield additional coupling between the modes and significant damping. It has been suggested to either consider the aerodynamic effects in the modeling task or to isolate the effect by installing the disk in a vacuum chamber [113]. Although the rotational speeds in the current experiment were not sufficiently high to demonstrate the behavior of the disk in the instability regions, the experiments conducted at the available speeds showed the forward and backward traveling waves of the in-plane modes. Moreover, the in-plane modes are known to be relatively less sensitive to the rotational speed than the out-of-plane modes. The experiment speed limit of 2000 rpm was thus

considered sufficient to study the combined effects of rotation and non-uniform supports, and to illustrate the forward and backward waves in the in-plane modes.

Uniform Boundary Conditions

The accelerometer and sound pressure signals acquired for the stationary disk with uniform flexible support at the inner edge and free outer edge were analyzed using the multi-channel signal analyzer. The measurements were subsequently performed at different rotational speeds (960, 1140 and 1920 rpm). Figures 5.12 and 5.13 illustrate frequency spectra of the measured sound pressure and acceleration, respectively, of the stationary disk subject to the impulse hammer excitation. The frequency spectra exhibit several in-plane and out-of-plane vibration modes. The spectra show the peeks corresponding to three in-plane vibration mode frequencies listed in Table 5.1, while all the outer peeks in the spectra correspond to the out-of-plane modes of vibration.
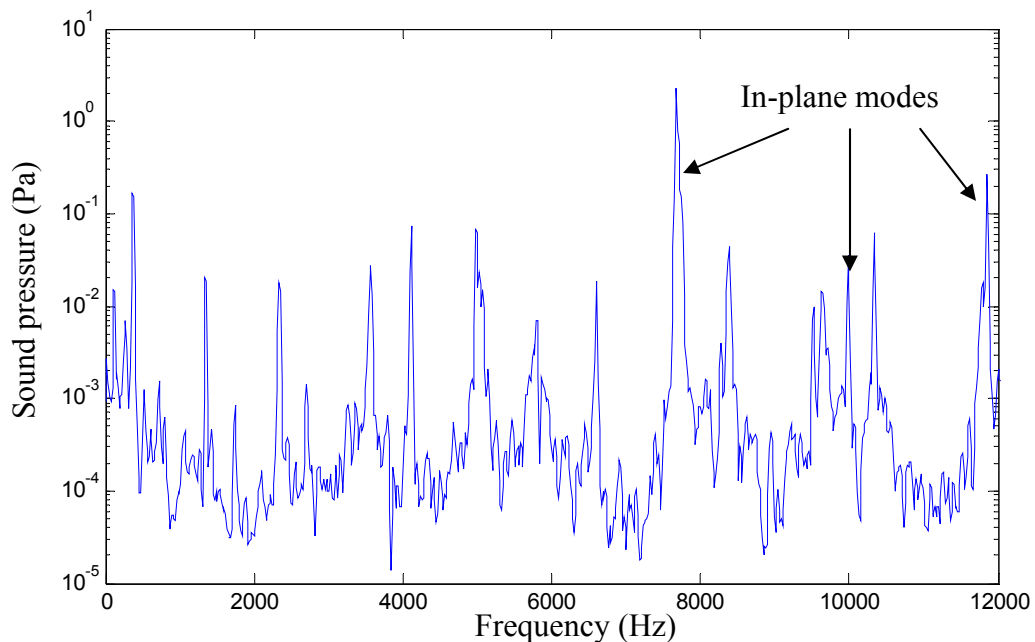
Figure 5.12: Frequency spectrum of the sound pressure measured near the stationary aluminum disk subject to an impulse hammer excitation (flexible inner edge and free outer edge).

187

Considering that a point-support would cause the in-plane frequencies to increase significantly and thereby may shift the higher mode frequencies beyond the frequency range of measurement, and the relative amplitude of the first mode is considerably higher, the discussions of the measured data are limited to the first mode only. Figures 5.14 to 5.16 illustrate the frequency spectra of the measured sound pressure response of the disk rotating at three different speeds to study the effects of rotation on the in-plane modes of vibration. The rotational effects are evident, Figure 5.14, on the frequencies of the out-of-plane modes. For instance, the modes in the 4-6.5 kHz range exhibit frequencies corresponding to the forward and backward traveling waves. The frequencies of the in-plane modes do not exhibit any split in frequencies at the lower speeds, as seen in Figures 5.14 and 5.15. It should be noted that the peak near the first in-plane mode (near 7.8 KHz) was found to correspond to an out-of-plane mode.
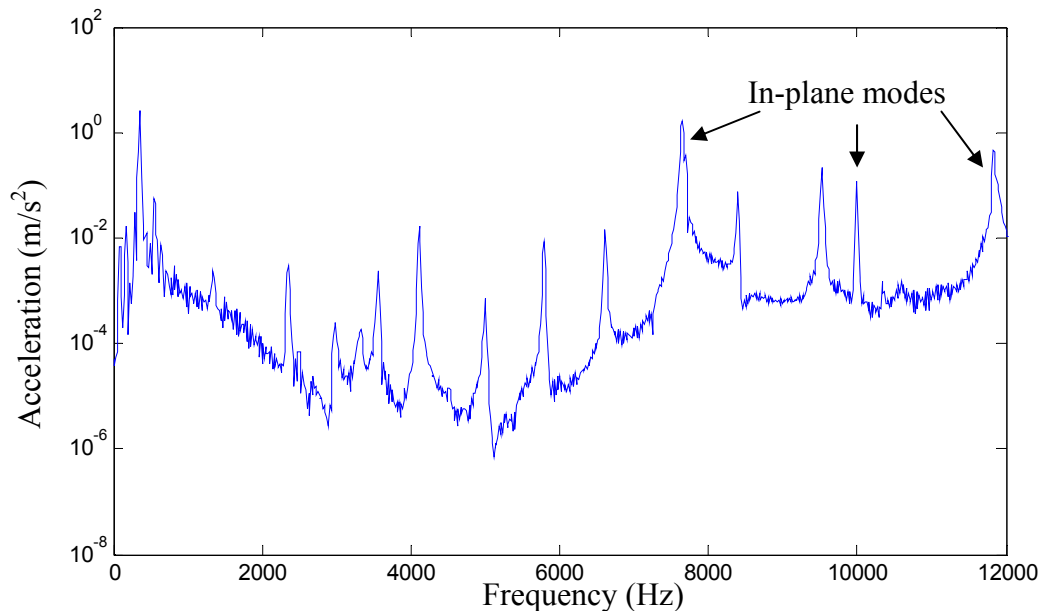
Figure 5.13: Frequency spectrum of the radial acceleration of the stationary aluminum disk subject to an impulse hammer excitation (flexible inner edge and free outer edge) along the in-plane direction.

Figure 5.14: Frequency spectrum of the sound pressure measured near the rotating aluminum disk subject to an impulse hammer excitation (flexible inner edge and free outer edge) at 960rpm.
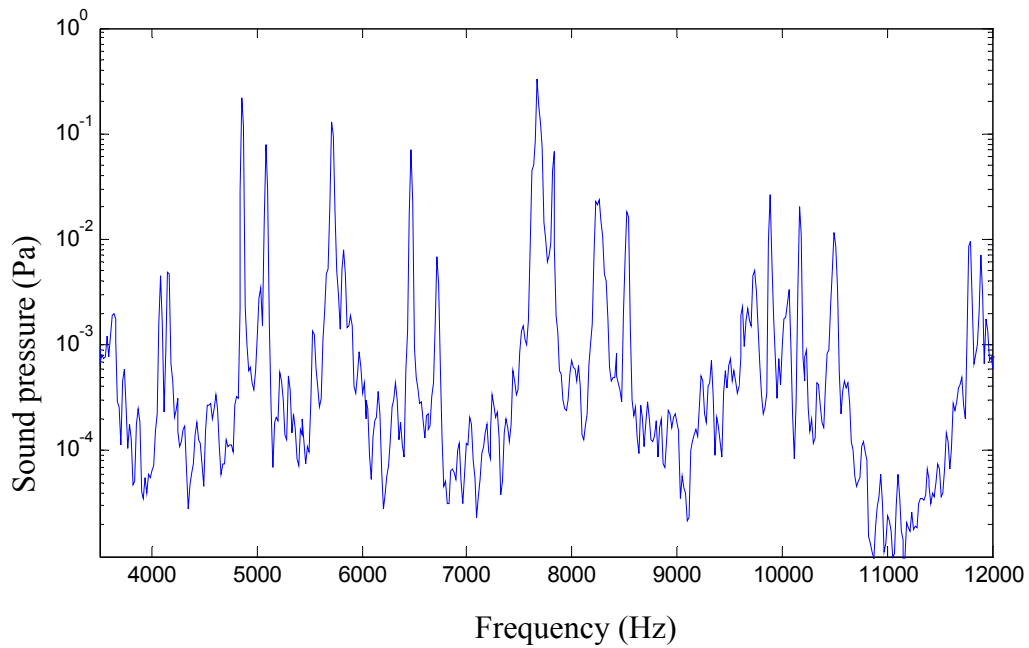
Figure 5.15: Frequency spectrum of the sound pressure measured near the rotating aluminum disk subject to an impulse hammer excitation (flexible inner edge and free outer edge) at 1140rpm.
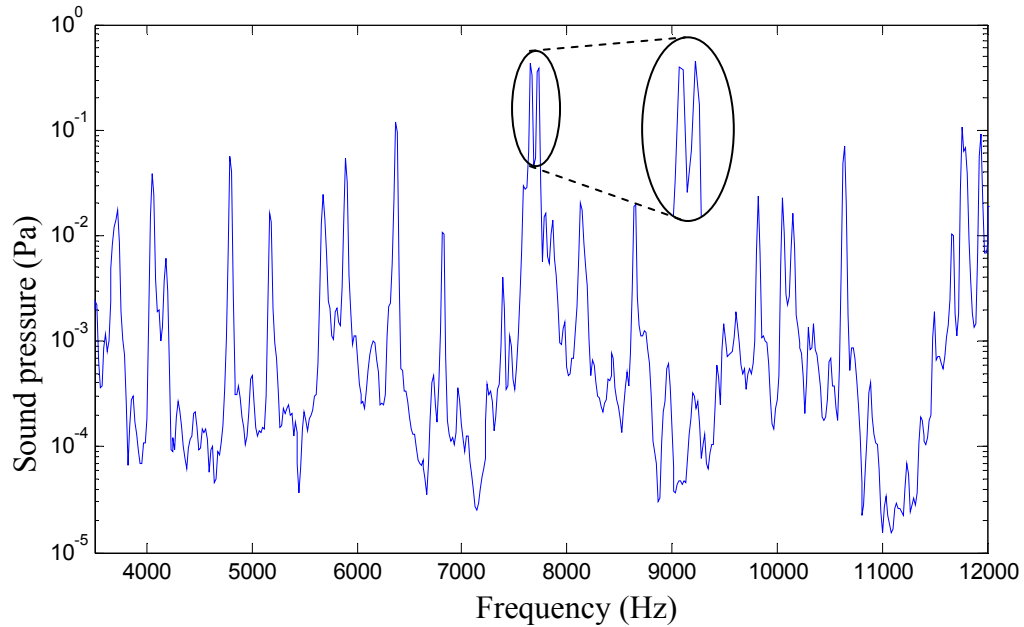
Figure 5.16: Frequency spectrum of the sound pressure measured near the rotating aluminum disk subject to an impulse hammer excitation (flexible inner edge and free outer edge) at 1920rpm.

A split in the first in-plane mode frequency, however, is clearly evident in the spectrum of the sound pressure measured at the higher speed of 1920 rpm, as shown in Figure 5.16. The results show two peaks in the spectrum that correspond to be the backward and forward wave frequencies at 7.68 and 7.73 kHz, respectively. The experimental results thus confirm the presence of the forward and backward wave frequencies of the disk under a uniform support that were observed in the simulation results at higher disk speeds. Although the results were obtained for the disk under radial excitation only, the frequency spectra show significant contribution from the out-of-plane modes which illustrate the strong coupling between modes of the disk. It has to be noted that disks with larger diameter would have in-plane modes with frequency values much lower than those of the disk considered in the experiment, as can be seen in Figure 3.7

190

which showed the variations of in-plane modes with disk diameter. These modes would have higher nodal diameter number n, which yields larger split between forward and backward waves.

Point-Supported Disk

The previous results show the split or bifurcation of natural frequency due to rotational effects only. In the previous chapter, the effect of point support on stationary disk was also studied. The current results explore the combined effect of rotation and point support on the disk. The point support is applied to the disk by pushing the bearing with rubber casing against the outer edge of the disk. The measurements were taken first for the disk while it is in stationary position. Figure 5.17 show the frequency distribution of the stationary disk with the support. The split of the in-plane mode is clearly shown in the figure which suggests that the point support effect is evident even without considering the rotational effect. The support is pushed against the disk with maximum allowable force and the frequency response is shown in Figure 5.18. Comparison between the responses in Figures 5.17 and 5.18 shows that the split between the frequencies becomes larger as the force of the support increases.

Then, the disk is allowed to rotate while the support is applied. Figure 5.19 illustrate the frequency distribution of the disk rotating at 500 rpm. The backward and forward waves are clearly shown in the figure as two peaks. The third peak that exists right after the forward peak frequency is an out-of-plane mode. The distribution of the frequencies for the disk rotating at 960 rpm is shown in Figure 5.20, which also shows the three peaks close to each other. Comparison between the responses at the same speed

191

without the support, shown in Figure 5.14, and with the support, shown in Figure 5.20, show that the response without the support did not show any split in the natural frequencies. The effect of the support is, therefore, helps to produce forward and backward frequencies at lower rotational speeds than those without support.

Further increase in the rotational speed increases the noise and vibrations from the rotor, bearings and motor. The bearing noises become larger due to the support force against the bearings. Moreover, the heating generated at the contact at high speeds cause damage to the outer layer of the rubber and produce excessive fluctuation of the disk. These reasons make it difficult to run the disk at higher speeds as in the case of freely rotating disk. The results shown are, however, sufficient to prove that the support or contact condition has significant effect on the modal characteristics of the circular rotating disk.
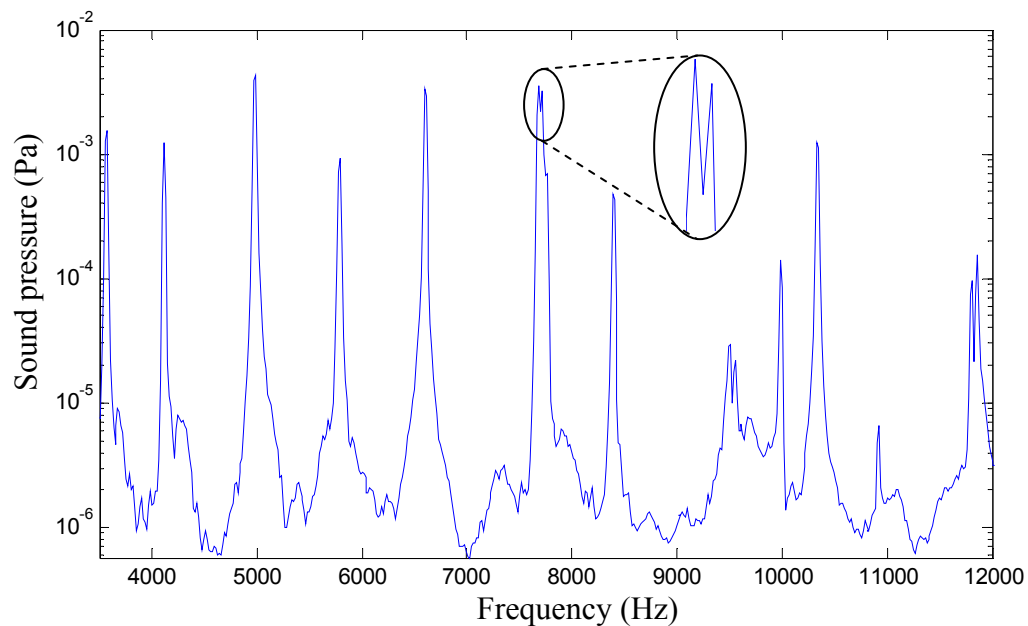
Figure 5.17: Frequency spectrum of the sound pressure measured near the stationary aluminum disk subject to an impulse hammer excitation (flexible inner edge and subject to an elastic point-support with low support force at the outer edge).
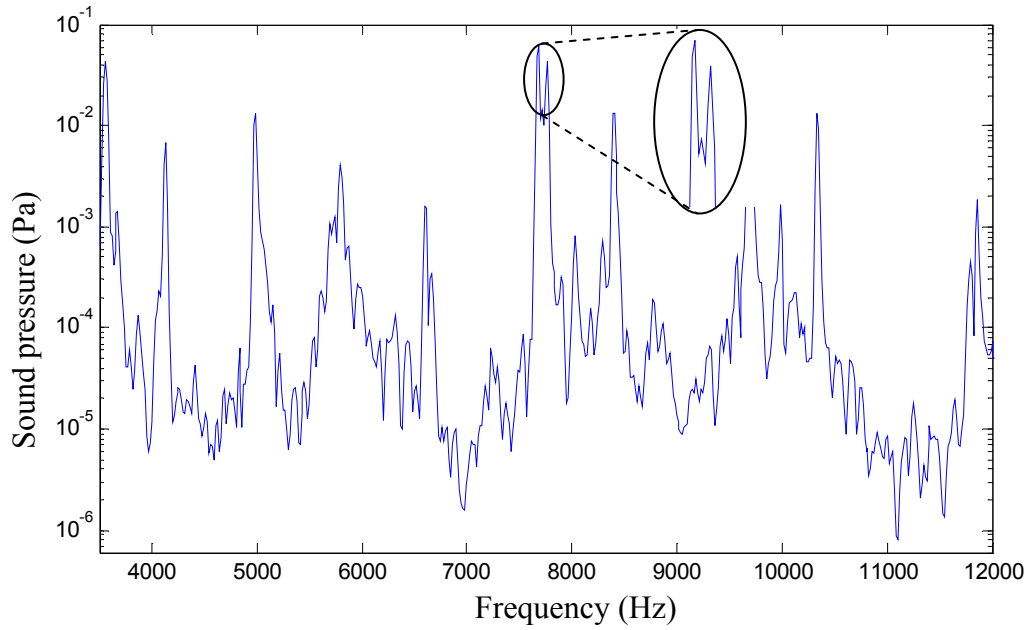
Figure 5.18: Frequency spectrum of the sound pressure measured near the stationary aluminum disk subject to an impulse hammer excitation (flexible inner edge and subject to an elastic point-support with high support force at the outer edge).
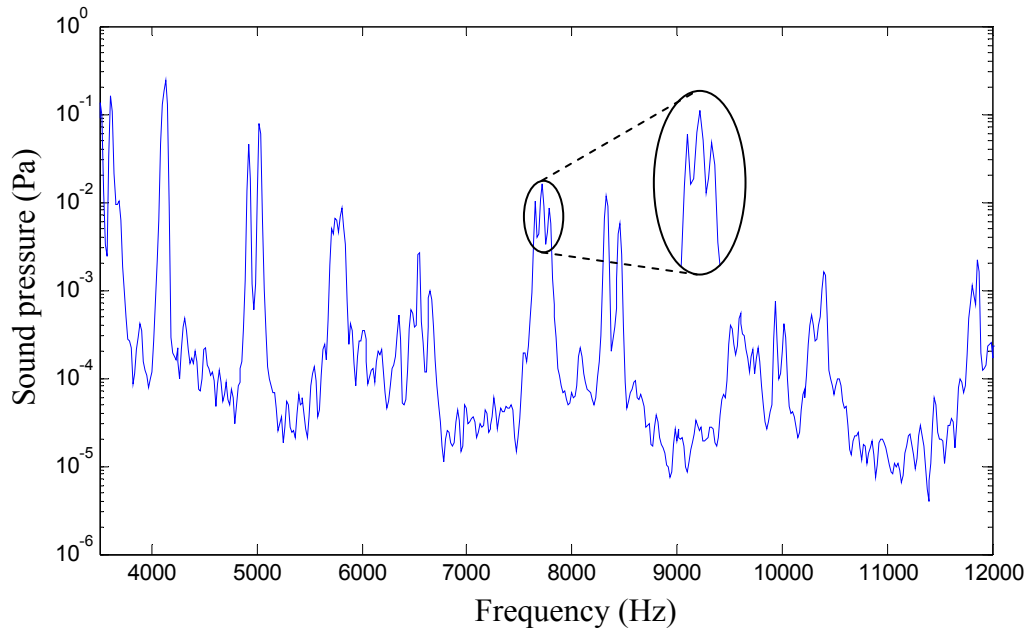
Figure 5.19: Frequency spectrum of the sound pressure measured near the rotating aluminum disk subject to an impulse hammer excitation (flexible inner edge and subject to an elastic point support at the outer edge) at 500 rpm.
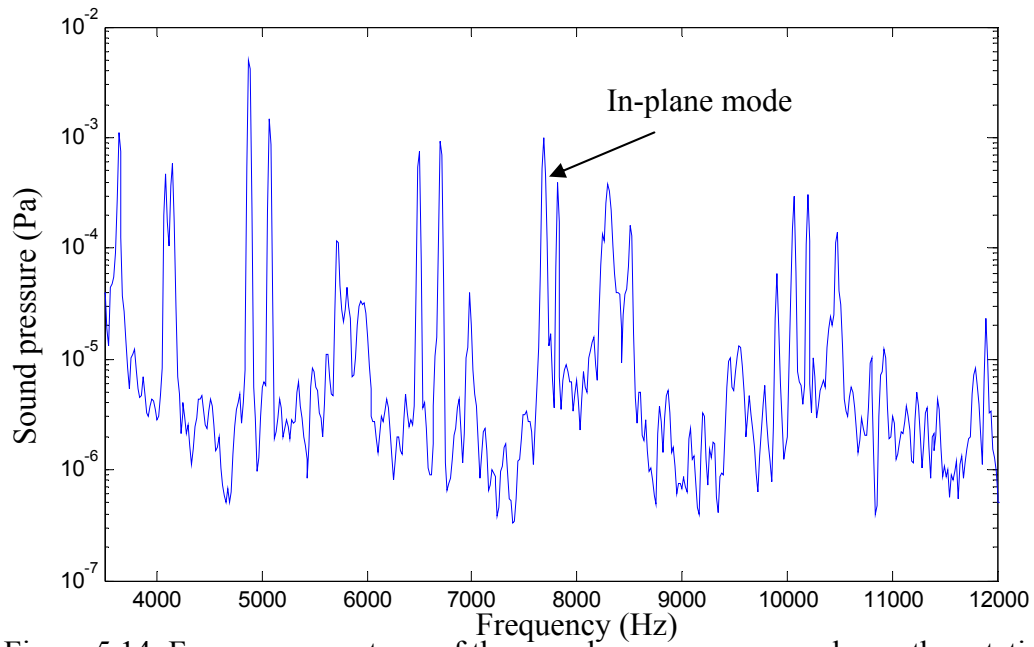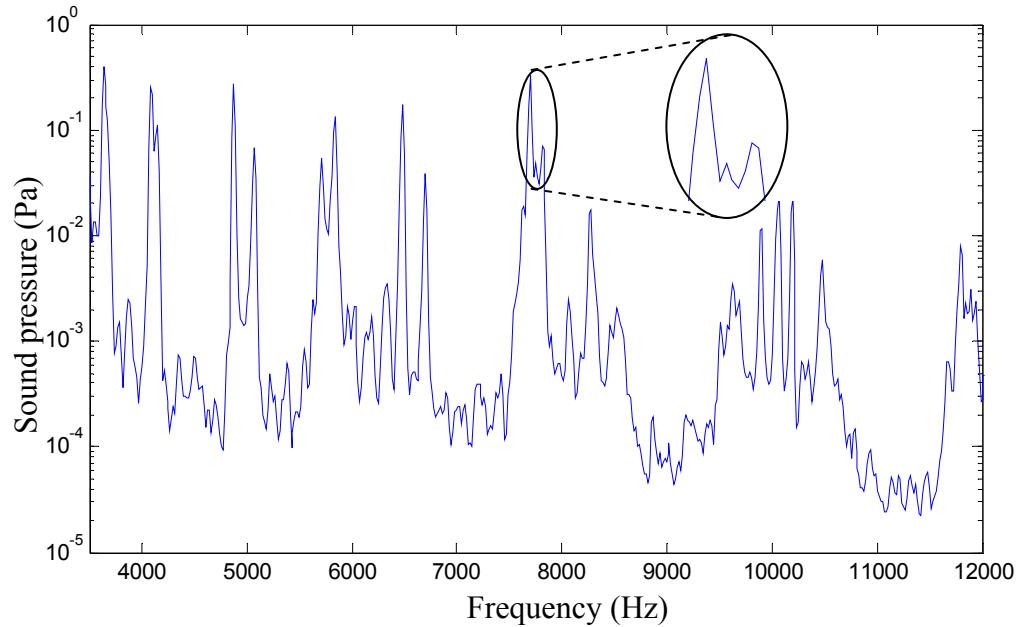
Figure 5.20: Frequency spectrum of the sound pressure measured near the stationary aluminum disk subject to an impulse hammer excitation (flexible inner edge and free outer edge) at 960 rpm subject to an elastic point support.

5.6.   Summary

The general problem of a rotating disk subject to non-uniform boundary conditions is explored. The variations of the forward and backward travelling waves are presented with respect to rotating and fixed coordinates to investigate the combined effect of rotation and boundary condition non-uniformity on the modal characteristics of the disk. Unlike the disks with uniform boundary conditions, the partial supports cause the frequencies to further split into two different values. This effect is added to the split caused by the gyroscopic effect of the rotating disk. Due to the additional coupling introduced by the non-uniform support, the forward, backward and the reflected waves tend to merge or separate from each other at different rotational speeds. The effect of additional stiffening is further explored on the in-plane vibration properties of disks with

194

non-uniform support conditions. The results clearly show the absence of critical speeds when the rotational stiffening is considered. An experimental study is performed to confirm the split in natural frequencies of the disk that was observed in the analytical results under both rotation and support non-uniformity. The experimental results thus confirm the presence of the forward and backward wave frequencies of the disk under a uniform support that were observed in the simulation results at higher disk speeds. The effect of the support, therefore, helps to produce forward and backward frequencies at lower rotational speeds than the case without support.

6. ANALYSIS OF THREE-DIMENSIONAL MODEL FOR THICK DISKS

It has been established that in-plane modes of vibration are significant in problems involving thick disks. In such problems, the contributions due to the out-of-plane modes are also equally important and could not be neglected. This is particularly significant considering the strong coupling between the in-plane and the out-of-plane modes for applications involving thick disks [2, 40, 74]. The analyses of noise and vibration responses of rotating thick disks thus necessitate considerations of the coupled in-plane and out-of-plane modes of vibrations.

A three-dimensional model of a thick disk is thus formulated in this chapter for analysis of coupled in-plane and out-of-plane modes of vibration. For this purpose, the in-plane formulations, presented in chapter 2, are extended to study the coupled modes of thick disks. Furthermore, the model is applied for analysis of vibration and noise of a railway wheel as a typical example involving rotational and constraint effects due to the contact with the rail. The point support and the rotation affect both in- and out-of-plane modes of vibrations of the railway wheel. In a reported study of the railway wheel noise radiation problem, Thompson [1] reported that the natural frequencies of the wheel could split into two values for some of the modes for a stationary wheel. The noise and vibration of a railway wheel were investigated by Sato and Matsuhisa [77] through an experiment. The experimental set up consisted of two wheels, representing the wheel and the rail, pressed against each other. The measurements were taken for several conditions including non-rolling and rolling disks at different pressing load conditions. Comparisons

between the experimental and analytical results suggested that the frequency distribution of the radiated noise is significantly affected by the wheel-rail contact. The analytical results showed that experimental results were best described by modeling the wheel as a disk with clamped inner edge and point-supported at the outer edge. The rotational effects were found to be insignificant for the rotational speeds considered in the analysis. Sakamoto et al. [78] conducted experimental investigations on rail-wheel interactions and concluded that one of the modes responsible for noise radiation could not be linked to any of the natural frequencies from the data acquired for the wheel without contact with the rail. The authors speculated that this mode could be attributed to the rail, while no explanation or justifications were provided. The authors also recommended for further investigations in this aspect. This mode of vibration could be associated to a mode that splits into two distinct frequencies in the presence of the wheel-rail contact or to the rail vibration caused by the wheel-rail contact forces. In both cases, this addresses the importance of the contact condition in the analysis of wheel vibrations. Thompson [42] showed that the analysis incorporating the rotational effects yields more accurate predictions of the natural frequencies and the acoustic properties of the rail-wheel system.

6.1. Analysis

In the previous chapters, the rotational and constraint effects have been addressed in the context of in-plane modes of vibrations only. Owing to the expected couplings between the in-plane and out-of-plane modes of thick disks, a three-dimensional model is proposed incorporating the uniform and non-uniform constraints and rotational effects. This model is formulated as an extension of the in-plane model developed in chapter 2,

which permits the analysis of the coupled in-plane and out-of-plane vibrations. The essential energy expressions for thick disks are derived for the three-dimensional model that also allows consideration of multiple disks connected by artificial springs to simulate abrupt variations in the thickness of the assembly. The non-uniform contact of the disk with a fixed surface could be represented by a point, line or an area spring with variations along the circumferential and the normal directions. Rotational effects and the additional stiffening due to initial rotation can be incorporated in the kinetic energy expression, as discussed earlier in section 2.5. Expressions are further formulated for estimating the acoustic properties associated with both the in-plane and out-of-plane modes of vibration.

6.1.1. Stationary Disk

A stationary annular thick disk of thickness h, outer radius R_o and inner radius R_i is shown in Figure 6.1. The displacement of an arbitrary point on the disk is described in the cylindrical coordinate system (r, θ and z) as u_r, u_θ and u_z, respectively. The strain energy can be written in terms of the stress and strain components as:

$$W = \frac{1}{2} \int_{-h/2}^{h/2} \int_0^{2\pi} \int_{R_i}^{R_o} (\sigma_r \varepsilon_r + \sigma_\theta \varepsilon_\theta + \sigma_z \varepsilon_z + 2\sigma_{r\theta}\varepsilon_{r\theta} + 2\sigma_{rz}\varepsilon_{rz} + 2\sigma_{z\theta}\varepsilon_{z\theta}) r\, dr\, d\theta\, dz \tag{6.1}$$

For an isotropic elastic disk that obeys Hooke's law, the stress-strain constitutive equations can be written as:

$$\begin{aligned}
\sigma_r &= \lambda\left(\varepsilon_r + \varepsilon_\theta + \varepsilon_z\right) + 2G\varepsilon_r \\
\sigma_\theta &= \lambda\left(\varepsilon_r + \varepsilon_\theta + \varepsilon_z\right) + 2G\varepsilon_\theta \\
\sigma_z &= \lambda\left(\varepsilon_r + \varepsilon_\theta + \varepsilon_z\right) + 2G\varepsilon_z \\
\sigma_{r\theta} &= 2G\varepsilon_{r\theta},\ \sigma_{rz} = 2G\varepsilon_{rz},\ \sigma_{z\theta} = 2G\varepsilon_{z\theta}
\end{aligned} \tag{6.2}$$

where the constants λ and G are called the *Lame* constants, given by:

198

$$\lambda = \frac{Ev}{(1+v)(1-2v)}; \text{ and } G = \frac{E}{2(1+v)}.$$ (6.3)

The constant G is also known as the shear modulus. The strain components can be expressed in terms of the three-dimensional displacements as:
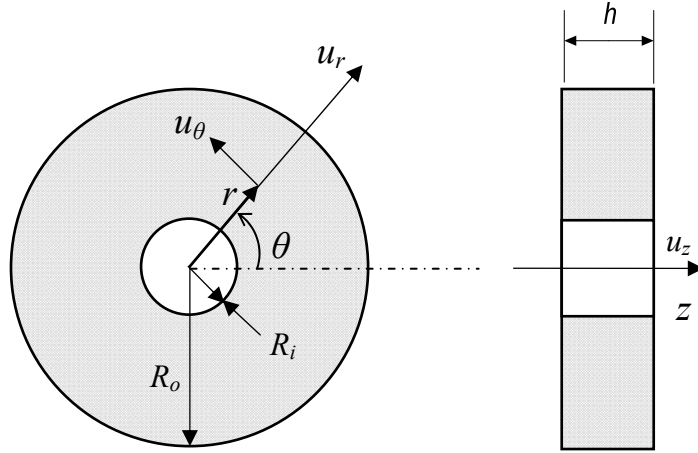
Figure 6.1: Geometry and coordinate system used for in-plane vibration analysis of a thick annular disk.

$$\varepsilon_r = \frac{\partial u_r}{\partial r}, \qquad \varepsilon_{r\theta} = \frac{1}{2}\left(\frac{1}{r}\frac{\partial u_r}{\partial \theta} + \frac{\partial u_\theta}{\partial r} - \frac{u_\theta}{r}\right)$$

$$\varepsilon_\theta = \frac{1}{r}\left(u_r + \frac{\partial u_\theta}{\partial \theta}\right), \qquad \varepsilon_{rz} = \frac{1}{2}\left(\frac{\partial u_r}{\partial z} + \frac{\partial u_z}{\partial r}\right)$$ (6.4)

$$\varepsilon_z = \frac{\partial u_z}{\partial z}, \qquad \varepsilon_{z\theta} = \frac{1}{2}\left(\frac{1}{r}\frac{\partial u_z}{\partial \theta} + \frac{\partial u_\theta}{\partial z}\right)$$

Substituting Eqs. (6.4) and (6.2) into (6.1) and introducing the non-dimensional parameters, $\xi = r/R_o$ and $\zeta = z/h$, the expression for the maximum strain energy ($\mathbb{U}_{max}$) of the disk in cylindrical coordinate system can be expressed as:

$$\mathbb{U}_{max} = \frac{1}{4} \frac{Eh}{(1+v)} \int\limits_0^{2\pi} \int\limits_{-0.5}^{0.5} \int\limits_{\beta}^1 \left\{ \frac{2v}{(1-2v)} \left(\frac{\partial u_r}{\partial \xi} + \frac{1}{\xi} \frac{\partial u_\theta}{\partial \theta} + \frac{u_r}{\xi} + \frac{R_0}{h} \frac{\partial u_z}{\partial \zeta} \right)^2 + 2 \left[\left(\frac{\partial u_r}{\partial \xi} \right)^2 \right. \right.$$

$$+ \left(\frac{u_r}{\xi} + \frac{1}{\xi} \frac{\partial u_\theta}{\partial \theta} \right)^2 \right] + \left(\frac{R_0}{h} \frac{\partial u_z}{\partial \zeta} \right)^2$$

$$+ \left(\frac{1}{\xi} \frac{\partial u_r}{\partial \theta} + \frac{\partial u_\theta}{\partial \xi} - \frac{u_\theta}{\xi} \right)^2 + \left(\frac{R_0}{h} \frac{\partial u_\theta}{\partial \zeta} + \frac{1}{\xi} \frac{\partial u_z}{\partial \theta} \right)^2$$

$$+ \left. \left(\frac{R_0}{h} \frac{\partial u_r}{\partial \zeta} + \frac{\partial u_z}{\partial \xi} \right)^2 \right\} \xi \, d\xi \, d\zeta \, d\theta \tag{6.5}$$

In the above equation, the coordinates r and z are expressed in terms of non-dimensional parameters leading to cylindrical coordinate as (ξ, θ, ζ). The expression for the maximum kinetic energy (T_{max}) is also expressed in the same coordinate system, as:

$$T_{max} = \frac{1}{2} \omega^2 h \rho R_0^2 \int\limits_0^{2\pi} \int\limits_{-0.5}^{0.5} \int\limits_{\beta}^1 (u_r^2 + u_\theta^2 + u_z^2) \xi \, d\xi \, d\zeta \, d\theta \tag{6.6}$$

The free in-plane vibration of the disk is assumed to have sinusoidal variations along the circumferential direction of the disk, and may be expressed in the form [2, 71]:

$$u_r(\xi, \zeta, \theta) = \sum_{l=0}^{\infty} \sum_{m=1}^{\infty} \sum_{n=0}^{\infty} [\bar{U}_{c,lmn}(t) \psi_l(\zeta) \phi_m(\xi) \cos(n\theta) \tag{6.7}$$

$$+ \bar{U}_{s,lmn}(t) \psi_l(\zeta) \phi_m(\xi) \sin(n\theta)]$$

$$u_\theta(\xi, \zeta, \theta) = \sum_{l=0}^{\infty} \sum_{m=1}^{\infty} \sum_{n=0}^{\infty} [\bar{V}_{c,lmn}(t) \psi_l(\zeta) \phi_m(\xi) \cos(n\theta) \tag{6.8}$$

$$+ \bar{V}_{s,lmn}(t) \psi_l(\zeta) \phi_m(\xi) \sin(n\theta)]$$

$$u_z(\xi, \zeta, \theta) = \sum_{l=0}^{\infty} \sum_{m=1}^{\infty} \sum_{n=0}^{\infty} [\bar{Z}_{c,lmn}(t) \psi_l(\zeta) \phi_m(\xi) \cos(n\theta) \tag{6.9}$$

$$+ \bar{Z}_{s,lmn}(t) \psi_l(\zeta) \phi_m(\xi) \sin(n\theta)]$$

where $\bar{U}$, $\bar{V}$ and $\bar{Z}$ are the radial, circumferential and transverse deflection coefficients, respectively. The first subscripts, c and s, refer to cosine and sine components of the deflections, respectively. The subsequent subscripts, l, m and n, describe the number of terms along the transverse, radial and circumferential directions, respectively. The functions $\phi(\xi)$ and $\psi(\zeta)$ are the assumed deflection shapes satisfying the geometric boundary conditions in the form of boundary characteristic orthogonal polynomials. The starting functions, $\phi_1(\xi)$ and $\psi_1(\zeta)$ where taken as 1, while distributed artificial springs were considered to represent the clamped boundary conditions. The successive polynomials were generated using the recurrence relation (2.46), while the associated constants b_k and c_k, for the polynomials along the normal directions $\psi(\zeta)$ are defined as:

$$b_k = \int_{-0.5}^{0.5} \zeta \psi_k^2(\zeta) d\zeta \Big/ \int_{-0.5}^{0.5} \psi_k^2(\zeta) d\zeta$$

$$c_k = \int_{-0.5}^{0.5} \zeta \psi_k(\zeta) \psi_{k-1}(\zeta) d\zeta \Big/ \int_{-0.5}^{0.5} \psi_{k-1}^2(\zeta) d\zeta$$

(6.10)

The assumed solutions (6.7) to (6.9) are substituted into the energy expressions, (6.5) and (6.6), to obtain natural frequencies of the disk using the Rayleigh-Ritz method. A point support condition at an edge is realized by introducing artificial springs along the radial, circumferential and transverse directions at the location of the support, as described in section 2.4.1 for the in-plane model. Figure 6.2 illustrates the disk supported on a point support idealized by the artificial springs in the three directions. For a disk supported at multiple points on the outer edge, the maximum potential energy W_p can be derived as:

$$\mathbb{U}_p = \frac{1}{2} \sum_{p=1}^{P} \left[K_{pr} \left[u_r \left(R_p, \theta_p, \zeta_p \right) \right]^2 + K_{p\theta} \left[u_\theta \left(R_p, \theta_p, \zeta_p \right) \right]^2 \right.$$

$$\left. + K_{pz} \left[u_z \left(R_p, \theta_p, \zeta_p \right) \right]^2 \right]$$

<div align="right">(6.11)</div>

where $p = 1, 2, \ldots P$ defines the number of point supports considered, and K_{pr}, $K_{p\theta}$ and K_{pz} are the stiffness constants per unit length of the point elastic support in the radial, circumferential and transverse directions, respectively; and R_p, θ_p and ζ_p are the radial and circumferential coordinates of the point support p, respectively. It is assumed that the point supports have a symmetric axis about $\theta = 0$. The total strain energy of the disk is then obtained by summing those defined in Eqs. (6.11) and (6.5). The energy equations are subsequently solved for the natural frequencies and mode shapes, using the methodology described in section 2.3.
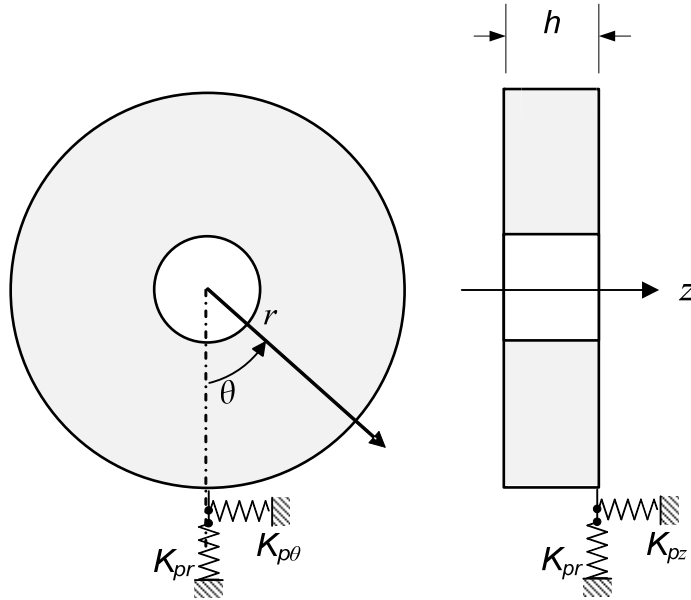
Figure 6.2: Annular disk with a three-dimensional elastic point support at the outer edge.

6.1.2. Rotational Effects

The formulation of the rotational effects is similar to that described in section 2.5. For the linear analysis and constant rotational speed about the normal axis, the expression for the kinetic energy can be written as:

$$T = \frac{1}{2} h \rho R_0^2 \int_0^{2\pi} \int_\beta^1 \left(\left(\dot{u}_r - \Omega u_\theta \right)^2 + \left(\dot{u}_\theta + \Omega u_r \right)^2 + \dot{u}_z^2 \right) \xi d\xi d\theta \qquad (6.12)$$

The kinetic energy expression can also be written with respect to fixed coordinate using the transformation given in Eq. (2.82). The kinetic energy expression, Eq.(6.12), along with strain energy expressions for the disk and boundary conditions, Eqs. (6.5) and (6.11), can be used to study the three-dimensional modal characteristics of a rotating disk.

The rotational and constraint effects yield coupling between different modes, as discussed previously in section 2.4.2. It was established that radial and circumferential displacements were coupled in thin disks, while the transverse displacement could be treated independently. For a thick disk, an additional coupling is introduced between in-plane and out-of-plane modes. This is evident from Eq. (6.5), which shows that the transverse displacement is coupled with both the radial and circumferential displacements. The severity of the coupling between the modes depends on the rotational speed and the boundary conditions, as described in section 2.4.2.

For axisymmetric modes ($n = 0$), the coupling exists between the radial and the transverse modes only. Therefore, for a stationary disk subject to uniform boundary conditions, the axisymmetric radial and transverse modes need to be solved

simultaneously, while the circumferential torsional modes can be treated independently. For modes with non-zero nodal diameter number ($n \neq 0$), radial, circumferential and transverse modes are coupled within the same nodal diameter number n. In this case, it is not necessary to solve for the even and odd subsystems since they would yield identical solutions for the eigenvalue problem. For stationary disks subject to non-uniform supports, the system can be conveniently expressed by decoupled even and odd subsystems, as described in section 2.4.2, where each subsystem would yield distinct values for of the natural frequencies. For rotating disks, however, both the subsystems need to be solved simultaneously. The non-uniform supports would further generate additional coupling between the modes with different nodal diameter number (n).

An additional symmetry is also observed at $\zeta = 0$ for disks subject to uniform boundary conditions at both faces. The modes, therefore, can be divided into symmetric and anti-symmetric modes with respect to the mid-plane of the disk. The symmetric modes can be obtained by taking $l = 0, 2, 4, \ldots$ in Eqs. (6.7) and (6.8) and $l = 1, 3, 5, \ldots$ in Eq. (6.9), while $l = 1, 3, 5, \ldots$ in Eqs. (6.7) and (6.8) and $l = 0, 2, 4, \ldots$ in Eq. (6.9) would yield the anti-symmetric modes [71].

6.1.3. Out-of-Plane Sound Radiation

In section 2.6, an acoustic analysis was performed to obtain the sound radiation characteristics due to in-plane modes of vibration of the disk. The acoustic properties associated with the out-of-plane modes of vibrations can also be evaluated in a similar manner. The three-dimensional model, presented in this section, however, can predict the

acoustic properties of the thick disk attributed to both the in-plane and out-of-plane modes.

The far field sound pressure can be obtained by solving the Helmholtz integral equation, such that:

$$P(r_p) = -\int_S \left(P\frac{\partial \overline{G}}{\partial \gamma} + j\rho_0 \omega \dot{w}(r_s)\overline{G} \right) dS \tag{6.13}$$

where P is the sound pressure generated at a sphere of radius r_p by the normal velocity $\dot{w}$ of the disk surface at r_s. The term $\overline{G}$ is free space Green's function, γ is the angle between the disk normal surface and the point where the pressure is measured and S is the boundary surface of the acoustic volume. For the vibrating body located in on an infinite rigid plane (see Figure 6.3), the sound pressure can be estimated from the Rayleigh integral equation [103]:

$$P(r) = \rho_0 c_0 k \int_S j\omega \dot{w}(r) \frac{e^{-jkR}}{2\pi R} \ dS \tag{6.14}$$

where ρ_0 is mass density of air, c_0 is the speed of sound, k is the acoustic wave number, R is the distance between the receiver and disk center, and $\dot{w}$ is the normal velocity amplitude. For a vibrating annular plate, the $(m,n)^{\text{th}}$ modal sound pressure associated with mode (m,n), P_{mn}, can be expressed, using the Hankel transform as [104]:

$$P_{mn}(R, \theta, \phi) = \frac{\rho_0 c_0 k e^{ik_{mn}R}}{R}(-i)^{n+1} \cos(n\theta) B_n[\dot{w}(r)] \tag{6.15}$$

where

$$B_n[\dot{w}(r)] = \int_0^\infty \dot{w}(r)J_n(kr\sin\phi)r dr$$

The surface velocity $\dot{w}(r)$ can be obtained by solving for the structural response, such that:
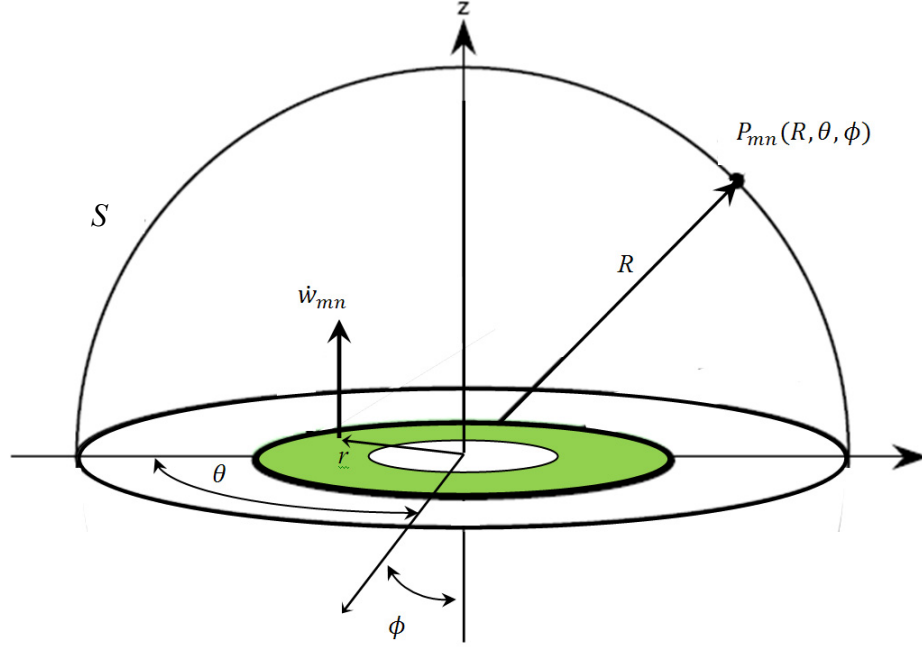
Figure 6.3: Sound radiation due to the out-of-plane vibration modes [23].

$$\dot{w}_{mn}(r,\theta,t) = -\omega_{mn} \sum_{m}^{M} C_m \phi_m(\xi) \cos(n\theta)\, e^{i\omega_{mn}t} \tag{6.16}$$

where C_m are arbitrary constants. Substituting Eq. (6.16) into Eq.(6.15), the far field modal sound pressure can be written as:

$$P_{mn}(R,\theta,\phi) = \frac{\rho_0 c_0 k e^{ik_{mn}R}}{R}(-i)^{n+1}\cos(n\theta)\sum_{m}^{M} C_m \int_{b}^{a} \phi_m(\xi)J_n(kr\sin\phi)dr \tag{6.17}$$

where J_n is the Bessel function of the first kind and k_{mn} is the modal acoustic wave number. The modal directivity function $D_{mn}(\theta,\phi)$ can be written in terms of the sound pressure, as:

$$D_{mn}(\theta,\phi) = RP_{mn}(R,\theta,\phi)e^{ik_{mn}R} \tag{6.18}$$

The modal sound power Π_{mn}, associated with mode (m,n), can also be derived as:

$$\Pi_{mn} = \frac{1}{2} \int_0^{2\pi} \int_0^{\pi} \frac{P_{mn}^2}{\rho_0 c_0} \sin(\phi) d\theta d\phi \qquad (6.19)$$

The modal radiation efficiency σ_{mn} is related to the sound power, such that:

$$\sigma_{mn} = \frac{\Pi_{mn}}{\langle |\dot{w}_{mn}|^2 \rangle} \qquad (6.20)$$

where

$$\langle |\dot{w}_{mn}|^2 \rangle = \frac{1}{2\pi(R_0^2 - R_i^2)} \int_{R_i}^{R_0} \int_0^{2\pi} \dot{w}_{mn}^2 \, d\theta dr$$

For thick disks, the sound radiation from both the surfaces needs to be considered. The following expressions are thus used to calculate the sound pressure, instead of Eq. (6.15), [23]:

$$P_{mn}^u(R,\theta,\phi) = \frac{\rho_0 c_0 k_{mn} e^{ik_{mn}R}}{2R} e^{-\frac{ik_{mn}h}{2}\cos(\phi)} (-i)^{n+1} \cos(n\theta) B_n[\dot{w}(r)] \qquad (6.21)$$

$$P_{mn}^l(R,\theta,\phi) = \frac{\rho_0 c_0 k_{mn} e^{ik_{mn}R}}{2R} e^{-\frac{ik_{mn}h}{2}\cos(\phi)} (-i)^{n+1} \cos(n(\theta + \pi)) B_n[\dot{w}(r)] \quad (6.22)$$

where P_{mn}^u and P_{mn}^l are the sound pressure from upper and lower surfaces, respectively. The total sound pressure is expressed by the sum of both the surface pressures leading to:

$$P_{mn}(R,\theta,\phi) = (1 + \cos(\theta))P_{mn}^u(R,\theta,\phi) + (1 - \cos(\theta))P_{mn}^l(R,\theta,\phi) \qquad (6.23)$$

Equation (6.23) along with Eq. (2.95) for the in-plane sound radiation yield the total sound pressure radiated from the thick disk.

6.2.   Free Vibration Response and Model Validation

The previous section presented a brief formulation to illustrate the generalization of the two-dimensional analytical formulations to a three-dimensional disk model. It is, therefore, essential to examine the validity of the current analysis through comparisons

with results reported for the three-dimensional models. Moreover, the applicability of the model is demonstrated by relating it to a railway wheel while comparison with measured railway wheel data is performed to illustrate the accuracy and versatility of the developed model. For the purpose of validation of the model with non-uniform boundary conditions, the approximate numerical results are obtained from a three-dimensional finite element model. The three-dimensional model for the annular disk is illustrated in Figure 6.4(a), while the model of the railway wheel is shown in Figure 6.4(b).

(a)   (b)
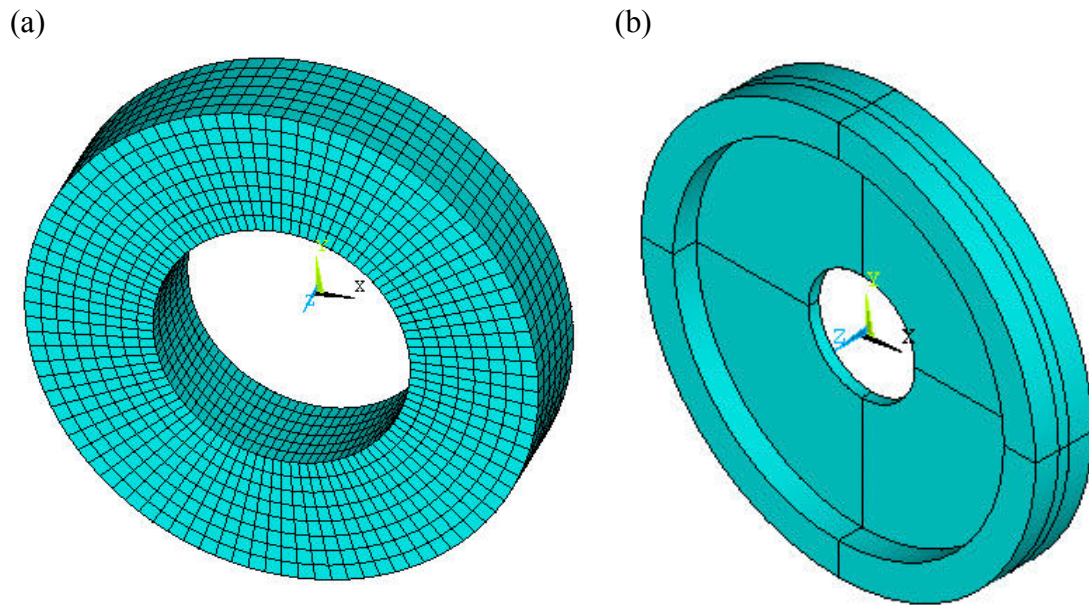
Figure 6.4: Three-dimensional finite element model of: (a) a thick annular disk; and (b) a railway wheel.

6.2.1. Free Vibration of Thick Disks

The natural frequencies are obtained for a thick disk with free boundary conditions and compared with those reported by So and Leissa [71] to demonstrate the model validity. Table 6.1 shows the comparisons of the frequency parameters, $\lambda^2 = \rho\omega^2 R_0^2/G$, of a solid disk with free boundary conditions for two different thickness to

diameter (*h/D*) ratios. The comparisons of the frequency parameters of the annular disks are shown in Table 6.2. The comparisons suggest very good agreements between the frequency parameters obtained from the model and the reported results. This also confirms the applicability of the analysis to study three-dimensional vibration problem. Further analysis is performed to examine the accuracy of the computed frequencies of the disk under the non-uniform boundary conditions.

Table 6.1: Comparisons of the frequency parameters of a solid disk with free conditions with the reported values ($v = 0.3$).

	Mode	$h/D = 0.2$		$h/D = 0.5$	
		Present study	Reference [71]	Present study	Reference [71]
$n=1$	1	2.731	2.731	2.705	2.705
	2	5.864	5.864	4.595	4.595
	3	6.812	6.812	4.836	4.836
	4	9.905	9.903	6.439	6.439
$n=2$	1	2.345	2.345	2.345	2.345
	2	4.230	4.230	3.966	3.966
	3	7.501	7.501	4.867	4.867
	4	8.561	8.560	5.623	5.623
$n=3$	1	3.600	3.600	3.591	3.591
	2	5.793	5.793	4.612	4.612
	3	8.832	8.832	6.045	6.045
	4	10.105	10.105	6.498	6.498

Table 6.2: Comparisons of the frequency parameters of an annular disk with free conditions with the reported values ($\beta = 0.5, v = 0.3$).

	Mode	$h/D = 0.2$		$h/D = 0.5$	
		Present study	Reference [71]	Present study	Reference [71]
$n=1$	1	1.943	1.943	1.999	1.999
	2	8.039	8.039	3.930	3.930
	3	8.534	8.534	5.839	5.839
	4	8.945	8.945	7.706	7.706
$n=2$	1	0.691	0.691	1.039	1.039
	2	3.123	3.123	2.846	2.846
	3	8.400	8.400	5.172	5.172
	4	8.793	8.793	6.157	6.157
$n=3$	1	1.680	1.680	2.320	2.320
	2	4.450	4.450	3.946	3.946
	3	8.808	8.808	6.392	6.392
	4	8.986	8.986	6.805	6.805

Table 6.3 compares the frequency parameters obtained from the even and odd systems for an annular disk free at the inner edge and point-clamped at the outer edge. Table 6.3 also shows the frequency parameters of the disk when the point-clamp is relaxed (free condition). The results are compared with those attained from the finite element model. The labels a and s represent anti-symmetric and symmetric modes with respect to the $z = 0$ plane, respectively. The results show good agreement between the frequency parameters derived from the proposed method and those estimated from the finite element model. The comparison shows that the results derived from the finite element model are very close to the analytical results for the free disk. Some differences, however, are evident in both the even and odd subsystem frequency parameters of the disk with the point support. This is most likely attributed to the localization effect around the point support, which requires a more refined mesh around the support. The results, however, are considered to be within an acceptable accuracy considering that the peak error is less than 2% for most of the listed frequencies.

Table 6.3: Comparisons of the even and odd frequency parameters of an annular disk with those estimated from the finite element model ($\beta = 0.5, h/D = 0.2, v = 0.3$).

Constraint	Free disk		Point Clamped at the outer edge (even)		Point Clamped at the outer edge (odd)	
(*m,n*)	Present study	FE Model	Present study	FE Model	Present study	FE Model
(1,2)*a*	0.691	0.691	1.130	1.112	0.920	0.917
(1,2)*s*	0.949	0.949	1.298	1.268	1.070	1.050
(1,0)*a*	1.388	1.387	1.465	1.466	-	-
(1,3)*a*	1.680	1.681	1.888	1.887	1.712	1.707
(1,1)*a*	1.943	1.944	2.238	2.237	1.943	1.944
(1,0)*s*	2.233	2.230	2.253	2.252	-	-
(1,3)*s*	2.249	2.249	2.529	2.509	2.251	2.247

a: anti-symmetric, *s*:symmetric

In order to show the significance of coupling between in-plane and out-of-plane motions of thick disk, the frequency response of a thick disk with $v = 0.3$, $\beta = 0.5$ and $h/D = 0.2$ subject to free and point-supported conditions is investigated. The in-plane and out-of-plane responses of the thick disk are illustrated Figure 6.5(a) and (b), respectively, due to a harmonic excitation along the radial direction only. It is evident in Figure 6.5(b) that an excitation along the radial direction also excites the out-of-plane modes of vibrations. This suggests that the coupling of the in-plane modes with the out-of-plane modes for thick disks would contribute to the noise radiation properties, even though in-plane modes did not contribute directly to the noise radiation. The coupling is significant and has been observed in disks with low thickness ratios such as the one used in the experimental investigations (Figure 4.23).

The frequency responses, in Figure 6.5, show also the significant effect of the point support on both in-plane and out-of-plane modes of vibrations. As stated earlier, the point support would introduce additional coupling between radial, transverse and circumferential modes with different n numbers. This coupling effect is additional to the primary effect of the point support which results in increasing the natural frequencies and splitting of some modes into two distinct values. The frequency response of a point-supported disk is quite different from the response of a disk with free edges for both in-plane and out-of-plane modes of vibrations. It is, therefore, recommended to consider a coupled in-plane and out-of-plane model with the proper consideration of the boundary conditions for applications involving thick disks, especially when excitations are along the in-plane directions or when the boundary conditions are non-uniform.

a)

b)
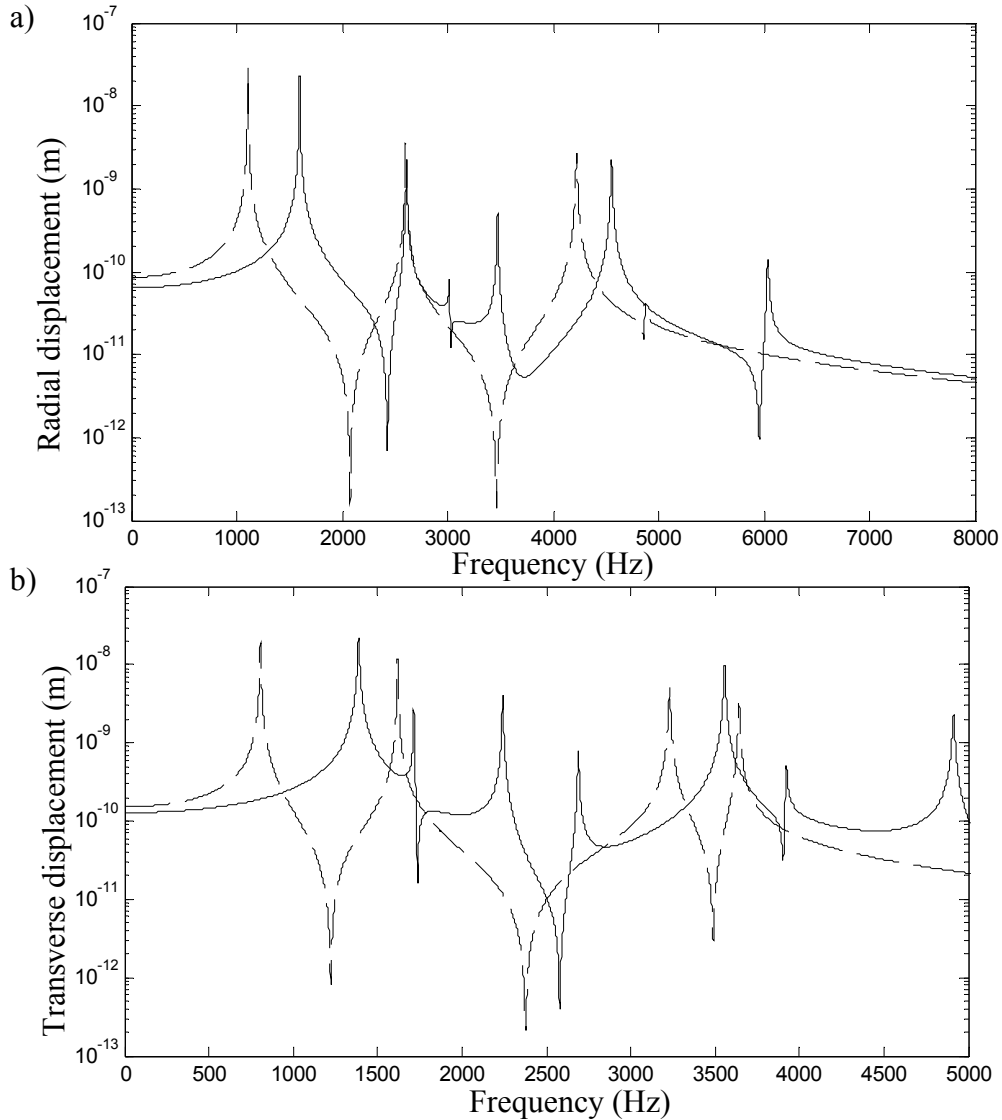
Figure 6.5: Frequency response characteristics of the annular thick disk with different boundary conditions subject to harmonic radial force: _ _ _ _ _ free, ———— point support (a) radial displacement, (b) transverse displacement.

6.2.2. Acoustic Model Validation

It is also essential to validate the accuracy of the analysis in predicting the out-of-plane acoustic properties of thick disks. The directivity patterns of two out-of-plane modes are illustrated in Figure 6.6. The pressure distributions agree very well with those obtained by Lee and Singh [23]. Further validation is performed with the sound power and radiation efficiency of specific out-of-plane modes, as shown in Table 6.4. The

212

calculated sound power and radiation efficiency are found to be similar to those reported in [108] for annular disks suggesting the validity of the current analysis. The formulation presented in this chapter along with the analysis of sound radiation due to in-plane modes, illustrated in sections 2.6 and 4.8, provide the essential foundation for the analysis of thick disks with any possible combination of boundary conditions. It is important to emphasize that the current formulation for acoustic properties is limited to stationary disks only. The formulation of the acoustic properties of rotating disks necessitate the employment of the far-field Green's function of a moving source instead of the stationary disk used in deriving the sound pressure expression [114]. For applications such as railway wheels, which involve relatively low speeds, the acoustic properties of rolling wheel can be approximated by those of a stationary disk simply-supported at one point on the outer edge [77].

Table 6.4: Comparison of acoustic power and radiation efficiency levels for selected out-of-plan modes.

mode	Present		Reference [108]	
(m,n)	Π_{mn}	σ_{mn}	Π_{mn}	σ_{mn}
(1,1)	69.5669	0.9162	70.1	1.06
(0,3)	74.95	1.1015	75.1	1.14

6.3.   Application to a Railway Wheel

The proposed three-dimensional model is employed to study the vibration properties of a railway wheel. The flange and the web of the railway wheel are idealized by two disks with different thicknesses. The disk representing the web is assumed to be fixed at the axle shaft. The two disks are connected to each other by artificial springs that are uniformly distributed at radius R_i. Figure 6.7 illustrates the axisymmetric view of the

213

two-disk model of the railway wheel. The geometric and material properties of the idealized wheel model are summarized in Table 6.5.

(a)

(b)
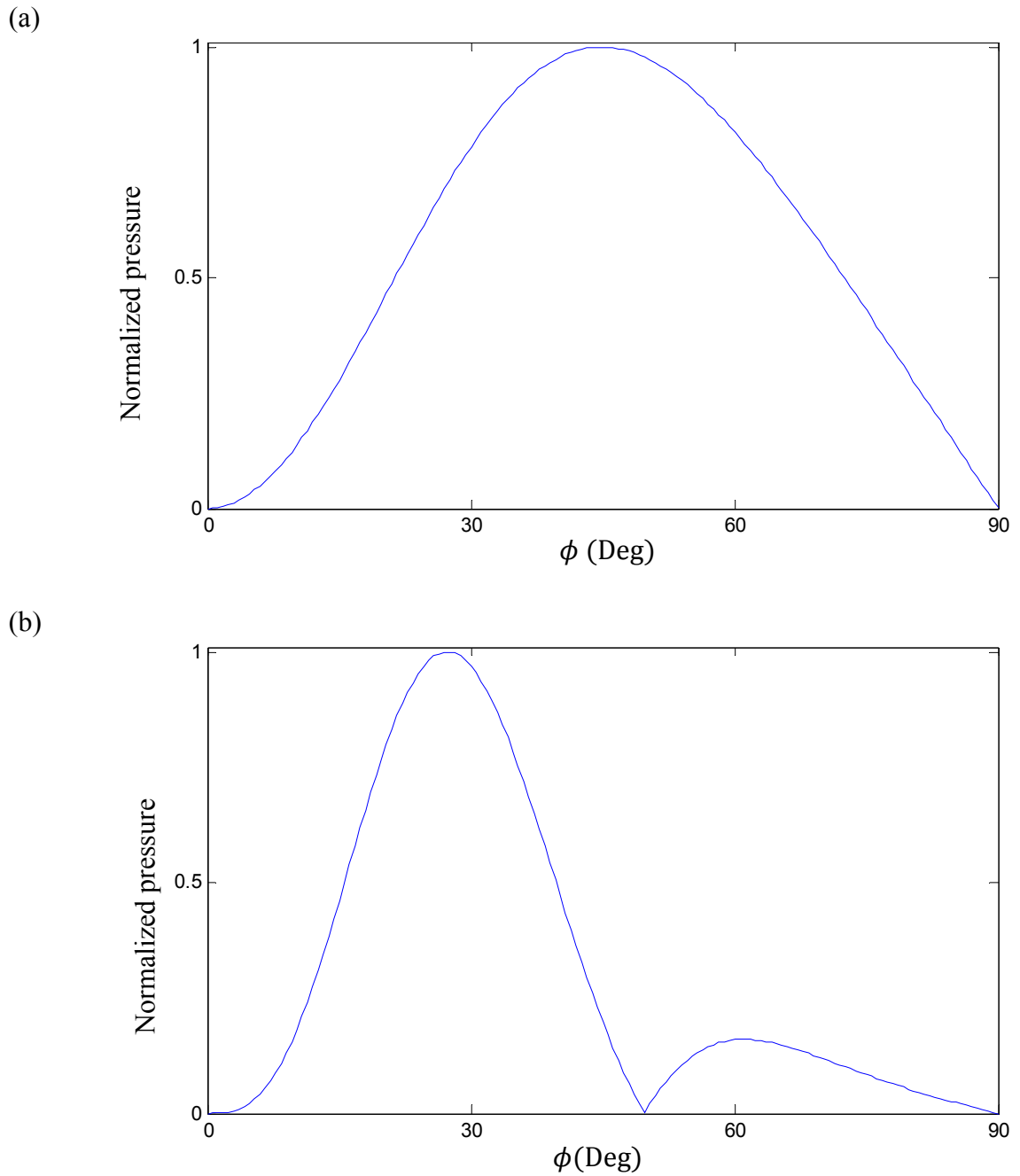
Figure 6.6: Directivity pattern for selected out-of-plane modes of the annular disk with free edges along ϕ direction: (a) mode (0,2); (b) mode (0,3).
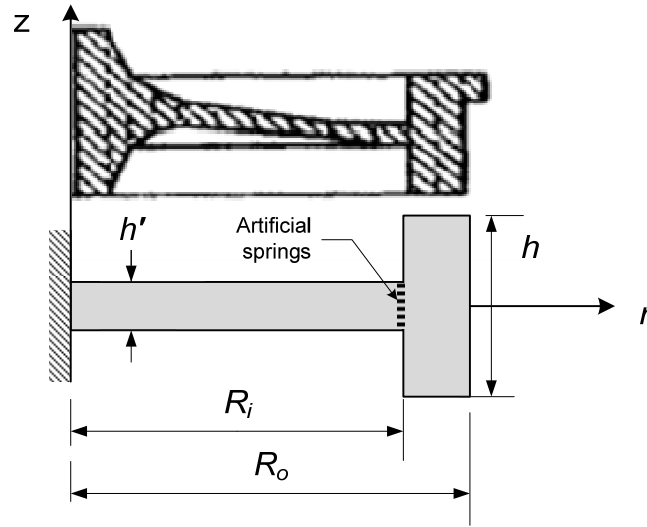
Figure 6.7: Idealization of a railway wheel by two disks with different thickness coupled through artificial springs.

In Table 6.6, the in-plane and out-of-plane natural frequencies of the idealized model are obtained and compared with the experimental and analytical results reported for selected modes in [78]. The comparisons reveal good agreements between the model results and the reported analytical and experimental values. The natural frequency results suggest that the frequencies obtained from the proposed model are in closer agreements with the measured values reported in [78], for all modes considered. Relatively greater differences, however, are evident between the reported measured and the reported model results. It needs to be emphasized that the methodology used in deriving the reported analytical values was limited to prediction of the first natural frequency for each nodal diameter number n. Moreover, the comparisons are confined to modes with $n \geq 2$, since prediction of the natural frequencies of modes with zero or one nodal diameter necessitates a proper idealization of the axle as well as the wheel.

Table 6.5: Geometric and material properties of the idealized railway wheel model [78].

material properties	density (ρ)	7800 kg/m^3
	Modulus of elasticity (E)	205.8 x 10^9 N/m^2
	Poisson's ratio (v)	0.3
Geometrical properties	Outer disk thickness (h)	125 mm
	Inner disk thickness (h')	23 mm
	Outside radius (R_o)	434 mm
	Inside radius (R_i)	364 mm

A point support is introduced on the outer edge of the wheel to simulate the wheel contact with the rail. The support is uniformly distributed along the normal direction and could be best described by a line support in the three-dimensional model. The natural frequencies obtained from the even and odd subsystems of the model are computed and compared with those attained from the finite element model in Table 6.7. The effect of the wheel-rail contact on the natural frequencies of both the in-plane and out-of-plane modes is clearly evident. The addition of the point support causes the natural frequencies corresponding to the selected modes to increase. The frequency of the first out-of-plane mode is nearly twice compared to that of the free wheel. The results suggest that the modal characteristics of the wheel with the contact are quite different from those obtained for the wheel with free edges.

Table 6.6: Comparisons of the in-plane and out-of-plane natural frequencies of the idealized railway wheel model with the reported measured and analytical values.

Mode number	In-plane modes (Hz)			Out-of-plane modes (Hz)		
	Present study	Measured [78]	Analytical [78]	Present study	Measured [78]	Analytical [78]
2	1719	1720	1778	435	430	435
3	2603	2620	2577	1097	1110	1069
4	3335	3339	3337	2004	2005	1767

Table 6.7: Comparisons of the in-plane and out-of-plane natural frequencies of the idealized railway wheel with contact support with these derived from the FE model.

Constraint		Free disk		Point contact at the outer edge (even)		Point Contact at the outer edge (odd)	
		Present study	FE Model	Present study	FE Model	Present study	FE Model
In-plane		1719	1697	1721	1725	1851	1857
		2603	2611	2691	2687	2682	2684
		3335	3289	3515	3520	3452	3462
Out-of-plane		435	435	635	631	825	809
		1097	1104	1340	1324	1225	1227
		2004	2029	2329	2329	2105	2073

The proposed model and the formulations permit study of the effects of several parameters on the modal and acoustic characteristics of the wheel. As an example, the effect of wheel diameter on its free vibration response is illustrated in Figure 6.8. The figure shows the variations in the natural frequencies of the railway wheel with variations in the web radius R_i. It is evident from the figure that the wheels with larger radius have relatively smaller natural frequencies of both the in-plane and the out-of-plane modes. Both the in-plane and out-of-plane modes tend to be more sensitive to variation in the web radius as the n increases.

Figure 6.9 (a) and (b) show the variations in the frequencies associated with the forward and backward waves with the rotational speed for out-of-plane and in-plane modes, respectively. It is shown that higher modes are more sensitive to variations in the rotational speed than the lower modes. The results also show absence of instability in the speed range considered. It is also important to note that the presented analysis employed the linear strain measure, which neglects the additional stiffening effect due to

(a)

(b)
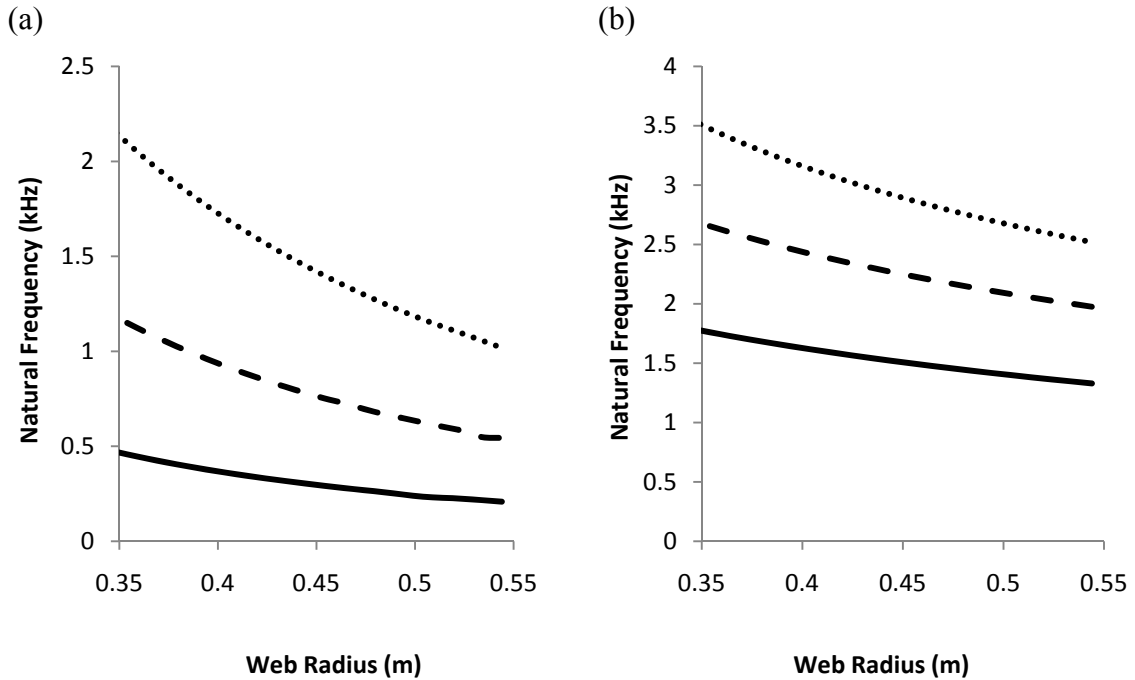
Figure 6.8: Variations in the natural frequencies of a railway wheel with the web radius: (a) In-plane modes, (b) out-of-plane modes. ——— $n = 2$, – – – – – $n = 3$ and ....$n = 4$.

rotation. This assumption was considered justifiable since the rotational speed is lower than the threshold speed specified by Deshpande and Mote [36]. A non-linear strain measure would be essential for higher speeds. The rotation, however, affects the natural frequencies in a considerable manner, as shown in Figure 6.9, and needs to be considered to accurately predict the modal characteristics of the wheel. Although the contact support does not affect the variations in the waves with the rotational speed but it significantly affects the initial values of the frequencies corresponding to zero rotational speed. as described above in Table 6.7. The effect of rotation on the modal characteristics of the wheel is relatively small compared to the significant effects associated with the wheel-rail contact.

(a)

(b)
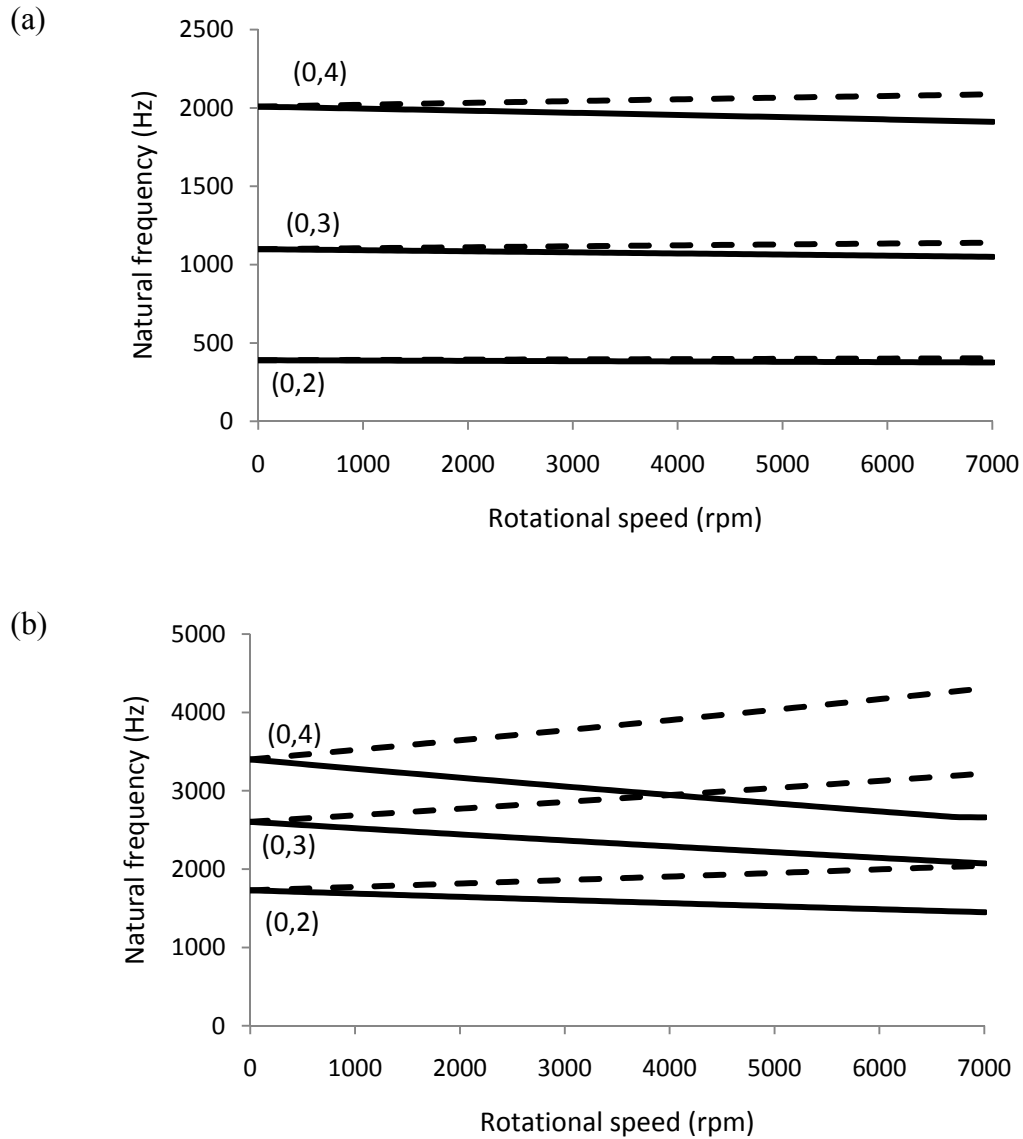
Figure 6.9: Effect of rotational speed on variations in the natural frequencies of a railway wheel with respect to the fixed coordinate: _____ backward waves, _ _ _ _ forward waves, (a) out-of-plane modes, (b) in-plane modes.

6.4. *Summary*

In this chapter, the formulations developed in the previous chapters are extended to analyze the vibration characteristics of thick disks. The validity of the three-dimensional model is demonstrated through comparisons of the results with the reported

data. The in-plane and out-of-plane natural frequencies are subsequently used to obtain the total sound radiation from the wheel. This allows further analysis of the sound radiation properties of the wheel under the effect of a contact support. The independent formulations derived for the sound radiation attributed to in-plane and out-of-plane modes permit analyses of contribution of different modes to the total sound radiation, and identifications of the most significant modes. The non-uniform contact or support has significant influence on the modal characteristics of the thick and thin disks. For thick disks, additional coupling between in-plane and out-of-plane modes is introduced due to the non-uniformity of the support. The proposed model is also applied to predict the natural frequencies of a railway wheel.

7. CONCLUSIONS AND RECOMMENDATIONS

The overall objective of this dissertation research was to investigate the effects of rotation and non-homogeneous constraint on the modal characteristics of circular disks with particular focus on the in-plane modes of vibrations. An analytical method is developed in this dissertation research, in which a simple comprehensive approach has been put forward for the treatment of disks subject to any combination of the classical boundary conditions and/or elastic supports, and rotational effects. The major highlights of this dissertation work are briefly summarized in the following:

7.1. *Major Contributions*

Exact frequency equations have been derived for the general case of annular disks subject to different combinations of uniform boundary conditions. In previous studies, the frequency equations were presented for solid disks with free or clamped outer edge only. The present study proposed a generalized and accurate formulation which has the capability to predict the modal characteristics for annular disks subject to flexible boundary conditions as well as the classical clamped or free boundaries. Simplified forms of frequency equations are presented for solid disks and axisymmetric modes of annular disks. The proposed frequency equations could serve as the reference for approximate methods on in-plane vibration characteristics of the annular disks with different combinations of uniform edge conditions.

Since exact solutions are limited to uniform boundary conditions only, the Rayleigh-Ritz method is used to develop a model that incorporates various classical and

non-uniform boundary conditions. The boundary characteristic orthogonal polynomials are employed as admissible functions to represent the radial variations in the displacements. The clamped and flexible supports are described by sets of artificial springs at the free outer and inner edges to study their effects on the vibration properties. For non-uniform supports, the stiffness parameter $K(\theta)$ is expanded using the Fourier series to simulate single, multiple points or line support conditions.

The proposed formulation is extended to study the effects of rotation on the in-plane modal characteristics to identify the bifurcation in the frequencies. Nonlinear strain relations are employed to account for the stiffening effect on the rotation. While previous studies considered the stiffening to be axisymmetric along the circumferential direction, the present formulation is generalized to account for the stiffening effects for disks subject to uniform as well as non-uniform boundary conditions, where the initial displacement cannot be considered to be axisymmetric.

The dissertation research is the first to illustrate the splitting of the in-plane natural frequencies due to the non-uniformity of boundary conditions and due to rotational effects through laboratory experiments. The measurements are performed for the disks with different boundary conditions including free and point-support conditions and to experimentally investigate the coupling between the in-plane and the out-of-plane modes of vibrations.

The acoustic properties associated with in-plane and out-of-plane modes of annular disks are further analyzed. For this purpose, the three-dimensional model of the disk is used to derive the expressions for the sound pressure, the sound power and the sound radiation efficiency for the general case of non-uniform boundary conditions. The

three-dimensional model is further employed to investigate the rotational and constraint effects on thick annular disks. The applicability and accuracy of the formulations is further explored through analysis of modal characteristics of a railway wheel in contact with the rail.

7.2.   Conclusions

The major conclusions drawn from the present research work are summarized below.

- The exact frequency equations for flexible boundary conditions involve combinations of the equations for free and clamped edge conditions. The model reduces to that for the clamped conditions by selecting high support stiffness values and to the free conditions when the stiffness parameters vanish.

- Analytical results suggest that the non-uniformity of the support along the circumferential directions of the boundaries affects the modal characteristics of the disk along the in-plane and out-of-plane directions, while introducing additional coupling between the two. The system of equations can be represented by those of two independent subsystems, associated with coupled radial cosine and circumferential sine, and radial sine and circumferential cosine modes, respectively. The odd and even subsystems, however, will be coupled in the case of rotating disks. In each subsystem, the modes associated with different nodal diameter number n are coupled for non-uniform boundary conditions while they are uncoupled for uniform boundaries. Rotation of the disk produces additional coupling between these two subsystems through the gyroscopic matrix.

223

- The results obtained from the parametric study show considerable effects of the geometric parameters on the in-plane natural frequencies. While some of the modes are significantly affected by variations in the geometric parameters such as radius ratio, only minimal effects were observed on the other modes. Modes with same nodal diameter number n tend to have the same variation pattern with geometric parameters. The comparisons of the analytical results with the laboratory-measured data confirmed the variation patterns of different modes.

- The results obtained for the point-supported disk show that the addition of a point support disturbs the axisymmetry of the modes with zero nodal diameter number, which makes the first torsional mode, for example, neither purely circumferential nor axisymmetric.

- Some of the peaks in the frequency spectrum obtained under uniform boundary conditions split into two distinct peaks in the presence of a point support. These peaks correspond to the frequency parameters obtained from the two subsystems, which yield different values due to the non-uniformity of the boundary conditions.

- The frequency parameters differ considerably with changes in the orientation of the point supports. The mode shapes are also strongly affected by the locations of the point supports. This effect is the smallest when the point supports are located near a nodal point of a specific mode.

- Consideration of the radial expansion due to rotation yields additional stiffening effects, which affects the frequencies correspond to the forward and backward waves considerably. A critical speed could not be observed when the rotational stiffening

effect is considered. The results suggest that instability may occur in the absence of the additional stiffening at speeds above the critical speeds.

- The results show that the in-plane modes of vibration are comparable with those associated with out-of-plane modes and contribute considerably to the total noise radiation. The experimental results also confirmed the splitting of some of the modes into two distinct pairs with a difference that could be few hundred Hertz for some modes. The experimental and analytical results also confirmed that an in-plane excitation could excite the out-of-plane modes in a manner similar to that caused by an out-of-plane excitation. Furthermore, the in-plane modes could be easily detected from the responses measured along the out-of-plane direction, suggesting strong coupling between the in-plane and out-of-plane modes, even though the thickness to radius ratio is relatively low.

- The accuracy of the proposed model in the analysis of the railway wheel problem suggested the validity of the method in problems involving multi-span disks and three-dimensional coupled vibrations under several constraints and rotational effects.

7.3.   Recommendation for Future Work

The present work provided significant insights into the problems associated with rotating disks subject to contact or supported at different points, particularly the in-plane modes of vibration. In view of the potential applications of the present study in many engineering problems, further investigations are essential for comprehensive understanding of the modal and acoustic characteristics of the disks in practical systems. Some of the recommended directions for further work are summarized below:

225

- The proposed model assumed uniform thickness along radial and circumferential directions. A direct extension of the current analysis is to consider disks with varying thickness. This would better simulate for some engineering applications involving non-uniform disks.

- The expressions for acoustic properties have been formulated for stationary disks only. The sound emission from rotating structures requires implementation of Green's function form moving sources instead of the one used for stationary sources.

- A detailed analysis of the three dimensional model of thick disks under the effect of point, line or area supports are also recommended. The variations of the frequency parameters with the number of support or their orientations can be discussed. The non-uniform support can be expanded using Fourier double series to represent the variations in the stiffness parameters along the circumferential and normal directions.

- The current study predicts the natural frequencies of a railway wheel. It is possible to combine the disk model with a beam model to develop a simplified wheelset model that would permit analyses of natural frequencies and mode shapes of the wheels and the axle, and the coupling between them. The axle could be connected to the wheels by means of artificial springs. This is of particular importance for predicting the modes with zero or one nodal diameter where the coupling is significant between wheels and axle modes.

- It is anticipated that wheels defects such as flats would emphasize the contributions due to in-plane vibration modes. It is thus suggested to extend the analytical and experimental studies to investigate the effects of wheel defects on the noise emission due to defective wheels.

REFERENCES

1.   Thompson D., 1993, Wheel-rail noise generation, Part II: Wheel vibration. *Journal of Sound and Vibration* 161, 401-419.

2.   Tzou K., Wickert J. and Akay A., 1998, In-plane vibration modes of arbitrarily thick disks, *Journal of Vibration and Acoustics*. 120, 384-91.

3.   Thompson D. and Jones J., 2000, A Review of the modelling of wheel/rail noise generation, *Journal of Sound and Vibration*, 231, 519-536.

4.   Fingberg U., 1990, A model of wheel-rail squealing noise, *Journal of Sound and Vibration*, 143, 365-377.

5.   Leissa A., *Vibration of plates*, Nasa SP-160,1969.

6.   Rao J., *Dynamics of Plates*, Narosa Publishing House, 1999.

7.   Ferguson N. and White R., 1989, The free vibration characteristics of a clamped-free disc under the action of a static in-plane load and constraint on the outer periphery, *Journal of Sound and Vibration*, 121, 497-509.

8.   Srinivasan V. and Ramamurti V., 1980, Stability and vibration of an annular plate with concentrated edge load, *Computers and Structures*, 12, 119-129.

9.   Yano S. and Kotera T., 1991. Instability of the vibrations of a rotating thin disk due to an additional support. *Archive of Applied Mechanics*, 61, 110-118.

10.   Yano S. and Kotera T., 1991, Instability of a rotating disk with a support under the action of a static in-plane load, *Archive of Applied Mechanics*, 61, 110-118.

11.   Lee H. and Singh R., 2005, Self and mutual radiation from flexural and radial modes of a thick annular disk, *Journal of Sound and Vibration*, 286, 1032-1040.

12.   Knothe K. and Grassie S. 1993, Modelling of railway track vehicle/track interaction at high frequency, *Vehicle System Dynamics*, 22, 209-262.

13.   Love, *A Treatise on the Mathematical Theory of Elasticity*, Dover Publications, New York, 1944.

14.   Onoe M., 1956, Contour Vibrations of Isotropic Circular Plates, *Journal of the Acoustical Society of America*, 28, 1158-1162.

15.   Holland R., 1966, Numerical studies of elastic-disk contour modes lacking axial symmetry, *Journal of Acoustical Society of America*, 40, 1051-1057.

16. Farag N. and Pan J., 2003, Modal characteristics of in-plane vibration of circular plates clamped at the outer edge, *Journal of the Acoustical Society of America*, 113, 1935-1946.

17. Park C., 2008, Frequency equation for the in-plane vibration of a clamped circular plate, *Journal of Sound and Vibration*, 313, 325-333.

18. Ambati G., Bell J. and Sharp J., 1976, In-plane vibrations of annular rings, *Journal of Sound and Vibration*, 47, 415-432.

19. Srinivasan V. and Ramamurti V., 1980, Dynamci response of a annular disk to a moving concentrated, in-plane edge load, *Journal of Sound and Vibration*, 72, 251-262.

20. Irie T., Yamada G. and Muramoto Y., 1984, Natural frequencies of in-plane vibration of annular plates. *Journal of Sound and Vibrations*, 97, 171-175.

21. Wu T., 2006, Analytical study on torsional vibration of circular and annular plate, *Proceedings of the Institution of Mechanical Engineers, Part C: Mechanical Engineering Science*, 220, 393-401.

22. Leung R. and Pinnington R., 1987, Responses of an elastic disc to in-plane forces, *Journal of Sound and Vibration*, 112, 355-368.

23. Lee H. and Singh R., 2005, Acoustic radiation from out-of-plane modes of an annular disk using thin and thick plate theories, *Journal of Sound and Vibration*, 282, 313-339.

24. Lee H. and Singh R., 2005, Comparison of two analytical methods used to calculate sound radiation from radial vibration modes of a thick annular disk, *Journal of Sound and Vibration*, 286, 1032-1040.

25. Chen J. and Jhu J., 1997, In-plane stress and displacement distributions in a spinning annular disk under stationary edge loads, *Journal of Applied Mechanics*, 64, 897-904.

26. Bhuta P. and Jones J., 1963, Symmetric planar vibrations of a rotating disk, *The Journal of the Acoustical Society of America*, 35, 982-989.

27. Burdess J., Wren T. and Fawcett J., 1987, Plane stress vibrations in rotating disks", *Proceedings of the Institution of Mechanical Engineers, Part C: Mechanical Engineering Science*, 201, 37-44.

28. Chen J. and Jhu J., 1996, On the in-plane vibration and stability of a spinning annular disk, *Journal of Sound and Vibration*, 195, 585-593.

29. Chen J. and Jhu J., 1996, In-plane response of a rotating annular disk under fixed concentrated edge loads, *International Journal of Mechanical Sciences*, 38, 1285-1293.

30. Hamidzadeh H. and Dehgani, M., 1999, Linear in-plane free vibration of a rotating disk, *Proceedings of the ASME Design Engineering Technical Conferences*, Las Vegas, USA.

31. Hamidzadeh H., 2002, In-plane free vibration and stability of rotating annular disks, *Proceedings of the Institution of Mechanical Engineers, Part K*, 216, 371-380.

32. Endo M., Hatamura K., Sakata M. and Taniguchi, 1984, Flexural vibrations of a thin rotating ring, *Journal of Sound and Vibration*, 92, 261-272.

33. Huang S. and Soedel W., 1987, Effects of coriolis acceleration of the free and forced in-plane vibrations of rotating rings on elastic foundation, *Journal of Sound and Vibration*, 115, 253-274.

34. Naguleswaran S., 1994, Lateral vibration of a centrifugally tensioned uniform Euler-Bernoulli beam, *Journal of Sound and Vibration*, 176, 613-624.

35. Mote C., 1965, Free vibration of initially stressed circular disks, *Transactions of the ASME Journal of Engineering for Industry*, 87, 258-264.

36. Deshpande M. and Mote C., 2003, In-plane vibrations of a thin rotating disk, *Journal of Vibration and Acoustics*, 125, 68-72.

37. Koh C., Sze P. and Deng T., 2005, Numerical and analytical methods for in-plane dynamic response of annular disk, *International Journal of Solids and Structures*, 43, 112-131.

38. Leung R. and Pinnington R., 1987, Vibration of a rotating disc subjected to an in-plane force at its rim, or at its centre, *Journal of Sound and Vibration*, 114, 281-295.

39. Lee H., 2004, Influence of in-plane modes of a rotor to brake noise, *Proceedings ASME Applied Mechanics Division*, 255, 553-558 California, USA.

40. Kirillov O., Hagedorn P., Hochlenert D. and Spelsberg-Korspeter G., 2009, In- and out-of-plane vibrations of a rotating plate with fricitional contact: investibations of Squeal phenomena, *Transactions of the ASME. Series E, Journal of Applied Mechanics*, 76, 041006.

41. Lee H. and Singh R., 2004, Determination of acoustic radiation from a simplified disk-brake rotor using a semi-analytical method, *Noise Control Engineering Journal*, 52, 225–239.

42. Thompson D. J., 1993, Wheel-rail noise generation, Part I: Introduction and interaction model, *Journal of Sound and Vibration*, 161, 387-400.

43. Wu X. and Thompson, D., 2002, A Hybrid model for the noise generation due to railway wheel flats, *Journal of Sound and Vibration*, 251, 115-139.

44. Talotte C., Gautier P., Thompson D. and Hanson C., 2003, Identification, modelling and reduction potential of railway noise sources: a critical survey, *Journal of Sound and Vibration*, 267, 447-468.

45. Popp K., Kruse H. and Kaiser I., 1999, Vehicl-track dynamics in the mid-frequency range, *Vehicle System Dynamics*, 31, 423-464.

46. Baddour N. and Zu J., 2001, A revisit of spinning disk models. Part I: derivation of equations of motion. *Applied Mathematical Modelling*, 25, 541-559.

47. Baddour N. and Zu J., 2001, A revisit of spinning disk models. Part II: linear transverse vibrations, *Applied Mathematical Modelling*, 25, 561-578.

48. Baddour N. and Zu J., 2007, Nonlinearly coupled in-plane and transverse vibrations of a spinning disk, *Applied Mathematical Modelling*, 31, 54-77.

49. Chonan S. and Hayase T., 1987, Stress analysis of a spinning annular disk to a stationary distributed, in-plane edge load, *Journal of Vibration, Acoustics, Stress and Reliability*, 109, 277-282.

50. Irretier H., 1983, The natural and forced vibrations of a wheel disc, *Journal of Sound and Vibration*, 87, 161-177.

51. Hirano Y. and Okazaki K., 1976, Vibrations of a circular plate having partly clamped or partly simply supported boundary, *Bulletin of JSME*, 19, 610-618.

52. Keer L. and Stahl B., 1972, Eigenvalue problems of rectangular plates with mixed edge conditions, *Transactions of the ASME. Series E, Journal of Applied Mechanics*, 39, 513-520.

53. Irie T. and Yamada G., 1978, Free vibration of circular plate elastically supported at some points, *Bulletin of JSME*, 21, 1602-1609.

54. Leissa W., Laura P. A. A. and Gutierrez R. H., 1979, Transverse vibrations of circular plates having nonuniform edge constraints, *Journal of Acoustical Society of America*, 66, 1180-1184.

55. Laura P. A. A. and Ficcadenti G. M., 1980, Transverse vibrations of circular plates of varying thickness with non-uniform edge constraints, *Applied Acoustics*, 13, 227-236.

56. Narita Y. and Leissa A. W., 1980, Transverse vibrations of simply supported circular plates having partial elastic constraints, *Journal of Sound and Vibration*, 70, 103-116.

57. Narita Y. and Leissa A. W., 1981, Flexural vibrations of free circular plates elastically constrained along parts of the edge, *International Journal of Solids and Structures*, 17, 83-92.

58. Amabili M., Pierandrei R. and Frosali G., 1997, Analysis of vibrating circular plates having non-uniform constraints using the modal properties of free-edge plates: application to bolted plates, *Journal of Sound and Vibration*, 206, 23-38.

59. Torvik P., 1984, A variational approach to the dynamics of structures having mixed or discontinuous boundary conditions, *Transactions of the ASME. Journal of Applied Mechanics*, 51, 831-836.

60. Febbo M., S. And Laura V. P., 2005, Free, transverse vibrations of thin plates with discontinuous boundary conditions, *Journal of Sound and Vibration*, 281, 341-356.

61. Eastep F. E. and Hemmig F. G., 1982, Natural frequencies of circular plates with partially free, partially clamped edges, *Journal of Sound and Vibration*. 84, 359-370.

62. Bauer H. F. and Eidel W., 2006, Determination of the lower natural frequencies of circular plates with mixed boundary conditions, *Journal of Sound and Vibration*, 292, 742-764.

63. Mindlin R., 1951, Influence of rotary inertia and shear on the flexural motion of isotropic, elastic plate, *Journal of applied Mechanics*, 18, 31-38.

64. Mindlin R. and Deresiewicz H., 1954, Thickness-shear and flexural vibration of a circular disk, *Journal of applied Physics*, 25, 1339-1332.

65. Irie T., Yamada G. and Takagi K., 1982, Natural frequencies of thick annular plates, *Transactions of the ASME. Series E, Journal of Applied Mechanics*, 49, 633-638.

66. Irie T., Yamada G. and Aomura S., 1979, Free vibration of a Mindlin annular plate of varying thickness, *Journal of Sound and Vibration*, 66, 187-197.

67. Hutchinson J., 1984, Vibrations of thick free circular plates, exact versus approximante solutions, *Transactions of the ASME. Journal of Applied Mechanics*, 51, 581-585.

68. Hutchinson J. and El-azhari S., 1986, On the vibratio of thick annular plates, *Proceedings of the Euromech-Chollquium,* 219, 102-111.

69. Leissa A.W. and So J., 1995, Accurate vibration frequencies of circular cylinders from three-dimensional analysis, *Journal of the Acoustical Society of America*, 98, 2136-2141.

70. Leissa A.W. and So J., 1995, Comparisons of vibration frequencies for rods and beams from one-dimensional and three-dimensional analyses, *Journal of the Acoustical Society of America*, 98, 2122-35.

71. So J. and Leissa, A.W., 1998, Three-dimensional vibrations of thick circular and annular plates, *Journal of Sound and Vibration*, 209, 15-41.

72. Kang J. and Leissa, A.W., 1998, Three-dimensional vibrations of thick, linearly tapered, annular plates, *Journal of Sound and Vibration*, 217, 927-944.

73. Kang J., 2003, Three-dimensional vibration analysis of thick, circular and annular plates with nonlinear thickness variation, *Computers and Structres*, 81, 1663-1675.

74. Hashemi S., Farhadi S. and Carra S., 2009, Free vibration analysis of rotating thick plates, *Journal of Sound and Vibration*, 1-2, 366-384.

75. Kane and Levinson, D., *Dynamics: Theory and Application*, McGraw-Hill, New York, 1985.

76. Knothe Kl., Strzyzakowski Z. and Willner K., 1994, Rail vibrations in the high Frequency Range, *Journal of Sound and Vibration*, 169, 111-123.

77. Sato S. and Matsuhisa H., 1978, A study of the mechanism of train noise and its countermeasure, part I: characteristics of wheel vibration, *Bulletin of JSME*, 21, 1475-1481.

78. Sakamoto H., Hirakawa K. and Toya Y., 1996, Sound and vibration of railroad wheel. *Proceedings of the IEEE/ASME Joint Railroad Conference*, 75-81.

79. Bogacz R. and Dzula S., 1998, Stability of a wheelset modelled as linear and non-linear continuous System. 6th Mini Conference on Vehicl System Dynamics, 229-239, Budapest.

80. Szolc T., 1998, Medium frequency dynamic investigation of the railway wheelset-track system using a discrete-continuous model, *Archive of Applied Mechanics* 68, 30 - 45.

81. Meywerk M., 1999, Polygonalization of railway wheels, *Archive of Applied Mechanics*, 69, 105-120.

82. Johansson A., 2006, Out-of-round railway wheels assessment of wheel tread irregularities in train traffic, *Journal of Sound and Vibration*, 293, 796-806.

83. Meirovitch L., *Fundamentals of Vibrations*, McGrow-Hill, 2001.

84. Bhat R., 1985, Natural frequencies of rectangular plates using characteristic orthogonal polynomials in Rayleigh-Ritz Method, *Journal of Sound and Vibrations*, 102, 493-499.

85. Kim C. S., The vibration of beams and plates studied using orthogonal polynomials, PhD Thesis, The University of Western Ontario, 1988.

86. Rajalingham C. and Bhat R., 1991, Vibration of elliptic plates using characteristic orthogonal polynomials in the Rayleigh-Ritz method, *International Journal of Mechanical Sciences*, 33, 705-716.

87. Rajalingham C. and Bhat R., 1993, Axisymmetric vibration of circular plates and its analog in elliptical plates using characteristic orthogonal polynomials, *Journal of Sound and Vibrations*, 161, 109-118.

88. Bhat R., 1985, Vibration of sturctures using characteristic orthogonal polynomials in Rayleigh-Ritz method, *Proceedings of the 10th Canadian Congress of Applied Mechanics, London, Ontario.*

89. Bhat R., 1987, Flexural Vibrations of polygonal plates using characteristic orthogonal polynomial in two variables. *Journal of Sound and Vibrations.* 114, 65-71.

90. Kim C. and Dickinson. S., 1989, On the lateral vibration of thin annular and circular composite plates subject to certain complicating effects, *Journal of Sound and Vibration*, 130, 363-77.

91. Kim C. S. and Dickinson S., 1986, The flexural vibration of slightly curved slender beams subject to axial end displacement, *Journal of Sound and Vibration*, 104, 170-175.

92. Kim C. and Dickinson. S., 1987, Flexural vibration of rectangular plates with point support, *Journal of Sound and Vibration*, 117, 249-261.

93. Yuan J. and Dickinson S., 1994, Free vibration of circularly cylindrical shell and plate systems, *Journal of Sound and Vibrations*, 175, 241-263.

94. Reddy J., *Energy Principles and Variational Methods in Applied Mechanics*, John Wiley & Sons, 2002.

95. Ilanko S., 2002, The use of negative penalty functions in constrained variational problems, Communications in Numerical Methods in Engineering, 18, 659-668.

96. Singa Rao K. and Amba-Rao C. L., 1972, Lateral vibration and stability relationship of elastically restrained circular plates, *AIAA*, 10, 1689-1690.

97. Laura P. A. A., Paloto J. C. and Santos R. D., 1975, A note on the vibration and stability of a circular plate elastically restrained against rotation, *Journal of Sound and Vibration*, 41, 177-180.

98. Laura P. A. A., Luisoni L. E. and Lopez J. J., 1976, A note on free and forced vibrations of circular plates: the effect of support flexibility, *Journal of Sound and Vibration*, 47, 287-291.

99. Kim C. S. and Dickinson S. M., 1990, The flexural vibration of thin isotropic and polar orthotropic annular and circular plates with elastically restrained peripheries, *Journal of Sound and Vibration*, 143, 171-179.

100. Eringen A. C. and Suhubi E. S., *Elastodynamics*, Volume II, Academic Press, 1975.

101. Zill D. G., Cullen M. R., *Advanced Engineering Mathematics*, Jones and Bartlett Publishers, 2006.

102. Bhat R. and Chakraverty S., *Numerical Analysis in Engineering*, Alpha Science, 2004.

103. Junger M. C. and Feit D., *Sound, Structures, and their Interactions*, New York: MIT Press, 1985.

104. Williams E. G., *Fourier Acoustics*, Academic press, 1999.

105. *ANSYS* Verification Manual, Release 10.0, 2005.

106. Xing Y. and Liu B., 2009, Exact solutions for the free in-plane vibrations of rectangular plates, *International Journal of Mechanical Sciences*, 51, 246-255.

107. Kane T. R. and Mindlin R. D., 1956, High-frequency extensional vibrations of plates, *Journal of Applied Mechanics*, 23, 277-283.

108. Lee H., Modal acoustic radiation characteristics of a thick annular disk, PhD Thesis, The Ohio State University, 2003.

109. Perkins N. and Mote J., 1986, Comments on curve veering in eigenvalue problems, *Journal of Sound and Vibration*, 106, 451-463.

110. Bhat B., 2000, Curve veering: Inherent behavior of some vibrating systems, *Shock and Vibration*, 7, 241-249.

111. Young T. and Wu M., 2004. Dynamic stability of disks with periodically varying spin rates subject to stationary in-plane edge loads. *Journal of Applied Mechanics*, 71, 450-458.

112. Chen J., 1994, Stability analysis of a spinning elastic disk under a stationary concentrated edge load, *Journal of Applied Mechanics*, 61, 788-792.

113. Raman A. and Mote C., 2001. Experimental studies on the non-linear oscillations of imperfect circular disks spinning near critical speed, *International Journal of Non-linear Mechanics*, 36, 291-305.

114. Lee M. and Singh R., 1994. Analytical formulations for annular disk sound radiation using structural modes, *Journal of Acoustic Society of America,* 95, 3311-3323.